SPINNING MODES IN ORDERLY JET STRUCTURE

AND JET NOISE

by

PAUL JONATHAN RAILTON STRANGE

Being an account of research work carried out in the Department of Applied Mathematical Studies, University of Leeds and at the Advanced Research Laboratory, Rolls Royce Ltd., Derby under the joint supervision of Prof. D.G. Crighton and Dr. C.J. Moore.

Submitted in fulfilment of the requirements for the degree of Doctor of Philosophy.

February, 1981.

Abstract

The structural response of a subsonic turbulent jet to controlled forcing has been investigated both theoretically and experimentally. An experimental study has been carried out in which a model jet was subjected to acoustic excitation in the form of circumferential modes of azimuthal wavenumber m = 0, 1 and 2. Detailed aerodynamic measurements on the initial region of the jet indicate that the m = 0 and m = 1 modes have comparable axial growth rates. Further, when forcing was applied in a combination of first (m = ±1) or second (m = ±2) order modes, substantial changes in the mean flow were evident over the first twelve diameters of the jet.

A linear stability analysis of higher order azimuthally coherent wave-like disturbances on a slowly diverging mean flow has been used to predict the axial growth rates, phase speeds and radial distributions of the flow characteristics in the forced turbulent jet. Similar axial growth rates result for the m = 0 and m = 1 modes but, in both these cases, they compare unfavourably with the measured rates which reflect the highly non-linear response of the instability wave to the strong forcing level used. The phase speeds are well predicted, as are the measured radial structures of the instability wave velocity components. The latter agree surprisingly well in view of the highly non-linear axial development of these quantities and this interesting result lends support to the previously unwarranted use of "shape functions" in non-linear stability calculations.

Finally the effects of an external flow on a forced jet have been considered. Linear stability theory has been used to examine the

axial development of a plane wave disturbance on a slowly diverging jet embedded in an infinite co-flowing stream. The results indicate that at a diameter-based Strouhal number of 0.5 the disturbance suffers very little downstream amplification in the presence of a significant external flow. This is in agreement with increasing experimental evidence which casts doubt on the significance of jet forcing when the device producing the jet is in flight relative to the ambient medium.

ACKNOWLEDGEMENTS

I wish to express sincere thanks to my academic supervisor, Professor David Crighton, for his enthusiastic approach and encouragement during the course of these studies. My thanks are also due to him for his patience and careful guidance in the preparation of this thesis.

The keen interest of my industrial supervisor Dr. Chris Moore of Rolls Royce Ltd., is also much appreciated, as are the helpful suggestions he made both during the course of the experimental work and in the preparation of this thesis.

Many thanks are also due to Mr. David Brierley of Rolls Royce Ltd., for his invaluable assistance with the experimental work and whose meticulous attention to detail was a great asset.

My thanks must also go to Dr. Julian Scott and Dr. Patrick Huerre, both formerly of the Department of Applied Mathematical Studies at Leeds University, for many useful discussions.

I gratefully acknowledge the financial support of the Science Research Council through the "CASE" award scheme, and Rolls Royce Ltd., the industrial collaborator on this project.

Finally I am indeed grateful to Mrs. J.L. Bunn for her careful typing of the thesis.

To

Mum and Dad

CONTENTS PAGE

List of Figures

Page

Page

Chapter 4

Chapter 5

CHAPTER 1 INTRODUCTION

Jet exhaust noise has developed into a pressing environmental problem during the last 20 years. Yet even many years after the introduction of the first commercial jet passenger service it was still regarded as a relatively insignificant though undesirable by-product of jet transport. Since that time ever-increasing payloads and more frequent flights have necessitated the introduction of strict legislation at both local and national levels to establish "acceptable" limits on aircraft noise. Consequently, noise considerations, including changes brought about by different aircraft installations, have become a significant design constraint for jet engine manufacturers. Industrial and academic research programmes have multiplied in a consolidated effort to identify, and to obtain a basic understanding of the dominant noise generation mechanisms from both a theoretical and an experimental standpoint.

As early as 1952, in anticipation of such problems, Lighthill [41,42] formulated his theory of "sound generated aerodynamically" which is probably still the most important basic tool we have with which to analyse jet noise. Lighthill's theory applies to sound generated by finite regions of turbulent flow embedded in an infinite homogeneous fluid in the absence of solid boundaries. In an analogy with a fictitious medium at rest the turbulent jet is represented by a quadrupole source distribution. The theory has proved to be extremely versatile in that effects such as refraction, source convection and fluid shielding have subsequently been sketched in qualitatively with a reasonable amount of success. Notable additions

in these and other respects appear in papers by Ffowcs Williams & Hawkings [28] (the effects of solid boundaries), Mani [45] (shielding effects), Ribner [62] and Ffowcs Williams [27] (convective amplification).

The noise fields of cold model jets, where care has been taken to minimise internal noise and turbulence, follow the predicted eighth power law variation with exhaust velocity of this "pure jet mixing noise" fairly well over a wide range of velocities as shown in,e.g., Lush [44] or Ahuja [3]. However, the noise fields of real engines show large increases above the levels obtained by scaling up mixing noise data from model jets, particularly at low exhaust velocities (see, for example, Bushell [13]). This is the so-called "excess noise problem" and the "excess" noise has usually been attributed to internal sources such as those associated with combustion or turbomachinery. In imperfectly expanded supersonic jets, shock associated noise (generated by the interaction of shear layer turbulence with the steady cellular shock-cell pattern in the jet exhaust) is considered to be the major contributing factor.

Since 1970 two highly significant experimental results have greatly influenced the position regarding "excess" noise. In 1977, Moore [52] discovered that very low levels of acoustic forcing could increase the radiated broadband noise of a subsonic jet by as much as 6 dB. This result was also obtained quite independently by Bechert & Pfizenmaier [5] at about the same time. Such an increase, it was found, could be produced from either tonal or broadband forcing. Moreover, the far-field spectra and directivity patterns of the noise

from the excited and unexcited jets were very similar. Earlier, in 1972, a less convincing but still noteworthy result was obtained by Crow [21]. An experiment was conducted on a hot model jet which showed that an internal tone could be greatly amplified on such a high speed turbulent jet (by up to 34 dB!). Moore found no such amplification of an internal tone and suggested that Crow's apparent amplification might be symptomatic of the measuring environment and caused by standing waves, for example, though there are many possible reasons why Crow's results might be expected to differ from Moore's.

Crow's explanation as to how a turbulent jet could act as a high gain amplifier was based on what has now become a well-established fact - that such a jet is unstable and, even in its natural (unforced) state, supports a large scale wave-like structure. The state of turbulence research at that time, however, was such that workers were only just beginning to unravel the essential features of this latent organised structure which is not confined to the turbulent jet, and has now been widely recognised in many kinds of free turbulent shear flows (as reviewed by, e.g., Roshko [64]). It had been known for over a hundred years that "high" Reynolds number (10^2 - 10^3) laminar jets were unstable, but it was only in 1964 that the first conclusive evidence appeared to suggest that this might also be a property of turbulent jets. In that year, Bradshaw, Ferriss & Johnson [9] produced a Schlieren photograph of a turbulent jet (Re $\sim 3 \times 10^5$) in which a large scale wave structure could be seen over and above the fine-scale mixing turbulence. Previously, experimental studies had concentrated on the mixing region of the jet because of the high

turbulence levels there, and the fluctuating quantities had been found to be broadband, suggesting that the fluctuations were random in nature. However, the measurements of Bradshaw et al. clearly pointed to the existence of a more regular coherent structure both in the mixing region (see also Davies, Fisher & Barratt [23]) and in the potential core.

Mollo-Christensen [50] found from pressure measurements in the near field that this coherence encompassed an even wider cross-section of the flow field. In the following years this experimental work was greatly extended. Techniques such as signal eduction and periodic forcing were used to facilitate the measurement of the coherent structures by extracting them from or raising their levels above the background turbulence. Individual papers are too numerous to mention but one fairly comprehensive study was that of Crow & Champagne [22]. In their experiments a model jet was forced with an incident plane wave generated inside the tailpipe. In common with other workers they found that there was a characteristic Strouhal number for the forcing at which the induced axisymmetric instability wave achieved the greatest total downstream amplification. The Strouhal number of this "preferred" mode was given by Crow & Champagne to be 0.3 and the maximum amplification was attained at about four diameters downstream of the nozzle exit. Wave modes at lower frequencies peaked further downstream and those at higher frequencies, further upstream. (It is interesting to note that as early as 1967, Ronneberger [63] performed a similar experiment at a number of flow speeds and excitation frequencies in which he measured the amplitude of the reflected pressure

signal inside the jet pipe to discover that the reflection coefficient reached a maximum value, greater than unity, at approximately the same preferred Strouhal number as that later obtained by Crow & Champagne. Ronneberger would no doubt have observed the growth of the jet instability wave, too, had he taken any measurements outside the jet pipe.)

The value of 0.3 for the Strouhal number of the preferred mode, however, did not appear to be unique. Fuchs [30], for instance, obtained 0.5, as later did Moore [52], and Lau, Fisher & Fuchs [38] gave a value of 0.6. These discrepancies were partly resolved by the work of Chan [15] which showed that the preferred Strouhal number depends very much on the radial position at which the measurements are taken. In 1977, Moore pointed out that disagreements might also result from the use of different forcing levels in these experiments. He found that non-linear effects are evident at forcing levels as low as 0.1% (fluctuating pressure in the nozzle exit plane re the jet dynamic head). The forcing levels (1 - 4%) used by Crow & Champagne, for instance, were therefore all in the non-linear range. Indeed, they found that the centre line velocity fluctuation in the preferred mode reached a saturation amplitude of only 18% under an exit plane forcing level of 4%, whereas Moore obtained an amplification factor of around 60 for this quantity at a forcing level of 0.08% (fluctuating pressure, normalised as above). Significant changes in the structure and response of the jet at <u>linear</u> forcing levels have also been shown to be produced by a number of workers e.g. Moore [52], Chan [15] and Lee [40].

Moore observed that in addition to the axisymmetric mode, the unforced jet could also support a helical wave train with azimuthal wavenumber 1. Further experiments conducted by Chan [17] involved a partial study of the fluctuating pressure field of this asymmetric mode together with that of the second order (m = 2) mode.

The type of instability to which all of these experiments refer is the jet column instability which scales on the diameter of the jet. It has been observed in the region $D < x < 8D$ on both clean model rigs and hot engine exhausts at Reynolds numbers between 10^4 and 10^7. Another instability mode which can occur on laminar jets is the quasi-two-dimensional shear layer instability with wavelength the order of the initial shear layer momentum thickness. In practical situations, however, the turbulent initial shear layer of the high Reynolds number jet is prohibitive towards this type of instability mechanism as the corresponding waves are inextricably coupled to the turbulent eddies already present in the shear layer. In contrast, the azimuthally coherent jet column instability in a (forced) turbulent jet may contain a considerable amount of the overall turbulent energy (Fuchs [31]) and in some cases virtually all of this energy ($\sim$ 90%) as indicated by the centre line axial velocity measurements of Crow & Champagne [22].

An alternative description of the axisymmetric coherent motions pictures them as a sequence of ring vortices being convected along the jet. This view is most readily appreciated from the flow visualisation results of Moore, say. Previous studies demonstrating the existence of such structures on two-dimensional shear layers (e.g. Brown & Roshko

[11] and Damms & Küchemann [24]) indicated that the observed increased vortex spacing with shear layer divergence was due to the occurrence of vortex pairing events. This process was also observed by Winant & Browand [67] whose results Laufer, Kaplan & Chu [39] generalised to describe, qualitatively, the equivalent process in the mixing layer of the circular jet. In Moore [52], forcing the circular jet was seen to "lock" the eddies to the forcing frequency and produce a regular spacing between the pairing events. Moore also showed that pairing processes took place in the unforced jet but in a much more random fashion.

Theoretical models of the jet column instability reflect these two points of view. Much of the early work concentrated on the wave theory model, initially in the form of a simple linear analysis of the instability modes of an "equivalent" laminar jet. Crow & Champagne's first attempts to provide a theoretical account of the observed structural behaviour were, however, unsuccessful. On the basis of linear stability theory, either temporal or spatial, they were unable to predict the existence of a preferred mode on a top hat mean velocity profile. Furthermore, they completely ruled out the possibility that the large scale structures could be modelled as spatially growing instabilities because the calculated dispersion relationship was incompatible with their experimental results. They proposed that the downstream wave growth should rather be modelled as a temporal instability in a frame of reference moving at the phase velocity which (although completely lacking justification) at least gave a satisfactory dispersion relationship.

However, the mean flow displays a top hat profile only very

close to the nozzle exit and the shear layer rapidly spreads out to a thickness which is a significant fraction of the jet radius. Michalke [48] showed that when a more representative mean velocity profile with a finite shear layer thickness is chosen, a preferred mode can indeed be predicted by the spatial theory. In particular, using an analytical form for the mean velocity profile which was in close agreement with Crow & Champagne's measured profile at x = 2D, he found that the phase speeds and amplification rates compared very favourably with their wave measurements. Michalke indicated further that "spinning" modes, those with azimuthal wavenumber 1, should be amplified at a rate comparable with that of the axisymmetric mode on the initial mixing region of the jet on the basis of the linear stability theory.

Mattingly & Chang [47] also recognised that the detailed structure of the mean velocity profile strongly affected the selection of a preferred mode and they applied spatial stability theory to m = 0, 1 and 2 disturbances on a quasi-parallel mean flow profile. In 1976, however, Crighton & Gaster [19] showed that the axial variations in phase speed and growth rate could not properly be accounted for using a quasi-parallel flow theory. They adopted a multiple scales expansion scheme to incorporate the effects of flow divergence in a linear stability analysis of axisymmetric modes on a circular jet. Variations in axial growth rates and phase speeds were found to occur with changes in flow characteristic and radial position and it was shown that peak amplitudes would not necessarily be reached at the axial positions at which the local parallel flow sustained a neutral wave.

A significant improvement in these models should be brought about by taking into account the turbulence-wave interaction. Crow's viscoelastic model [20] whereby the wave is able to give up some of its energy to the fine-scale turbulence is one such method but has yet to be incorporated successfully in a stability analysis for a circular jet. The non-linearity of the instability wave, another important aspect in the selection of a preferred mode, has received much attention in recent years. As far back as 1971, Crow & Champagne recognised that non-linear effects might be important. Having observed the production of a second harmonic in their forcing experiments they proposed a selection mechanism whereby the preferred mode could be considered to be the wave which is least capable of generating a harmonic and therefore more likely to reach a large amplitude prior to saturation. It is only recently, though, that any detailed calculations have been presented in this respect (those of Huerre [34] and Huerre & Scott [35] show that weakly non-linear stability for parallel shear flows is still far from understood.)

Integral formulations on a two-dimensional free shear layer, which take weak non-linear effects and the interaction of the large scale structure with the fine-scale turbulence into account have been pursued in the temporal case by Alper & Liu [4] and in the spatial case by Liu & Merkine [43], amongst many others. These studies have now been extended to the circular jet by Mankbadi & Liu [46], although Chan [15,16] had already used similar but more drastically simplified methods. Stability theory is here combined with an eddy viscosity model in a useful way. The flow field is split up into its mean, large scale wave and turbulent components. The integrated forms of

the three coupled kinetic energy equations are then solved using a "shape assumption" for the transverse structure of the large scale wave (the profile being given locally from linear parallel stability theory) and a further closure assumption, based on experimental results, relating the mean stresses of the fine-grained turbulence to the mean flow. Three non-linear ordinary differential equations result involving the shear layer momentum thickness, the wave amplitude and the kinetic energy density of the fine-grained turbulence. The equations are integrated from specified nozzle exit conditions and the axial development of the flow is given in terms of these three characteristic functions. Studying the energy transfer mechanisms in this way provides much insight into the physical processes involved in the interactions between the different scales of motion. The large scale structure is seen to extract energy from the mean flow as it grows on the initial region of the jet and some of this energy is fed to the fine-grained turbulence, which also takes a certain amount of energy from the mean flow directly. The transfer of energy from the mean flow to the fine-grained turbulence is greatly enhanced by the growth and decay of the large scale structure. The fine-grained turbulence energy is eventually converted into heat by viscous dissipation.

Mankbadi & Liu have been able to study the axial development of the $m = 0$ and $m = 1$ modes in this manner well into the flow region where these structures are decaying. The linear stability calculations, which are used to determine the local radial "shape" of the coherent structures, produce damped solutions in this region and the possibility that energy can be fed back from the large scale structures to the mean flow arises. It is pointed out that the use of an eddy viscosity model

for the wave-mean flow interaction, which permits only a one-way energy transfer, is completely inconsistent with the physical behaviour.

The development of the instability wave is well predicted by this method, but the turbulent energy levels (overall) fall well short of the measured ones. The main disadvantages are that the method relies entirely on shape functions providing the radial distributions of the wave amplitude, that non-linear interactions take place only in the axial direction and that local turbulence spectra are left unresolved.

The second approach mentioned above in which the shear layer of the jet is represented by a row of ring vortices has also reproduced a number of the features of the large scale structures found experimentally. The numerical modelling of Acton [1,2], Grant [33] and Morfey [55] in which vortices evolve under their mutual interaction whilst convecting downstream predicts a flow pattern very similar to that which is observed. The vortex interactions are fully non-linear, but the model is restricted to incompressible flow and further, only strictly axisymmetric modes can be treated in this manner.

Returning to the noise aspect, it is not surprising that after the work of Crow & Champagne there was a growing awareness that the coherent structures found on a turbulent jet were likely to contribute, directly or indirectly, to the radiated sound field and that such a contribution might well form a substantial part of the excess noise. Accordingly, Crow [21] made a radical move away from mixing noise theory by calculating the sound field due to a growing and decaying

instability wave with a Gaussian envelope along the jet column (at a prescribed phase velocity) to try to predict the results he had obtained experimentally. Although it was known that an instability wave with subsonic phase velocity (as in the experiment) should radiate only weakly, Crow's predictions and experimental results appeared to fit surprisingly well. Crow himself found that his experimental results were repeatable but they remain unique up to the present day.

The rôle of large scale structures is still unclarified as far as real engines in flight are concerned, but the many forcing experiments which have been carried out on model jets cover a wide range of flow conditions. In an extensive survey of these experiments Crighton [18] observes that the effects of forcing on the radiated sound field can be placed into two distinct categories. One type of response is a uniform broadband noise increase over the entire frequency spectrum at all angles to the jet. This effect has been found in the experiments of Moore [52] and Bechert & Pfizenmaier [5] on cold subsonic jets, as mentioned earlier, and subsequently in those of Jubelin [36] on hot subsonic jets, although the broadband increase produced here is somewhat less uniform both in frequency and angle. The second type of response which Crighton describes involves a suppression of the broadband noise except for limited frequency bands around the tone and its harmonics and subharmonics. Such a response has been observed by Kibens [37], for example, when forcing at the characteristic frequency of the shear layer instability was applied to a cold subsonic jet with a laminar nozzle boundary layer. Morrison & McLaughlin [59] found similar results in their experiments on cold

perfectly expanded supersonic jets at low Reynolds number, again with laminar nozzle boundary layers but subjected to forcing at the characteristic frequency of the jet column instability.

The type of response which will occur in a given situation might be considered to be determined by any of a number of factors such as the flow Mach number, temperature or Reynolds number or perhaps by whether the nozzle boundary layer is laminar or turbulent. From all of the available experimental evidence Crighton concludes that whether forcing a given jet, at a Strouhal number of about 0.5, will produce broadband suppression or broadband amplification would seem to be characterised by the Reynolds number, the criterion being that suppression or amplification will take place according as the Reynolds number is less than or greater than 10^5, or thereabouts. Why this is remains unclear at the present time. However, it is clear that at the flow conditions present in a full scale engine exhaust, broadband amplification is favoured under this hypothesis. Furthermore, Deneuville & Jacques [25] present experimental evidence which can be taken to support this belief, that jet noise from a gas turbine engine is in fact amplified jet noise.

Theoretical noise prediction schemes in which attempts have been made to take into account the existence of a large scale structure, in one form or another, have met with varying success. As discussed with regard to the modelling of the instabilities themselves, whether they are interpreted as waves or eddy structures is also reflected in the different methods used to determine the detailed velocity field for the purpose of the noise calculations.

Evidence to support the hypothesis that the dominant noise source in a forced jet derives from the transition of the instability wave from the growing to the decaying phase can be found in Moore [53]. Source location techniques used here indicated that whereas in the unforced jet the noise sources for different frequencies are distributed throughout the flow field, in the forced jet all the extra broadband noise comes from the same axial position, some three diameters or so downstream of the nozzle exit plane. Since the instability wave reaches its maximum amplitude at about the same axial position it must be considered to be a likely cause of the extra noise, either directly or through an increase in the background turbulence.

Ffowcs Williams & Kempton [29] calculated the sound radiated by a simulated instability wave; using a "source model" approach they extended Crow's model to take into account the fluctuating response of the instability wave to forcing with time. Their model assumes an element of randomness in the phase velocity of the wave at the nozzle exit, the randomness growing as the wave convects downstream, and it was shown that the spectrum of the radiated sound is broadband when the resulting phase distortion at the position of the maximum wave amplitude is large (a substantial fraction of 2π), but narrowband when this distortion is negligible. It was argued that the randomness in the phase should be large enough on both model jets and full scale engine exhausts to produce broadband noise. However, the model also predicted that the radiated noise at the Mach angle would always be narrowband whatever the value of the phase distortion

and the authors therefore believed the amplification of an internal tone, as found by Crow, to be an equally acceptable possibility at the Mach angle. In addition, the results of this analysis could be interpreted as indicating that forcing at a high frequency might be expected to reduce the radiated broadband noise, as found experimentally by Moore [52]. The sound field calculated in this way was thus shown to produce good qualitative agreement with a number of observations.

In 1973, Laufer, Kaplan & Chu [39] suggested that it is rather the vortex pairing mechanism which is primarily responsible for the noise generation in a subsonic jet. This alternative view was also considered in the paper by Ffowcs Williams & Kempton mentioned above. Again a source model was used and the spectrum of the radiated noise was in this case found to depend on the randomness in the pairing positions. The theory indicated that the radiated noise would be broadband when this variation was large in comparison with the eddy spacing which has indeed been found experimentally to be the case in the forced jet.

However, poor numerical agreement between theory and experiment has been obtained when noise calculations of this kind have taken the full flow field into account, as opposed to those which use a source model. Morfey's calculations [55], in which the vorticity distribution in the flow field is represented by discrete ring vortices, overestimate the noise field of a forced jet (St = 0.45, 0.66) by as much as 30 dB at 90° to the jet axis. Furthermore only small changes are predicted between the noise field of a jet subjected to 5% forcing

(perturbation velocity/mean velocity) at the nozzle exit plane and that of an unforced jet.

In 1975 Michalke & Fuchs [49] had suggested that representing the coherent structures using an axisymmetric ring vortex model was an oversimplification of the real situation in a round turbulent jet and that noise calculations based on this premise would indeed be inappropriate. They showed, by expanding the turbulent pressure fluctuations in terms of circumferential modes and calculating the respective source terms in the mean flow/turbulence interaction, that in the Strouhal number range $0.2 \leqslant St \leqslant 1.0$ the $m = 0$, 1 and 2 terms dominate the sound field of a low Mach number jet. Also the measurements of Morrison & McLaughlin [59] have shown that first order ($m = \pm 1$) modes are dominant in the near field of a high Mach number jet, natural or forced (using a point excitation technique), and moreover that the instability wave radiates to the far field.

There are a number of other reasons why the presence of higher order modes on a turbulent jet might be considered to be important. Michalke has shown in his 1971 paper [48] that on a linear theory the growth of an $m = 1$ mode on the initial region of the jet is comparable with that of the plane wave mode. Further, the $m = 1$ modes are the only modes which can grow on the far downstream profile of the fully developed jet. Also, at the frequencies of interest higher order modes do not generally propagate into the far field, but are cut off in the tailpipe. In this event it is therefore possible to have an excited jet in which the excitation signal is not detectable in the far field and recent experiments on a model jet (Bechert &

Pfizenmaier [6]) have shown that a broadband amplification comparable in level to that produced by plane wave excitation is also afforded by higher order mode excitation.

In comparison with the extensive theoretical and experimental studies of the axisymmetric large scale structures on a turbulent jet which have been carried out in recent years, relatively little work has been done in respect of the higher order modes. In view of the lack of empirical data, an experimental study of the structure of a turbulent jet subjected to forcing by higher order mode acoustic excitation has been carried out. A description of the model jet rig, the higher order mode generator and the flow visualisation and measuring techniques used is given in chapter 2. In the results section of the chapter, the effects of plane wave, first and second order mode excitations on the jet structure are described in relation to the structure of the unexcited jet in terms of the mean, instability wave and turbulent velocity fields.

In chapter 3, Crighton & Gaster's stability analysis of the axisymmetric structures on a slowly diverging circular jet [19] has been extended to include spiral modes of the first and second order. This theoretical study complements the experimental work and comparisons with the results presented in chapter 2, and also with some of the results of Chan [17], are shown in chapter 4. It is observed that a turbulent jet can support helical instabilities whose radial distributions and phase speeds are well modelled by linear stability theory. The instabilities grow and decay on the first few diameters of the jet in much the same way as plane wave disturbances and also have a marked influence on the development of the mean flow. In the

case of the first order "flapping" mode this effect is most pronounced and persists as far as twelve diameters downstream of the nozzle exit. A further result arising from the present study is that the "shape assumption" used in a number of stability calculations (e.g., Mankbadi & Liu [46], Chan [16] and Morris [57]) would seem to be a good approximation even when the forcing level is well into the range in which the instability wave responds in a non-linear manner.

The primary objective of jet noise research is ultimately to be able to predict the far field noise of an engine in flight. However, static to flight differences in noise levels are still far from understood. One particular aspect of this more far-reaching problem has been addressed in chapter 5 where the qualitative effects of an external flow on a forced jet are considered.

An informative study of forward flight effects was produced in 1975 by Bushell [14] in which experimental results covering a wide range of engine types were presented. From ground-based measurements of the sound field associated with a full scale jet engine in flight it was observed that the noise levels in the rearward arc are generally reduced whilst those in the forward arc are increased in comparison with the levels measured in static tests (similar results were also obtained by Brooks & Woodrow [10]). These results apply to jets at high subsonic velocities and in which the jet mixing noise would therefore have been expected to dominate over the tailpipe (core) noise.

On the other hand, aerodynamic noise theories based on Lighthill's

approach, e.g., Ffowcs Williams [27] and Ribner [62], predict that the level of the radiated noise should decrease at all angles to the jet axis as the flight velocity increases due to the reduced shear in the mixing layer. In particular, the overall sound pressure level of a turbulent jet in flight is determined to be proportional to the seventh power of the relative velocity (Vj - Va), where V_j is the jet exhaust velocity and Va is the forward flight velocity. The static to flight change predicted in the forward arc on this basis therefore has the opposite sign to that obtained experimentally. Further, in flight a reduction in the noise level at 90° to the jet axis is predicted theoretically, but the measurements generally show no change and sometimes even an increase in the noise level there.

Data from the "spinning rig" type of flight simulation facility (a flight simulation device used by Rolls Royce in which a model jet nozzle is mounted at the tip of a large rotating blade) in which the jet is moving relative to a stationary microphone, follow the same trend as the genuine flight data with the exception of some of the results obtained from the Bertin Aerotrain by Drevet, Duponchel & Jacques [26] which show a slight reduction in the noise level at 90° to the jet axis "in flight". The results obtained from flight simulation tests (wind tunnel tests) in which there is no relative motion between the jet nozzle and the microphone do at least show a reduction in the noise level at 90° to the axis "in flight", but the actual level "in flight" is proportional to a lower power of relative velocity than predicted. Indeed, static to flight differences do in general display a pronounced directional variation.

Possible explanations of the existing discrepancies have usually involved the consideration of additional noise sources on which the effects of forward flight are essentially different from those experienced by jet mixing noise. Sarohia & Massier [65] argued that the external boundary layer on the engine cowl shields the jet flow in flight and that this would indicate that at 90° to the jet axis, and in the forward arc, the far field noise scales with the absolute rather than the relative jet velocity. The scattering of sound by fins and tailplanes are amongst other installation effects which have been considered in the extensive experimental work which has been carried out at NGTE on the effects of flight (see Bryce's review [12]).

The effects of internal noise sources on the radiated noise from both hot and cold static jets (as discussed earlier) have also received much attention, e.g., Jubelin [36], Moore [52] and Bechert & Pfizenmaier [5]. However, doubt has been cast on the significance of internal noise sources in flight by the co-axial jet experiments of Moore & Brierley [54] and Jubelin [36]. Their results have indicated that jet noise amplification by internal sources is insignificant on a co-axial jet when the ratio of the secondary to the primary jet mean axial velocity is greater than about 0.5, irrespective of the "characteristic frequency" chosen and the results of a stability analysis on a circular jet in an infinite co-flowing stream presented here, in chapter 5, would seem to support these findings.

A satisfactory explanation of all of the effects of forward flight on jet engine exhaust noise has not yet been put forward and,

beyond that, accurate numerical prediction schemes must lie well into the future. Nevertheless, a far greater understanding of the general mechanisms at work has been achieved in recent years and future research programmes can now build on a more solid foundation. It is hoped that the present study of nonaxisymmetric large scale modes on a single stream jet, and of plane wave modes on a jet with external flow, will contribute to that foundation.

CHAPTER 2 EXPERIMENTAL STUDIES OF THE MEAN FLOW AND TURBULENCE STRUCTURE OF A JET FORCED BY HIGHER MODE EXCITATION

2.1 Introduction

In the introductory chapter we mentioned a few of the experimental techniques which have been used to study the large scale orderly structures found in a turbulent jet. In particular, we noted that a number of workers (e.g., Crow & Champagne [22], Moore [52], Jubelin [36]) had successfully carried out experiments in which they had forced the jet with controlled excitation at the preferred instability frequencies in order to raise the levels of the coherent motions above those of the background turbulence. We have also adopted this approach in a detailed study of the aerodynamic behaviour of higher order modes on a turbulent jet, which have received little attention in the past. First order modes have been shown to play an important rôle with regard to the radiated sound of a low Reynolds number (perfectly expanded) supersonic jet (Morrison & McLaughlin [59]) and Michalke & Fuchs [49] have indicated that the modes of order m = 0, 1 and 2 should dominate the noise produced by the mean flow - turbulence interaction of a subsonic jet.

We have chosen a forcing level at which the radiated broadband noise level is increased above that of the unforced jet since we believe the forced jet condition and the associated jet noise amplification to be highly relevant to the conditions in a full scale jet engine exhaust (see Deneuville & Jacques [25]). Mean, turbulence

and instability wave velocity measurements have been made, concentrating on the first four or so diameters of the jet, and these are complemented by flow visualisation results, in the same region, using ciné Schlieren photography.

2.2 Description of facility

The experimental results presented in this chapter were all obtained using the Rolls Royce Advanced Research Laboratory (A.R.L.) model jet rig as described in Moore [51]. The rig, shown in figure 1, consists of a 0.915 m. diameter plenum chamber which is supplied with air, from a 0.55 MPa works compressor, through a 100 mm. diameter pipe. The pipe is blanked inside the chamber and the air flow spreads into the plenum through a number of 12 mm. diameter holes in the side of the pipe. Blanking off the inlet pipe reduces the noise from the valves and this is further suppressed by a lining of acoustic absorbing material both on the inside of the plenum chamber and along a 2 m. section of the inlet pipe further upstream. The air accelerates into the nozzle through a bellmouth intake section and exhausts into the open atmosphere.

Previously, for the purpose of exciting the jet acoustically with a plane wave mode, a speaker system had been positioned inside the plenum chamber. However, because most of the higher order modes do not propagate inside the nozzle at the frequencies used, the forcing in the present experiments is applied very close to the nozzle exit. The acoustic excitation is thus provided by four

Vitavox S3 driver units arranged symmetrically around the nozzle and powered by two Quad 303 amplifiers. The driver units are fitted with inverse conical horns and each horn is connected to the nozzle by a short parallel tube, which is attached 1.270 cm. upstream of the nozzle exit plane.

A 0.635 cm. thick plug of 'Retimet', rounded off to the contours of the nozzle, was fixed at the end of the parallel section to give a smooth flow inside the nozzle. This material was found to decrease the sound pressure level by less than 0.5 dB.

The block diagram, figure 2, shows the system used to set up each mode. For this purpose, a Bruel and Kjaer 1/4 in. condenser microphone was positioned in the centre of the nozzle exit plane. A signal at the required frequency was fed to the reference speaker directly from the oscillator, i.e., without any change in the phase. The resulting microphone signal was filtered at the excitation frequency with a 3.16 Hz bandwidth phase locked filter and the phase (with reference to the excitation signal) and amplitude were used as references for the remaining speakers. Each of the other speakers was connected in turn and its phase shifter was adjusted to give the same amplitude and the appropriate phasing for the required mode, measured in the centre of the exit plane.

The output from the oscillator was set at 139 millivolts, which was the maximum drive level that could safely be fed to the speakers when they were fitted with inverse conical horns and were required to run continuously. The drive level used in each set of measurements will be given as an attenuation referred to this maximum level.

Plate 1 is a photograph of the top of the plenum chamber showing the speakers in position around the nozzle. The flexible pipe from each horn to the back of each speaker equalises the mean pressure across the diaphragm.

With this system of driver units a variety of modes of excitation can be generated and these are shown in figure 3. When all the speakers are in phase, then obviously a plane wave (m = 0) mode is produced. A phase lag of 90° between each successive speaker, moving in a clockwise sense, produces a first order mode spinning in the clockwise direction (m = +1), as in (a). The same phase changes in the opposite direction produce an anticlockwise spinning first order mode (m = -1).

A flapping first order mode is generated by the phase settings given in (b). This produces a standing circumferential wave of an elliptical shape.

The only second order mode obtainable with four speakers also has a standing wave pattern, the shape of which is shown in (c). In order to produce a second order mode spinning in one particular direction, at least one more speaker would be required to prevent any ambiguity.

Modal Analysis

A modal analysis was performed on the excited jet in order to determine, quantitatively, the efficiency of the loudspeaker system as a generator of higher order modes. The analysis system, figure 4, consisted of an array of six 1/4 in. Bruel and Kjaer condenser microphones positioned symmetrically around the nozzle and situated

0.317 cm. downstream of the nozzle exit plane in the near field of the jet. For each mode generated, the modal content of the near field, with and without flow, was evaluated in terms of the zeroth, first and second order modes.

The first and second order spinning mode components of the pressure distribution are given by

$$\frac{1}{6}\left\{\sum_{n=1}^{6} V_n \cos m\theta_n \pm i \sum_{n=1}^{6} V_n \sin m\theta_n\right\} \qquad (2.2.1)$$

where the positive sign is taken for the clockwise spinning modes and the negative sign for the anticlockwise modes, m being the mode order. V_n is the signal from the nth microphone, filtered at the excitation frequency with a 3.16 Hz bandwidth and θ_n is the "acoustic angle" of that microphone. In the case of a first order mode, the "acoustic angle" is simply the geometrical angle of the microphone measured from a reference microphone. For a second order mode it is twice that angle.

The level of the plane wave mode is given by

$$\frac{1}{6}\sum_{n=1}^{6} V_n \qquad (2.2.2)$$

and it can be seen from this and the preceding expression that, if aliasing is neglected, only the mode being measured will have contributed to these values.

The results, given in table 1, are for a nozzle exit Mach number of 0.5 and an excitation frequency of 2250 Hz, which corresponds to a

Strouhal number of 0.55. This frequency was chosen because it produces a large broadband noise increase when the jet is excited. The drive level was 0 dB.

The readings indicate that when the system was set up to produce the zeroth or the first order mode, the measured level of the required mode was at least 10 dB above the level of the unwanted modes, which therefore contained an insignificant amount of the energy being fed into the system. However, when the system was set up to generate the second order mode, a substantial amount of the plane wave mode was produced.

The results presented in table 1 are r.m.s. levels of the total filtered signals and in order to check the accuracy of these, a number of phase locked measurements were taken using a waveform averager. This check was performed on the measurements taken when the '±1' modes were being generated and the phase locked averages, shown in table 2, were obtained from 2^{14} samples.

2.3 Measuring Systems

Pitot Tube

Radial mean velocity profiles of the jet were obtained from a series of traverses with a pitot tube. A United Sensor tube was used, which had an outer diameter of 1.5 mm. and a hole diameter of 0.5 mm., and the pressure was read on a water manometer.

Since the pitot tube reads the mean total pressure in the flow, the mean axial velocity can be calculated from the steady flow form of Bernoulli's equation, as shown in Bradshaw [8] pp. 99-101, such

Table 1 Modal content of near field produced by prescribed mode of excitation.

Levels at nozzle exit

	Without Flow		With Flow	
'0' mode generated	Sum	Difference	Sum	Difference
0	133.3 dB	___	126.1 dB	___
1	101.6 dB	105.1 dB	102.3 dB	105.3 dB
2	97.6 dB	99.8 dB	99.1 dB	99.1 dB
'-1' mode generated				
0	87.6 dB	___	99.5 dB	___
1	81.6 dB	110.3 dB	98.7 dB	110.4 dB
2	80.6 dB	81.0 dB	92.3 dB	93.5 dB
'±1' modes generated				
0	85.0 dB	___	99.5 dB	___
1	106.0 dB	106.5 dB	105.6 dB	108.8 dB
2	79.3 dB	78.9 dB	96.8 dB	97.2 dB
'±2' modes generated				
0	95.8 dB	___	106.4 dB	___
1	< 76.3 dB (Background noise)	79.6 dB	92.0 dB	93.1 dB
2	93.9 dB	93.9 dB	103.5 dB	100.0 dB

——— denotes the mode generated and the terms "sum" and "difference" refer to the choice of sign made in (2.2.1) or (2.2.2), which determines whether the clockwise or anticlockwise mode was being measured.

Table 2 Comparison of the total and phase locked modal levels in the filtered near field pressure signal at the nozzle exit ('±1' modes generated)

Without flow

	Total		Phase locked	
	Sum	Difference	Sum	Difference
0	88.1 dB	___	87.9 dB	___
1	107.0 dB	107.5 dB	106.8 dB	107.2 dB
2	81.8 dB	80.6 dB	81.5 dB	80.6 dB

With flow

	Total		Phase locked	
	Sum	Difference	Sum	Difference
0	86.0 dB	___	87.5 dB	___
1	107.8 dB	108.3 dB	107.4 dB	108.0 dB
2	92.3 dB	90.8 dB	89.5 dB	86.2 dB

that

$$U = \sqrt{\frac{2g\ \rho_\omega\ h_\omega}{\rho_a}}$$

where g is the acceleration due to gravity, ρ_ω and ρ_a are the densities of water and air and h_ω is the height of the water read from the manometer. The value of ρ_a was determined from the equation of state

$$p_a = \rho_a R T_a$$

where the measured quantities are p_a, atmospheric pressure and T_a, the temperature in the plenum chamber.

A comparison of mean velocities calculated from pitot tube measurements and those obtained using hot wire and laser anemometry, presented in Moore [51], indicates that the steady flow assumption is a valid one in the case of the unexcited jet. This is also borne out to a good approximation in the present investigation (carried out at the same Mach number), as shown in section 2.5. However, there are certain discrepancies between the pitot tube and hot wire measurements obtained from the excited jet and these will be discussed in the results section.†

Hot Wire Anemometry

The turbulent velocity measurements were made using hot wire anemometry and, in particular, a DISA 55D constant temperature system. A crossed wire probe was used in order to provide sufficient

† Such discrepancies are to be expected, the pitot tube measurements can have significant errors due to the turbulence or the large scale fluctuations and it is not usually possible to correct the data.

information to calculate the axial and radial components of the fluctuating velocity as well as the mean axial velocity.

A single hot wire anemometer relies on the principle that the resistance of a wire is proportional to its temperature and also that the rate of cooling of the wire is proportional to the component of the flow velocity normal to the wire. The wire serves as one of the resistances in a Wheatstone bridge, as in the circuit diagram, figure 5, and its temperature is indirectly kept constant by keeping the bridge in balance, thus keeping its resistance constant. So the current fed to the bridge top from the amplifier serves the two-fold purpose of indicating the conditions for bridge balance and heating the wire. It is this feedback mechanism which facilitates the measurement of the high frequency fluctuations in the flow.

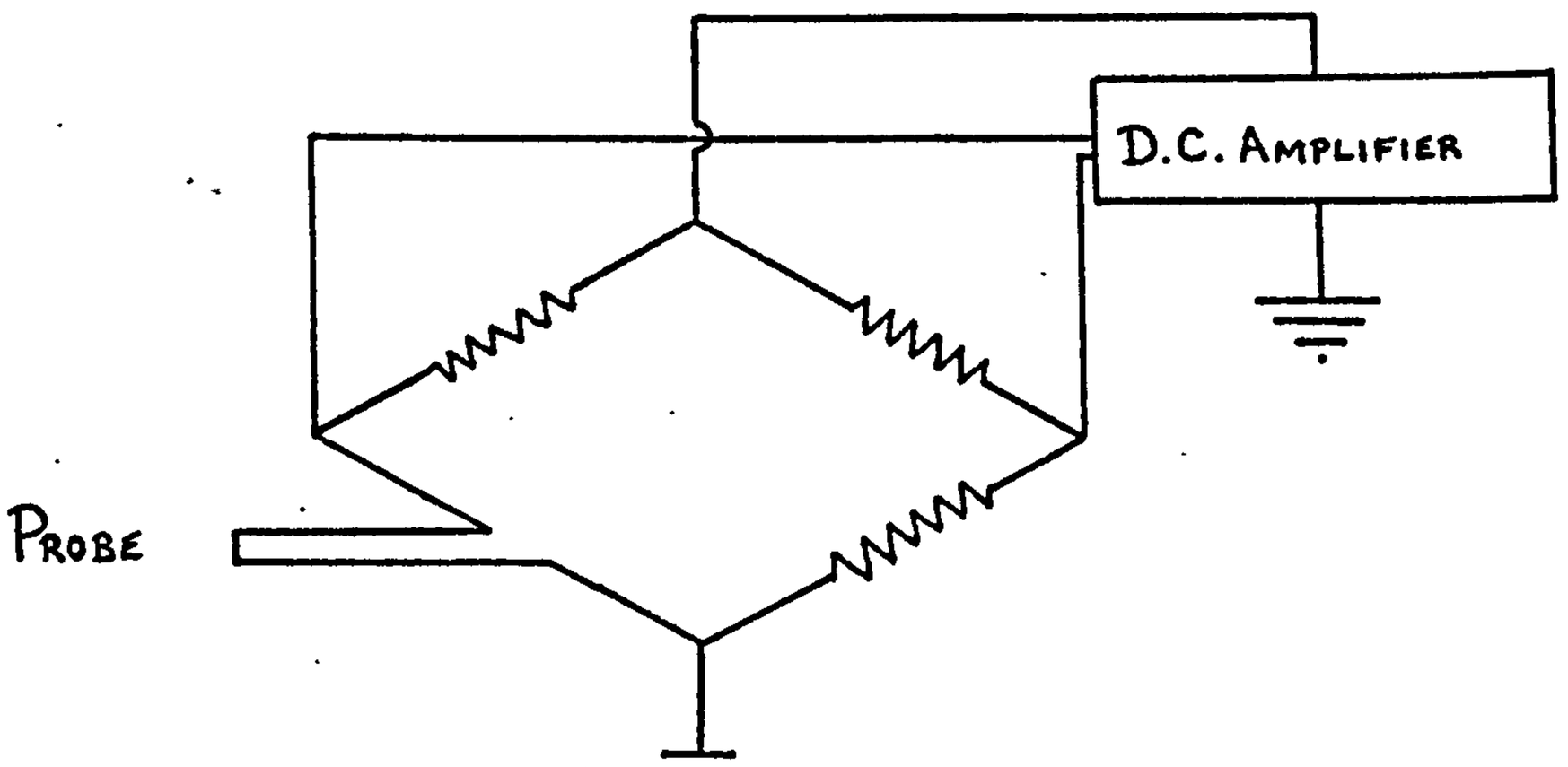

Figure 5. "Wheatstone bridge" circuit for hot wire probe

Since the output voltage of the constant temperature anemometer is a non-linear function of the flow velocity, the signal is passed through a linear iser with an offset zero.

Before making any measurements, both wires were calibrated against a pitot tube. The two probes were positioned as close as possible to each other, both well within the potential core region of the jet, at an axial distance of approximately one nozzle diameter downstream of the exit plane. A number of readings were taken at different velocities and the results were plotted out to determine the calibration factors, K_1 and K_2, in Volts/ms^{-1} (as defined in the Appendix). Calibrations were carried out at regular intervals throughout the experiments : an example of the calibration curves is shown in figure 6. To make the analysis system as simple as possible, the gain settings on the anemometers were adjusted to give the same calibration factor for each wire. Occasionally, however, these calibrations were found to drift more than expected and the analysis system had to be modified accordingly.

During the experiments the crossed wire probe was positioned such that the wires were inclined at 45° to the jet axis and the plane of the wires was coincident with the plane of each radial traverse in order to prevent any change in the effect of the azimuthal velocity on the wires in crossing the jet. The axial and radial velocities, as functions of the two wire signals, are then (see Appendix)

$$U_a = \frac{1}{2\sqrt{2}\,K_1\,K_2}\,[(K_2 + K_1)(V_1 + V_2) + (K_2 - K_1)(V_1 - V_2)]$$

and

$$U_r = \frac{1}{2\sqrt{2}\,K_1\,K_2}\,[(K_2 + K_1)(V_1 - V_2) + (K_2 - K_1)(V_1 + V_2)].$$

The sum and the difference of the two hot wire signals were recorded on magnetic tape at each position on the traverse. The sum was recorded both D.C. and A.C. coupled on channels 1 and 2, respectively, and the difference was recorded, D.C. coupled only, on channel 3. A.C. coupling filters out all frequencies below 4 or 5 Hz, that is, it is used to reject the steady part of the signal, whereas D.C. coupling admits the whole signal. In its simplest form, then, the recording system was arranged as shown in figure 7 (a). The voltage gain effected by each piece of equipment is shown for future reference (in the description of the analysis system). All the channels on each new tape were calibrated by recording signals of 0 volts and 1 volt and then adjusting the gains and zero settings of the replay amplifiers to reproduce the same levels during the analysis.

The recorded signals were analysed using a Hewlett-Packard 5420 twin channel digital signal analyser. To make the best compromise between economy and accuracy, the analyser was set to take fifty 10 millisecond samples, restricting the frequency range to 0 - 25.6 KHz and the resolution to a 300 Hz bandwidth. This produces a BT product† of 150, which means (as shown in Bendat and Piersol [7]) that the error involved in the estimate of the signal amplitude, using this system, is less than 5%. A 30 second recording was required at each position on the traverse in order to allow the analyser enough time to process each sample as it was obtained.

When the calibration factors of the two wires did not alter during a traverse, the analysis was straightforward, so we shall consider the more general case when K_1 or K_2 drifted and the

† Bandwidth-time product

correction terms, proportional to $(K_2 - K_1)$, had to be taken into account. These corrections were performed electrically using an operational amplifier , figure 7 (b). The diagram indicates how the signals from channels 2 and 3 were modified before being fed to the two analyser inputs. We restrict ourselves to a description of the processing required to obtain the fluctuating axial velocity.

To bring both channels to the same relative gain, the gain of the correcting channel, $(V_1 - V_2)$, was multiplied by the ratio of the two gains, G_2/G_3. The difference in the calibration factors, K_1 and K_2, was also rectified, at the same stage, by multiplying the correcting channel signal by the factor $(K_2 - K_1)/(K_2 + K_1)$, and the two channels were then added to give

$$0.98\ G_2(V_1 + V_2) + 0.98G_2\ \frac{(K_2 - K_1)}{(K_2 + K_1)}\ (V_1 - V_2)$$

The analyser could then be given the single gain of

$$\frac{1}{0.98G_2}\ \frac{(K_2 + K_1)}{2\sqrt{2}\ K_1\ K_2}$$

to produce the required velocity. The fluctuating radial velocity was obtained in a similar manner, as was the mean axial velocity.

The overall levels of the fluctuating axial and radial velocities, and also the levels of the components at the excitation frequency, were read from the analyser's display, and hard copies of the two spectra produced were then obtained on a Hewlett-Packard 9872 digital plotter for further analysis. The value of the mean axial velocity was simply the level of the frequency component at 0 Hz on the spectrum resulting

from the relevant combination of channels 1 and 3.

Any extraneous frequency components introduced by the analysis system, and in particular, the tape recorder, would show up in the spectra of the 0 volts and 1 volt calibration signals. The spectra of these signals from channels 1 and 3 of one of the tapes are shown in figure 8 (a) and (b). The scale of the abcissae in these and in all subsequent spectra is such that 0 dB corresponds to 1 m/s. A number of frequencies are seen to dominate the spectra when there is no externally applied A.C. signal present. However, the contributions from these frequencies are negligible when compared with the 1 volt signal, shown here, as they are in comparison with the hot wire signals, of which a number of spectra are included later on in this chapter.

Pressure Measurements

In addition to the velocity measurements, a number of pressure level readings were taken in the jet. A 1/4 inch Bruel and Kjaer condenser microphone, fitted with a nose cone, was used for this purpose and both phase and amplitude results were obtained by a signal eduction technique. The circuit diagram, figure 9 (a), shows how the filtered microphone signal was sampled.

To start each sample, a pulse was derived from the BFO output and fed to the trigger input on the correlator. When a sufficient number of samples had been taken, the educed signal was displayed digitally on an oscilloscope screen as a 512 point waveform. Figure 9 (b) shows this averaged signal together with the triggering signal and pulse. It is important that the pulse generator is not set to produce a pulse

at a zero crossing of the triggering signal. If, for instance, a pulse was generated at each zero crossing with positive gradient, it is possible that the noise accompanying the triggering signal could produce just this triggering condition immediately after a zero crossing with negative gradient.

The phase is worked out by noting the numbers of the points nearest to the first and second zero crossings with positive gradient, N_1 and N_2, respectively. To this end, the time window was chosen so that the 512 points encompassed a little over two cycles of the required signal. Denoting the triggering delay by ϕ_d, the phase then becomes

$$\phi = 360 - \left[\frac{360\ N_1}{(N_2 - N_1)} + \phi_d\right] .$$

2.4. Flow Visualisation

During the course of the aerodynamic measurements, a series of ciné Schlieren films of the excited jet were taken. It is useful to discuss these results at this stage in order to illustrate the structural behaviour of the jet, the quantitative measurements of which will be presented in section 2.5.

The first five or six diameters of the turbulent circular jet have a central cone, the potential core, where the mean axial velocity is constant and approximately equal to that in the nozzle exit plane, figure 10(a). An annular mixing region surrounds the core and it is this area of the jet where the use of Schlieren photography is most beneficial. The turbulent mixing process

between the jet and the ambient air gives rise to large density gradients which appear as light areas on the film sequences, shown in plates 2 to 8, where a dark background has been used. Regions of constant, but different, densities cannot be distinguished: only a spatial density change produces a contrast. In the case of still photography, the orderly structure can be reinforced by the use of a triggering system.

The optical system used was that described in Moore [51] and figure 10(b) shows a plan view of the apparatus. A parallel beam of light, derived from a mercury arc lamp source, illuminates the flow region and the image of the jet is focussed on the film at the back of a high speed ciné camera. An optical stop prevents the light which arrives directly from the source from swamping the image.

The films were taken at a Mach number of 0.3 and in order to enhance the image, the jet was heated to a temperature of 75°C, which increases the density gradients in the mixing region. The excitation frequency was 1380 Hz and the drive level 0 dB for all modes. A convenient frame speed of 14,000 frames/second was sufficiently large to avoid aliasing.

Films were taken of the jet under excitation by every mode described in 2.2 : two films were taken for each standing wave mode, viewing the wider and narrower cross-sections in turn. Plates 2 to 8 show 52 successive frames from each film. When the plate is viewed lengthways, the first frame is in the top left-hand corner and the sequence runs from left to right. At the bottom of each frame there is a record of the excitation signal fed to the reference

speaker. There are therefore just over 5 cycles on each plate or 3.7 milliseconds of elapsed time.

The excitation signal was turned on for 15 milliseconds in every 30 milliseconds and the first frame on each plate roughly corresponds to the start of a period of excitation. The effect is almost instantaneous as, in each case, a disturbance starts to propagate downstream and a large scale columnar structure quickly envelopes the whole jet.

Moore [52] describes how, in the case of plane wave excitation, at the onset of the shear layer instability a small wave-like perturbation develops on the initial region of the jet and, entraining the surrounding ambient air, grows to such an extent that it breaks up into a series of individual vortex rings. The growth continues as the rings travel downstream and often two adjacent vortices merge into a single large vortex. This pairing process can be detected, in the case of the plane wave excitation (plate 2), in the present work. (The phenomenon is shown more clearly on the moving film.) No similar mechanism appears to take place under the higher order mode excitation.

The spiral nature of the first order modes may be clearly seen in plates 3, 4, 5 and 6.

2.5. Results and Discussion

The Unexcited Jet

Since no aerodynamic measurements of the flow produced by the particular nozzle described in 2.2 have previously been made, we

begin this section by presenting some mean and r.m.s. turbulence velocity profiles to establish the basic structure of the unexcited jet. These profiles will also be used later, superposed on those of the forced jet, in order to illustrate the changes in aerodynamic behaviour brought about by the different modes of excitation.

The mean velocity profiles shown in figure 11 were obtained from a series of radial traverses made with the United Sensor pitot tube. On this graph, as in all subsequent axial and radial profiles, the velocities are normalised with respect to the mean axial velocity on the centre line of the jet at one diameter downstream of the nozzle exit plane, and the distances are normalised on the nozzle diameter. The curves shown correspond to axial positions of 1, 2, 4, 6, 8 and 12 diameters downstream of the nozzle exit, and they are staggered in such a way as to give some indication of the spatial structure of the flow. The readings were taken at a nozzle exit Mach number of 0.3.

Mean velocity measurements, made at the same Mach number, using the hot wire anemometry system are in good agreement with the pitot tube results. These results, at axial distances of 1, 2 and 4 diameters, are shown in figure 12, and the mean line through the pitot tube readings has been redrawn for comparison. The greater sensitivity of the anemometry system provided a more accurate representation of the shape of the profile at the outside edge of the shear layer, where the small changes from atmospheric pressure could not be detected on the manometer.

The unexcited jet displays the familiar "top hat" profile close to the nozzle exit, and the potential core region, shown more clearly in figure 13, ends at an axial distance of about five diameters.

Further downstream, the mean velocity gradually decreases and the more stable bell-shaped profile is already well established at a distance of twelve diameters.

The variations of the axial and radial turbulence velocity profiles with axial distance are shown in figures 14 and 15 (the r.m.s. axial and radial turbulence velocity components are denoted here and in subsequent figures in this chapter by u'_x and u'_r, respectively). Whilst the axial component is dominant in the centre of the shear layer it is noticeable, particularly at x = 1D, that it is the radial component which is the larger of the two in the potential core region. There are no published results known to the author with which the radial velocity component can be compared but the axial velocity component at x = 1D is in good agreement with the results of Moore [52] at the same nozzle exit Mach number. It must be noted, however, that the relative error in the radial component which would result from a small drift in the calibrations of the wires would be much larger than the relative error in the axial component.

Between x = 1D and x = 2D the only change in the profiles is a general widening of the shear layer which both reduces the width of the potential core and increases the overall width of the jet. There appears to be little change in the intensities on the lip line, but, as mentioned later, the true peaks may not have been resolved, so few measurements having been taken in respect of the steep gradient. At x = 4D, the radial component on the lip line has increased somewhat, the mixing region here covers almost the whole jet and the centre line turbulence has increased accordingly.

Figures 16, 17 and 18 are spectra of the fluctuating axial and radial velocity components at an axial distance of one diameter and at three different radial positions. The two spectra in figure 16 were taken on the axis of the jet and those in figure 17, in the centre of the shear layer. Figure 18 shows the two spectra at a position in the near field of the jet: these are dominated by the low frequency components, because only infrequently do the vortices grow sufficiently large to widen the jet enough to affect the probe at such a large radial distance. It should further be pointed out that the broad peak at 9KHz is inherent in the recording system (see figure 8 (a)).

The corresponding turbulence spectra at axial distances of two and four diameters are very similar: in particular, they also display a smooth broadband velocity distribution both on the axis of the jet and in the centre of the shear layer, and are free of any large amplitude discrete frequency components.

The Excited Jet

We next discuss the influence of the plane acoustic wave, and subsequently that of the higher order modes of acoustic excitation, on each of the basic flow quantities in turn.

We shall first look at the growth of the instability wave and consider the radial profiles of the axial and radial velocity components filtered at the excitation frequency. We then turn to quantities which can be compared with those already presented for the unexcited jet, showing the corresponding mean axial velocity profiles and the profiles of the turbulent axial and radial

velocities. All of these velocity measurements were taken at a nozzle exit Mach number of 0.3 and the excitation frequency was 1380 Hz. The drive level was 0 dB, which is a high excitation level and produces a non-linear response in the shear layer.

Finally, we present a number of filtered pressure level measurements taken in the flow region when the jet was excited by a first order (m = -1) mode. Readings were made with and without flow and two drive levels, - 20 dB and 0 dB, were used, which produce linear and non-linear responses, respectively.

The Growth of the Instability Wave

Measurements obtained using the anemometry system were made at axial distances of 1, 2 and 4 diameters. As mentioned in section 2.3, the filtered components were read from the spectra shown on the signal analyser's display. This method yields a fairly accurate result when the signal at the excitation frequency is strong enough to stand well above the background turbulence level, which it usually is at x = 1D and 2D. However, because of the high broadband turbulence level at the end of the potential core region, it is not possible to accurately estimate the excitation frequency signal level there in this way. Further narrowband analysis is therefore needed to extract the required instability wave components of the velocity fluctuations at the furthest downstream position above, and only those profiles obtained at the first two axial positions will be discussed in any detail here, though results at x = 4D are also shown.

Figures 19 and 20 are plots of the filtered axial and radial velocities ($\tilde{u}_x$ and $\tilde{u}_r$) produced by plane wave excitation at a Strouhal

number of 0.544 and a drive level of 0 dB. At each axial position, the two velocity components show similar behaviour at the edge of the jet, and although the radial component is very close to zero on the axis, as would be expected for a symmetric disturbance, they both display approximately the same peak value in the centre of the shear layer. Also, there is little amplification between one and two diameters, the centre line axial component increasing by a factor of only 1.3.

In the case of a first order mode (m = +1, figures 21 and 22), it is the axial velocity component which is almost zero on the axis. Again, as with the plane wave mode, the two profiles are very similar at x = 1D. However, between x = 1D and x = 2D, the peak radial velocity has moved well inside the lip line and this is accompanied by a substantial decrease in the peak value of the axial component. The axial velocity component also exhibits at least one secondary peak just inside the lip line (a secondary peak inside the lip line at x = 2D was also found by Lee [41] in his forcing experiments). Nevertheless, both components still undergo a small amplification at positions away from the centre of the shear layer, the centre line value of the filtered radial component increasing by a factor of 2.

The filtered axial velocity is again zero on the centre line when the jet is excited by the first order flapping mode (m = ±1), and a secondary peak is here evident at both axial positions, figures 23 and 24 (the profiles shown here were measured across the widest cross-section of the jet). These velocities attain by far the largest downstream amplification of all those induced by the available modes of excitation. Another point of note, peculiar to

this mode, is that the radial component is constant across the width of the potential core region.

The maximum and minimum cross-section velocity profiles for the second order "standing wave" mode are shown in figures (25,26) and (27,28), respectively. At x = 1D, larger fluctuations are found on the wider profile, across the whole jet diameter, and in the centre of the shear layer, in particular. A small axial growth is observed in all of the fluctuations, with the exception of the peak values. Secondary peaks are again present at x = 2D, notably on the filtered radial velocity profile obtained from the traverse of the wider cross-section of the jet, and also for which the main peak is found inside the lip line, as in the case of the m = +1 mode.

With the exception of the peak values on the radial profiles, there is a small amplification of the instability wave between one and two diameters downstream for every mode considered. (It must, however, be pointed out that in the regions of the peak values, there are very steep gradients in the radial direction and the true peaks have probably not been resolved.) Furthermore, at radial positions between the centre line and the lip line of the jet, where accurate measurements have been obtained at x = 4D, it appears that the maximum gains in the filtered axial and radial velocities are reached at axial positions which are certainly no further than four diameters downstream, for every mode.

Turbulence and Mean Velocity Profiles

The r.m.s. turbulence levels presented in figures 29 to 38 all exclude the contribution from the excitation signal. Similar

profiles are produced by all the different modes of excitation, and without examining the curves in fine detail it is difficult to differentiate between them. The levels in the excited jet, where measured (i.e., at x = 1, 2 and 4 diameters), were found to be at least as high as the corresponding levels in the unexcited jet at almost every position. The only exceptions, at any given axial position, are the peak values, about which it is not possible to draw any conclusions, on account of the poor resolution, as already discussed in the context of the instability wave results.

There is an apparent asymmetry, in the shear layer at x = 1D, in the radial velocity profiles for the m = +1, ±1 and ±2 modes. This does not manifest itself in the corresponding instability wave profiles, nor is it evident in any of the profiles taken at stations further downstream, and it does not appear in the case of the plane wave mode. However, the larger signal always occurs towards the end of the traverse, on the side of the jet where the whole length of the horizontal section of the crossed wire support is subjected to the force of the whole jet. It is therefore possible that this increase in the signal level is due to a low frequency vibration of the probe support system, but the processing technique also has many sources of error which could account for this discrepancy.

Comparisons of the spectra obtained on opposite sides of the jet are shown in figures 39 and 40. These particular spectra are taken from the first order standing wave mode results, but similar changes are observed in the radial velocity spectra of the other two modes.

In the potential core, at x = 1D and x = 2D, the turbulence level in the excited jet never exceeds that in the unexcited, but in

the shear layer (away from the central peak) the broadband turbulence is always larger when the excitation is present. It is of interest to note that on the radial velocity profiles produced by the second order standing wave mode, across the widest section of the jet, figure 36, and the m = +1 spinning mode excitation, figure 32, at x = 2D, the instability wave peaks nearer to the jet axis than does the turbulence. Furthermore, the turbulence peaks are situated very close to the radial positions at which the instability waves exhibit secondary peaks. Otherwise, the peaks of the gross turbulent fluctuations are coincident with those of the instability wave and, moreover, the radial distributions are qualitatively the same as for the unexcited jet.

The mean velocity profiles are shown in figures 41 to 46. Those calculated from pitot tube readings were taken at x = 1, 2, 4, 6, 8 and 12 diameters downstream of the nozzle exit. Hot wire measurements are also shown corresponding to the axial positions x = 1, 2 and 4D. The hot wire and pitot results agree fairly well at x = 1D and x = 2D with the surprising exception of the m = 0 mode results at x = 2D, figure 41. In the shear layer ($r \gtrsim D/2$) the velocities indicated by the pitot tube results are found to be much <u>higher</u> than those calculated from the hot wire data in this mode. It is not understood why a discrepancy of this magnitude should have occurred, but there is good evidence to suggest that it was not due to a fault in one of the measuring systems involved. The pitot tube results were found to be repeatable and the hot wire results must be considered to be reliable since the measurements in the m = 0 mode were obtained during the same radial traverse as those

for the unexcited jet (recordings being made with the excitation signal switched both on and off at each radial position) and in the case of the unexcited jet, excellent agreement was found between the hot wire and pitot tube results, as shown in figure 12.

It might be expected that when aligned parallel to the jet axis in a flow with a substantial mean swirl, the pitot tube would indicate a value for the mean axial velocity which was lower than that given by hot wire measurements. Although discrepancies of this nature do appear at x = 4D in the m = 1 mode (figure 42(b)), similar results are obtained at this axial position in the m = ±2 mode (figure 46(b)), too. At this axial position it was necessary to perform two radial traverses for each mode considered, because of the limited movement (10 cm.) of the traversing equipment, both traverses taking in half of the radial extent of the jet, starting on the centre line and moving outwards (in opposite directions). The most likely explanation of the above discrepancies would appear to be a drift in the calibrations of the wires during each traverse, the difference between the hot wire results and the pitot results increasing with radius on each side of the jet. The plane wave results at x = 2D, however, remain unexplained.†

The only observable change in the radial profile at x = 1D between the unexcited and the excited jets, irrespective of the mode of excitation, is a slight increase in the width of the jet. Further downstream, the essential effects of forcing become more prominent. There is again, as at x = 1D, an increase in the width of the jet: the shear layer thickens, increasing entrainment and although the overall diameter of the jet is larger than that of the unexcited jet,

† This statement must not be taken too literally (see footnote, p. 30).

the width of the potential core is actually reduced. In addition, at x = 2D and beyond, the mean velocity on the centre line is below the value for the unexcited jet, so that the length of the potential core is reduced. A comparison between the axial variation of the centre-line mean velocity for the excited and unexcited jets is shown in figure 47.

Quantitatively, the plane wave mode, figure 41, and the first order spinning mode, figure 42, produce similar effects. The effects are more exaggerated when we consider the maximum and minimum cross-sections of the jet produced by the standing wave modes. The first order "flapping" mode causes by far the largest deviation from the unexcited jet profiles, and it is perhaps significant that this deviation persists at least as far as x = 12D, the farthest downstream position at which measurements were taken. Indeed, at such a distance from the nozzle exit, the profile of the unexcited jet would be referred to as "fully-developed", but this is hardly a fitting description for the profile shown in figure 43.

This distortion is shown to greater effect in a contour plot, figure 48. At each axial station considered, a contour describes the radial positions, in the plane normal to the jet axis, at which the mean velocity has fallen to a value of 20% U_o. The curves have been drawn using very few data points and are by no means intended to be an accurate representation of the true shapes. However, they do serve as an additional illustration of the sizeable deformation in the mean flow profile afforded by such a low energy input as an acoustic wave.

The changes in the width of the jet effected by the second

order standing wave mode, figures 45 and 46, are less persistent. A notable feature here is the curious "arrowhead" profile which is seen at x = 4D and x = 6D on the maximum cross-section, in figure 45. Again, some indication of the change in the "shape" of the jet with axial distance is given by the contours, plotted in figure 49. In contrast to the flapping mode (figure 48), the distortion is less evident at the further downstream positions of x = 8D and x = 12D, the "square jet" profile having developed into an axisymmetric one.

Generation of Higher Harmonics

A number of spectra of the fluctuating velocity, figures 50 to 57, are now presented in order to illustrate the general effects of the non-linear forcing. Figures 50 to 55 are all taken from a radial traverse performed at an axial distance of one diameter and the mode of excitation is the plane wave. (The turbulence spectra of the unexcited jet are also shown for comparison.)

In the centre of the jet, figure 50, the axial velocity spectrum is dominated by the fundamental, the radial velocity at the excitation frequency is suitably low and the broadband turbulence level is also low. Moving radially outwards through the potential core, the turbulence level gradually increases, the level of the fundamental increases and, at a radial distance r = 0.193D, the second harmonic is seen well above the background turbulence on both graphs, but only at a very low level relative to the fundamental (figure 51).

A third harmonic, again common to both velocity components, is evident at r = 0.322D, figure 52, a position just outside the

potential core, (see figure 41), and in the plane perpendicular to the jet axis all three harmonics and the turbulence level attain their peak values very close to the centre of the shear layer (figure 53, r = 0.515D). A little way outside the lip line, the levels of the higher harmonics on the axial velocity spectrum are reduced and they are of comparable level with the broadband turbulence, figure 54. In contrast, the harmonics of the fundamental radial component are more persistent there, but both spectra display as many as five harmonics when the broadband turbulence level is low enough, a little further out (figure 55, r = 0.837D). This increasing number of harmonics with radius, however, may be due to the decreasing mark/space ratio of the signal.†

We have seen, though, that as near to the nozzle exit as x = 1D, the instability wave is of sufficiently large amplitude to be able to generate a second harmonic of sizeable proportions. This was also found to be the case with all the higher order modes of excitation, restricting the downstream growth of the fundamental. Indeed, excitation by the second order standing wave mode results in the level of the second harmonic, in both velocity fluctuations, at x = 1D, actually exceeding that of the fundamental at a number of radial positions on the narrower cross-section (see figures 56 and 57).

However, it must be appreciated that at the high forcing level used in the present experiments, the loudspeakers would be producing a certain amount of harmonic distortion. Consequently, the levels presented in figures 50 to 57 do not constitute a quantitative measure of the harmonics generated purely by the non-linear interaction

† The large number of harmonics observed at this outermost radial station could equally well be a feature of the hot wire behaviour in the presence of such a low mean flow, and possibly flow reversal.

of the fundamental with itself in the fluid. Some contribution from the amplification of existing exciter products is also expected to be present here.

Pressure Measurements

Further information on the internal behaviour of the jet, when subjected to excitation in the form of the m = -1 mode, was obtained by measuring the axial and radial variation of the static pressure fluctuation. The signals were filtered at the frequency of excitation using a phase locked 3.16 Hz bandwidth bandpass filter so that the development of the instability wave could be followed. The measurements were taken at a Mach number of 0.5, the excitation frequency was 2250 Hz and so the Strouhal number, 0.555, was close to that at which the crossed wire and pitot tube readings were made (0.544).

At each drive level, - 20 dB and 0 dB, axial traverses were made both inside and outside the nozzle using a $^1/_4$ inch diameter microphone. Inside the nozzle, the microphone was located at the radial position r = D/4, and outside the nozzle, the traverse was performed along the lip line, r = D/2. In both cases the microphone was situated equidistant from the nozzle connections of two adjacent loudspeaker horns. The results from these axial traverses, with and without flow, are presented in figures 58 to 62. Both the amplitude of the pressure signal and the phase angle, referred to the excitation signal, are shown in consecutive figures for each drive level. The axial position of the horn connection to the nozzle is indicated on each horizontal axis.

Standing waves are formed inside the nozzle, withor without flow, due to interference of the signal with its reflection from the nozzle exit. Outside the nozzle, without flow, the signal decays in accordance with spherical spreading over most of the traverse ($1D \lesssim x \lesssim 5D$) at the higher drive level, which is perhaps rather unexpected so close to the nozzle. Between six and eight diameters downstream, under the same conditions, reflections from the probe support affect the measured signal which no longer follows such a simple decay law. This also occurs at the lower drive level, closer to the nozzle, between three and four diameters downstream. A further complication arises from the fact that the extent of travel of the traversing system is only 2.5 diameters, so that the reflections change dramatically where the probe support is moved, at $x = 2.55D$ and $x = 5.10D$, as can be seen in figure 60. Without flow, both the sound pressure level and the phase angle are affected significantly in moving the support between one position and another, particularly at the low drive level.

With flow, the pressure signal outside the nozzle grows to a maximum in the axial direction, and then decays further downstream. The peak level is reached closer to the nozzle at the higher drive level, and the decay is more rapid, indicative of a non-linear response. At a drive level of - 20 dB, the maximum pressure fluctuation occurs between $x = 2.5D$ and $x = 3D$. It is also noticeable, from the amplitude results, figure 60, that at this level the onset of the growth region in the potential core is downstream of that in the centre of the shear layer. A similar behaviour was found by Chan [15] in the case of plane wave excitation. He determined that

the disturbance spreads from the shear layer into the core of the jet in a certain direction and that the spreading angle, with respect to the shear layer, decreases as the Strouhal number increases.

Measurements of the phase angle in the excited jet, figures 59 and 61, clearly define a region downstream of the nozzle exit where the instability wave is dominant. The slope gradually decreases downstream to the end of the potential core. Beyond this distance, the slope increases (i.e., the phase speed, figure 62, decreases) in the linear regime, but maintains a fairly constant value when the response is non-linear. Upstream of the horn connection, the phase angle starts to decrease at a constant rate as the sound wave propagates in the opposite direction.. The velocity calculated from the slope in this region is around 135 m/s, which is in agreement with theory, i.e., the speed of propagation should be approximately $a(1 - M)$, where a is the sound speed at $10^{\circ}C$ and M is the Mach number of the flow.

Figures 63 and 64 show the variation of pressure amplitude and phase angle with radial distance at $x = 2D$ and at a drive level of 0 dB, with and without flow. Since all the higher order modes are cut off inside the nozzle, the signal measured without flow is a consequence of plane wave propagation alone. The phase angle is therefore constant across any diameter and the signal also maintains approximately the same level in traversing the jet.

With flow, the spiral nature of the instability is clearly evident. The amplitude falls sharply as the centre line is approached and there is a phase change of approximately 180° as the centre line is crossed.

2.6 Conclusions

The results have shown that higher order mode excitation produces structural changes in the jet similar in many ways to those produced by a plane wave excitation though there are distinct differences also. Certainly the zeroth and first order modes exhibit comparable axial growth rates, although the downstream amplification of the second order mode does not appear to be uniformly as large. The radial instability wave structures are much as expected but display secondary peaks at x = 2D, most noticeably just inside the lip line (r = R) in the axial velocity measurements taken in the m = +1 and m = ±1 modes. In the case of the m = 0 mode it seems plausible that the two peaks in the axial velocity distribution mark the inner and outer edges of an axi-symmetric ring vortex, assuming there to be little change in axial or radial position between successive vortices. A similar argument is clearly possible for helical vortices, too.

There are noticeable increases in the turbulence levels in the shear layer of the excited jet for all circumferential modes, particularly at the x = 4D station where the shear layer envelops almost the whole jet. The highest turbulence levels at x = 2D and x = 4D are produced in the second order mode across the narrowest radial profile, and seemingly at the expense of the instability wave growth. The effect of excitation, in any mode, on the mean flow is to widen the shear layer and shorten the potential core. The m = ±1 and m = ±2 modes, which generate standing circumferential wave patterns, produce asymmetric mean velocity profiles and in the

case of the former the asymmetry is still strongly evident at $x = 12D$.

Low level acoustic disturbances in the flow just upstream of the nozzle exit are here seen to produce substantial changes in the structure of a turbulent jet regardless of whether the wave is above or below the cut-off frequency for the nozzle.

Appendix : Calculation of axial and radial velocities from the crossed wire signals.

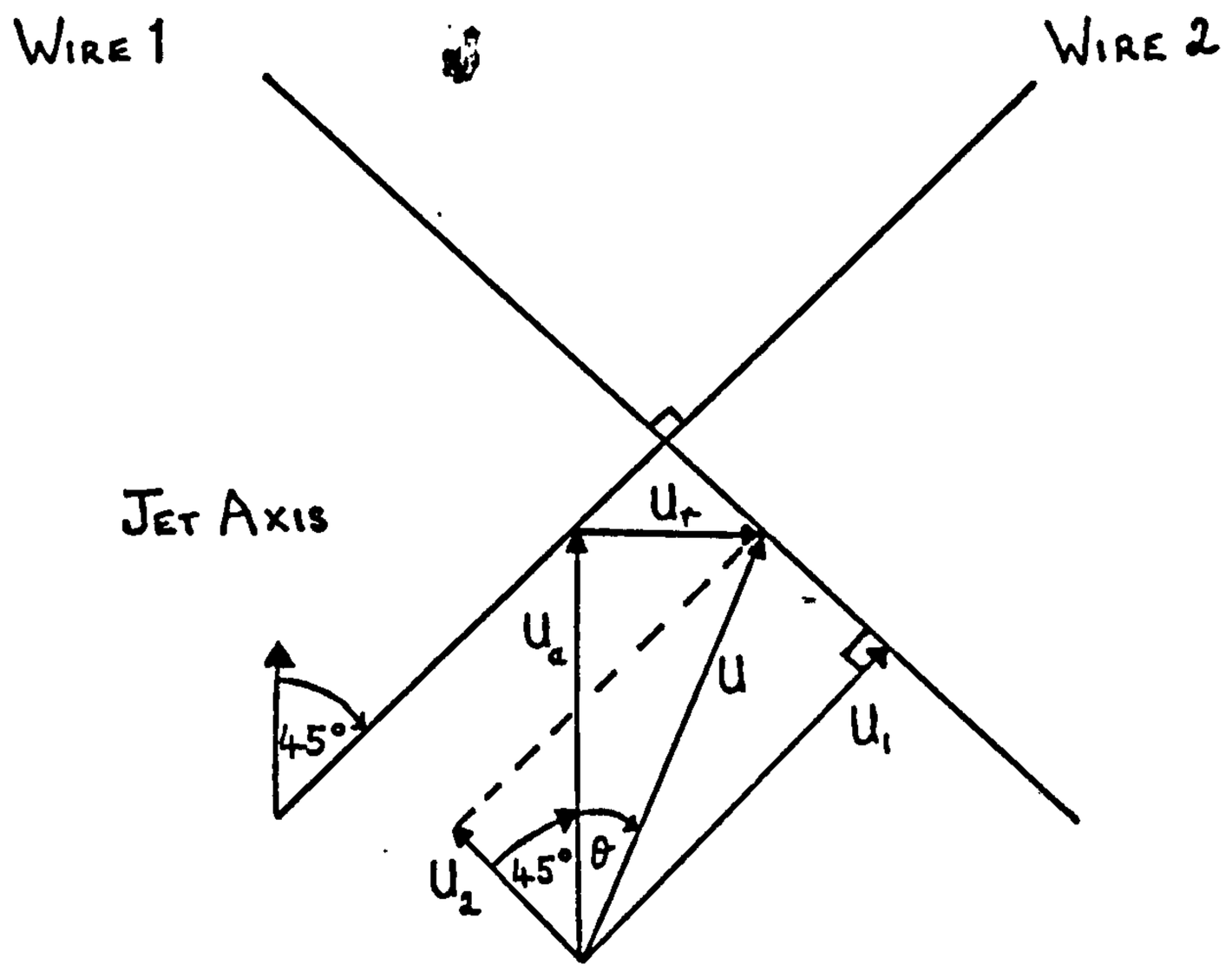

When the flow velocity is U, the required axial and radial components are $U_a = U \cos\theta$ and $U_r = U \sin\theta$. The signals from the wires V_1 and V_2, however, are proportional to the components of U normal to the wires, U_1 and U_2 respectively, where

$$U_1 = U \cos (45^\circ - \theta)$$

and

$$U_2 = U \cos (45^\circ + \theta),$$

so that

$$V_1 = K_1 U \cos(45^\circ - \theta)$$

and $$V_2 = K_2 U \cos(45^\circ + \theta) .$$

Rewriting these as

$$V_1 = \frac{K_1 U}{\sqrt{2}} (\cos\theta + \sin\theta)$$

and $$V_2 = \frac{K_2 U}{\sqrt{2}} (\cos\theta - \sin\theta)$$

we have

$$K_2 V_1 + K_1 V_2 = \sqrt{2} K_1 K_2 U \cos\theta$$

$$= \underline{\sqrt{2} K_1 K_2 U_a}$$

and similarly

$$K_2 V_1 - K_1 V_2 = \underline{\sqrt{2} K_1 K_2 U_r} .$$

Using the identities

$$2(K_2 V_1 + K_1 V_2) = (K_2 + K_1)(V_1 + V_2) + (K_2 - K_1)(V_1 - V_2)$$

and $$2(K_2 V_1 - K_1 V_2) = (K_2 + K_1)(V_1 - V_2) + (K_2 - K_1)(V_1 + V_2)$$

the axial and radial velocities are obtained in terms of the sum and difference of the signals from the two wires,

$$U_a = \frac{1}{2\sqrt{2}\, K_1\, K_2} \left[(K_2 + K_1)\,(V_1 + V_2) + (K_2 - K_1)\,(V_1 - V_2)\right]$$

and

$$U_r = \frac{1}{2\sqrt{2}\, K_1\, K_2} \left[(K_2 + K_1)\,(V_1 - V_2) + (K_2 - K_1)\,(V_1 + V_2)\right].$$

FIGURE 1 : SKETCH OF MODEL JET RIG.

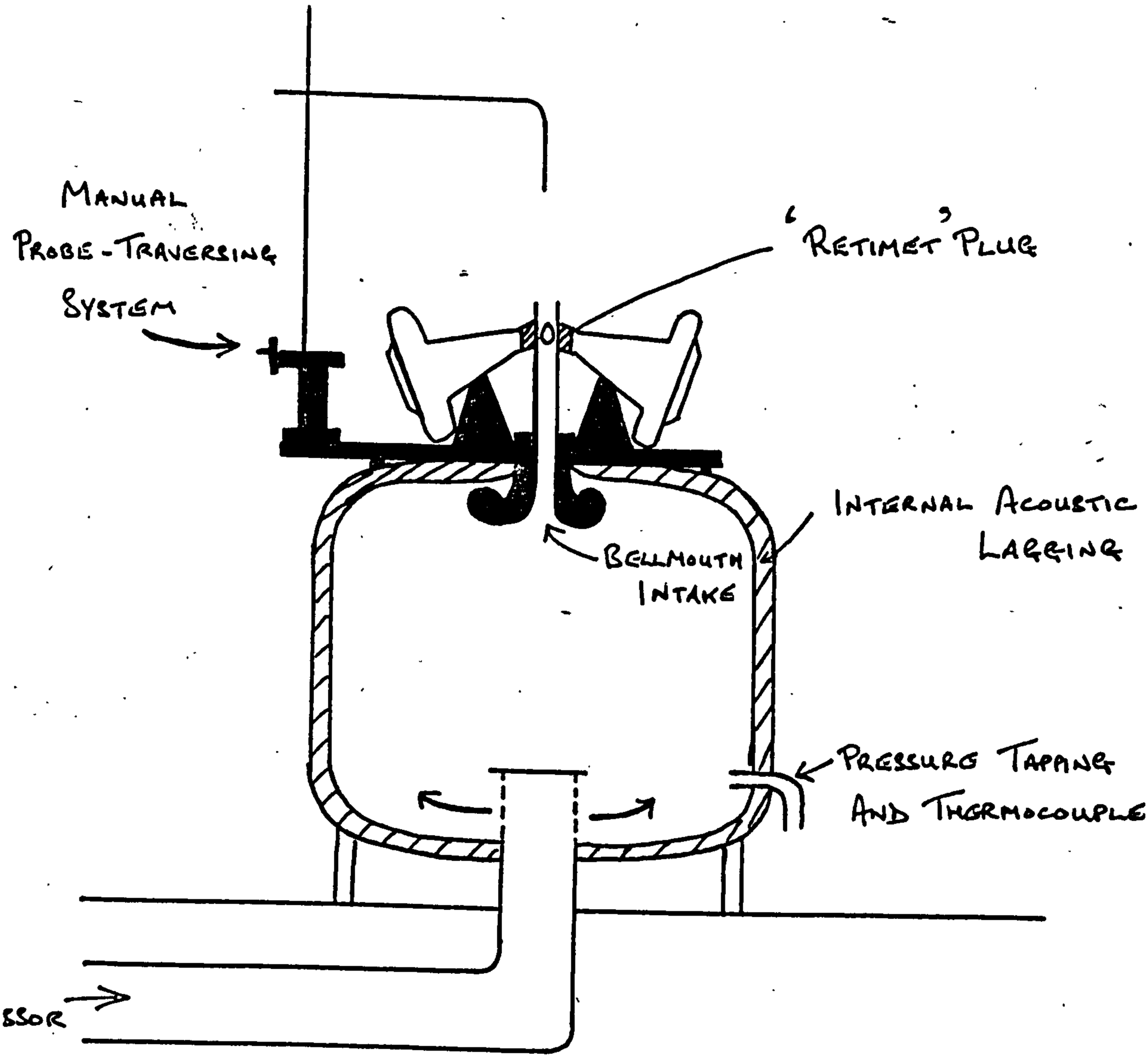

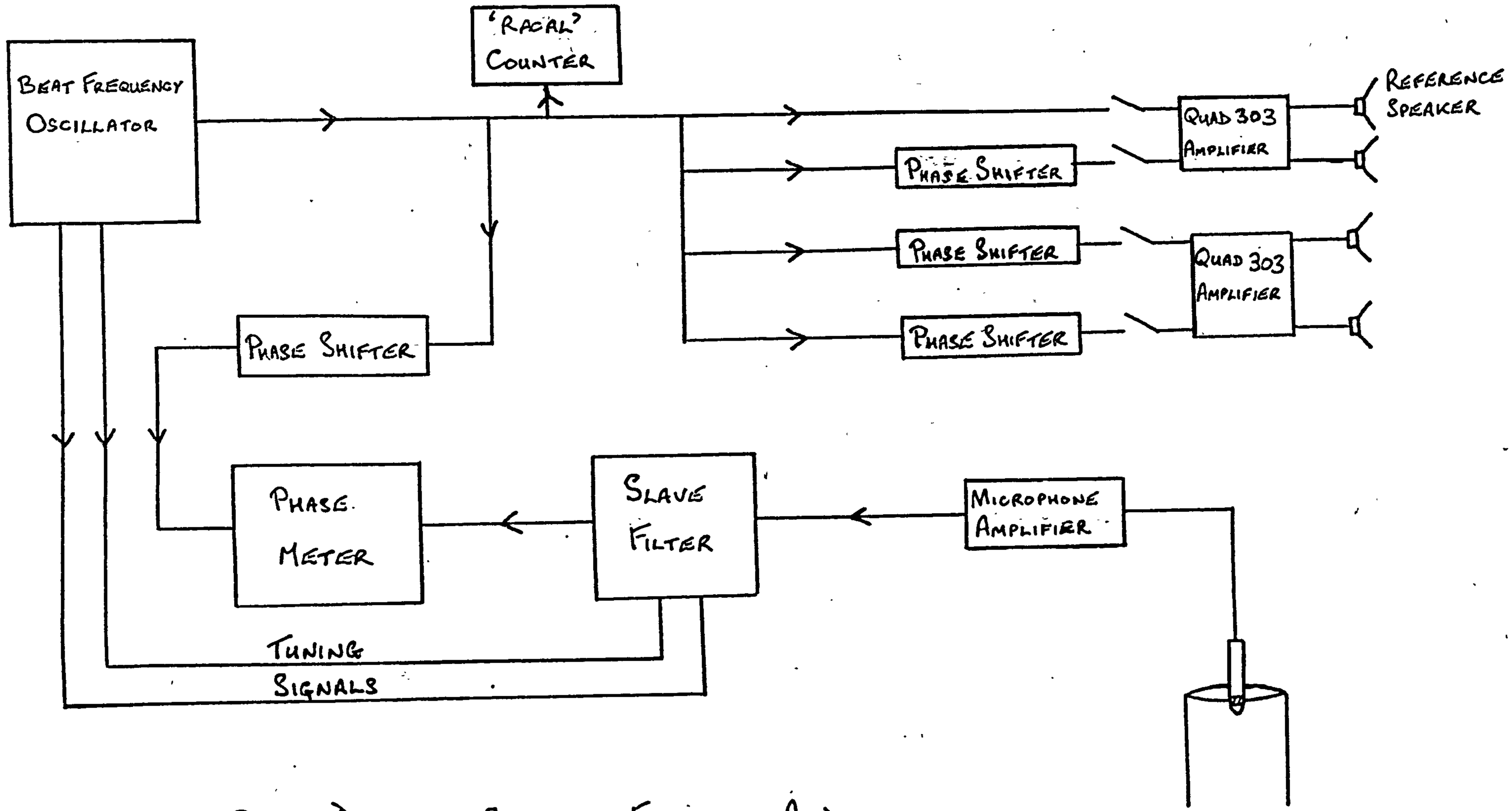

FIGURE 2 : BLOCK DIAGRAM SHOWING EXCITATION AND MONITORING SYSTEMS.

PLATE 1 HIGH ORDER MODE GENERATING SYSTEM

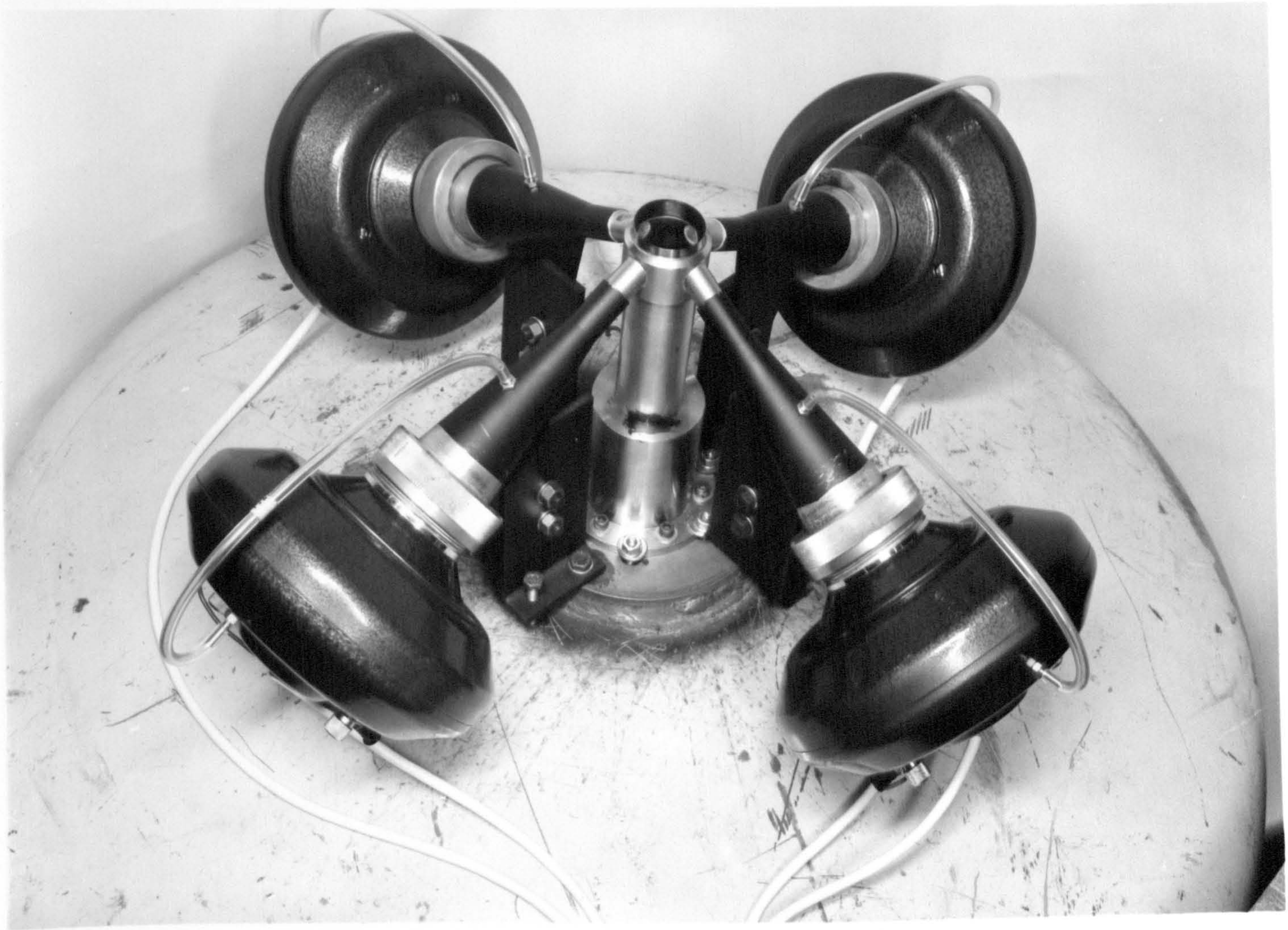

FIGURE 3 : MODES OF EXCITATION

(a) $m = +1$

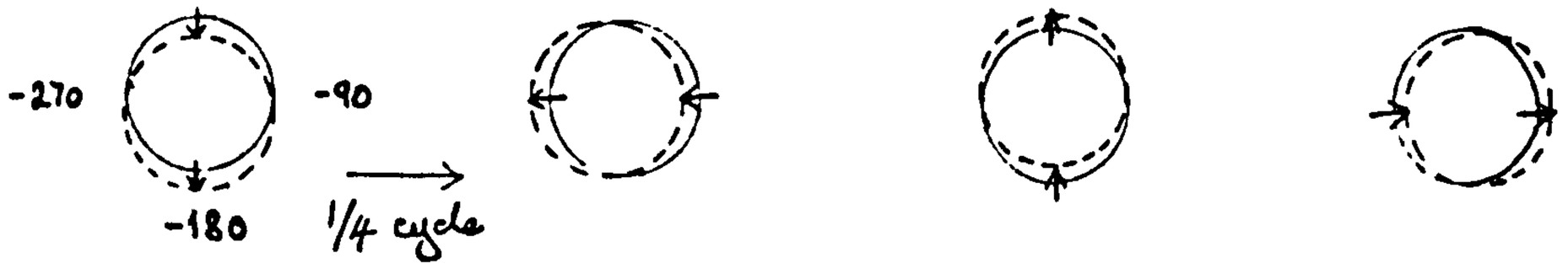

(b) $m = \pm 1$

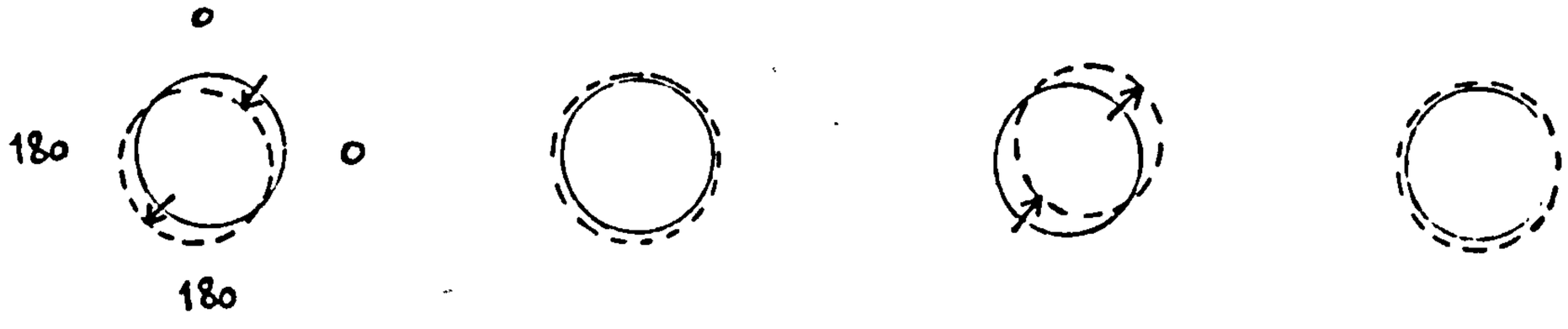

PRODUCING THE STANDING WAVE PATTERN

(c) $m = \pm 2$

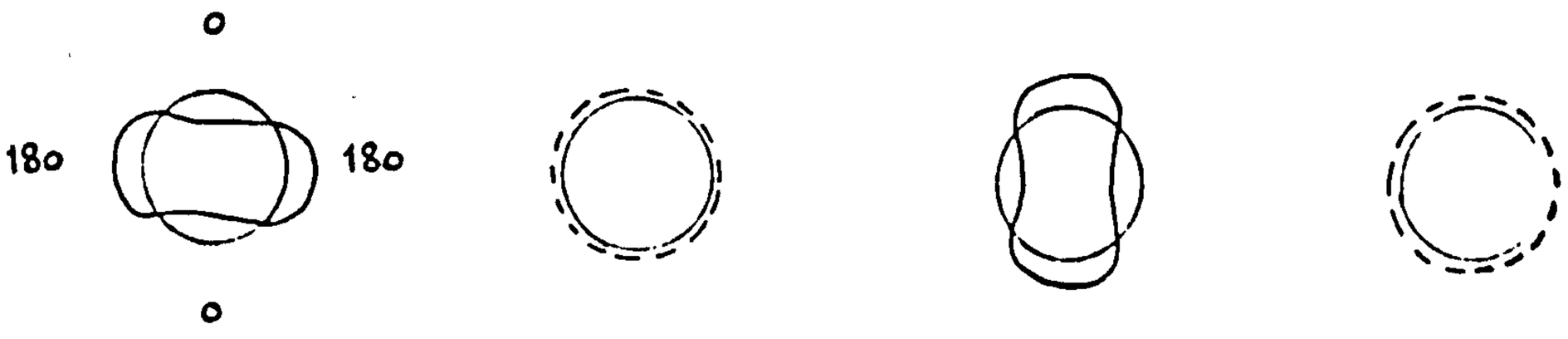

PRODUCING THE STANDING WAVE PATTERN

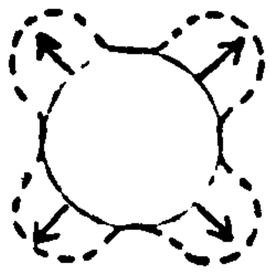

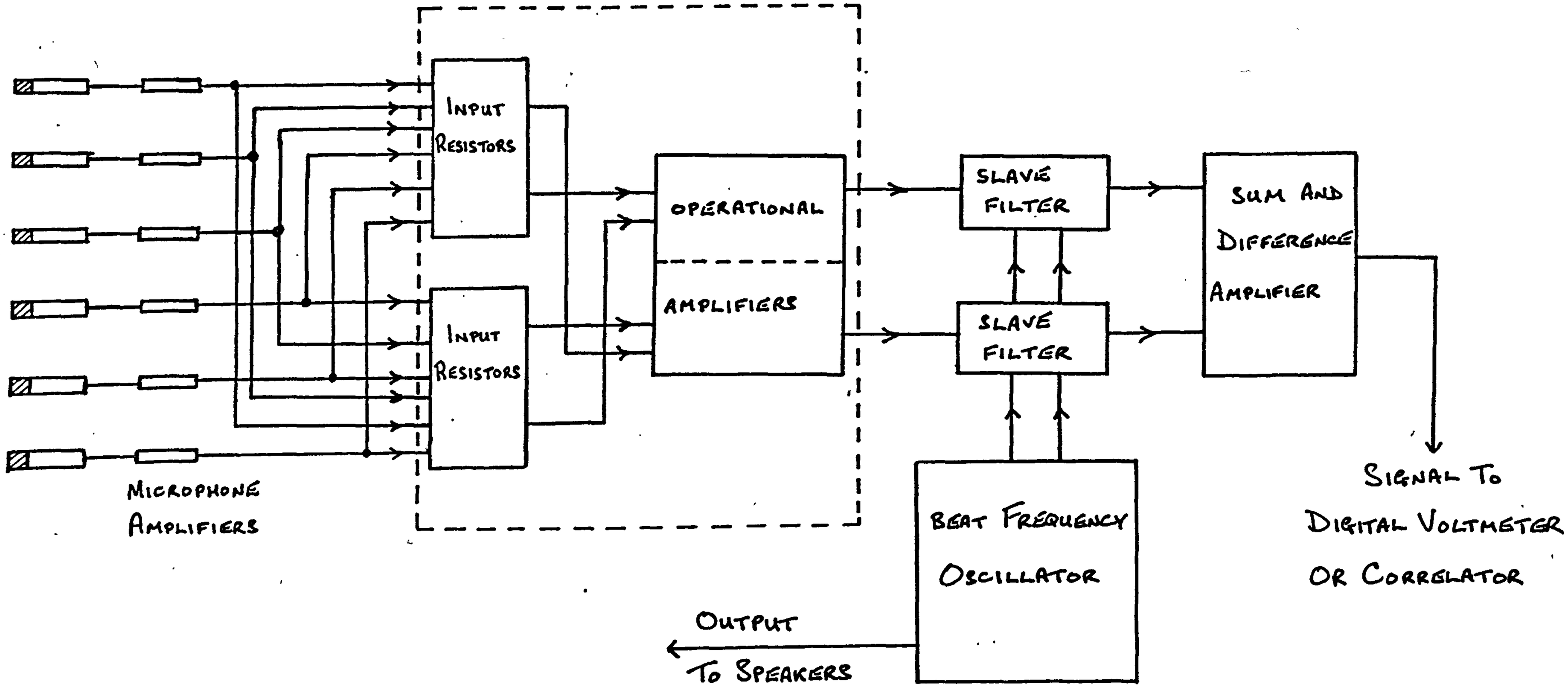

FIGURE 4: MODAL ANALYSIS SYSTEM

FIGURE 6 : HOT WIRE CALIBRATION CURVES

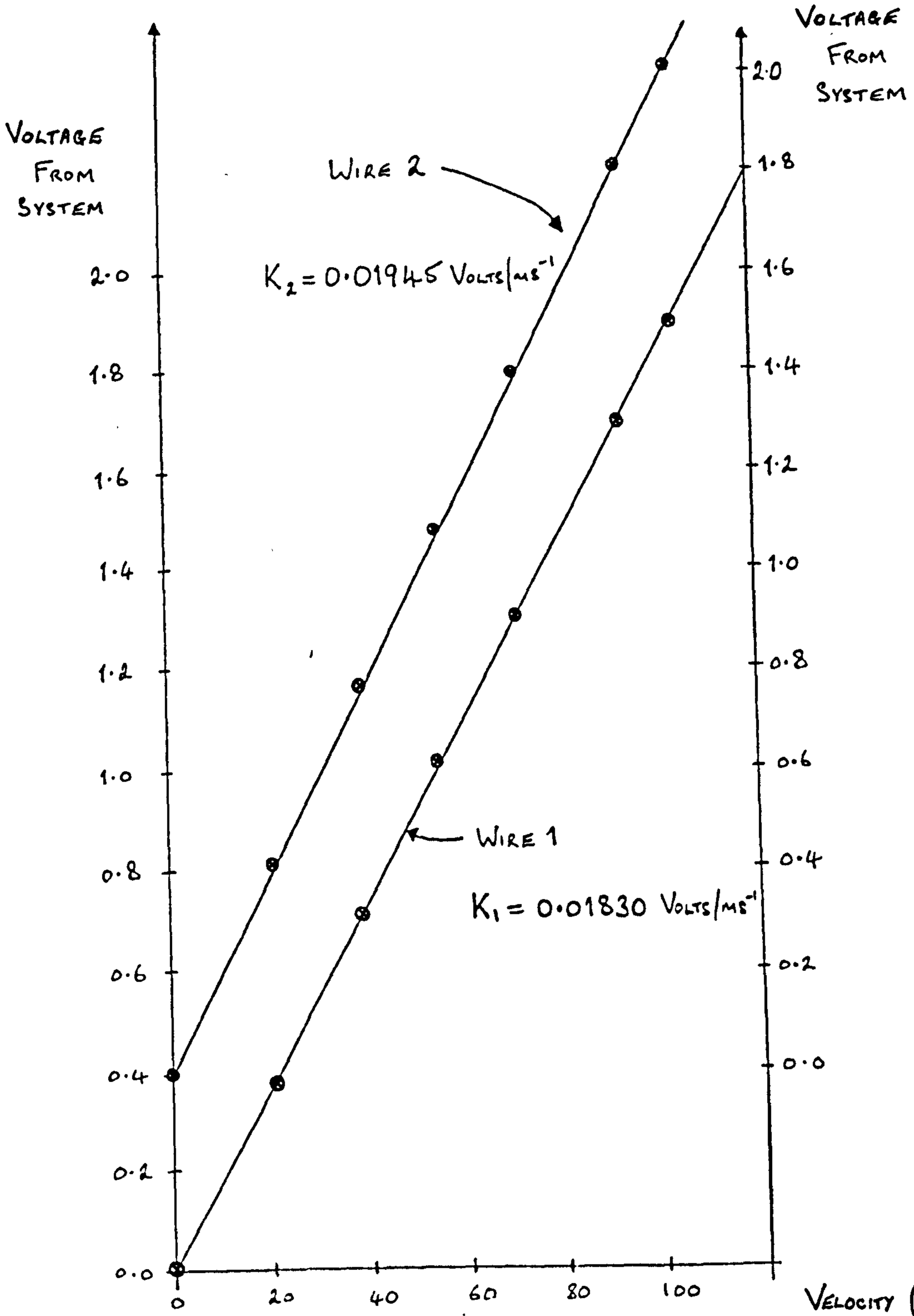

FIGURE 7 : CROSSED WIRE RECORDING AND ANALYSIS SYSTEM

(a)

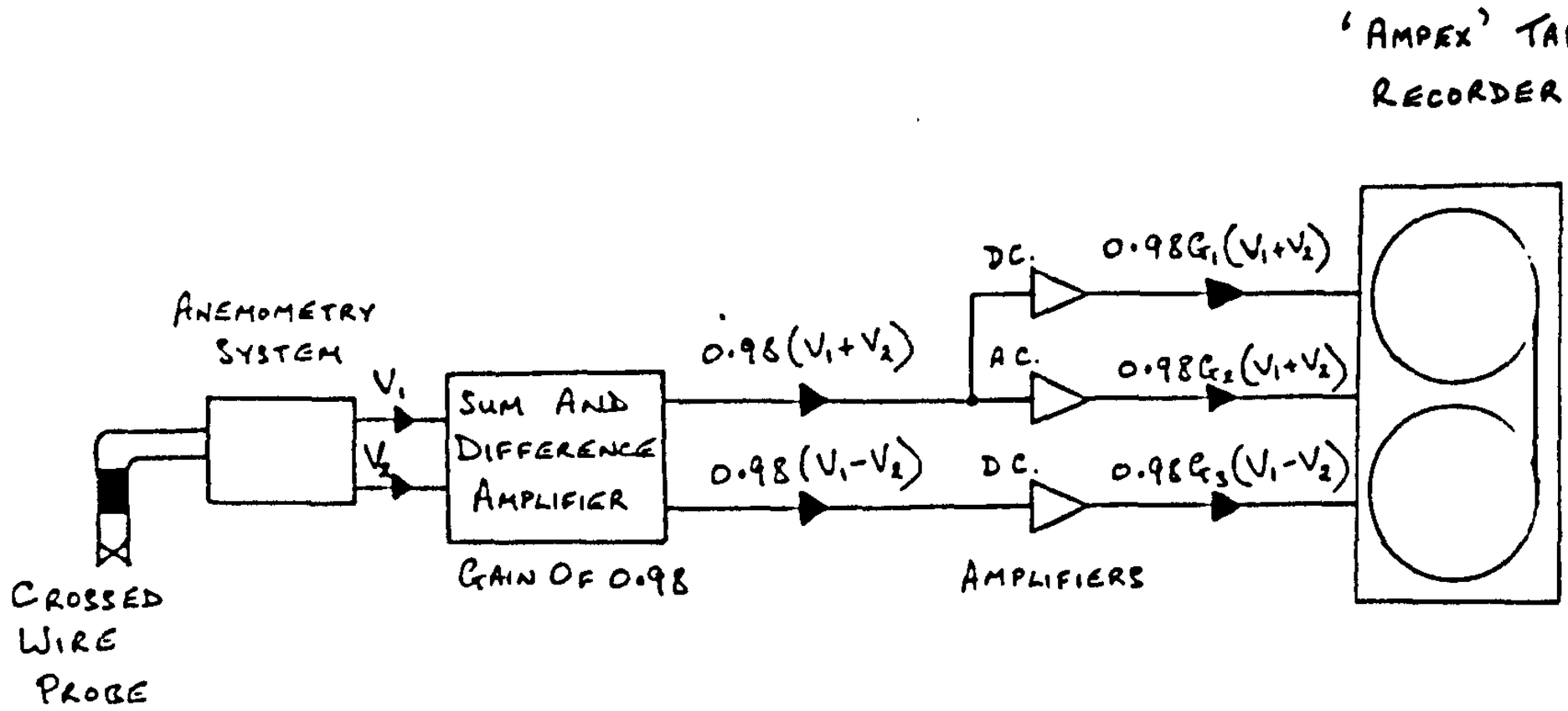

(b)

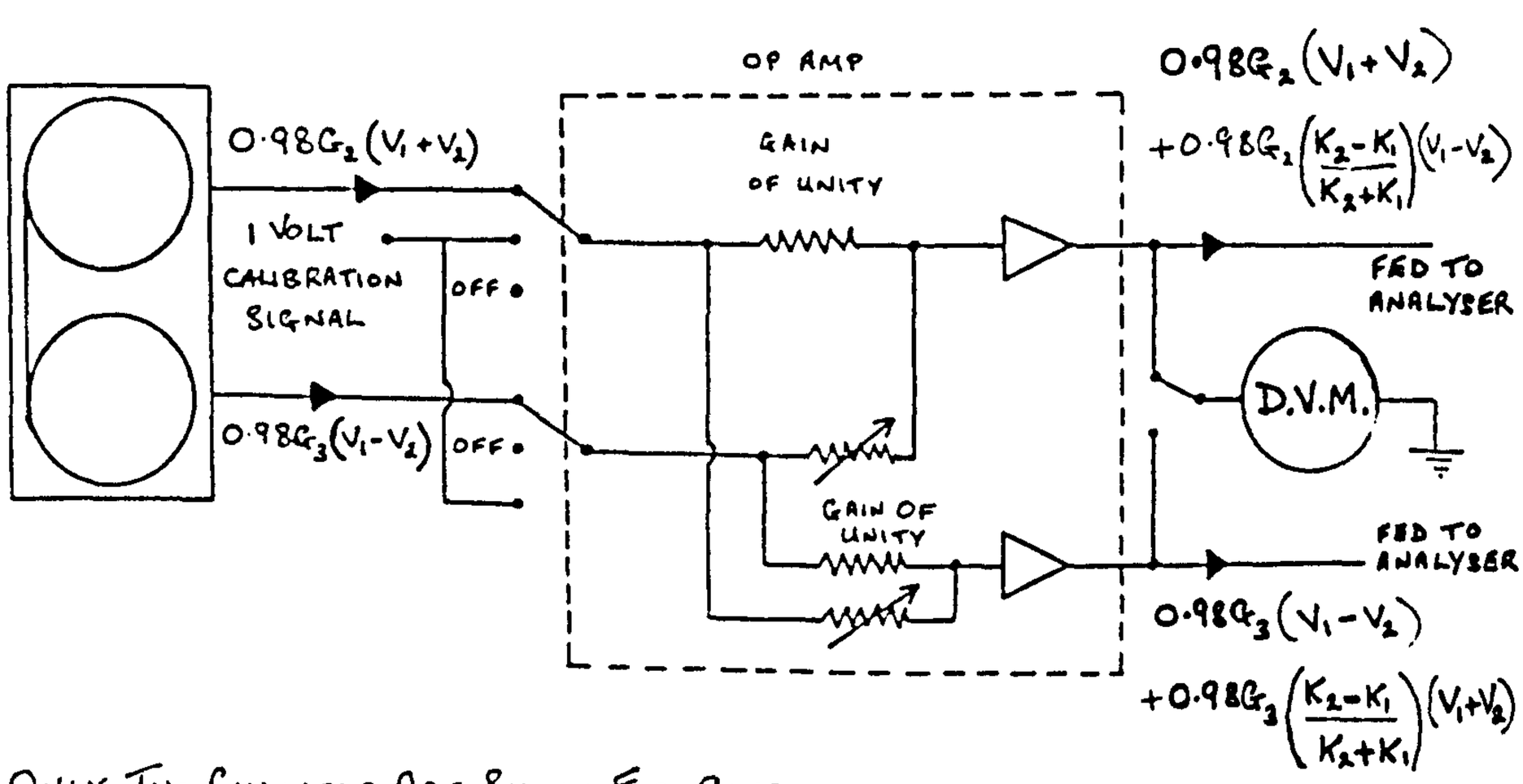

ONLY TWO CHANNELS ARE SHOWN, FOR CLARITY.

FIGURE 8(a): SPECTRA OF 0 VOLTS CALIBRATION SIGNAL ON CHANNELS 1 AND 3.

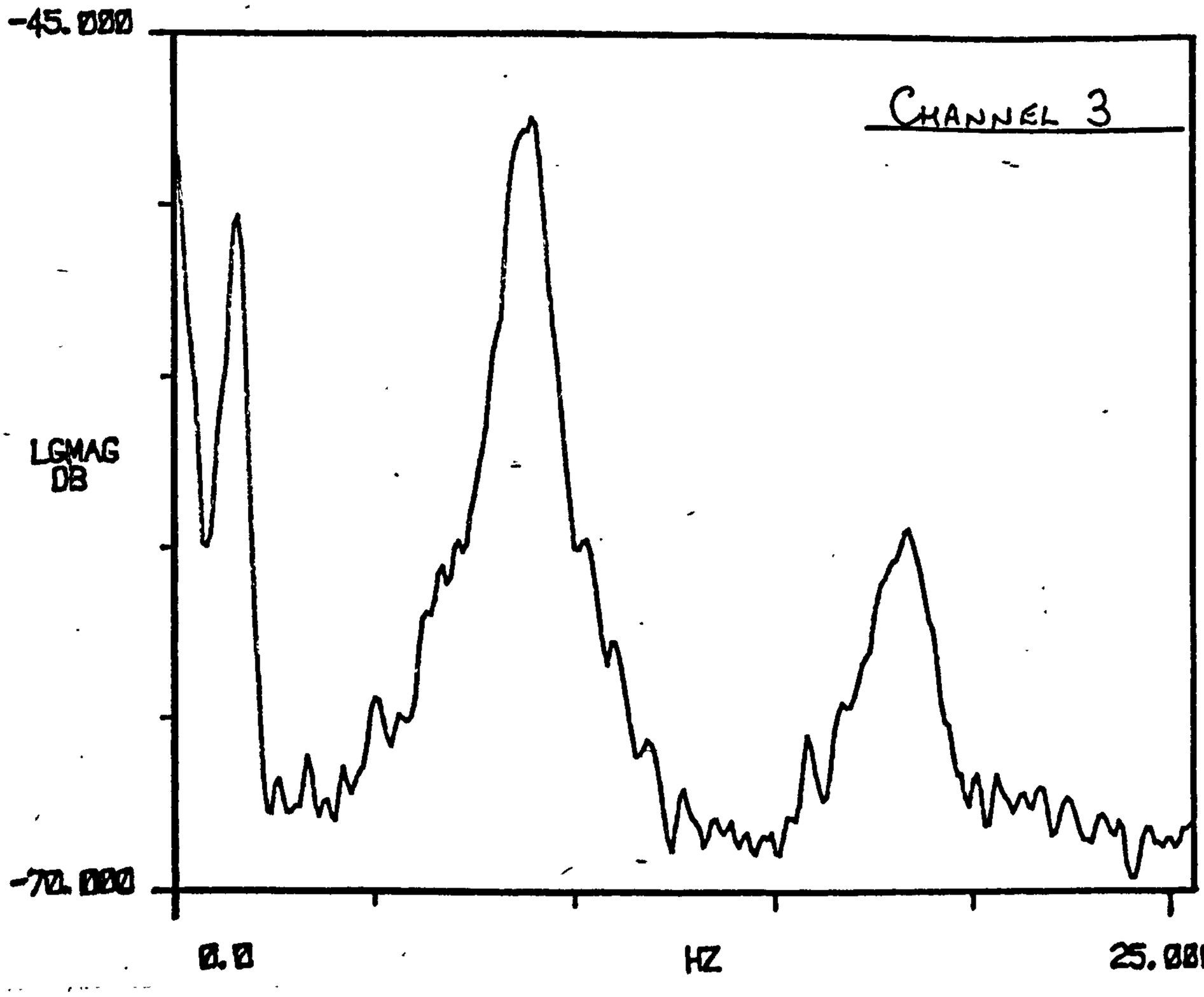

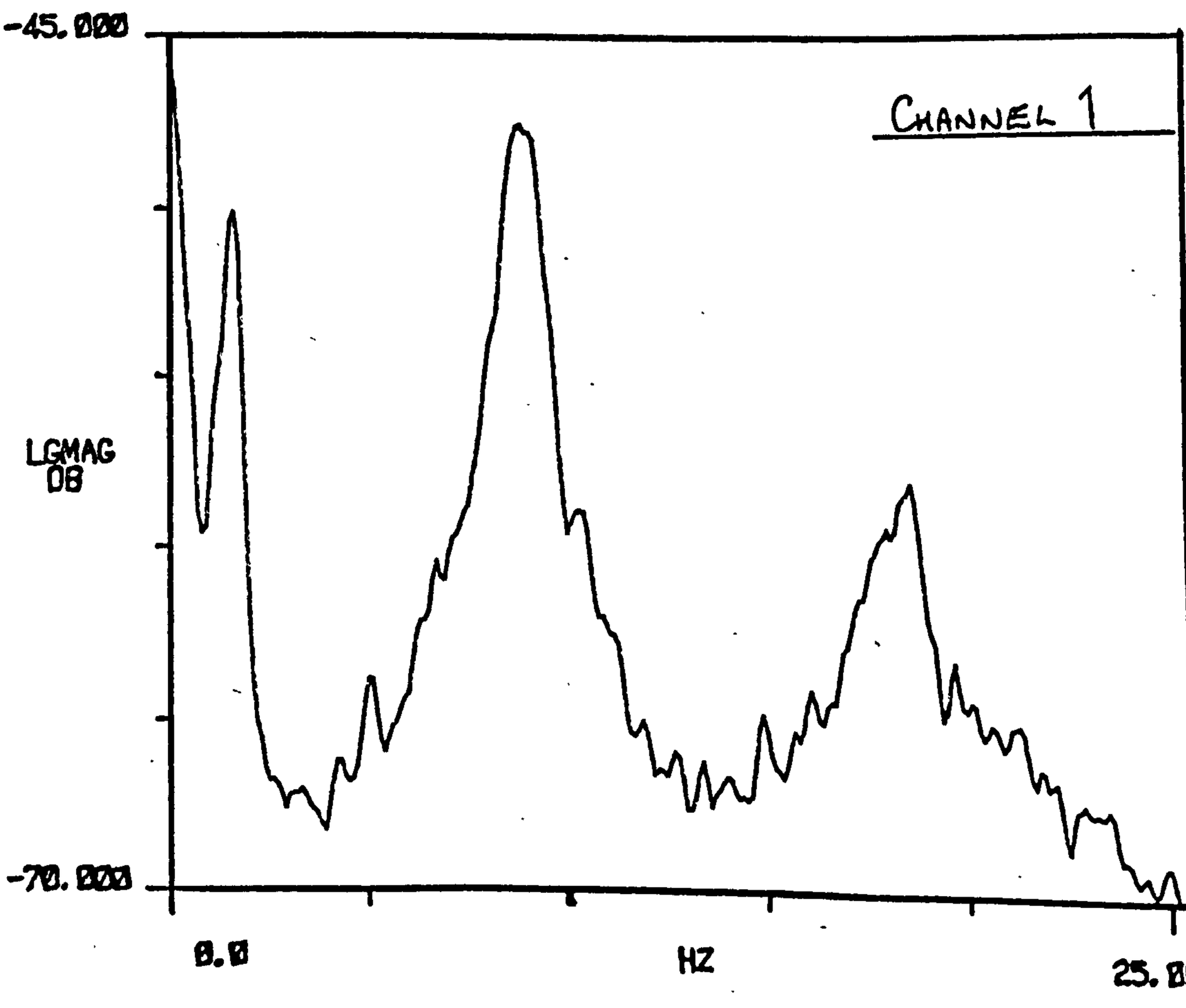

FIGURE 8(b): SPECTRA OF 1 VOLT CALIBRATION SIGNAL ON CHANNELS 1 AND 3

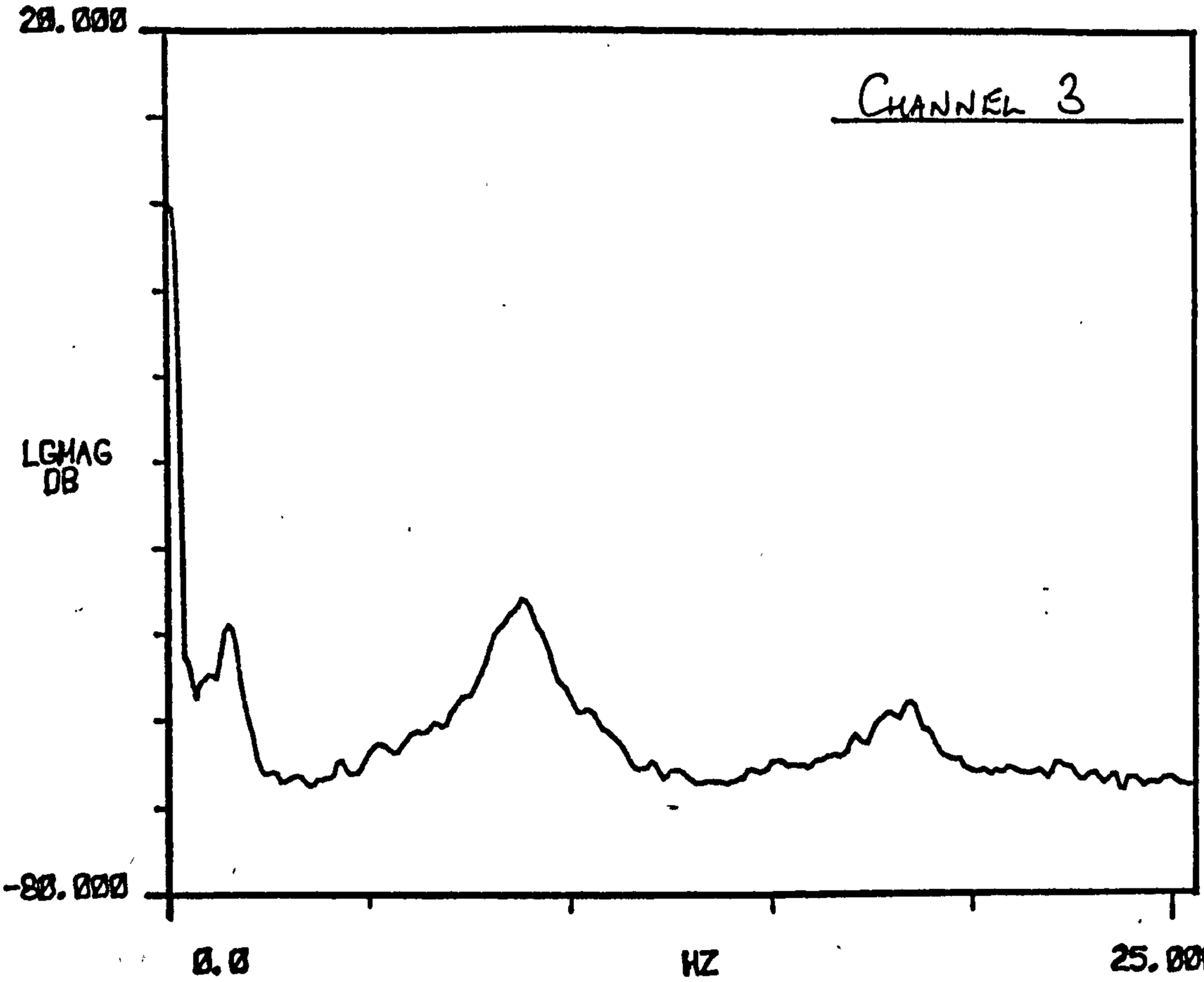

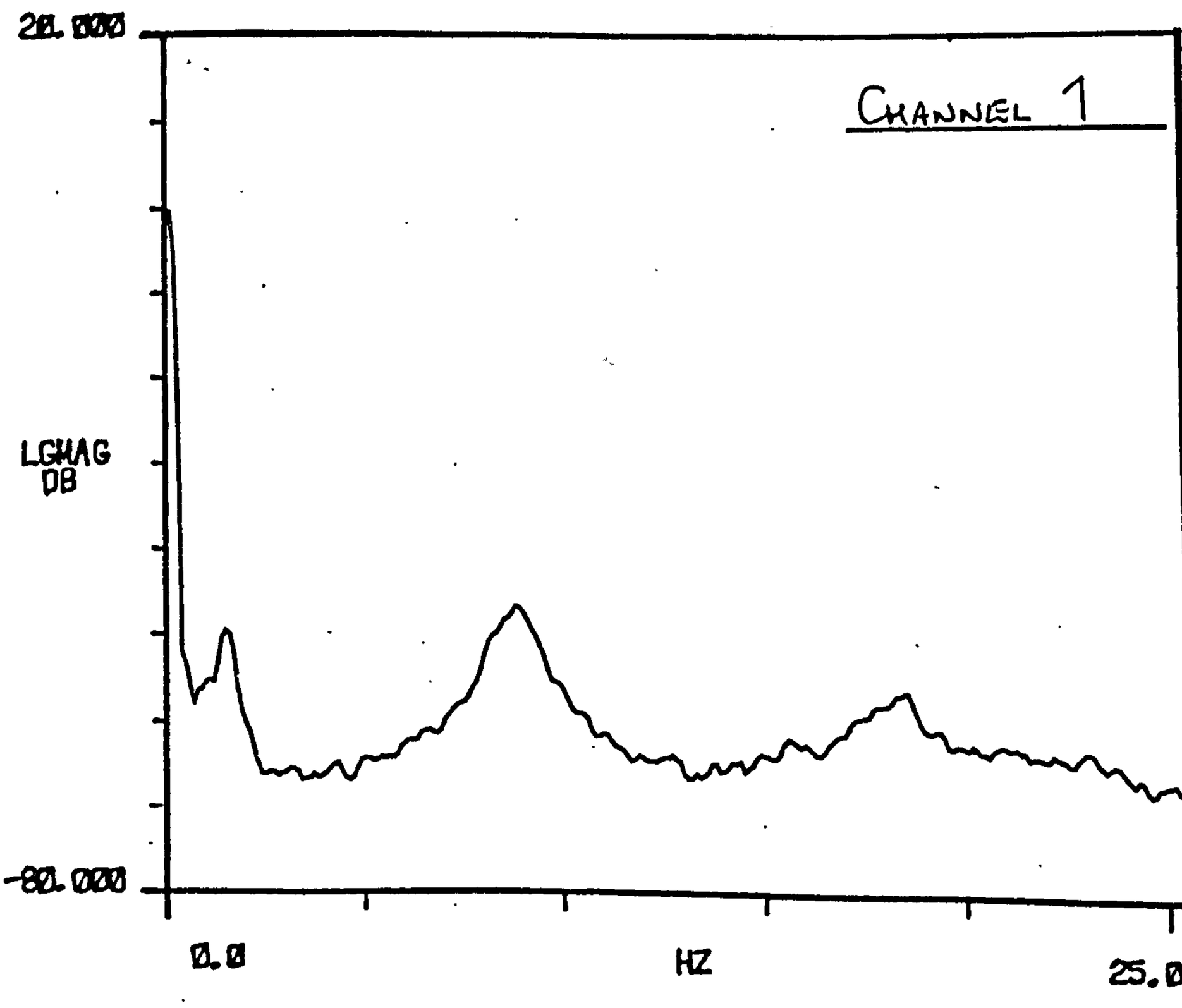

FIGURE 9: SIGNAL EDUCTION TECHNIQUE

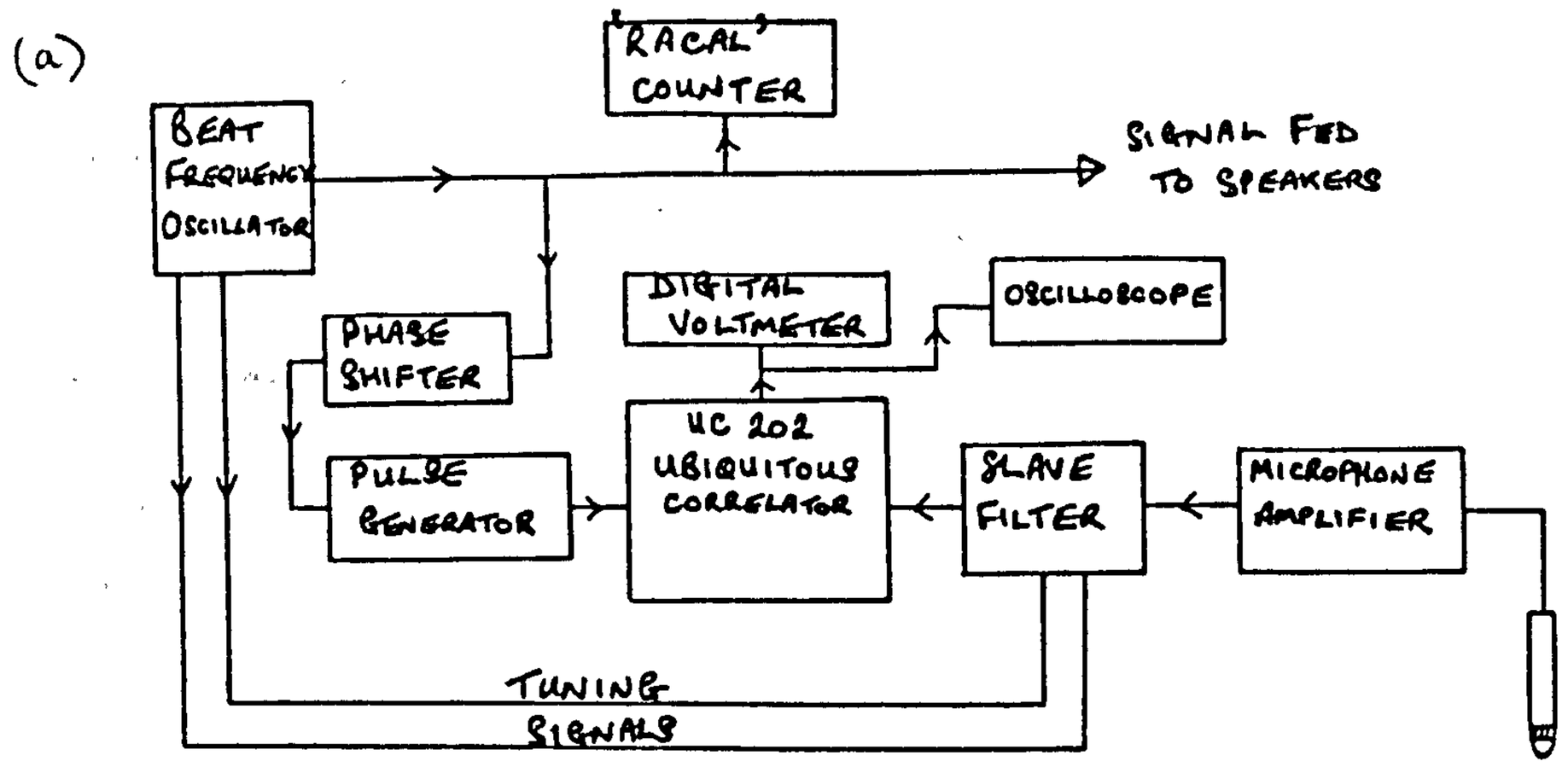

FIGURE 10(a): STRUCTURE OF THE TURBULENT JET

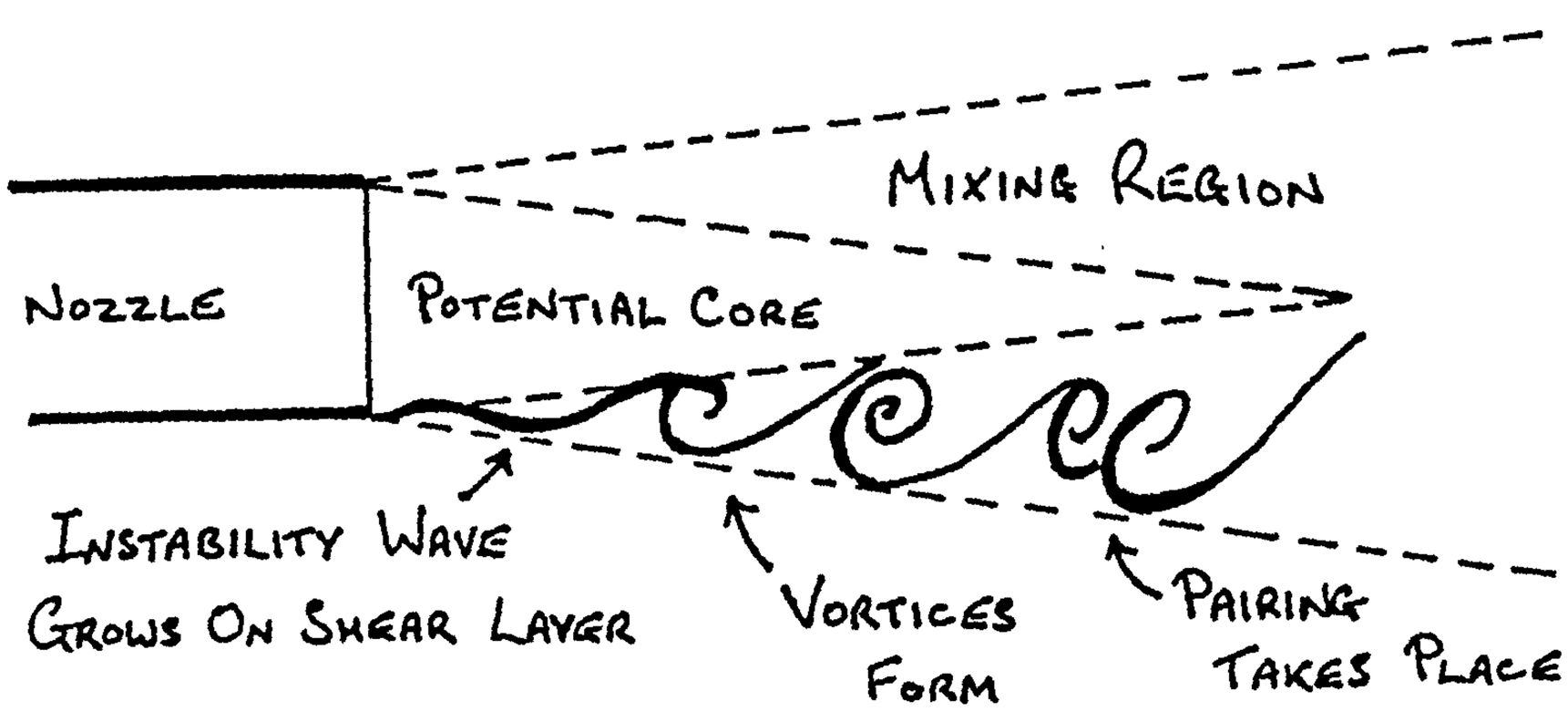

FIGURE 10(b): SCHLIEREN SYSTEM

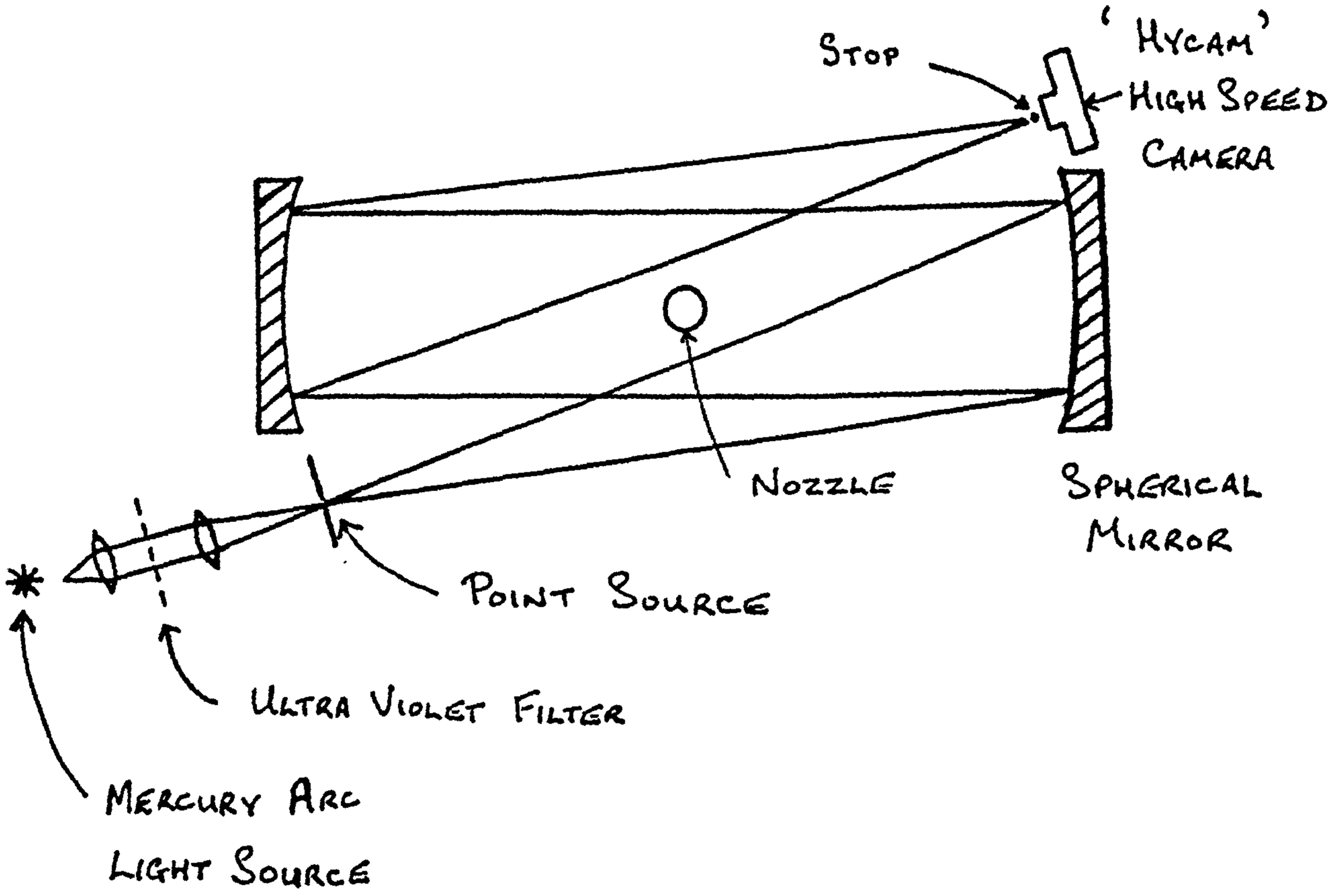

Copy No

Copy Neg: 790-4418
: 790-4428

PLATE 2 PLANE WAVE MODE

Copy Neg: 790-4421
No : 790-4431

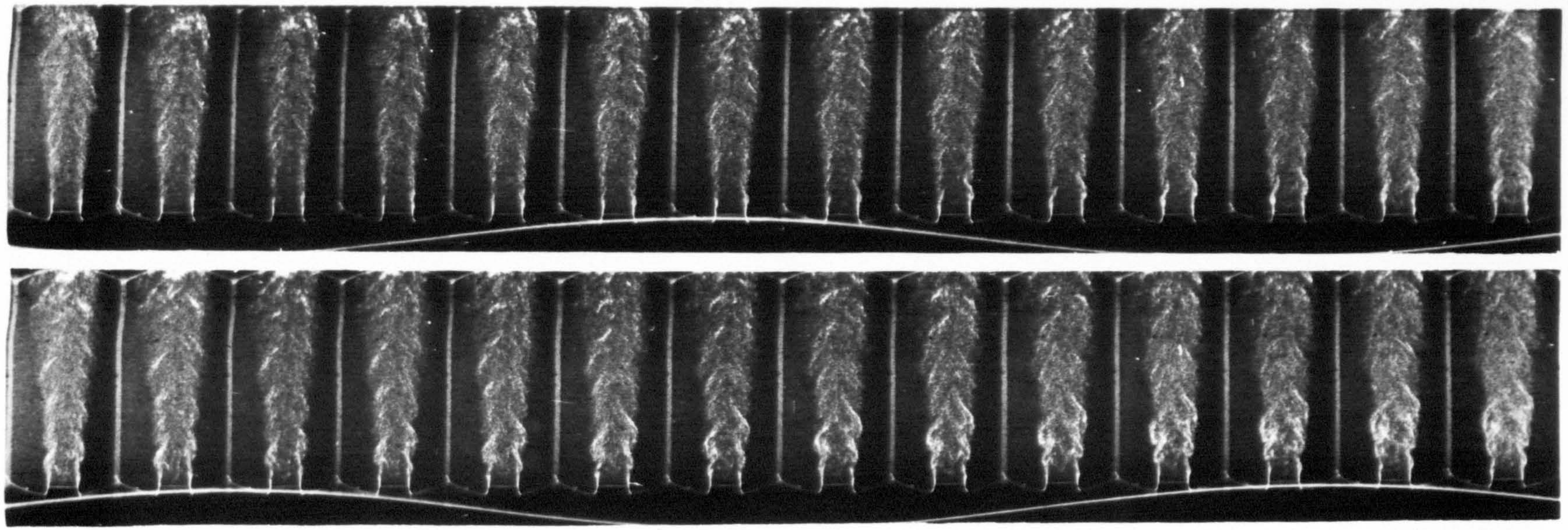

PLATE 3

+1 MODE

Copy Neg: 790-4423
No : 790-4424

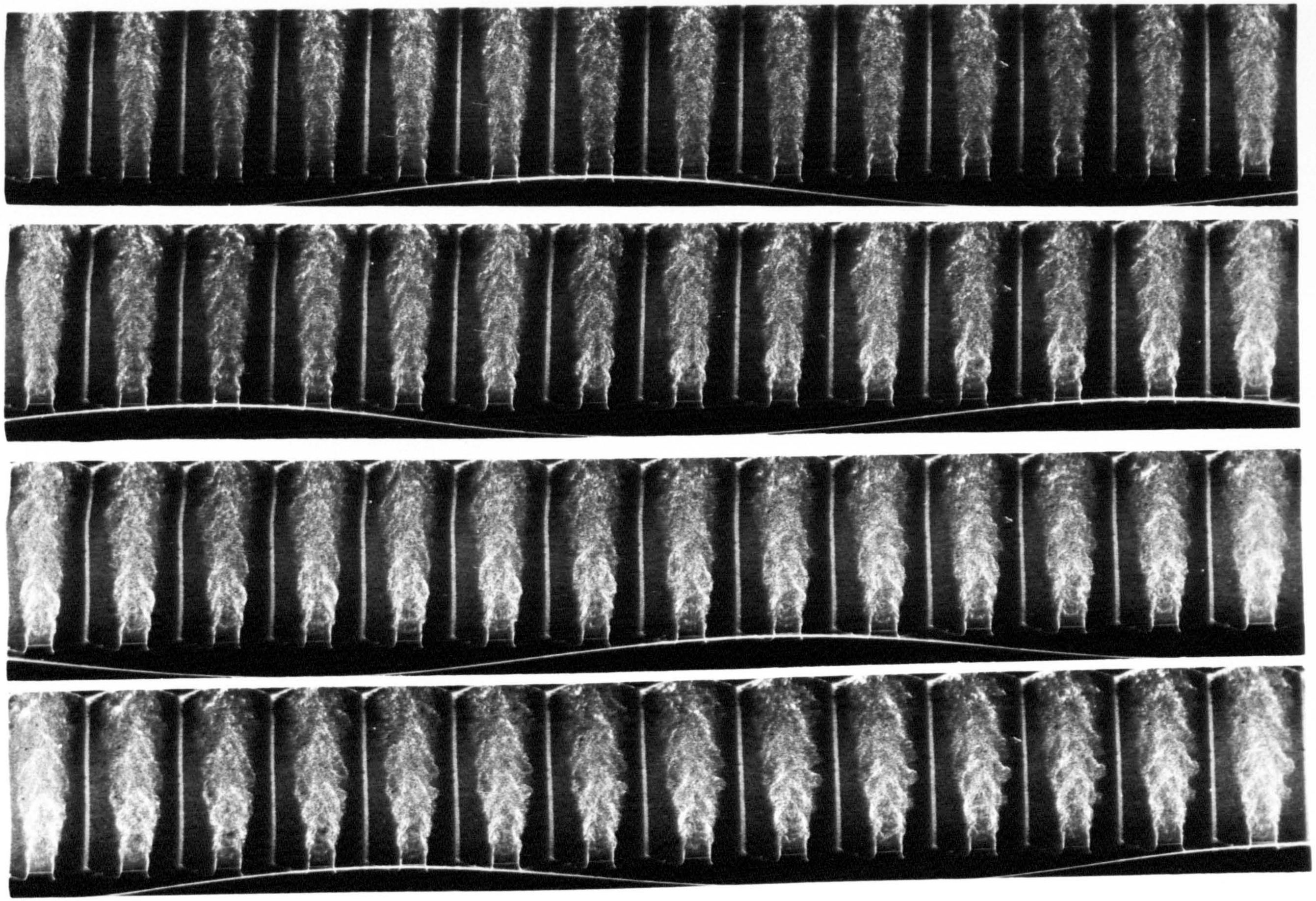

PLATE 4 -1 MODE

Copy Neg: 790-4415
No : 790-4425

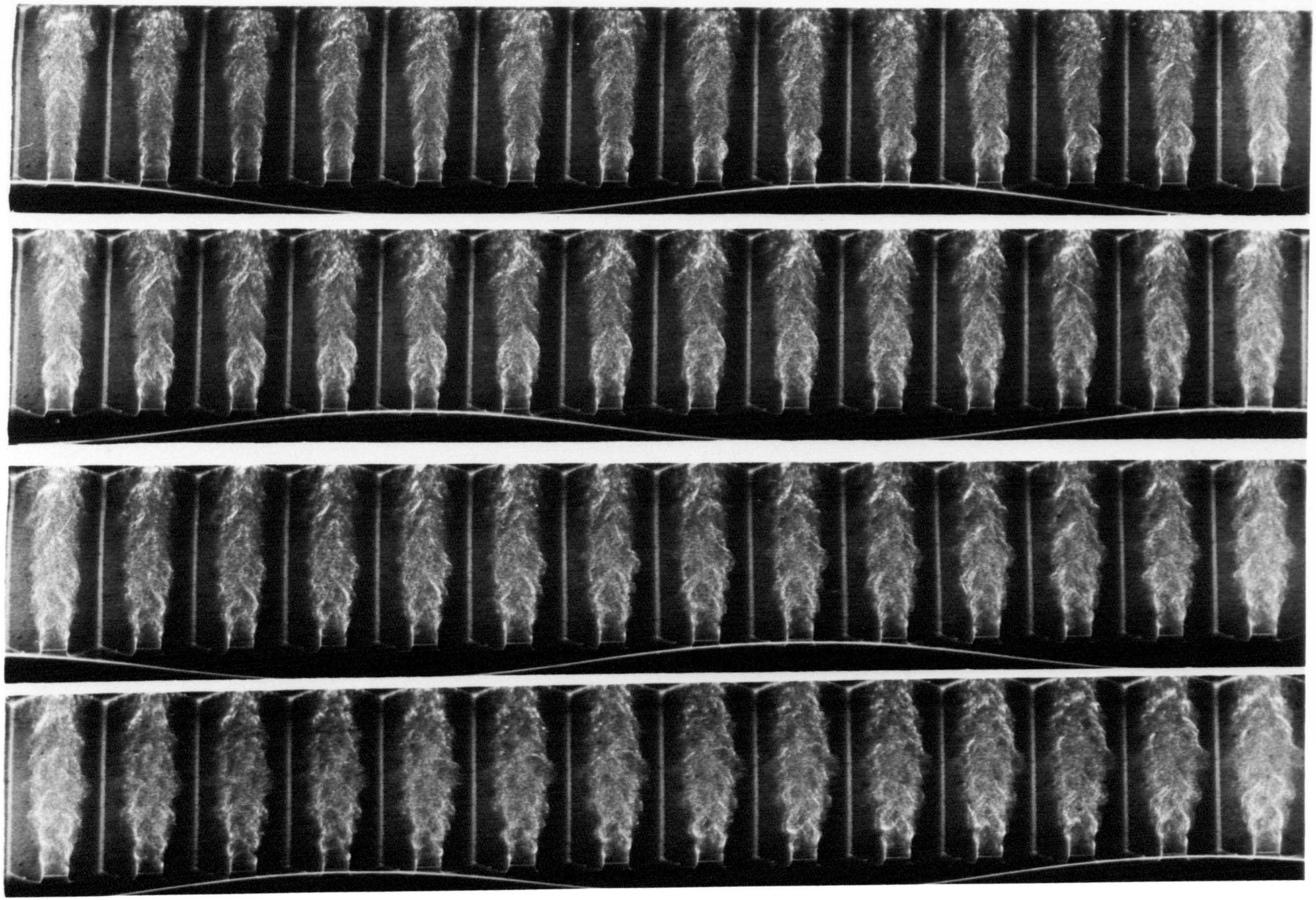

PLATE 5 ±1 MODE, WIDE VIEW

Copy Neg! 790-4416
No : 790-4426

PLATE 6 ± 1 MODE, NARROW VIEW

Copy Neg: 790-4419
No : 790-4429

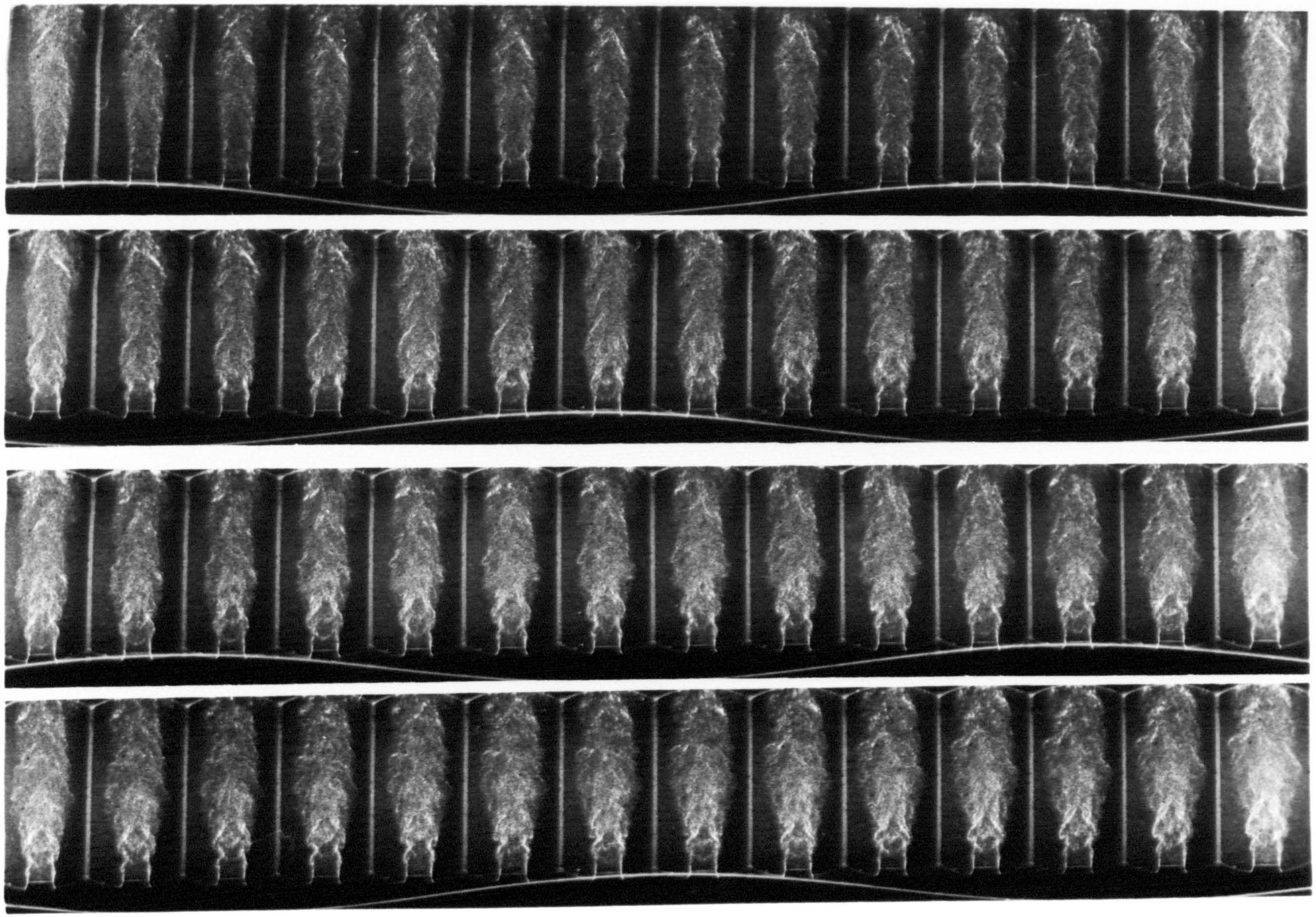

PLATE 7 ±2 MODE, WIDE VIEW

Copy Neg: 790-4417
No : 790-4427

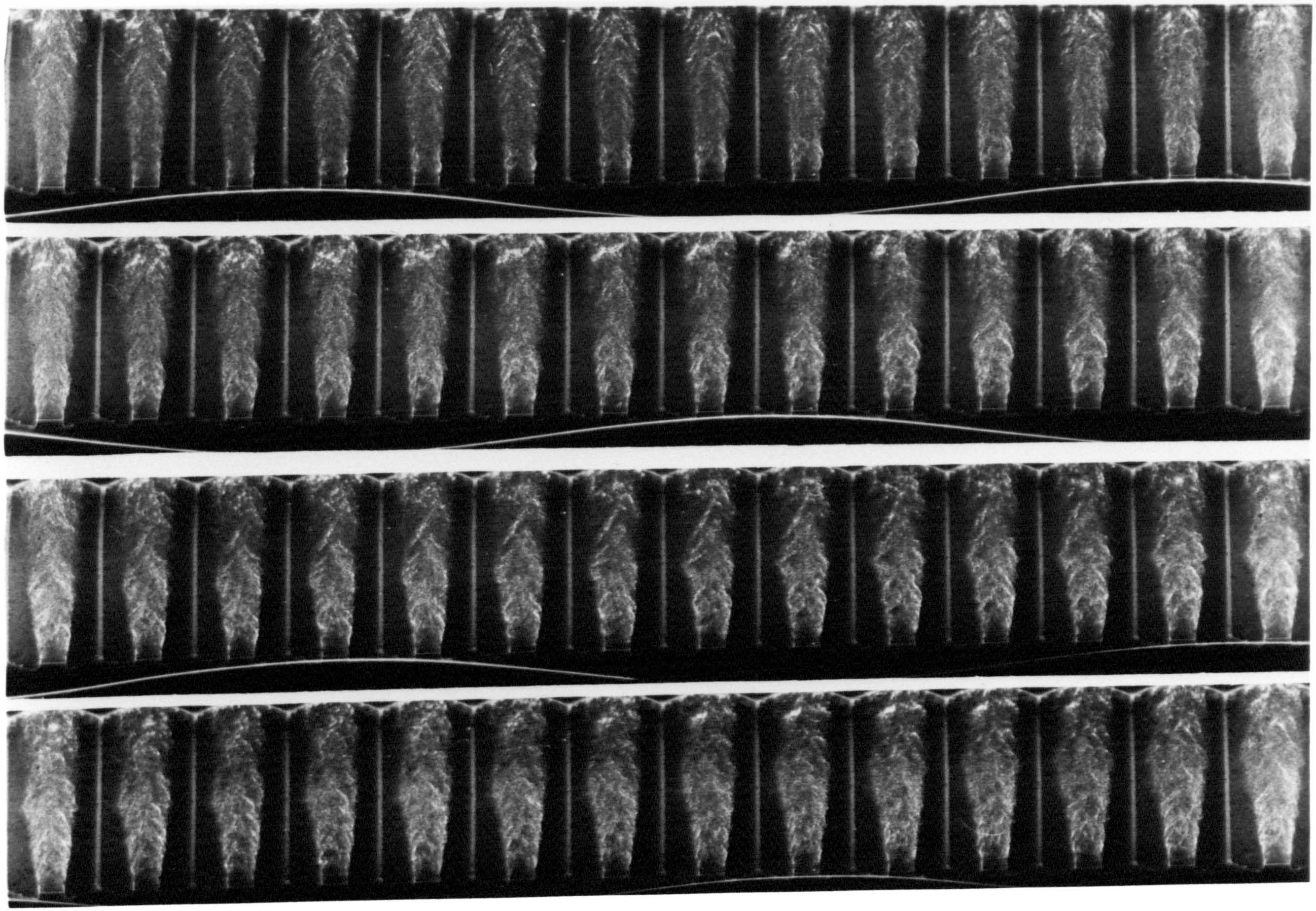

PLATE 8 ±2 MODE, NARROW VIEW

FIGURE 11 : VARIATION OF MEAN VELOCITY PROFILE WITH AXIAL DISTANCE AT M = 0·3, UNEXCITED JET, (PITOT RESULTS).

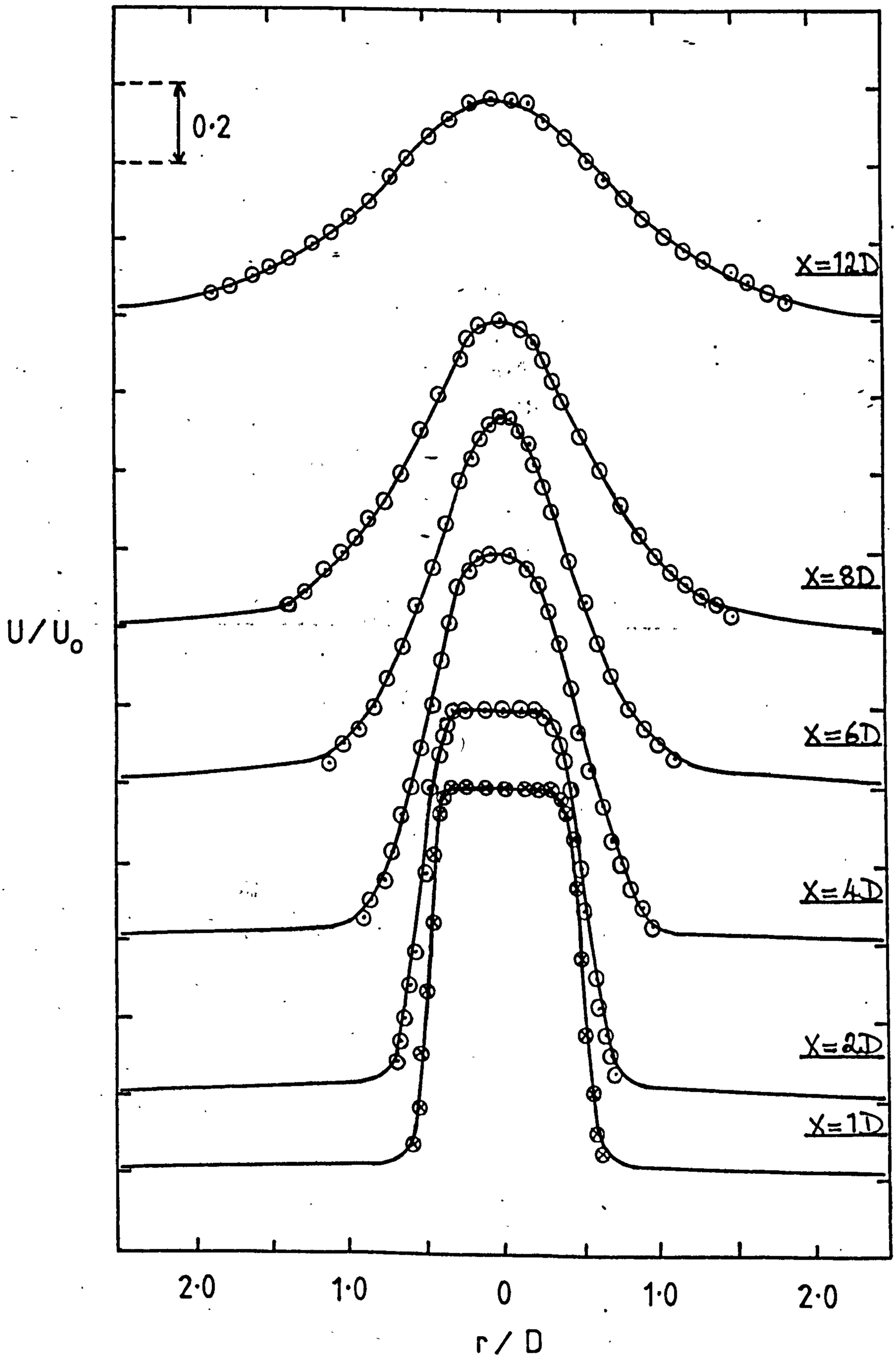

FIGURE 12 : VARIATION OF MEAN VELOCITY PROFILE WITH AXIAL DISTANCE AT M=0·3, UNEXCITED JET, (HOT WIRE RESULTS).

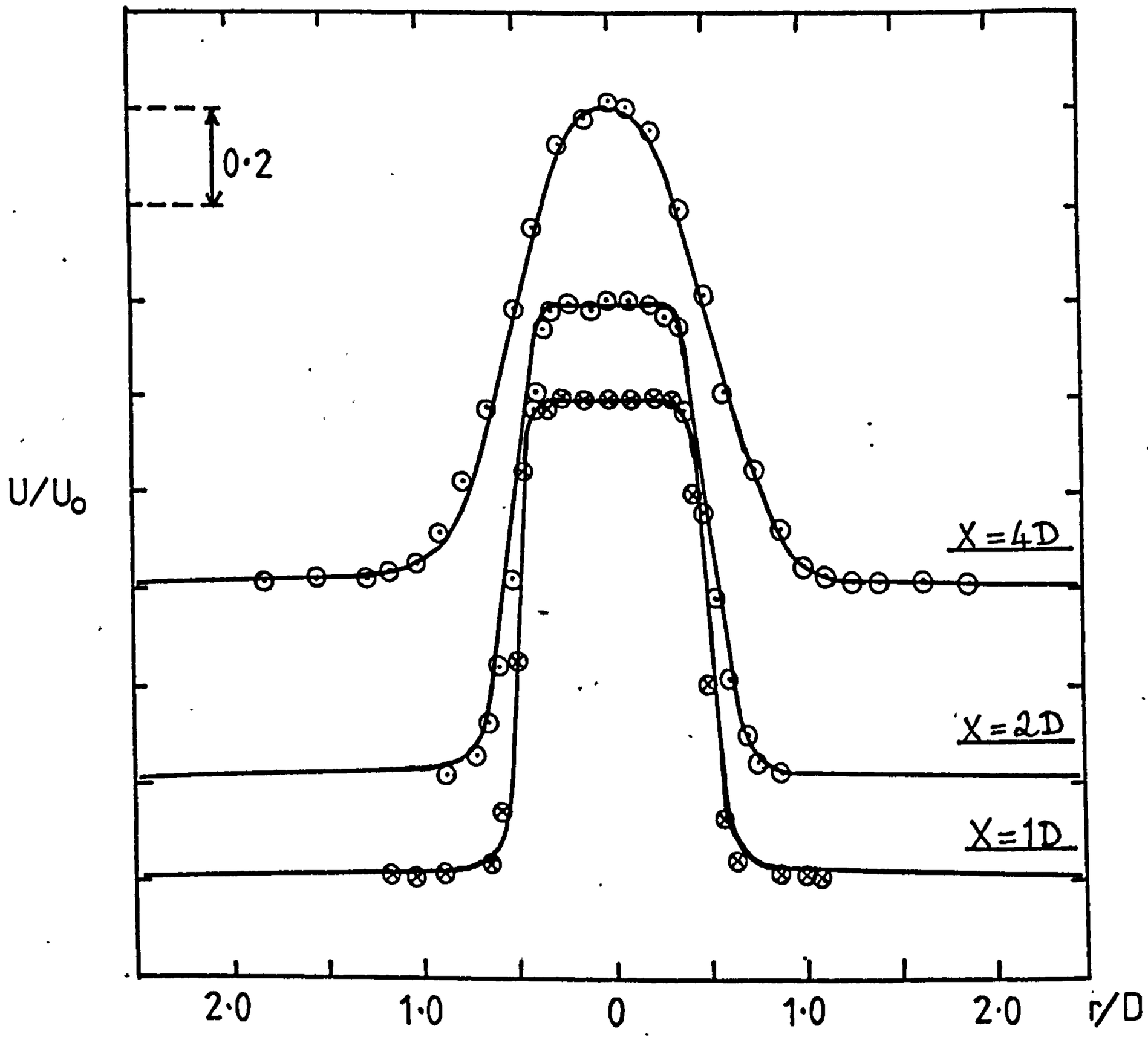

FIGURE 13 : VARIATION OF CENTRE-LINE MEAN VELOCITY WITH AXIAL DISTANCE AT M=0·3

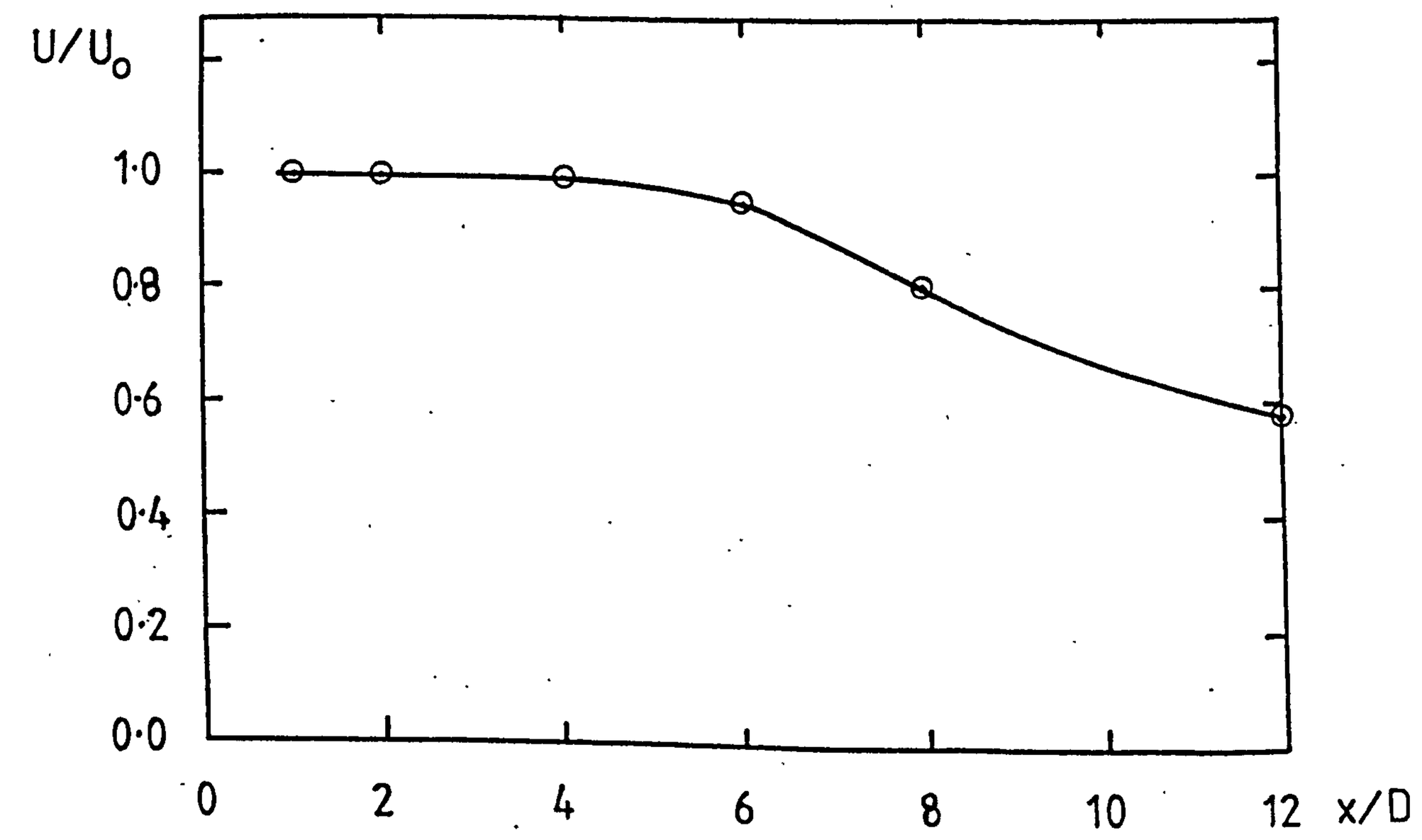

FIGURE 14

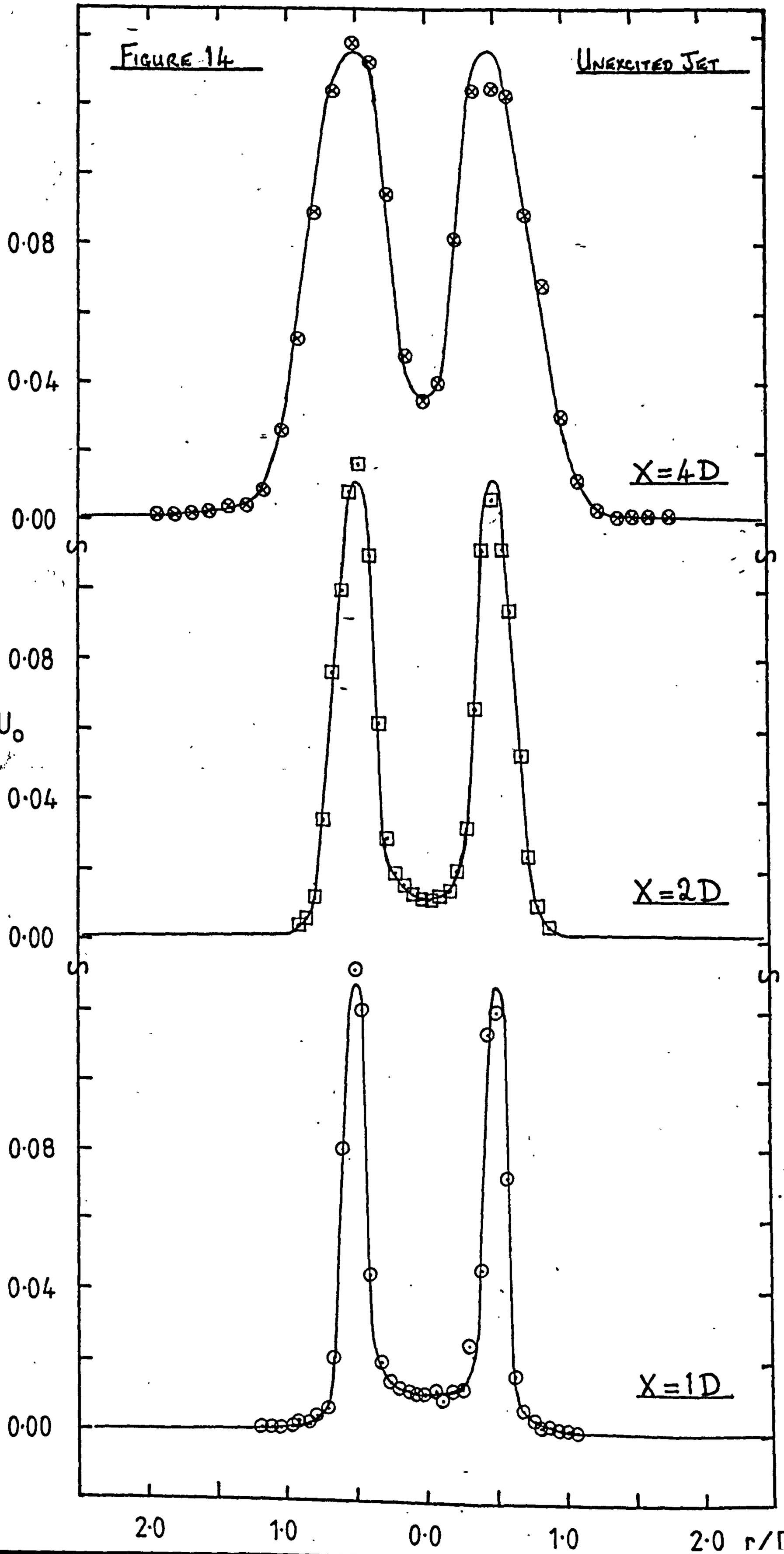
UNEXCITED JET
X=4D
X=2D
X=1D
0·08
0·04
0·00
0·08
u'_x/U_o
0·04
0·00
0·08
0·04
0·00
2·0
1·0
0·0
1·0
2·0 r/D

FIGURE 15

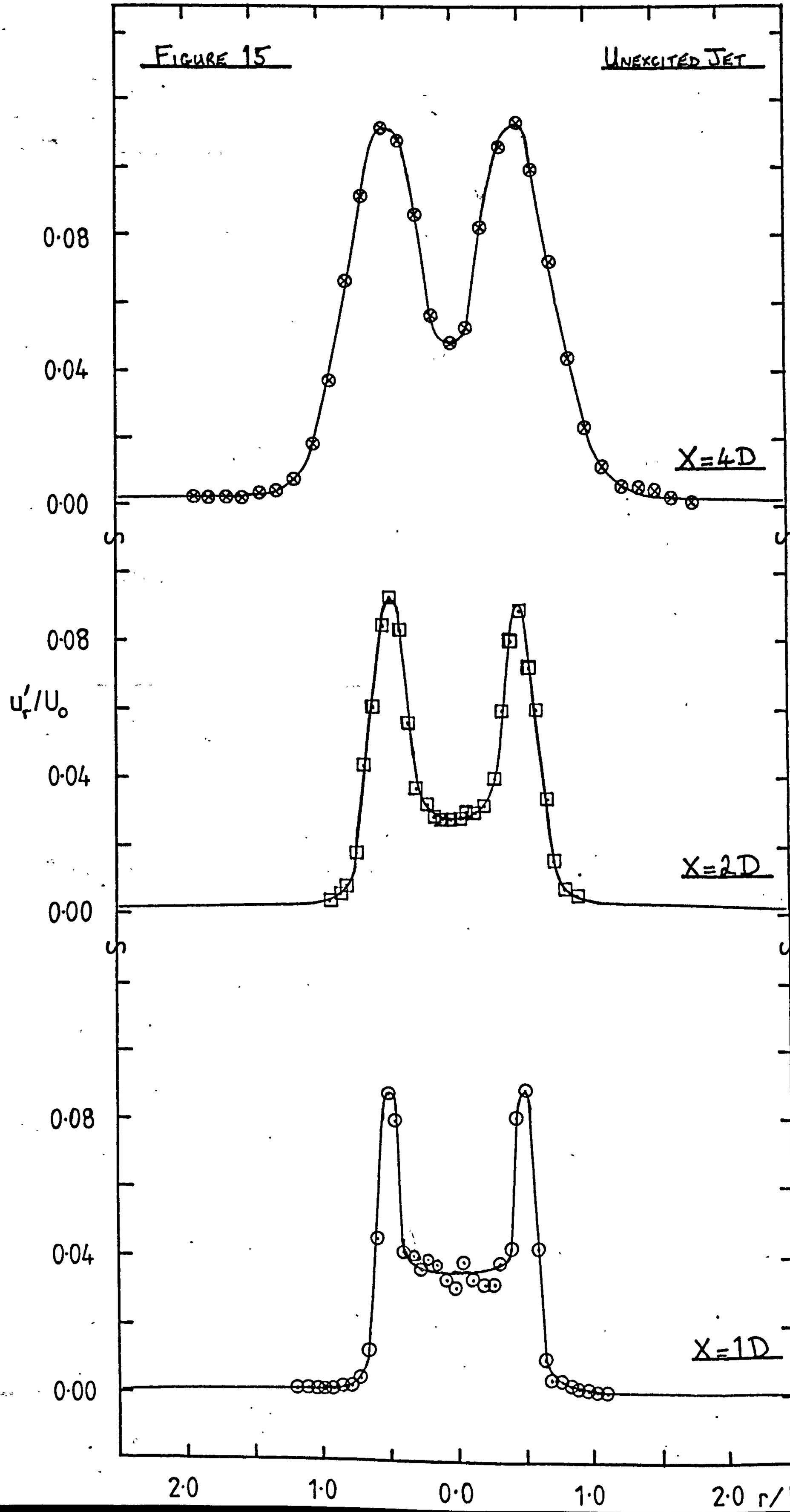
UNEXCITED JET
X=4D
X=2D
X=1D
u'_r/U_o
0·08
0·04
0·00
0·08
0·04
0·00
0·08
0·04
0·00
2·0
1·0
0·0
1·0
2·0 r/D

FIGURE 16 : FLUCTUATING VELOCITY SPECTRA AT X=1D, r=0.0D, UNEXCITED JET.

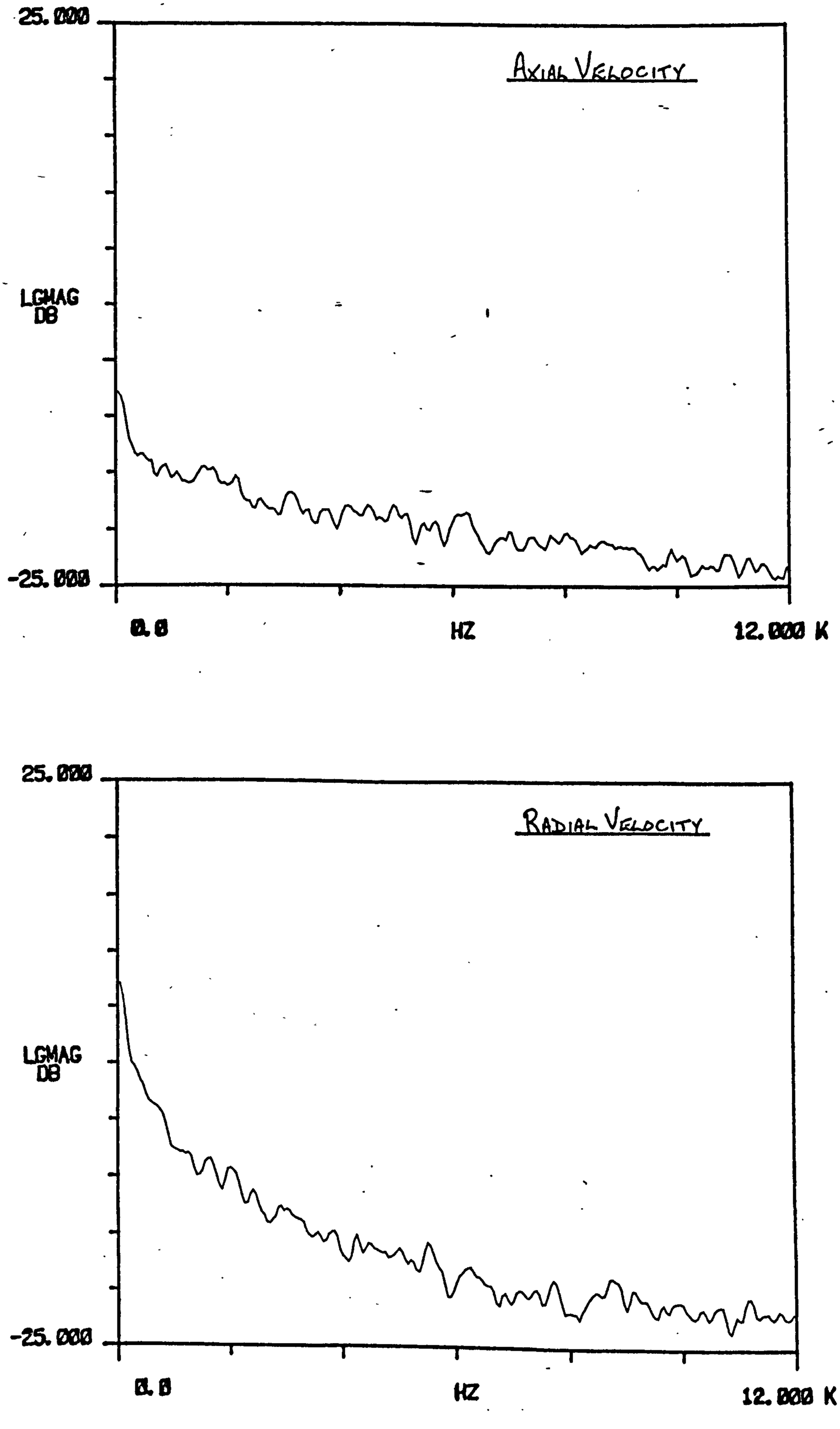

FIGURE 17 : FLUCTUATING VELOCITY SPECTRA AT X=1D, r=0·515D, UNEXCITED JET.

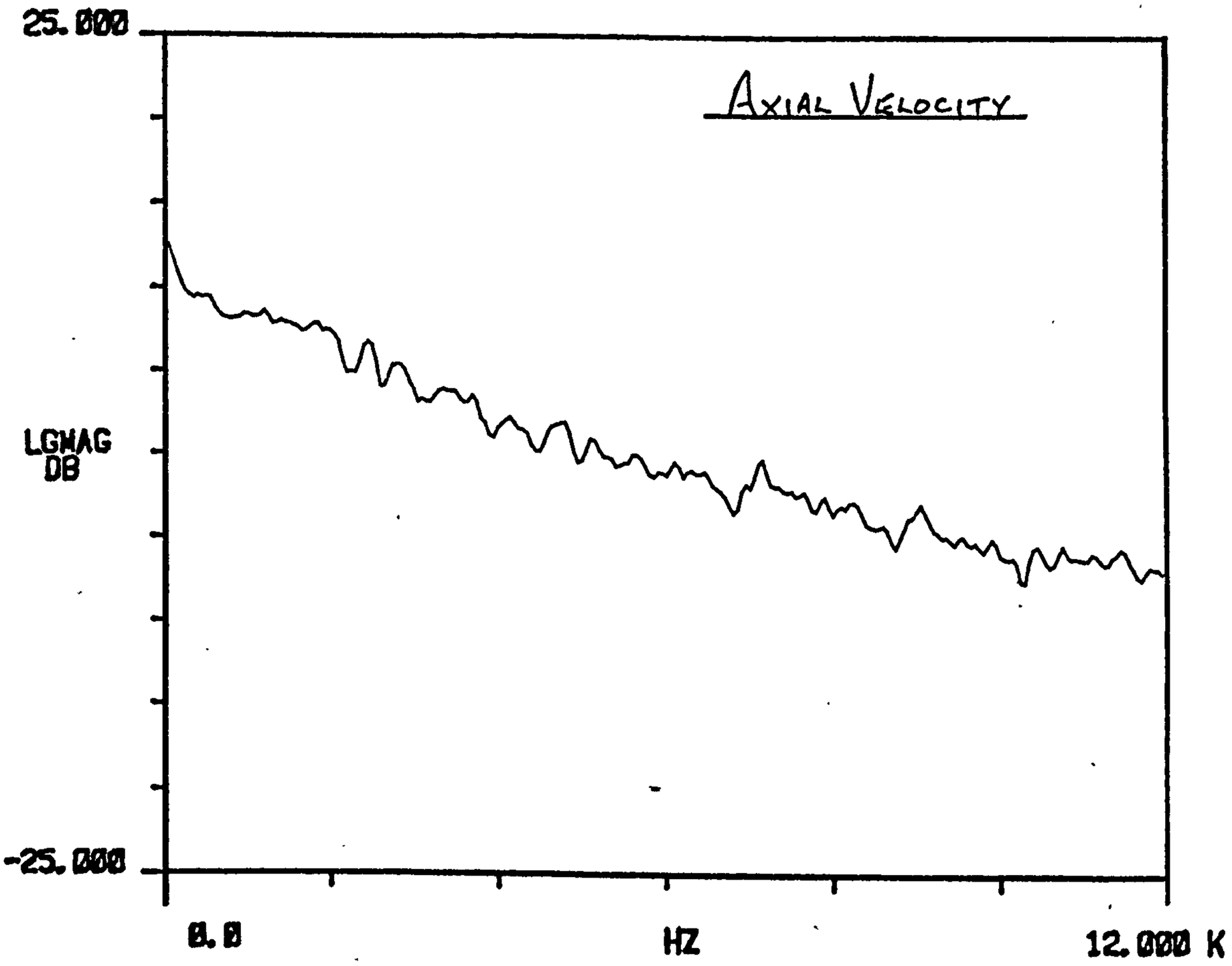

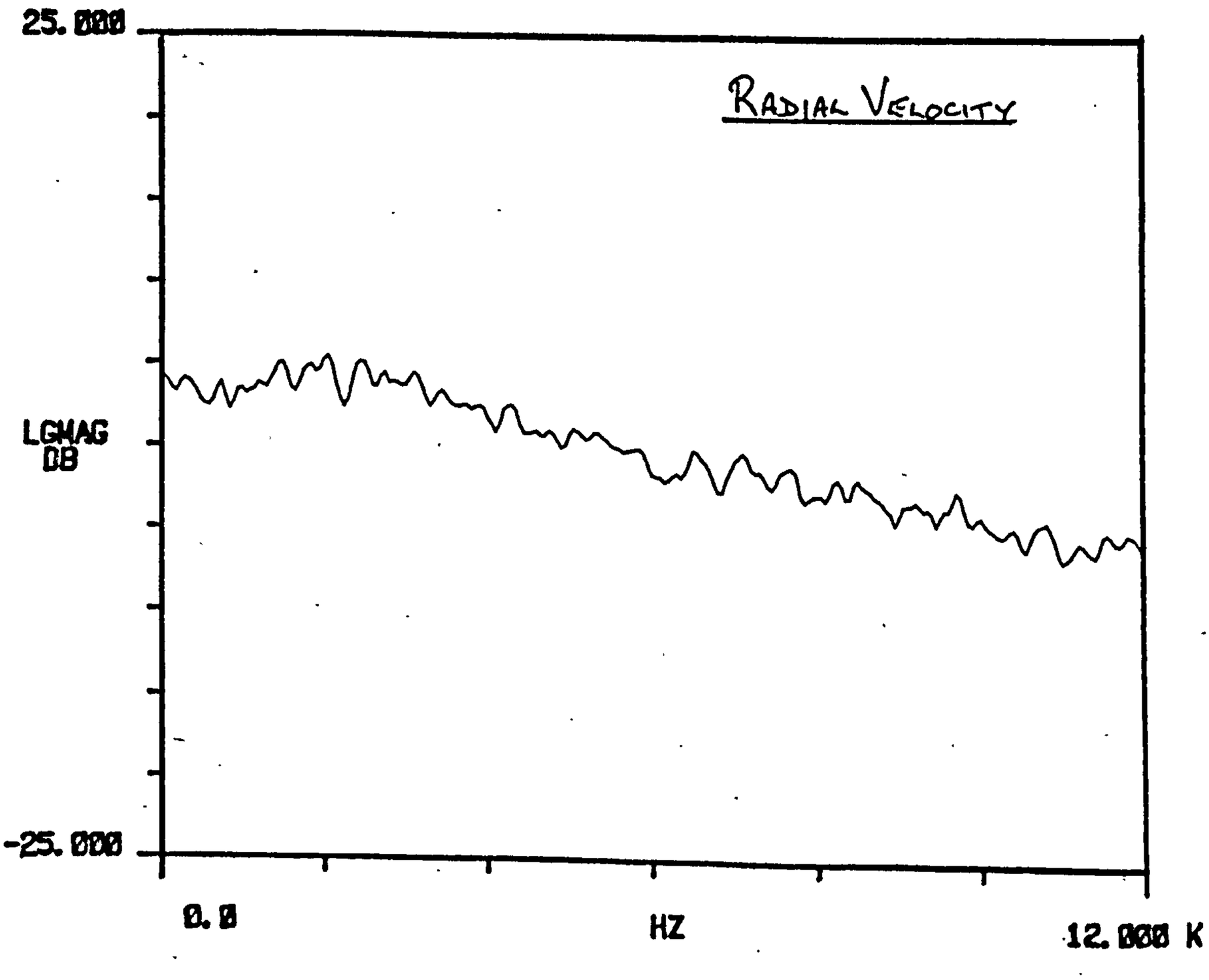

FIGURE 18 : FLUCTUATING VELOCITY SPECTRA AT X = 1D, $t = 1.095D$, UNEXCITED JET.

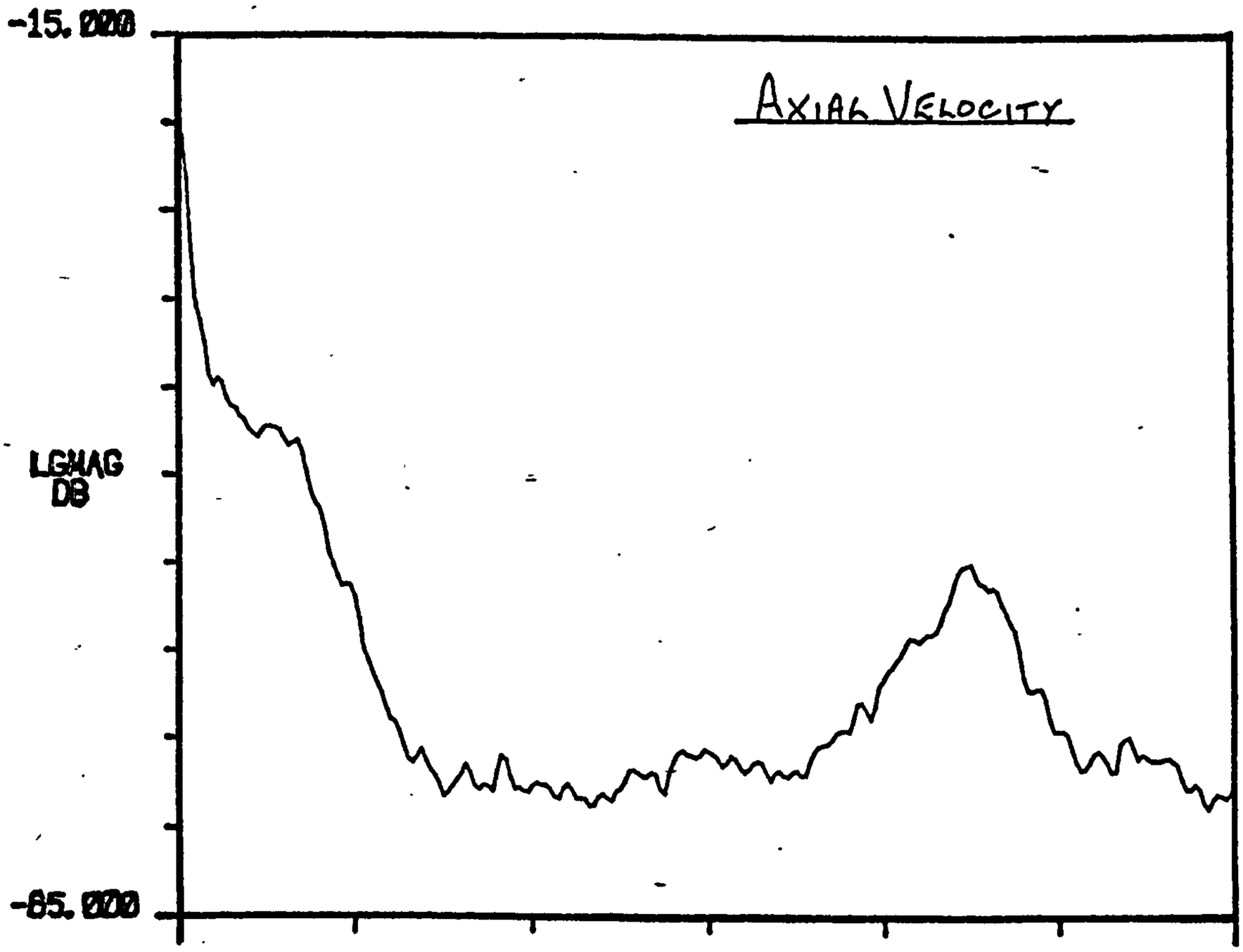

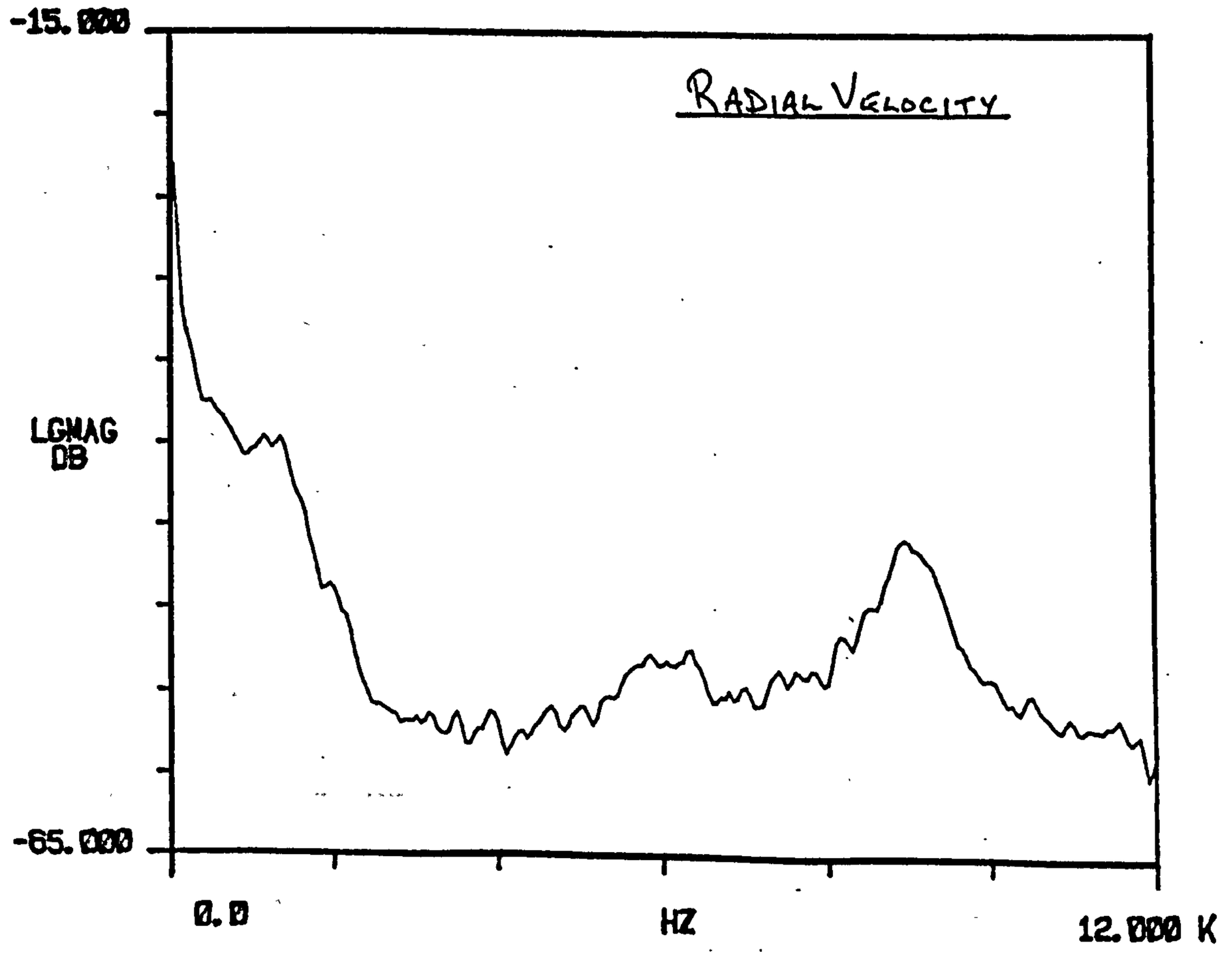

FIGURE 19 : m = 0

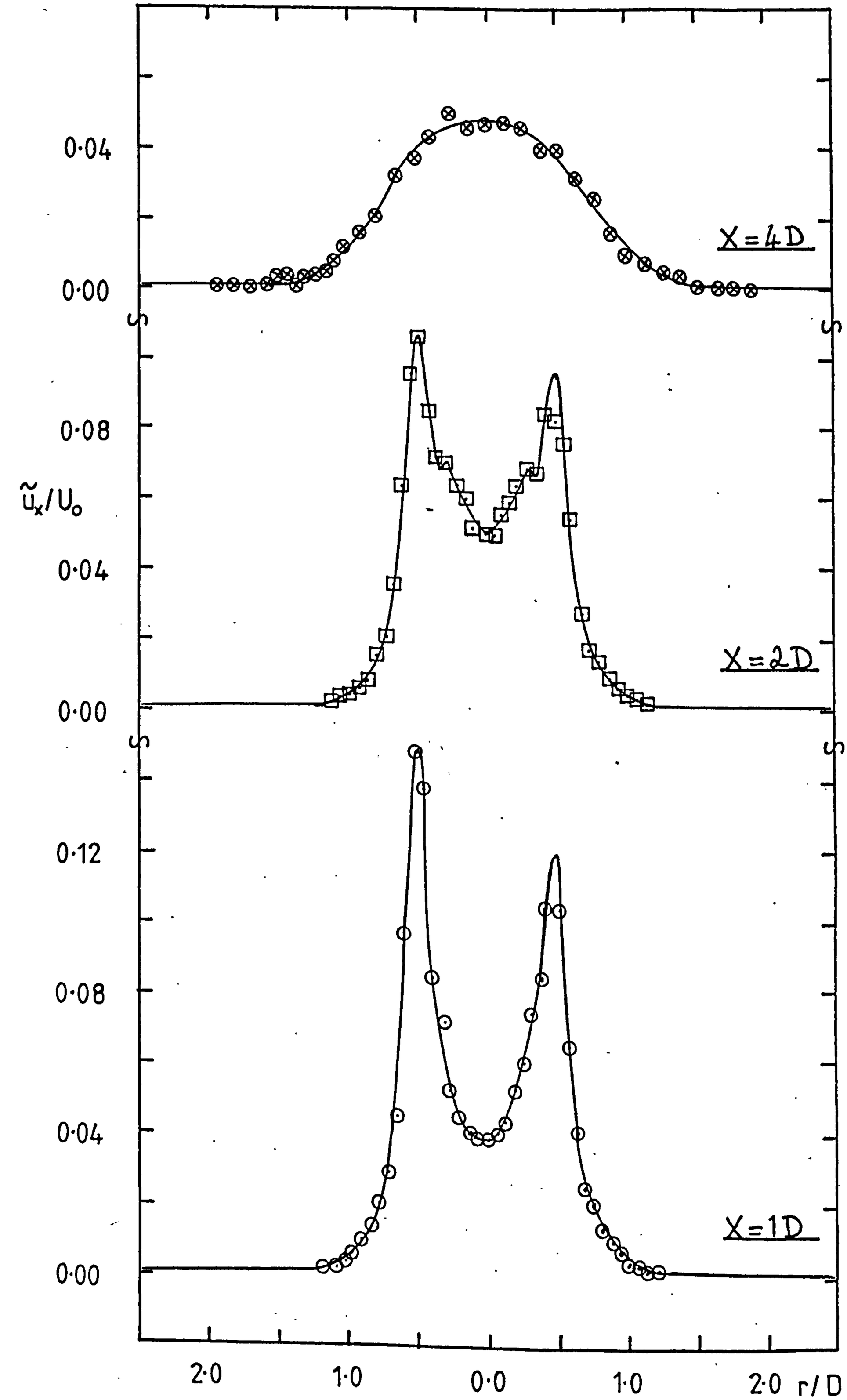
X=4D
X=2D
X=1D
$\tilde{u}_x/U_o$
0·04
0·00
0·08
0·12
0·04
0·00
0·08
0·04
0·00
2·0
1·0
0·0
1·0
2·0 r/D

FIGURE 20 : $m = 0$

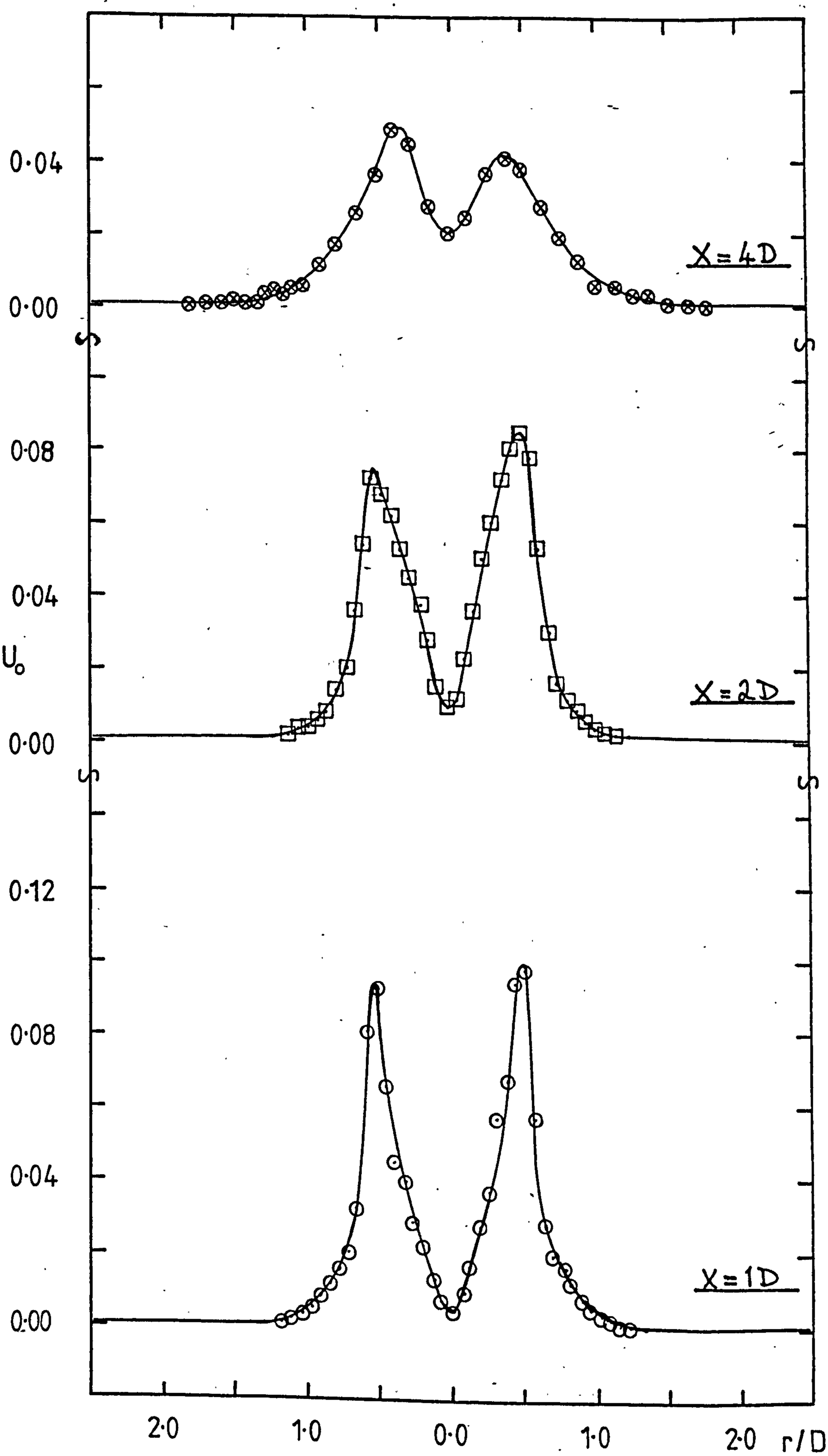

FIGURE 21 : m = +1

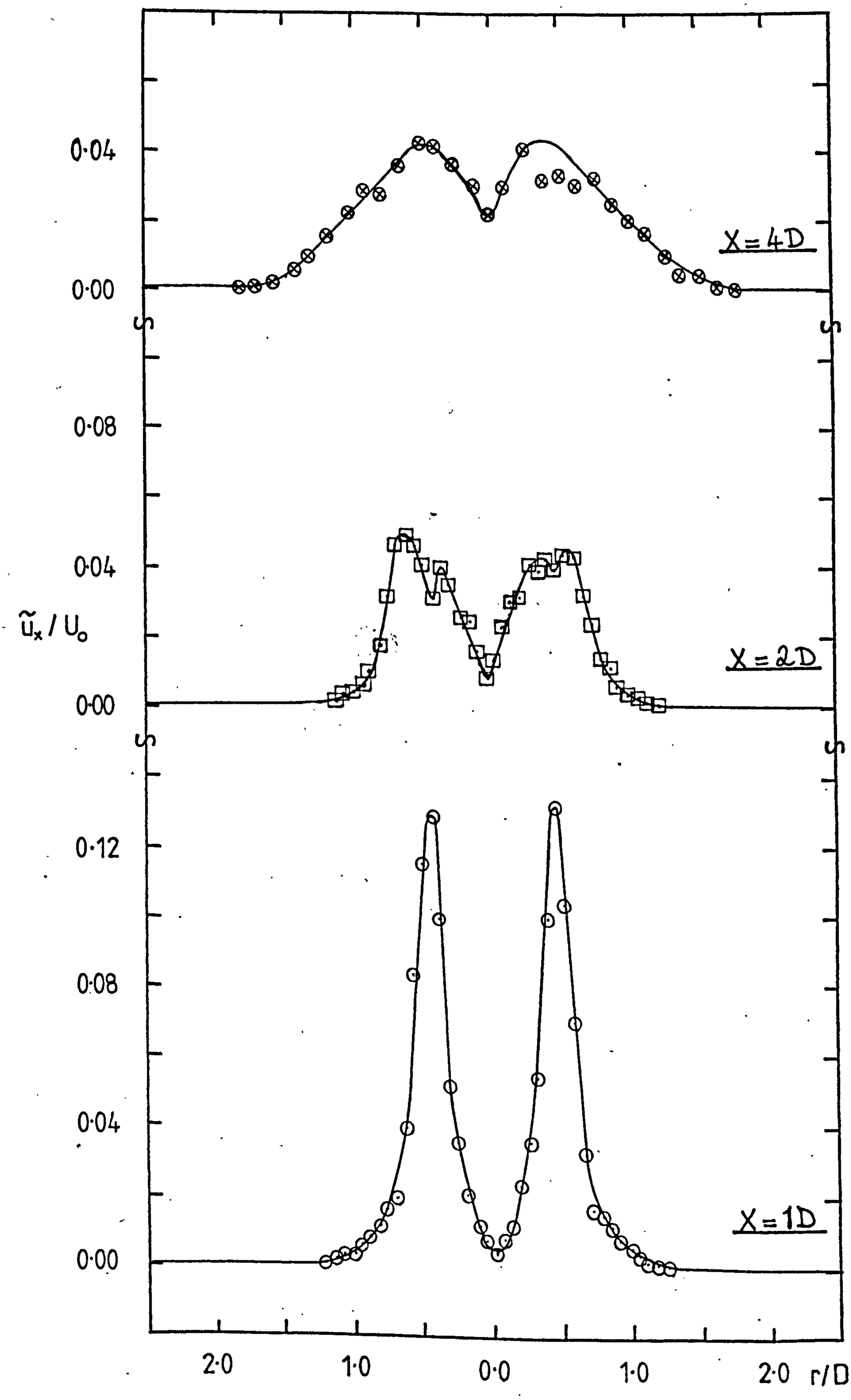
0·04
0·00
0·08
0·04
$\tilde{u}_x / U_o$
0·00
0·12
0·08
0·04
0·00
X=4D
X=2D
X=1D
2·0
1·0
0·0
1·0
2·0
r/D

FIGURE 22 : m = +1

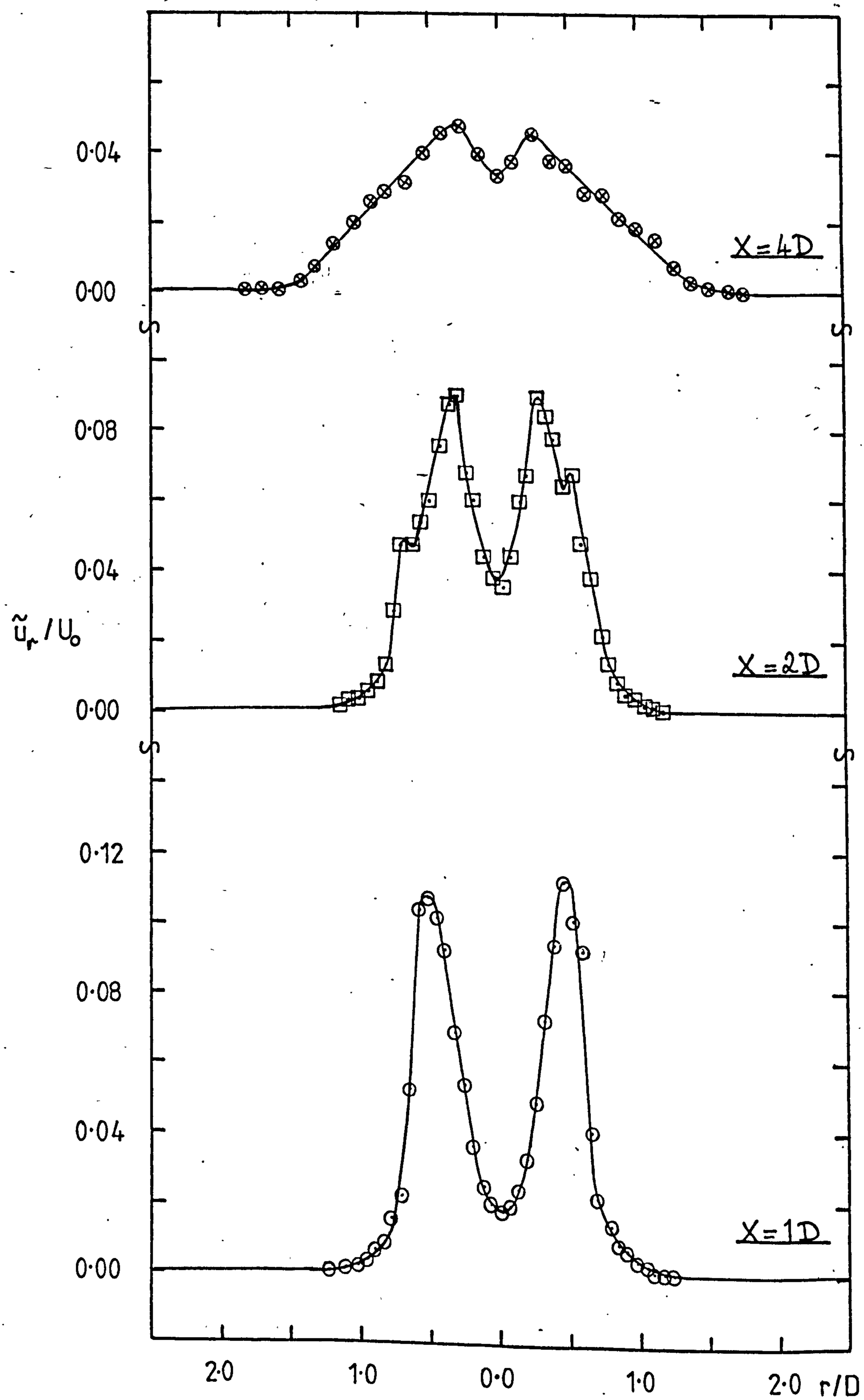
0·04
0·00
0·08
0·04
$\tilde{u}_r / U_o$
0·00
0·12
0·08
0·04
0·00
X=4D
X=2D
X=1D
2·0
1·0
0·0
1·0
2·0 r/D

FIGURE 23 : $m = \pm 1$ (MAX.)

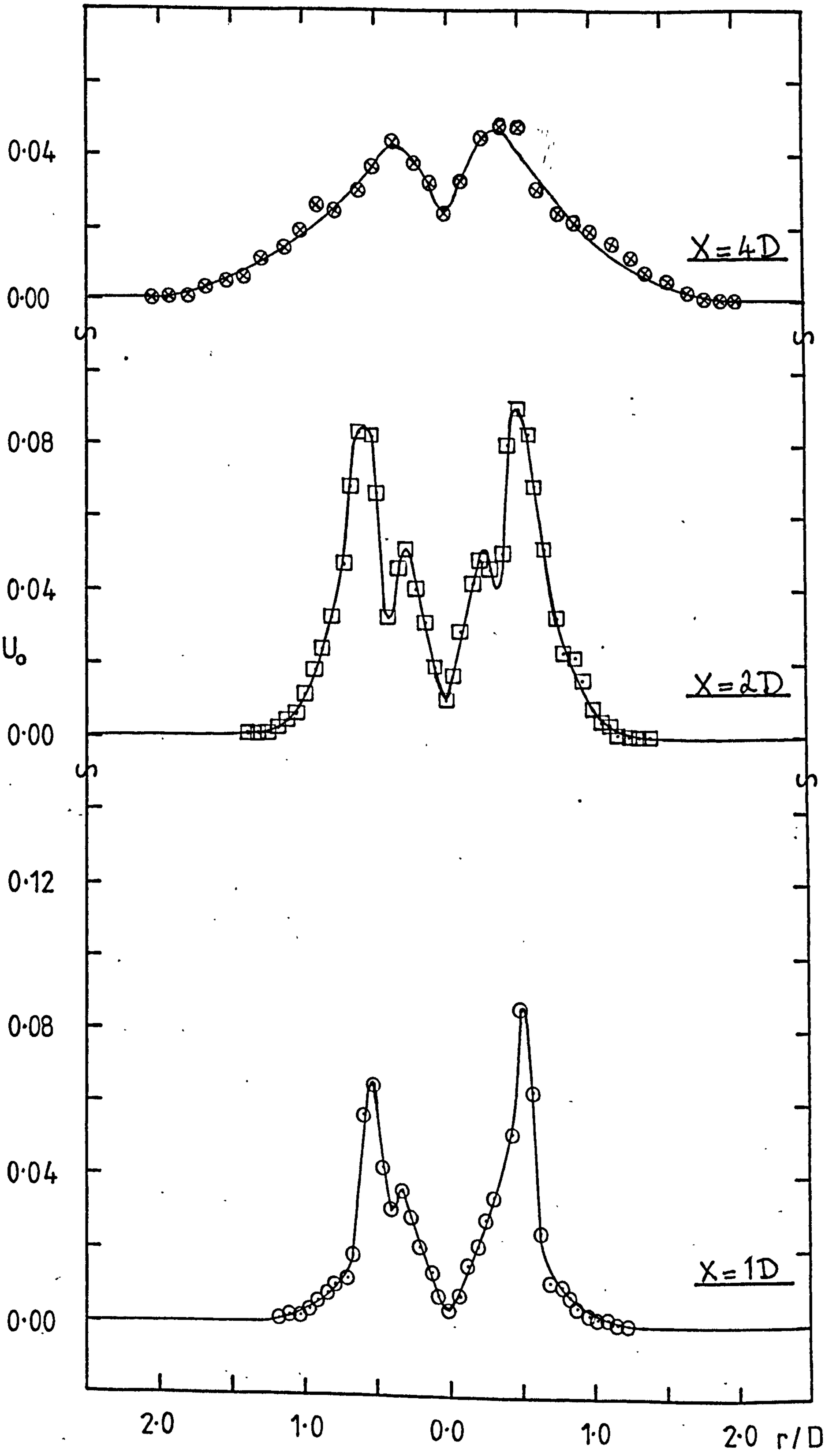

FIGURE 24 : m = ±1 (MAX.)

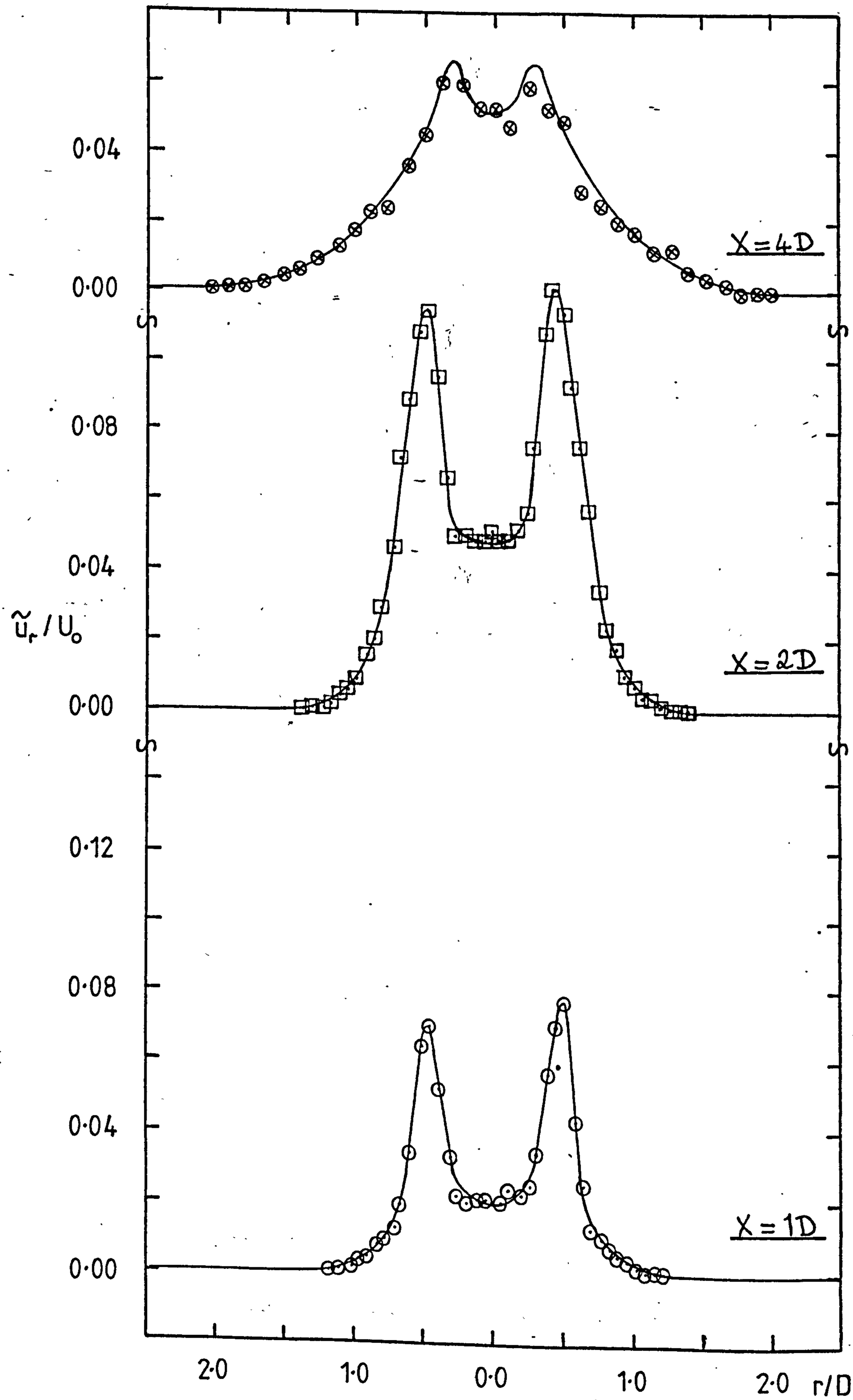

FIGURE 25 : m=±2 (MAX.)

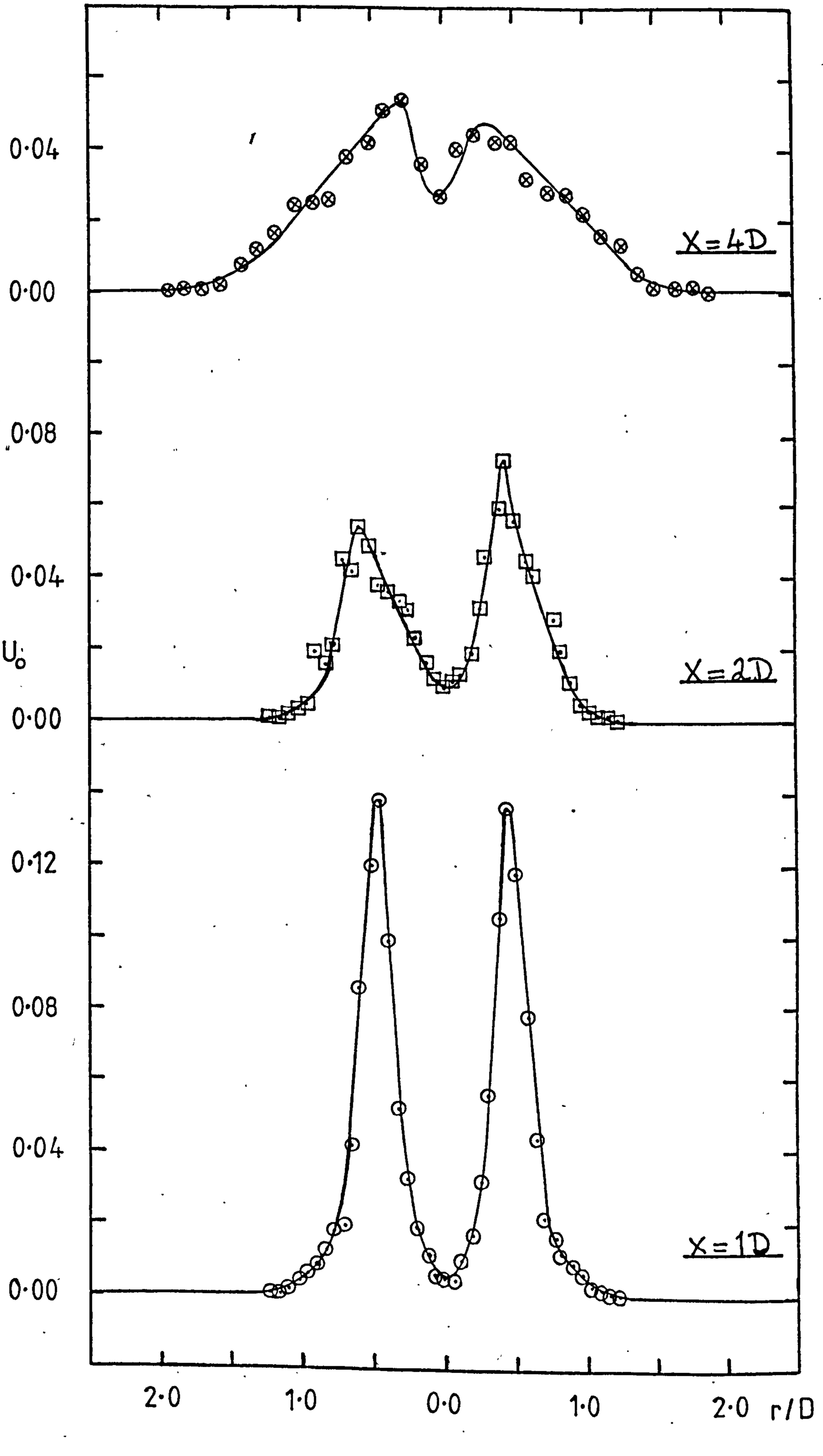

FIGURE 26 : m=±2 (MAX.)

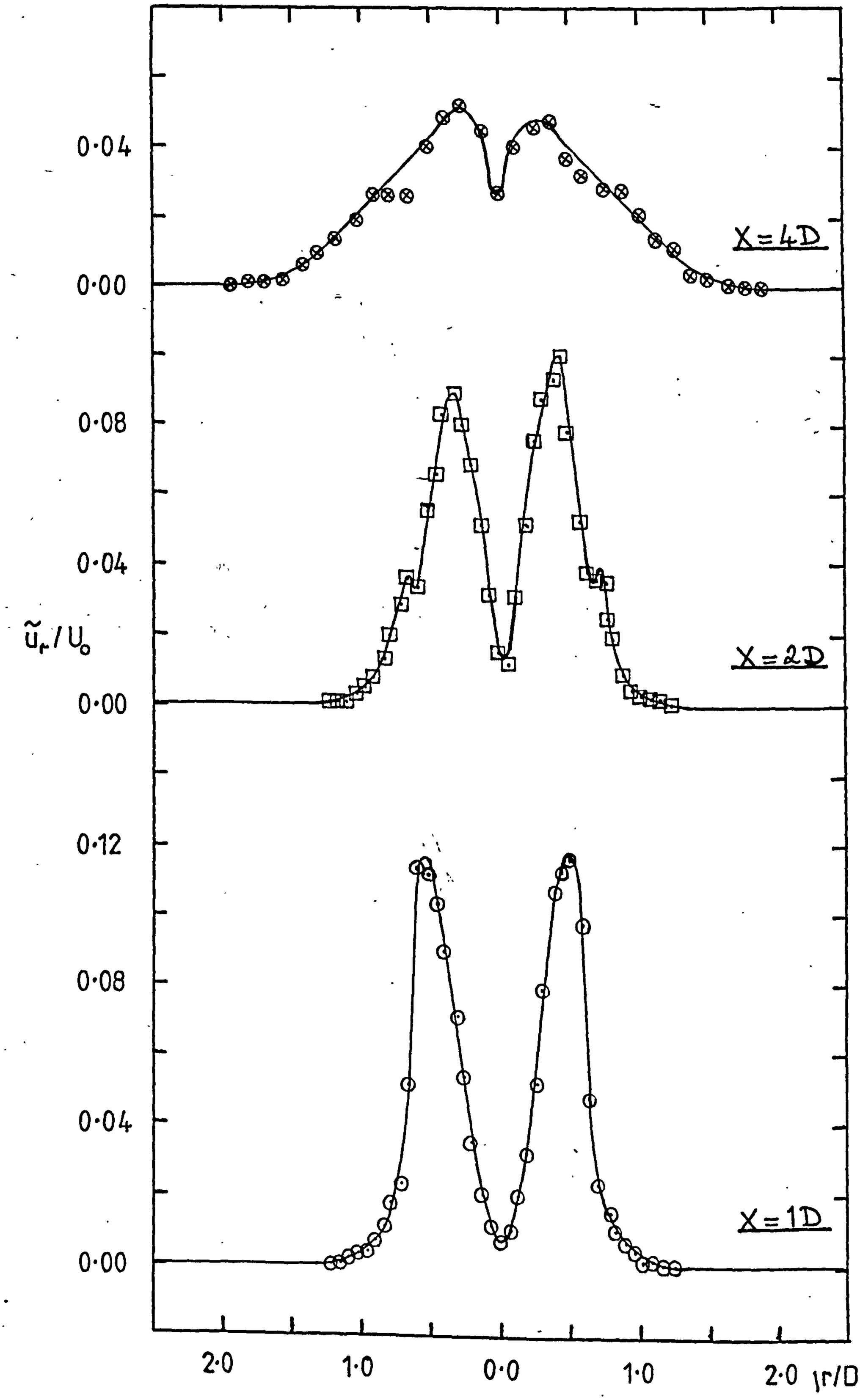

FIGURE 27 : $m = \pm 2$ (MIN.)

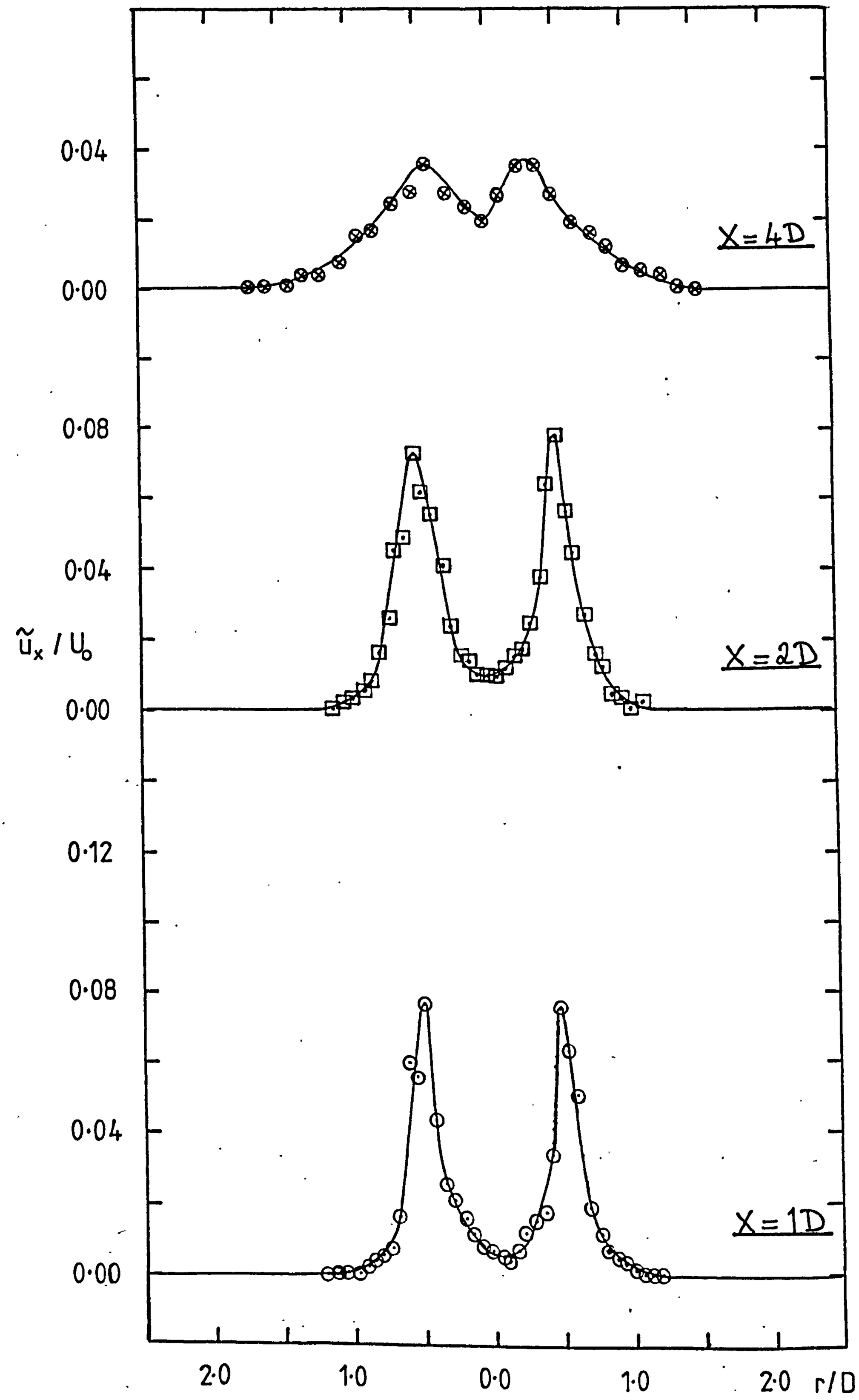

FIGURE 28 : m=±2 (MIN.)

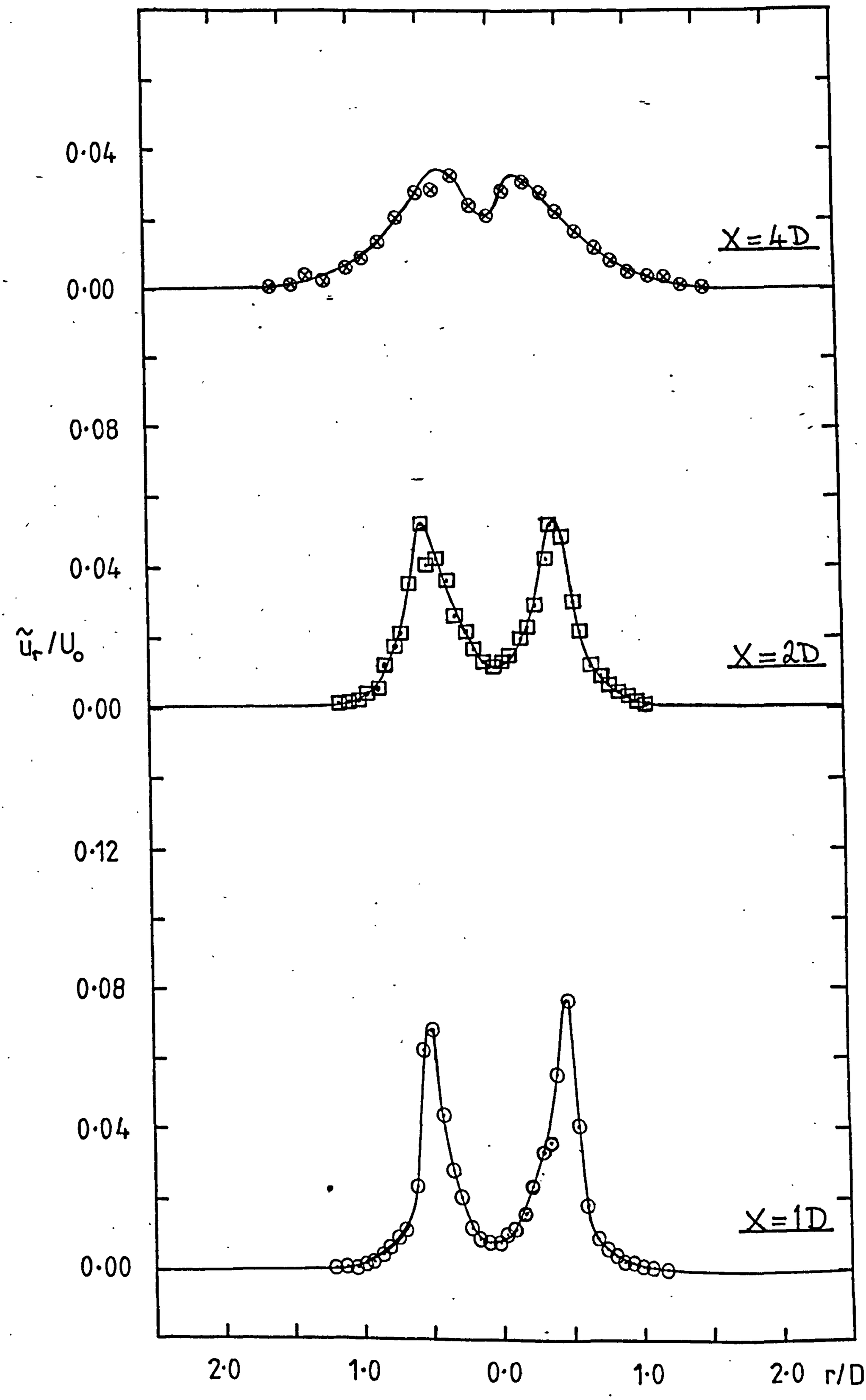

FIGURE 29

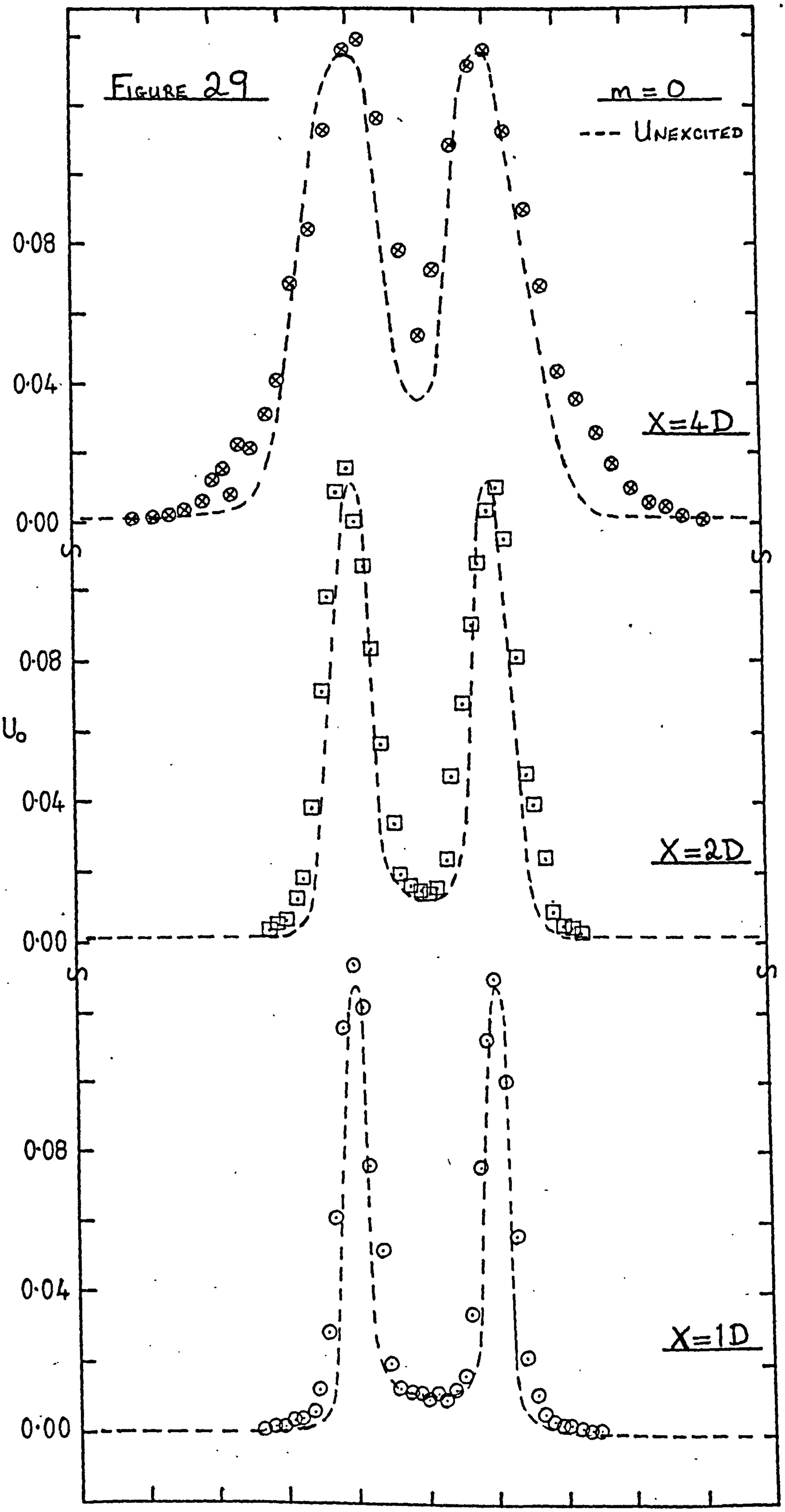
m = 0
--- UNEXCITED
X=4D
X=2D
X=1D
0·08
0·04
0·00
0·08
0·04
0·00
0·08
0·04
0·00
u'_x / U_o
2·0
1·0
0·0
1·0
2·0
r/D

FIGURE 30

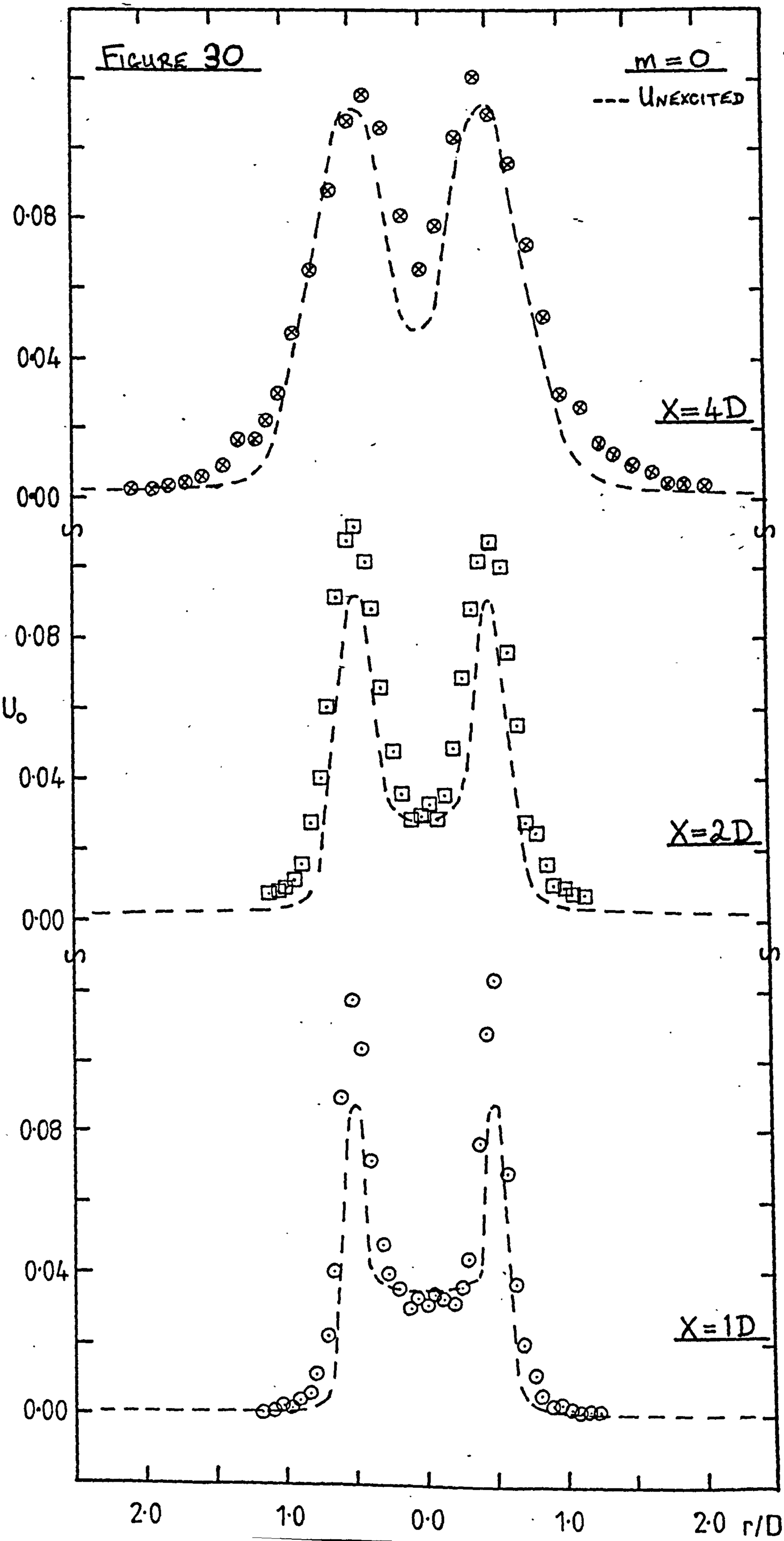
m = 0
--- UNEXCITED
X=4D
X=2D
X=1D
0·08
0·04
0·00
0·08
0·04
0·00
0·08
0·04
0·00
u_r'/U_o
2·0
1·0
0·0
1·0
2·0
r/D

FIGURE 31

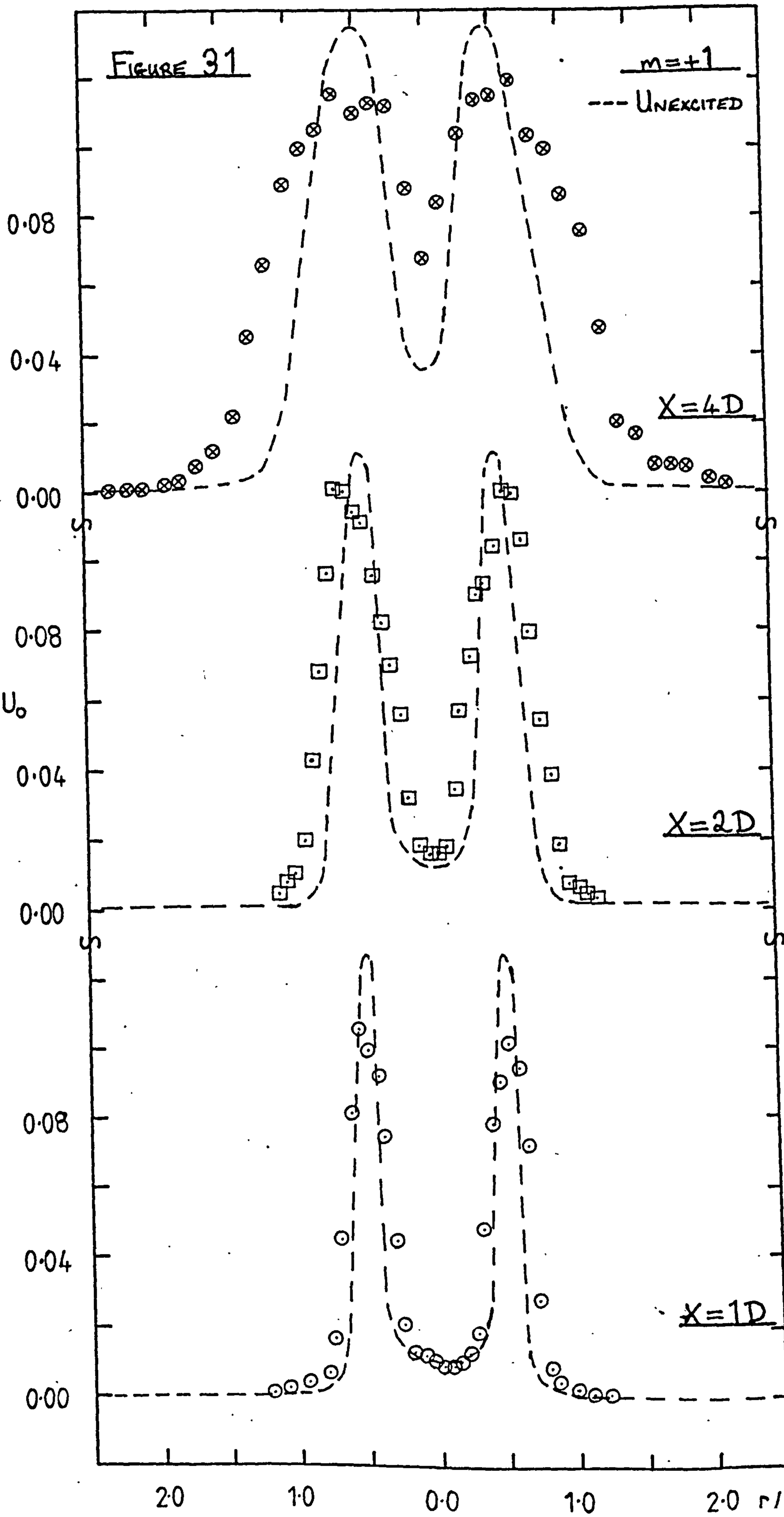
m=±1
--- UNEXCITED
X=4D
X=2D
X=1D
0·08
0·04
0·00
0·08
u'_x / U_o
0·04
0·00
0·08
0·04
0·00
2·0
1·0
0·0
1·0
2·0 r / D

FIGURE 32

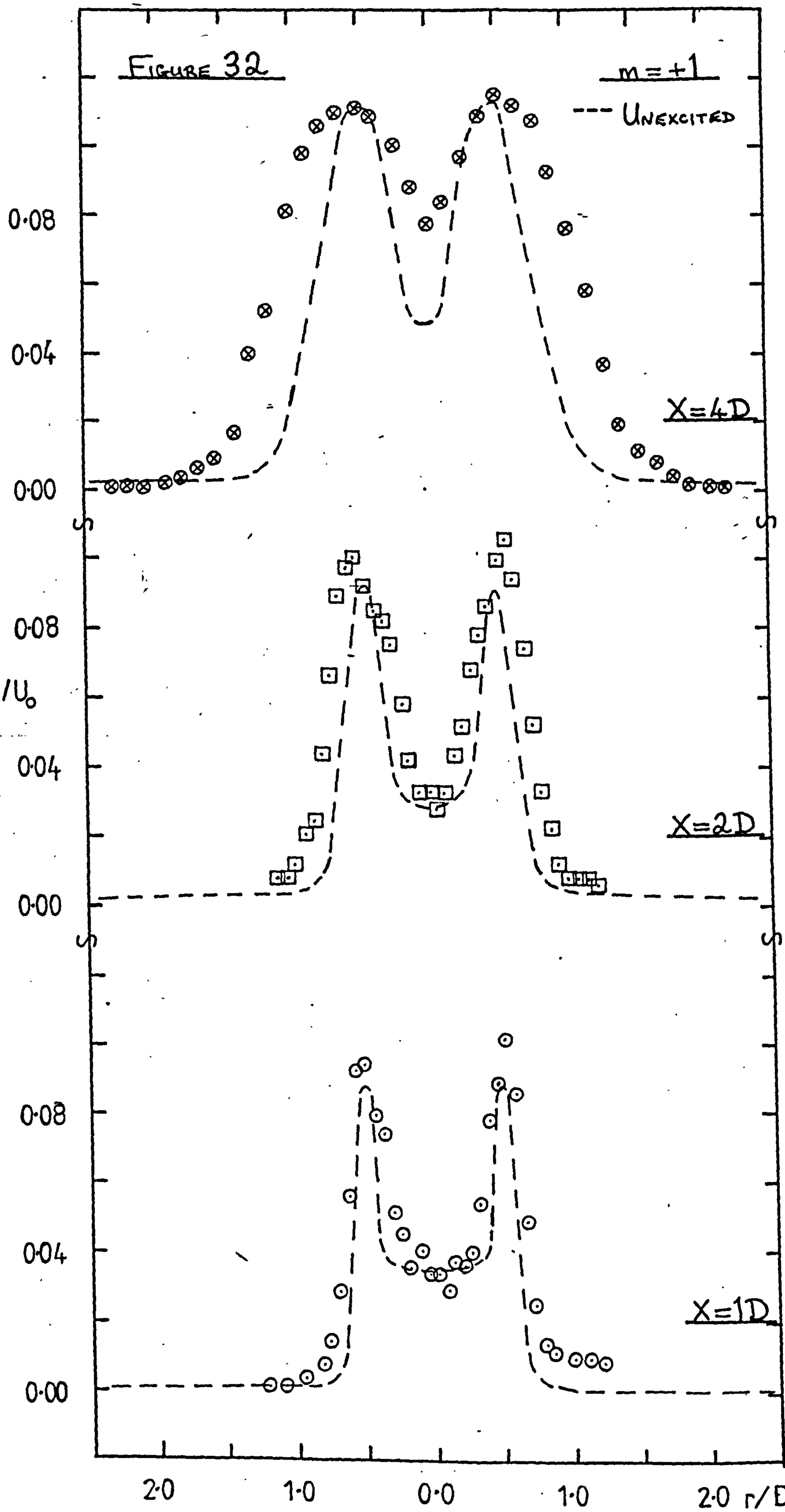
n=+1
--- UNEXCITED
X=4D
X=2D
X=1D
0·08
0·04
0·00
0·08
0·04
0·00
0·08
0·04
0·00
u'_r/U_o
2·0
1·0
0·0
1·0
2·0 r/D

FIGURE 33

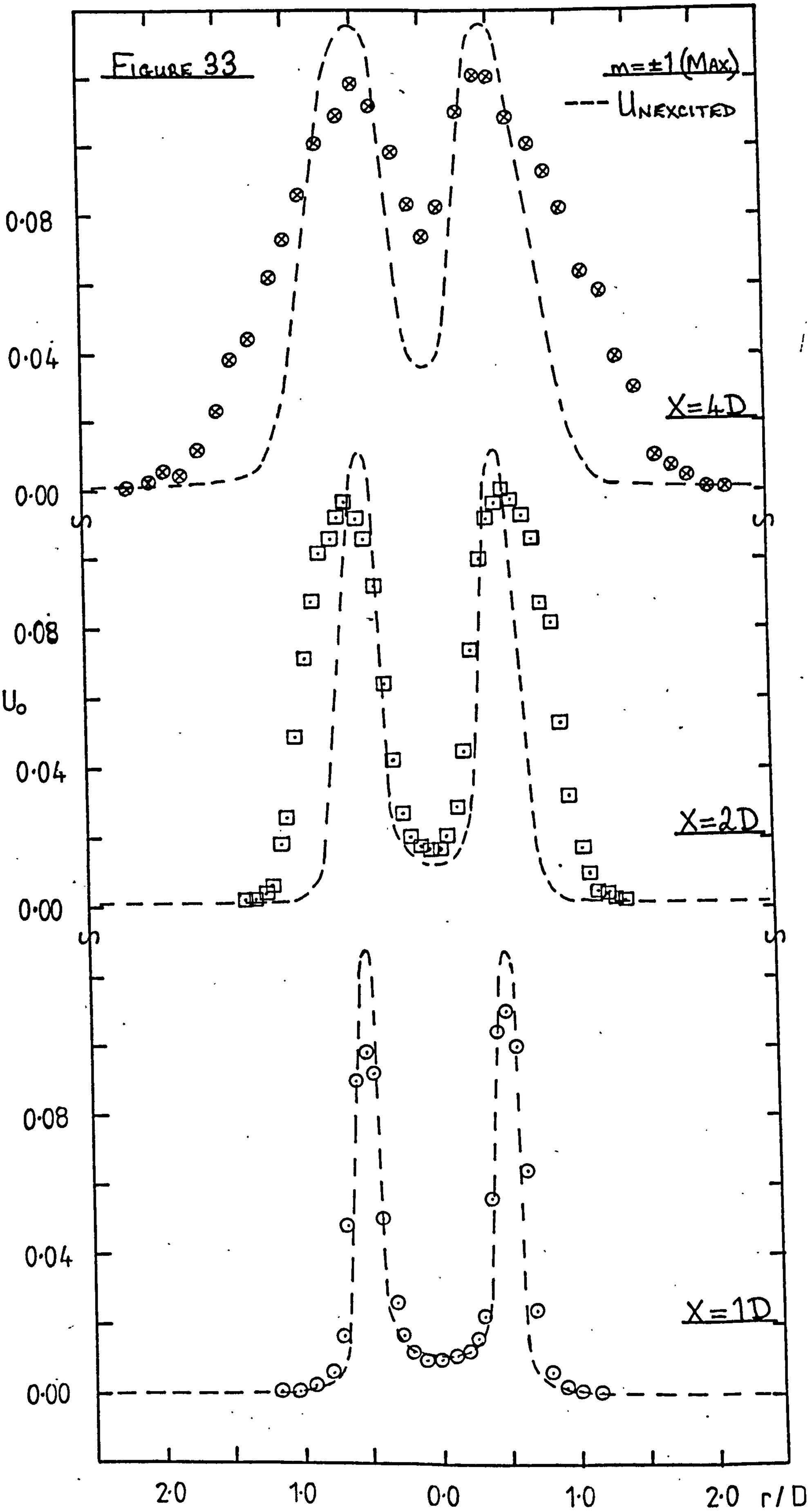
m=±1 (MAX.)
--- UNEXCITED
X=4D
X=2D
X=1D
0·08
0·04
0·00
0·08
u'_x / U_o
0·04
0·00
0·08
0·04
0·00
2·0
1·0
0·0
1·0
2·0
r / D

FIGURE 34

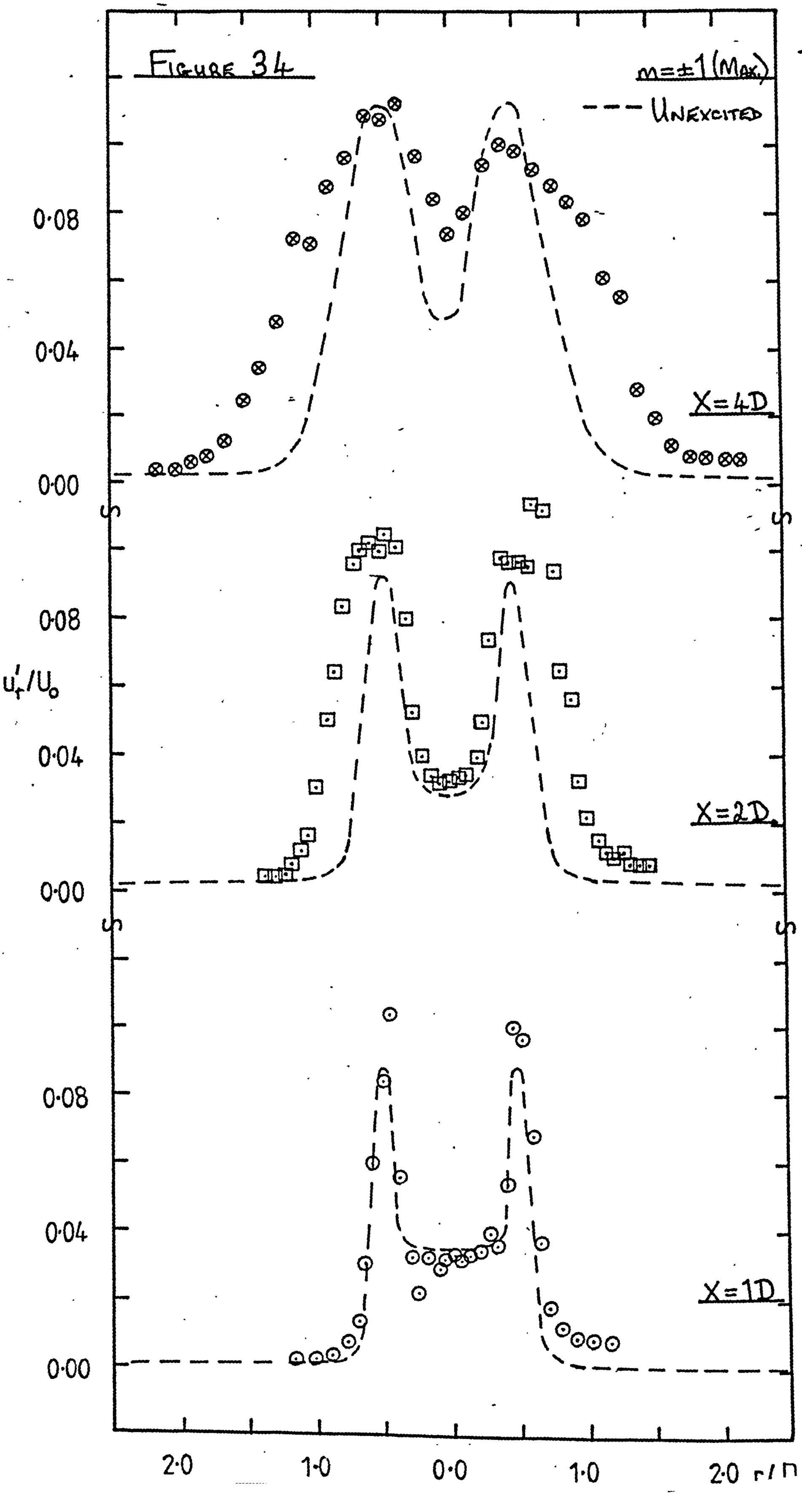

FIGURE 35

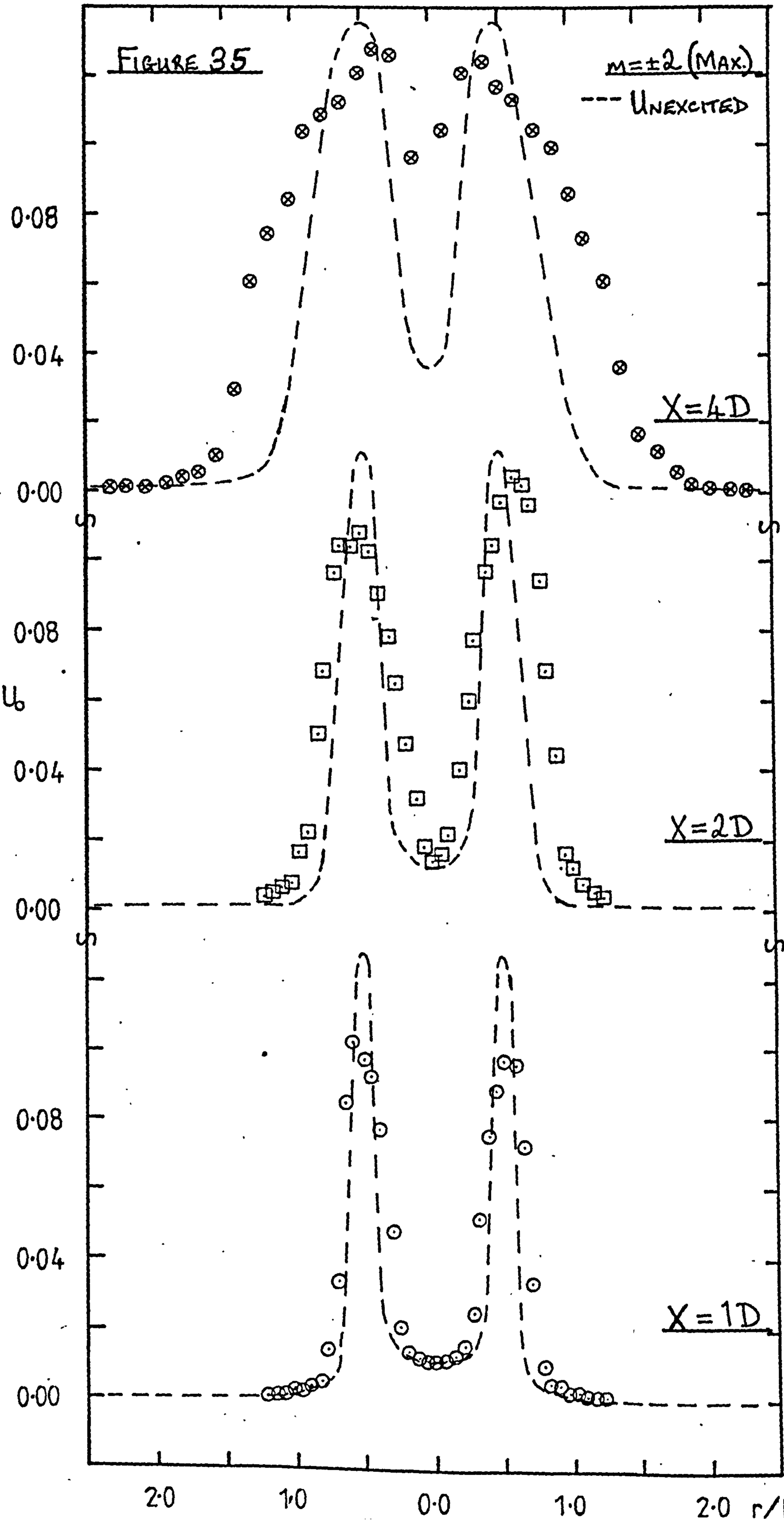
M=±2 (MAX.)
--- UNEXCITED
X=4D
X=2D
X=1D
0·08
0·04
0·00
0·08
0·04
0·00
0·08
0·04
0·00
u'_x / U_0
2·0
1·0
0·0
1·0
2·0
r/D

FIGURE 36

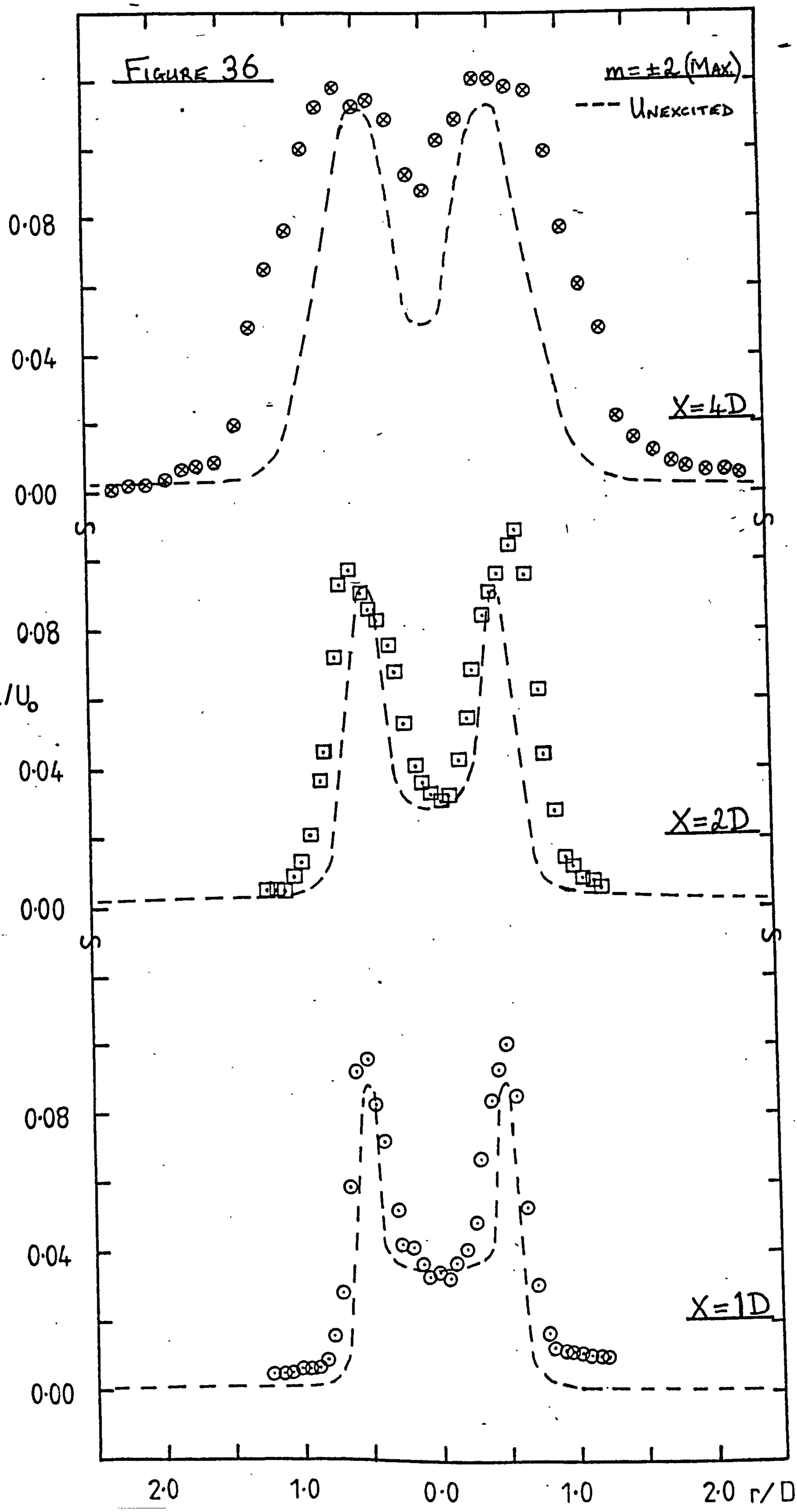
m = ±2 (MAX.)
--- UNEXCITED
X=4D
X=2D
X=1D
0·08
0·04
0·00
0·08
0·04
0·00
0·08
0·04
0·00
u_r'/U_o
2·0
1·0
0·0
1·0
2·0 r/D

FIGURE 37

m=±2 (Min.)
--- Unexcited
X=4D
X=2D
X=1D
u'x / U0
0·10
0·08
0·04
0·00
0·08
0·04
0·00
0·08
0·04
0·00
2·0
1·0
0·0
1·0
2·0 r/D

FIGURE 38

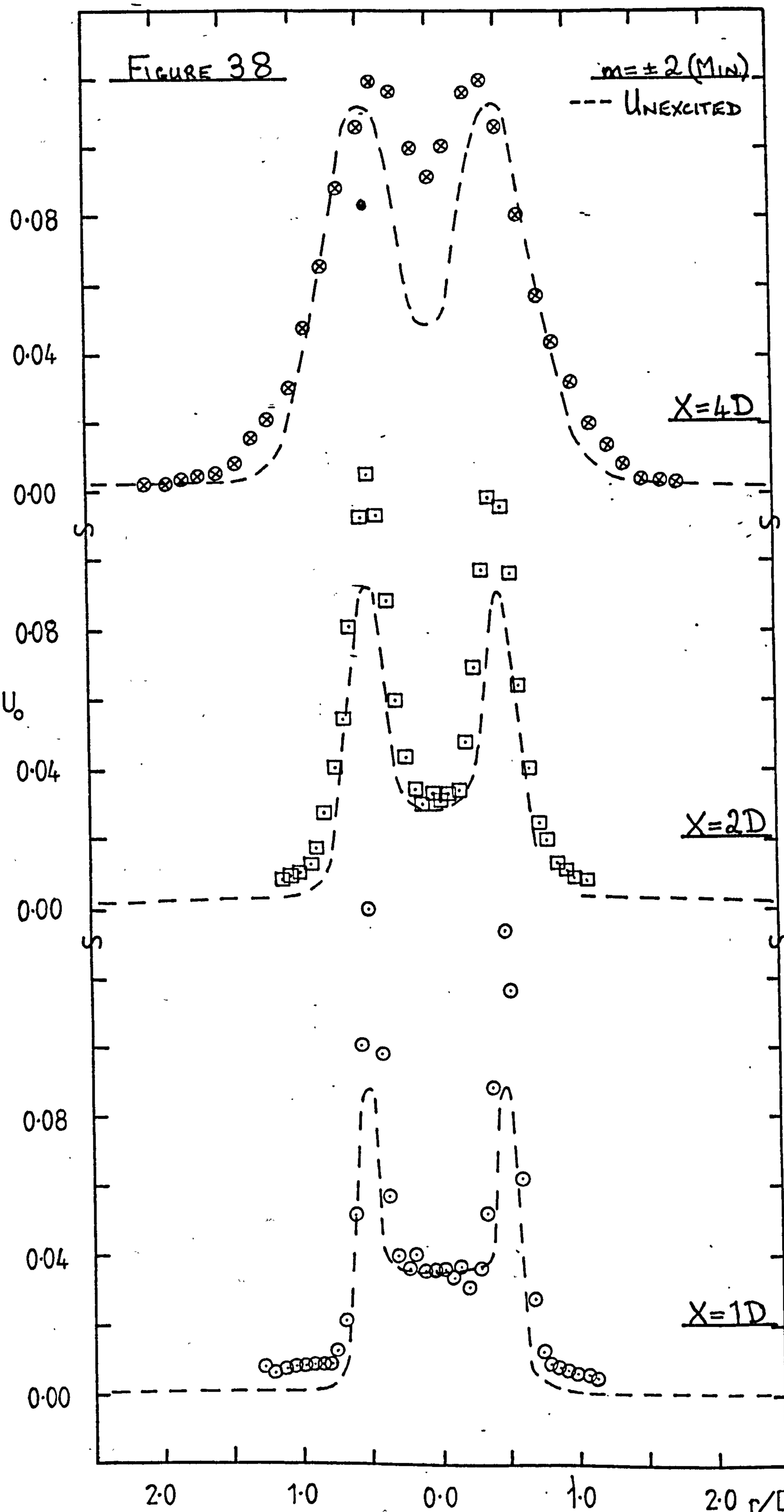
m=±2 (MIN.)
--- UNEXCITED
X=4D
X=2D
X=1D
0·08
0·04
0·00
0·08
0·04
0·00
0·08
0·04
0·00
u'_r/U_o
2·0
1·0
0·0
1·0
2·0 r/D

FIGURE 39: FLUCTUATING VELOCITY SPECTRA AT X=1D, r=1.159D, ±1 MODE, MAXIMUM WIDTH

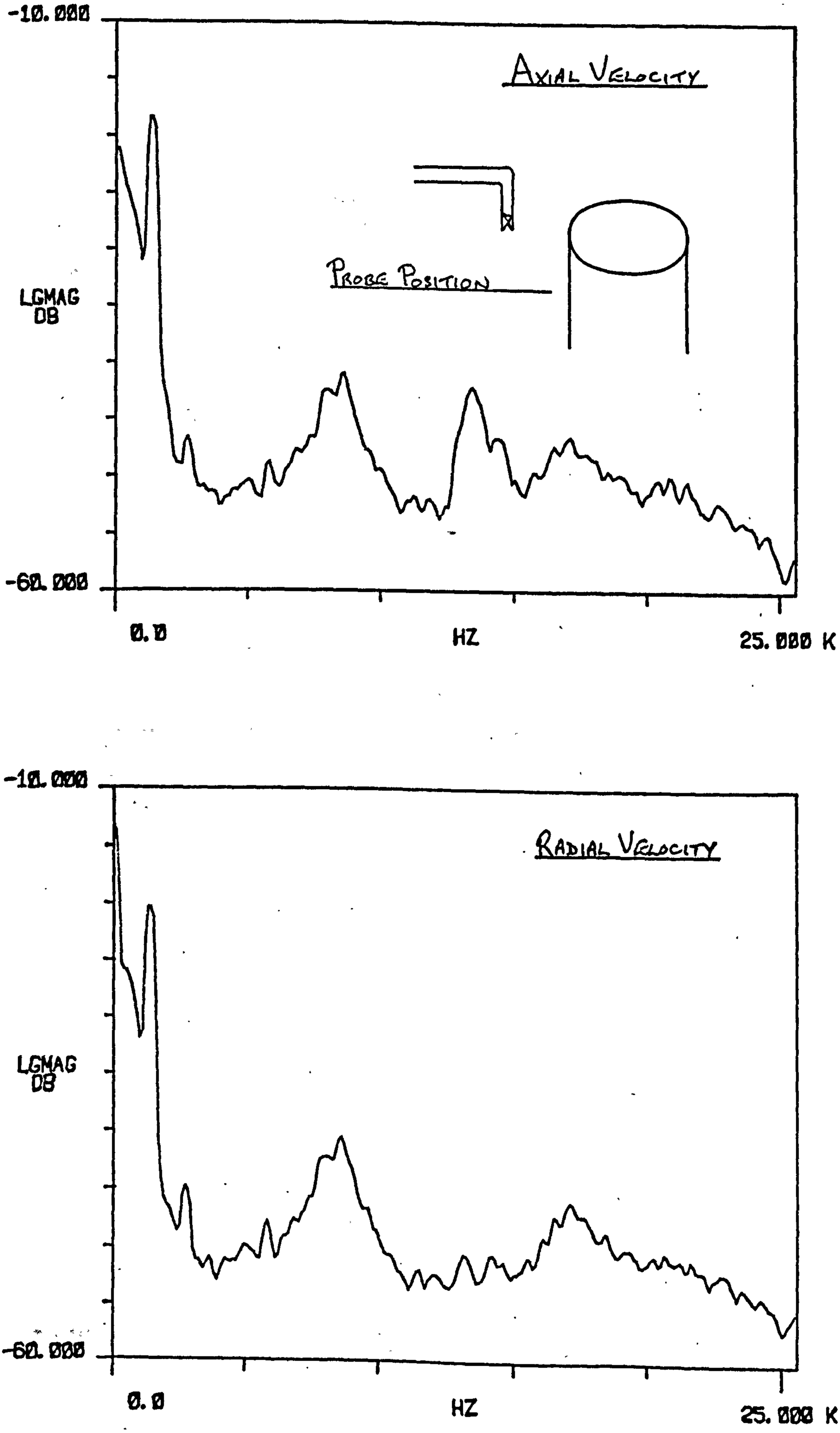

FIGURE 40: FLUCTUATING VELOCITY SPECTRA AT X=1D, r=1.159D, ±1 MODE, MAXIMUM WIDTH

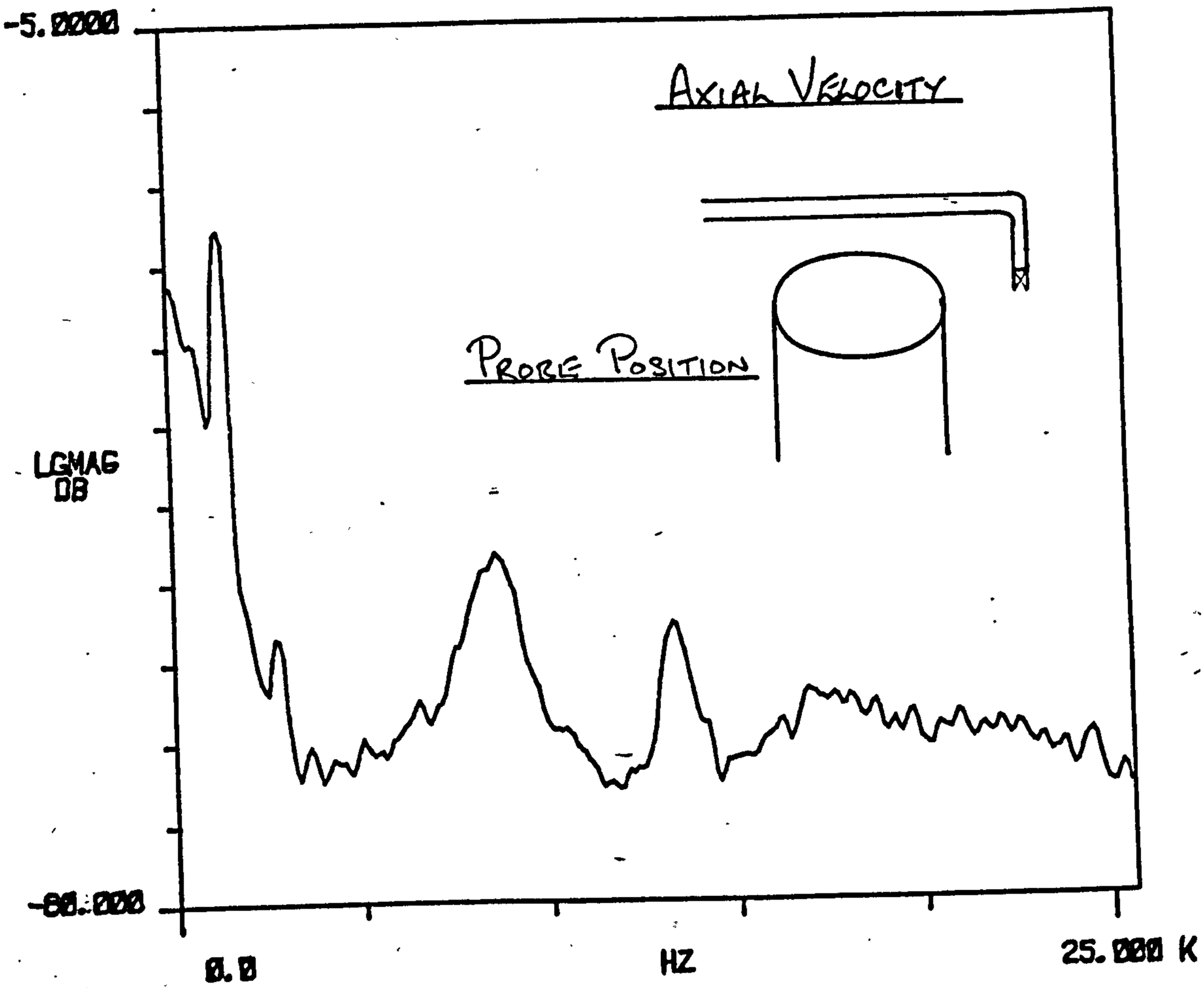

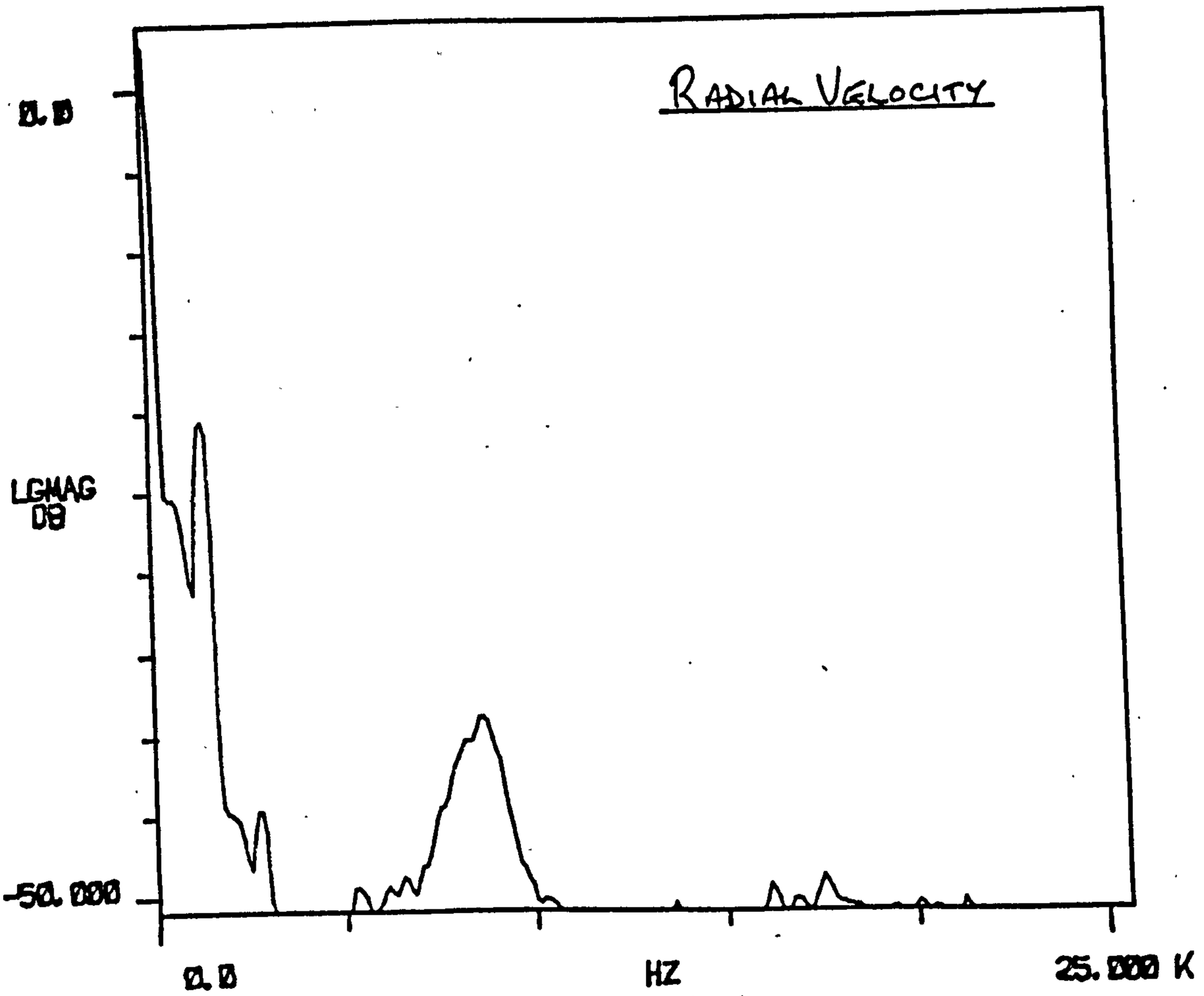

FIGURE 47: VARIATION OF MEAN VELOCITY PROFILE WITH AXIAL DISTANCE AT M = 0·3, m = 0 (a) PITOT RESULTS

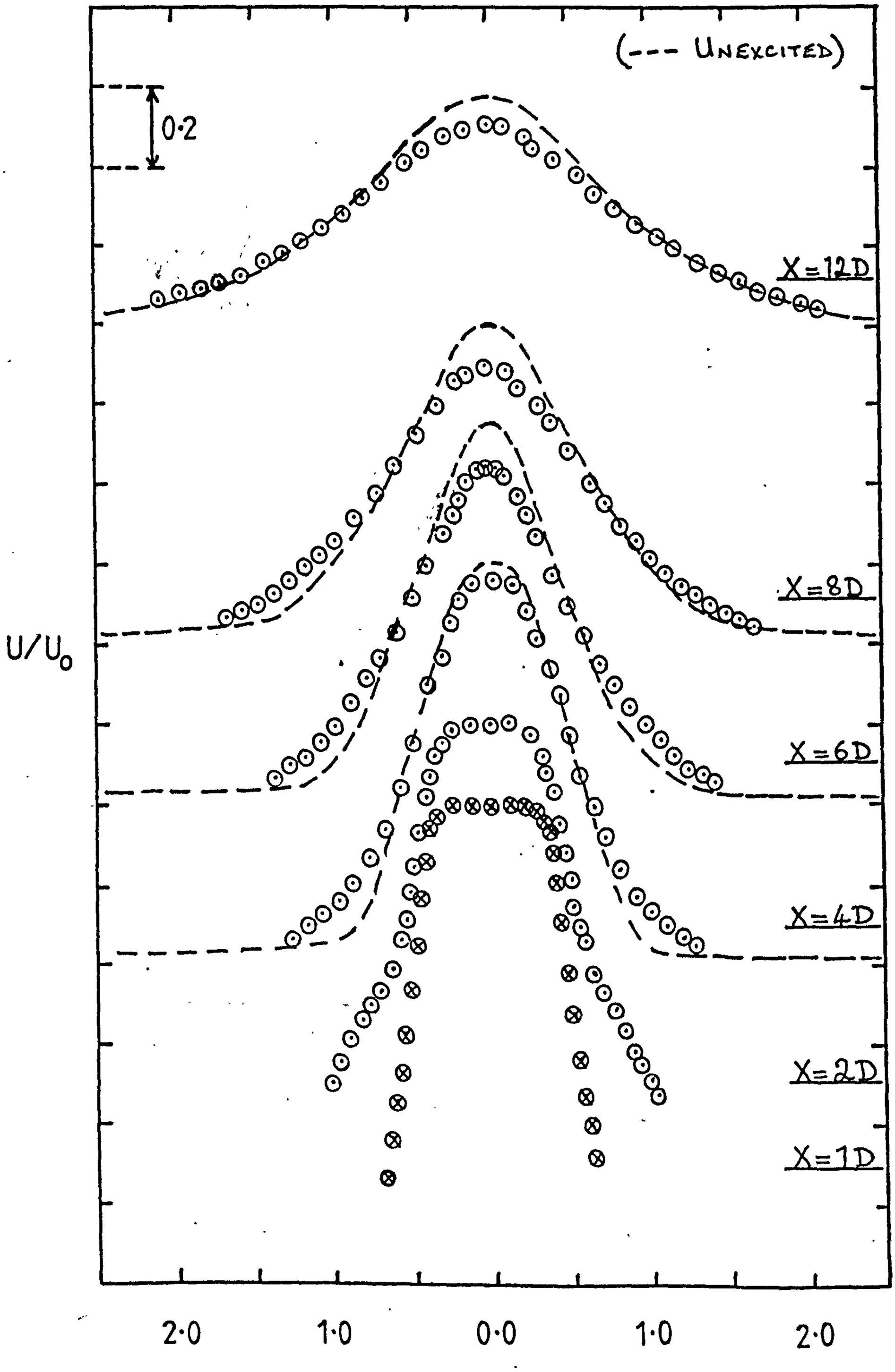

FIGURE 4.1 : (b) HOT WIRE RESULTS

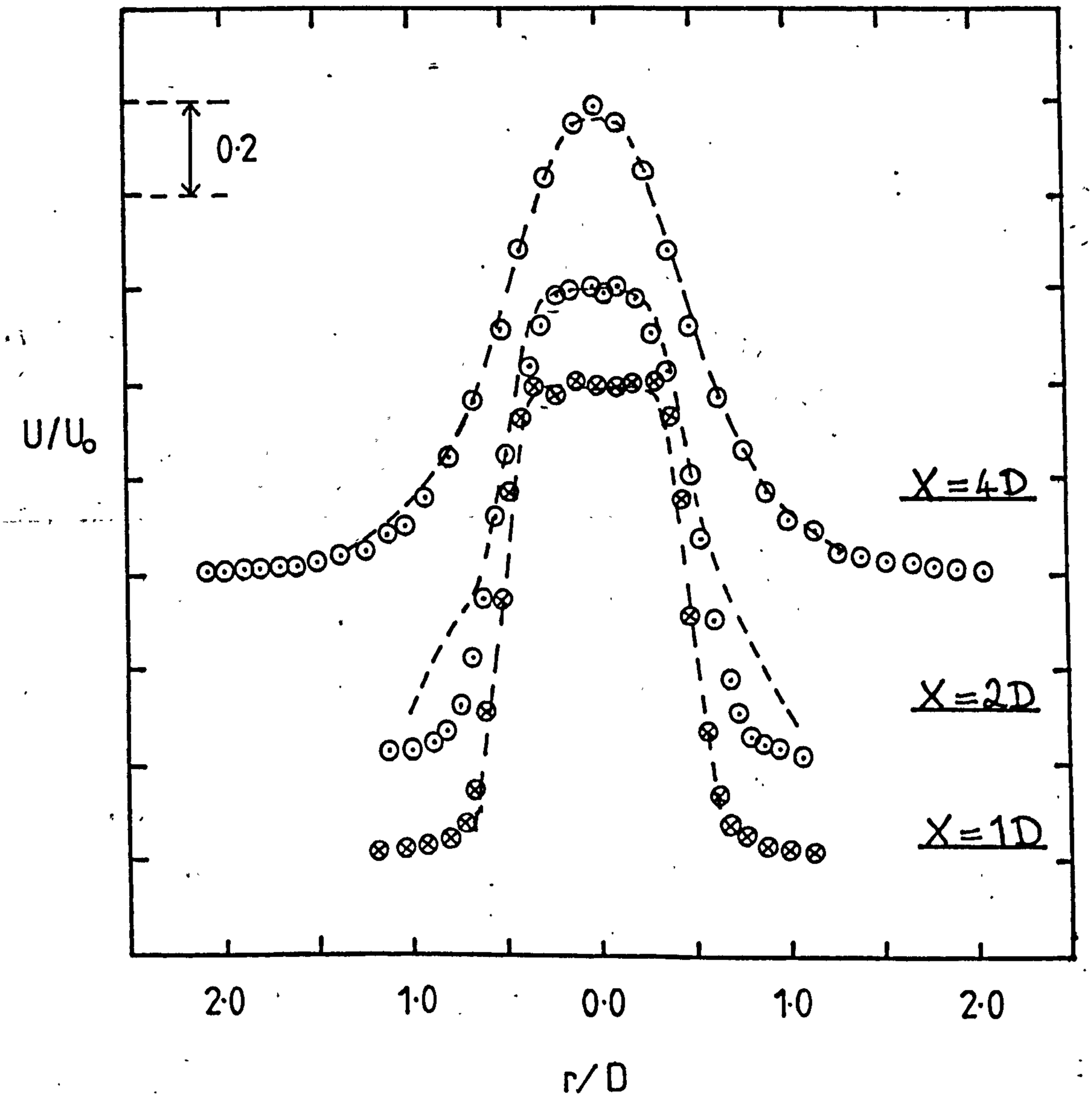

(--- PITOT RESULTS)

FIGURE 42 : VARIATION OF MEAN VELOCITY PROFILE WITH AXIAL DISTANCE AT M=0·3, m=+1 (a) PITOT RESULTS

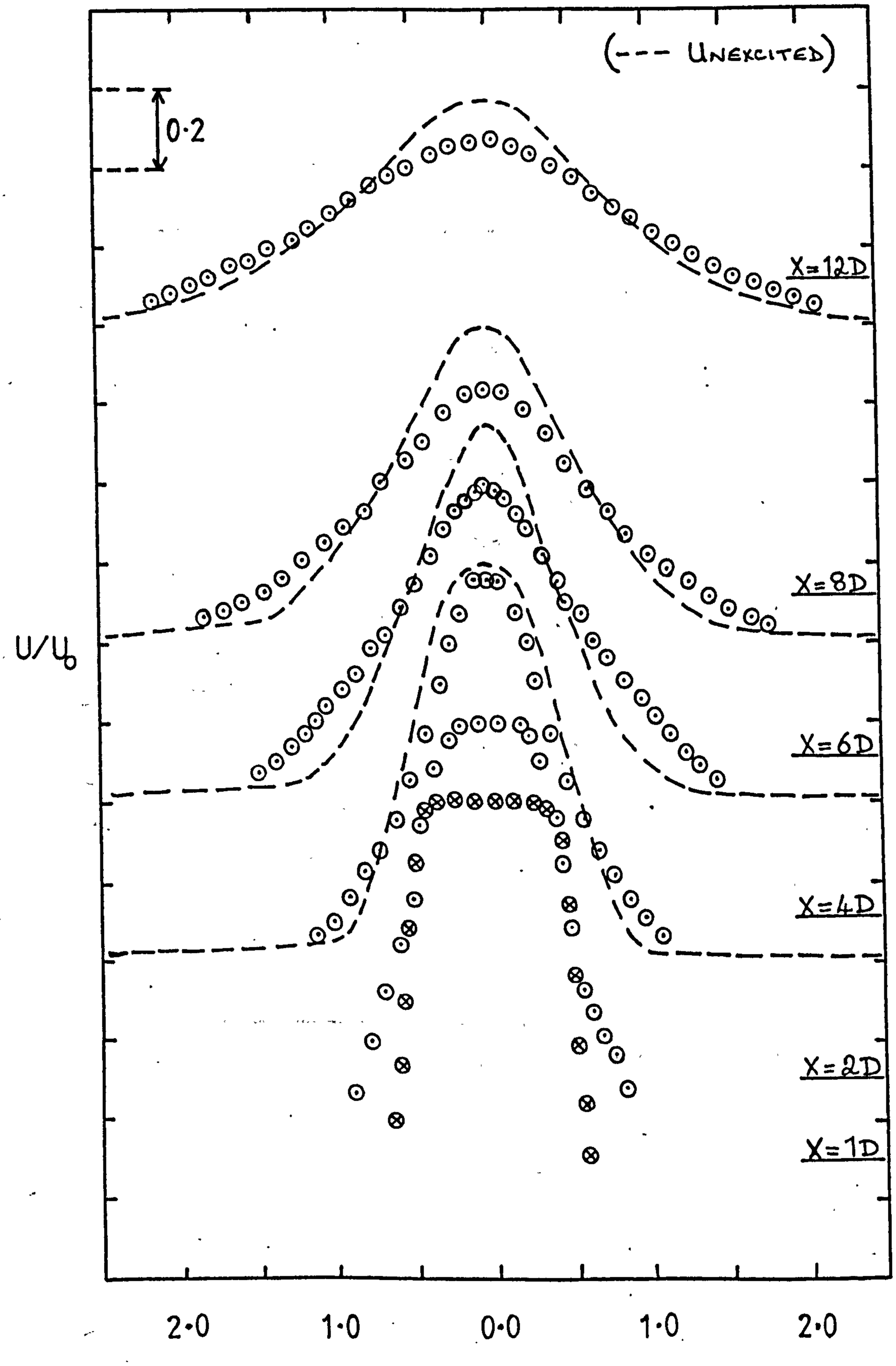

FIGURE 4.2 : (b) HOT WIRE RESULTS

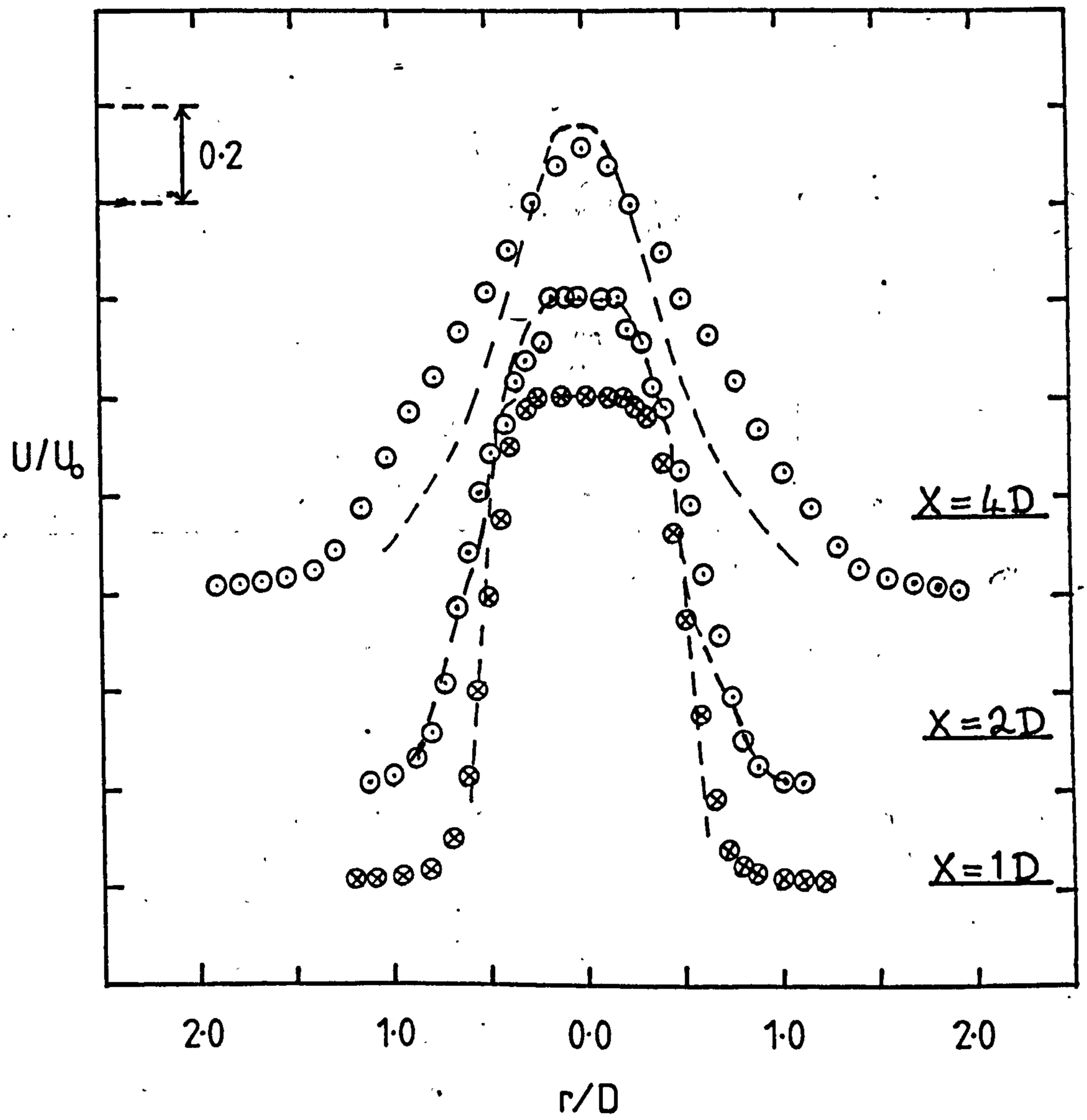

(--- PITOT RESULTS)

FIGURE 43 : VARIATION OF MEAN VELOCITY PROFILE WITH AXIAL DISTANCE AT M = 0·3 , M = ±1 (MAX.) , (PITOT RESULTS)

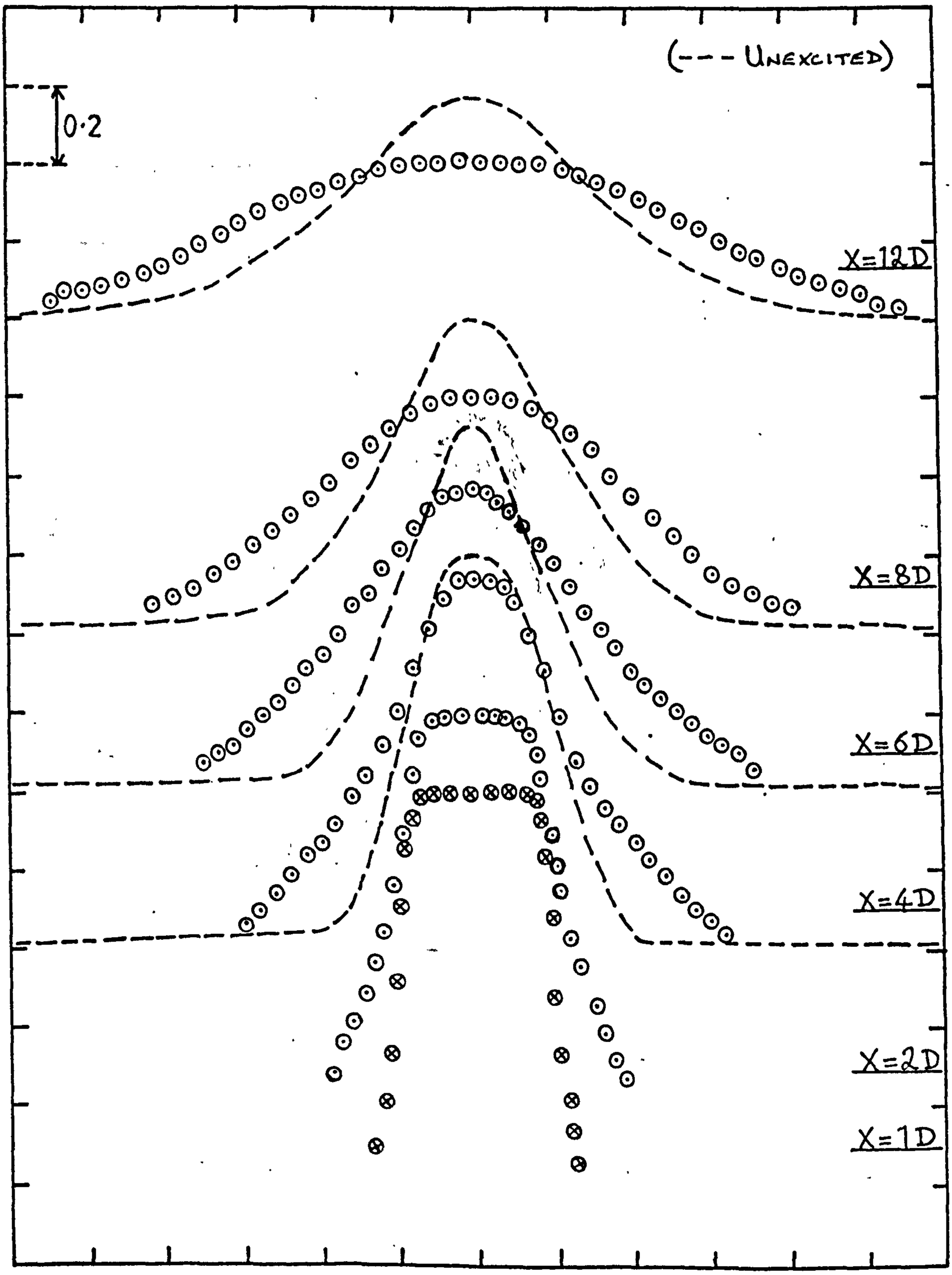

FIGURE 43 : (b) HOT WIRE RESULTS

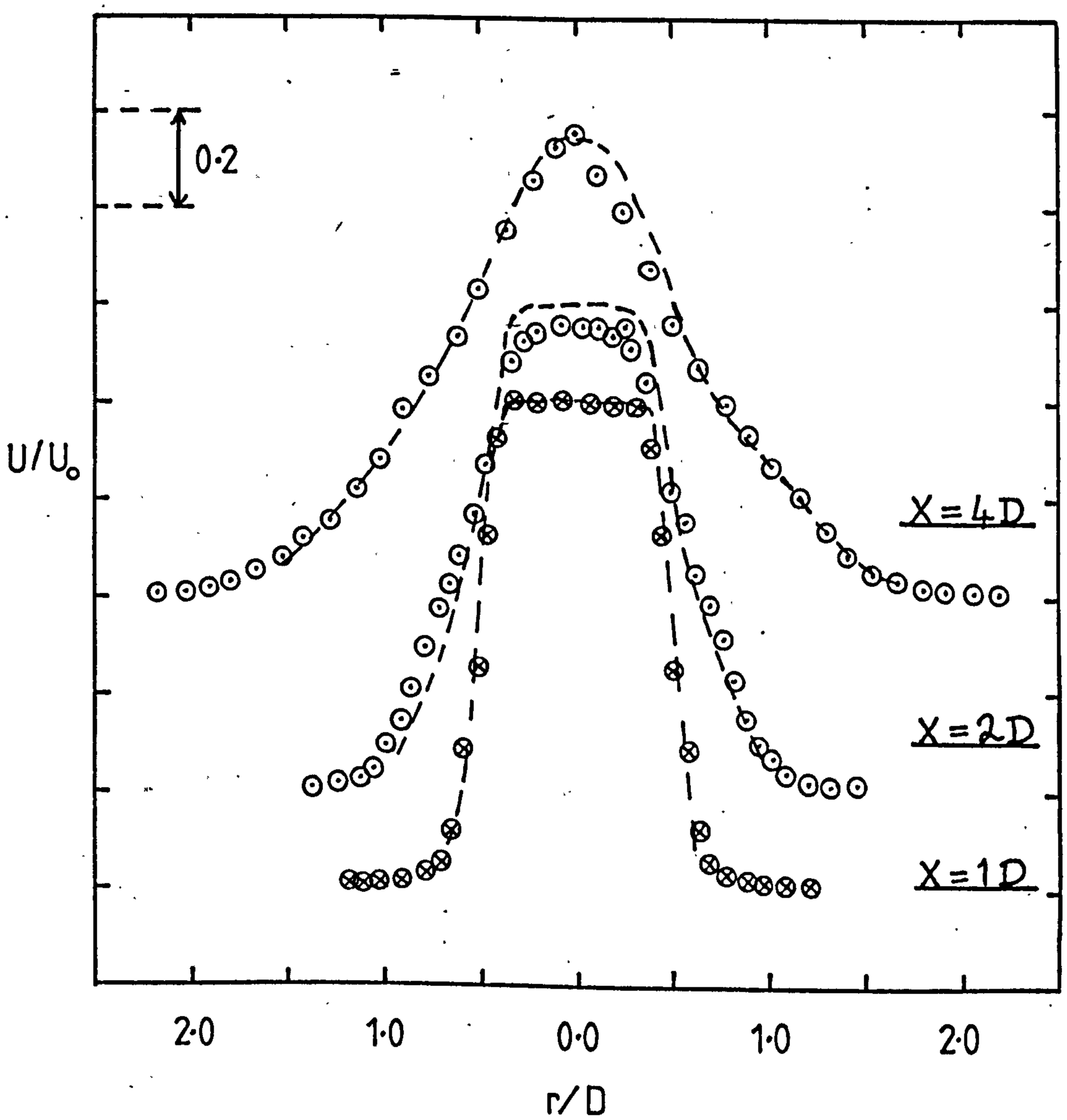

(--- PITOT RESULTS)

FIGURE 44 : VARIATION OF MEAN VELOCITY PROFILES WITH AXIAL DISTANCE AT M = 0·3, m = ±1 (MIN.), (PITOT RESULTS).

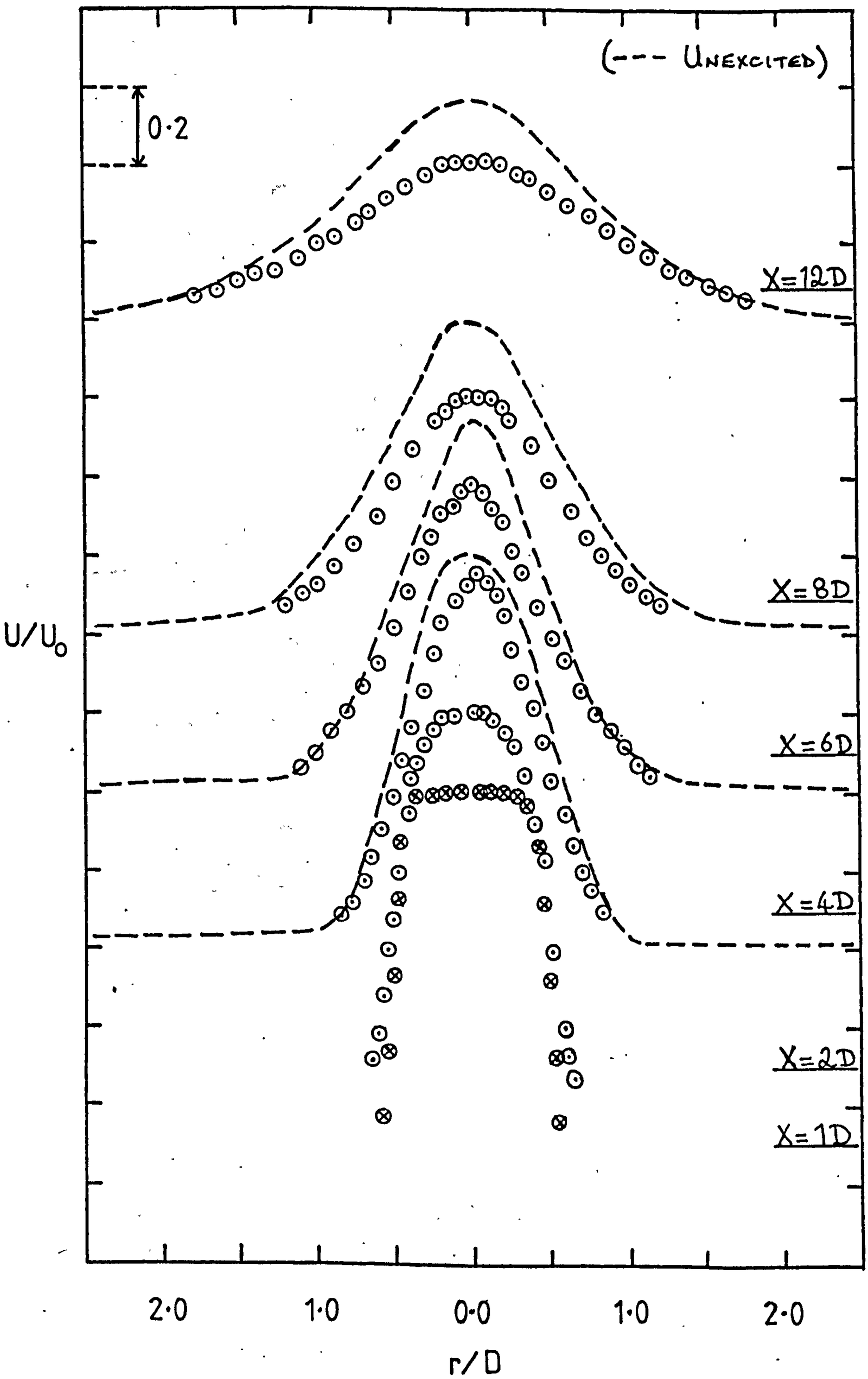

FIGURE 45 : VARIATION OF MEAN VELOCITY PROFILE WITH AXIAL DISTANCE AT M = 0·3, m = ±2 (MAX.), (PITOT RESULTS).

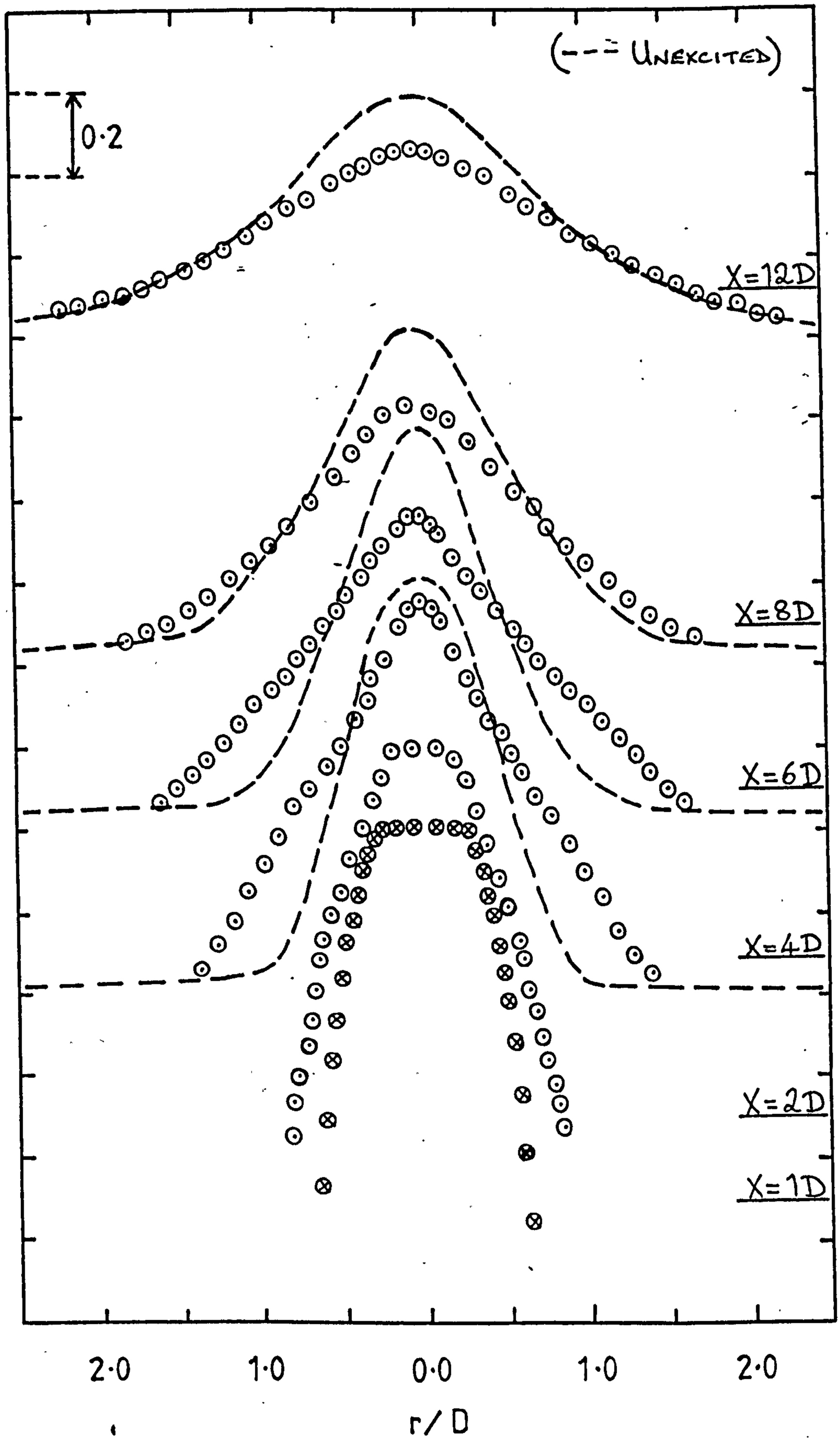

FIGURE 45 : (b) HOT WIRE RESULTS

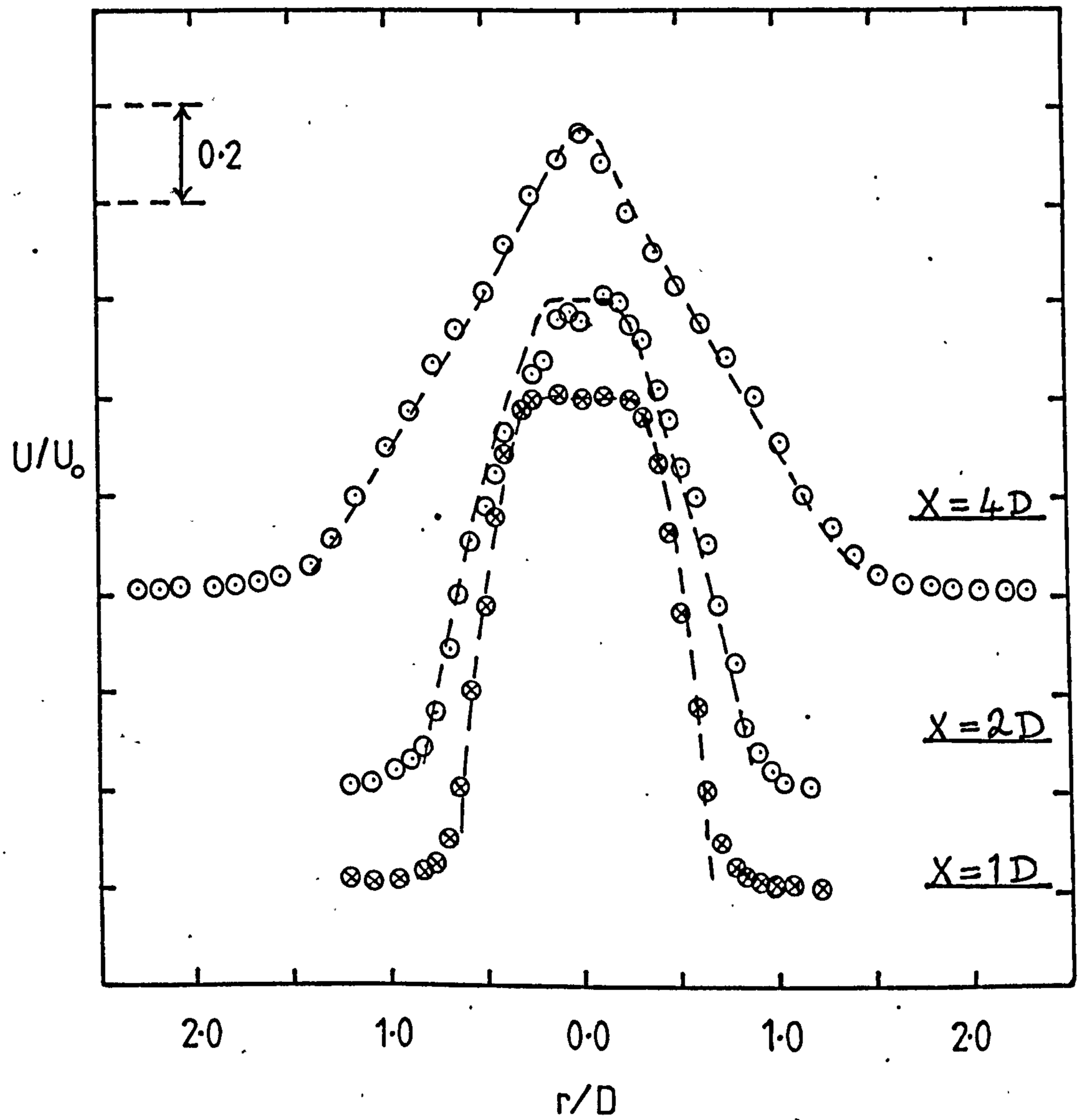

(--- PITOT RESULTS)

FIGURE 46: VARIATION OF MEAN VELOCITY PROFILE WITH AXIAL DISTANCE AT M=0·3, m=±2(MIN.), (PITOT RESULTS).

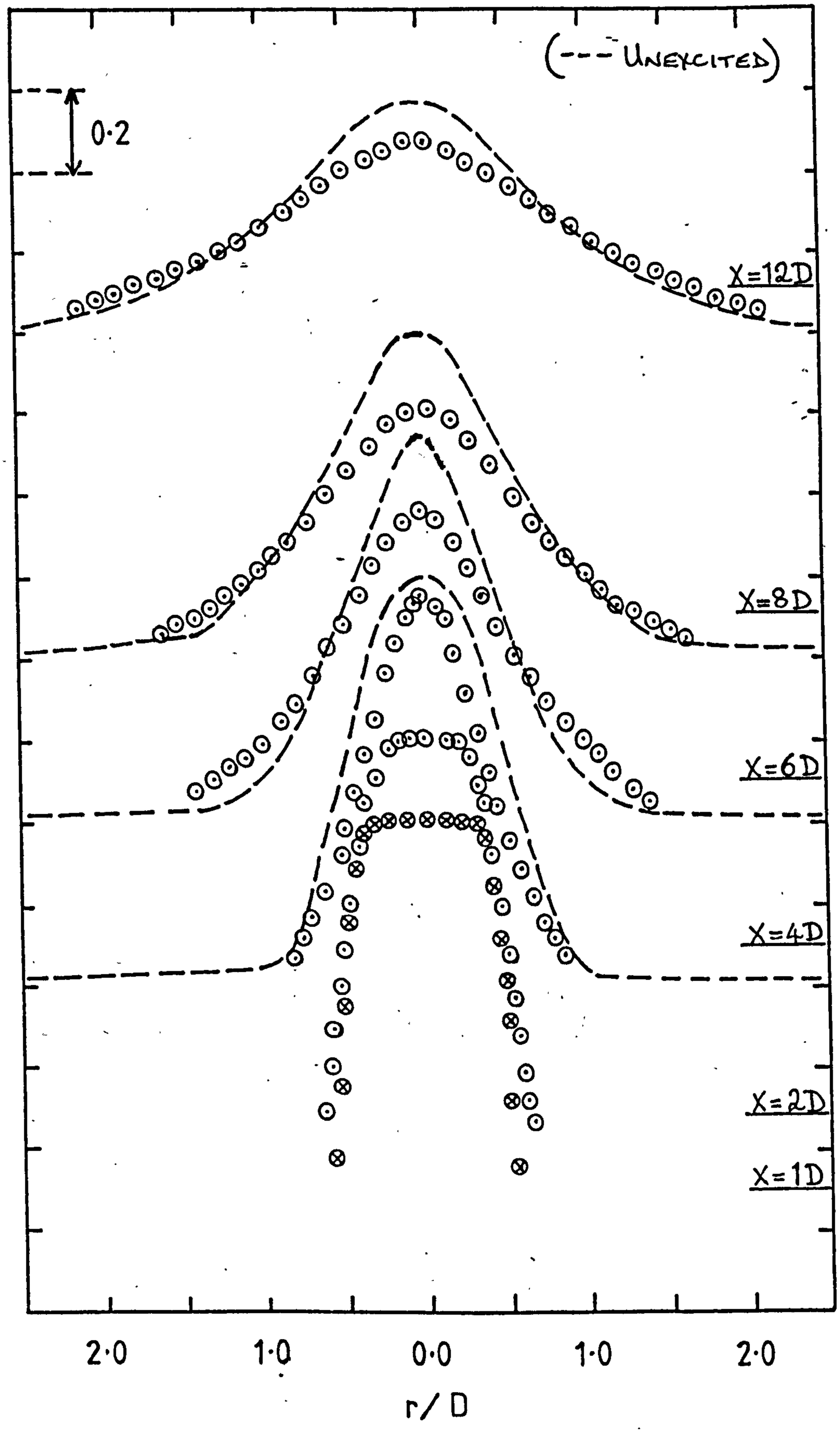

FIGURE 46 : (b) HOT WIRE RESULTS

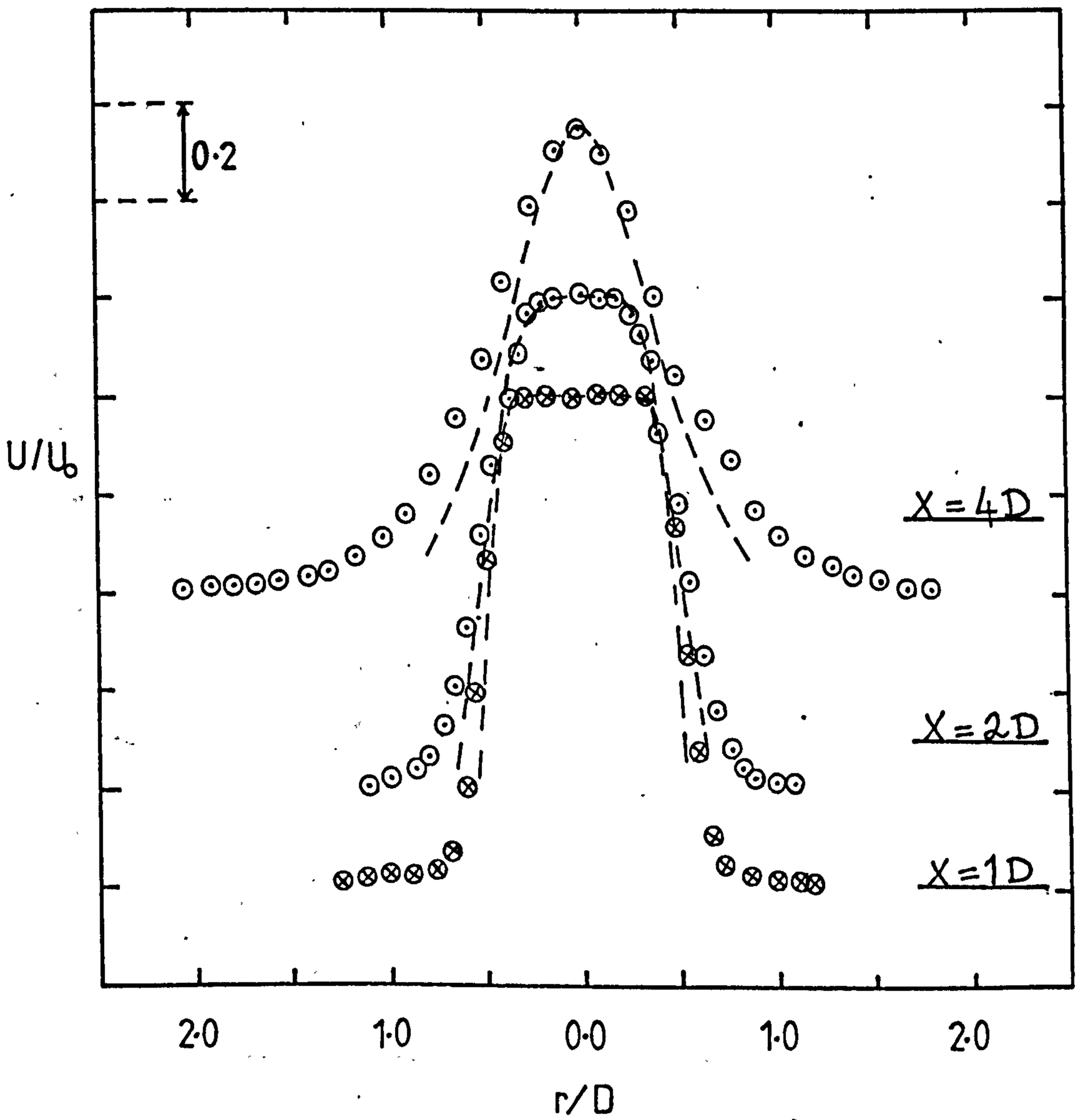

(--- PITOT RESULTS)

FIGURE 47 : VARIATION OF CENTRE LINE MEAN VELOCITY WITH AXIAL DISTANCE, M = 0·3

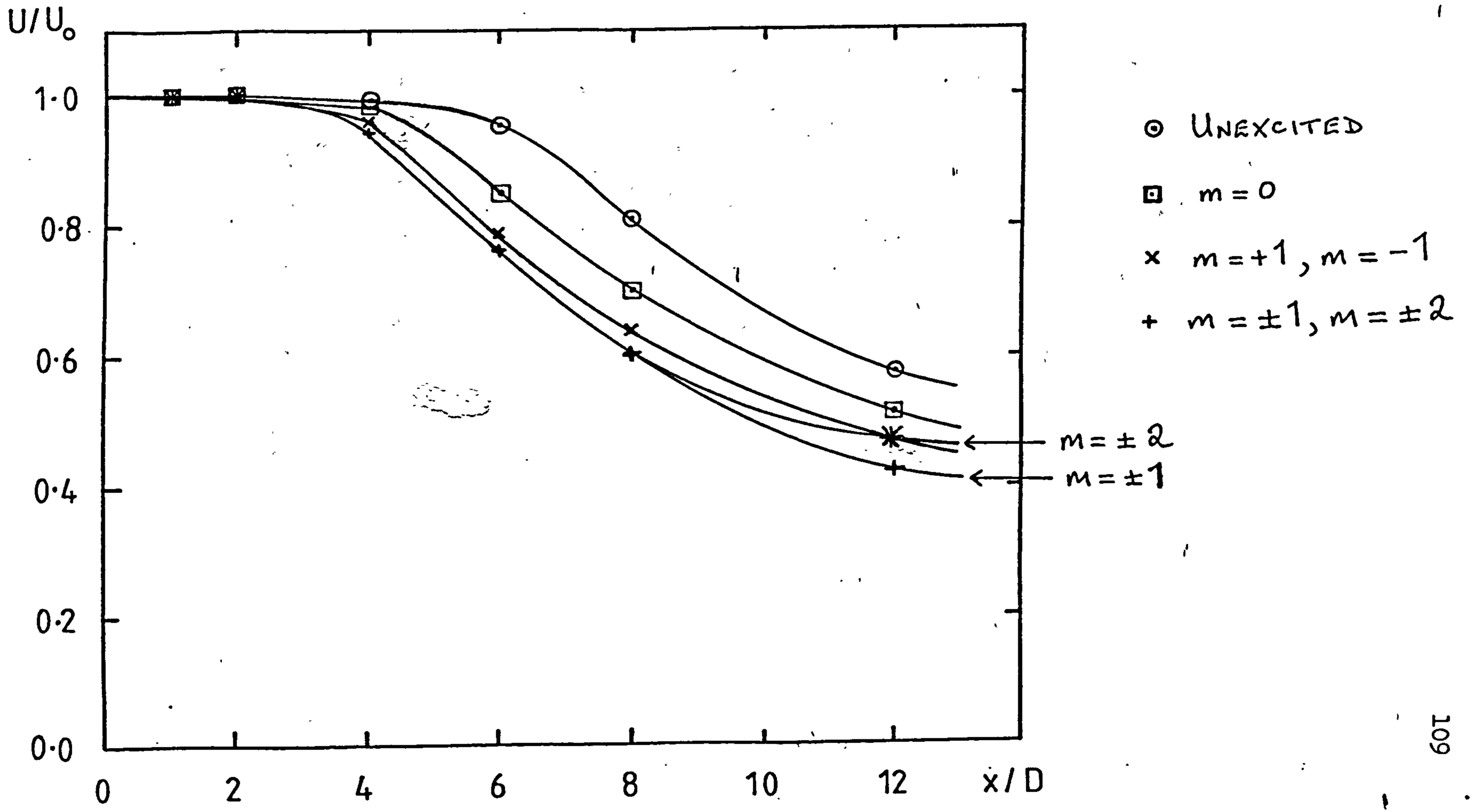

FIGURES 48 AND 49 : EXPERIMENTAL STANDING WAVE PATTERNS SHOWING THE ASYMMETRIC STRUCTURE OF THE JET WHEN SUBJECTED TO $m=\pm1$ AND $m=\pm2$ MODE EXCITATIONS. ($\diamond$ X=1D, $\square$ X=2D, $\circ$ X=4D, $\triangle$ X=6D, + X=8D AND × X=12D)

FIG. 48

$m=\pm1$

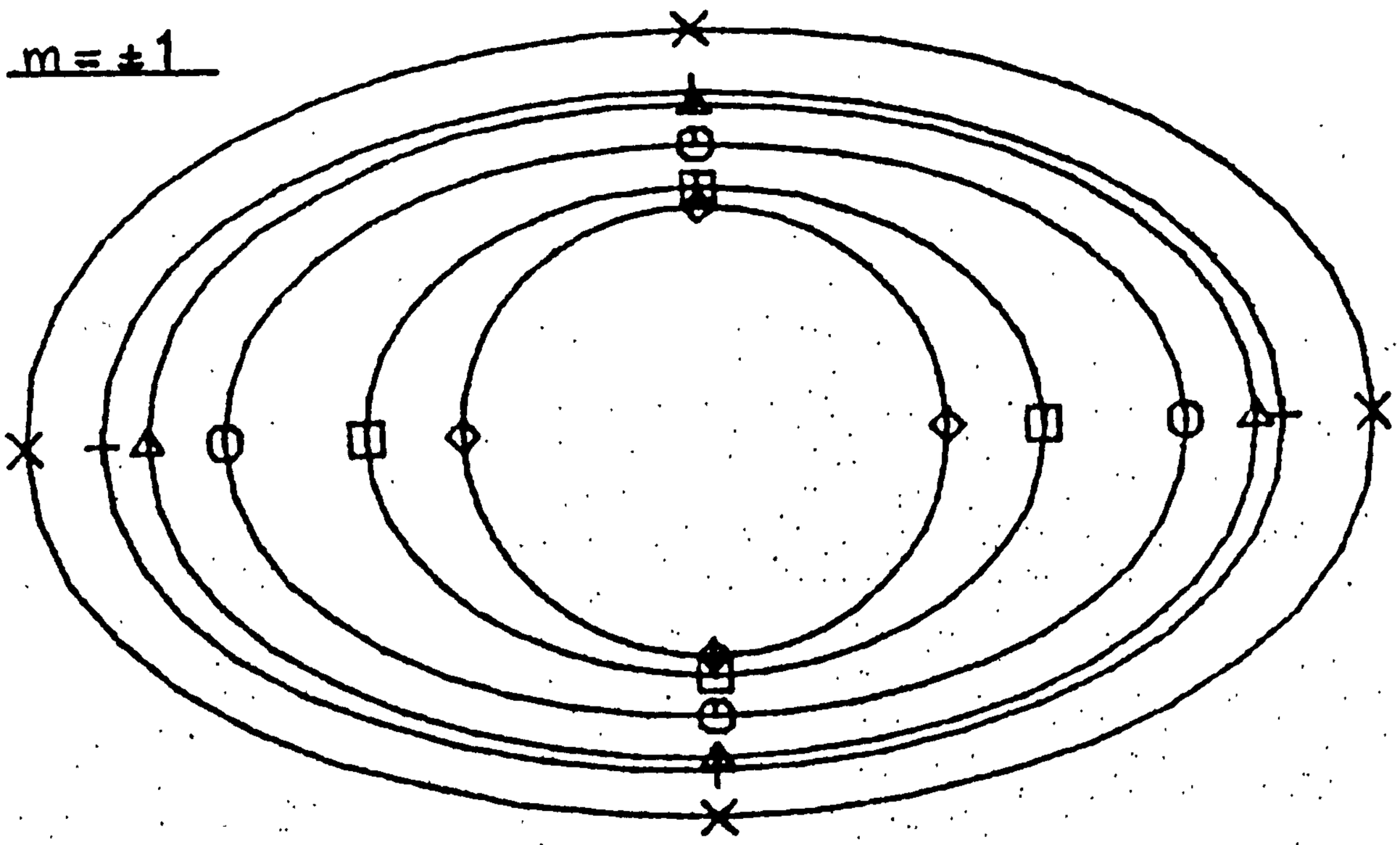

FIG. 49

$m=\pm2$

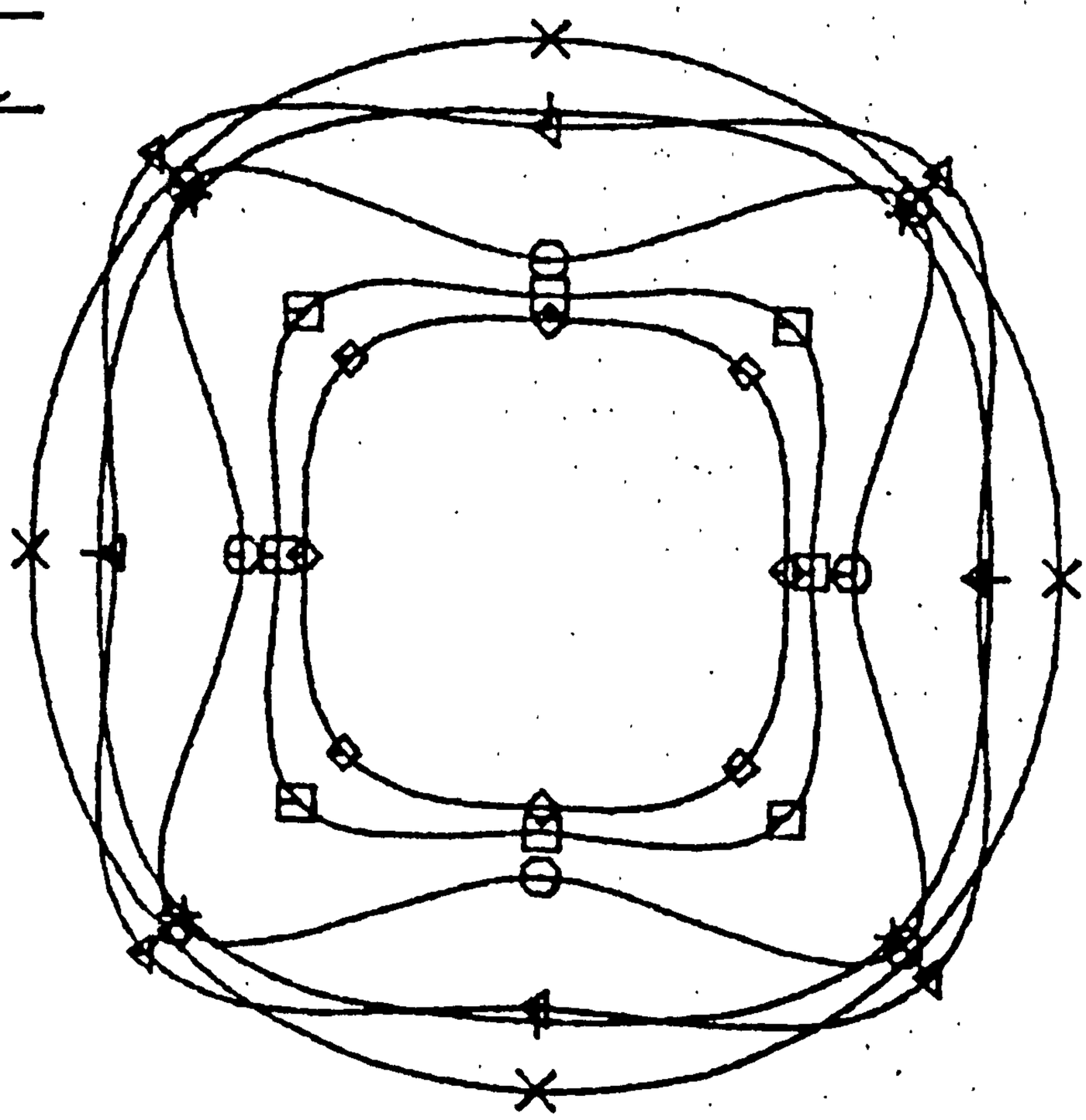

FIGURE 50 : FLUCTUATING VELOCITY SPECTRA AT X = 1D, r = 0.000D, M = 0 MODE

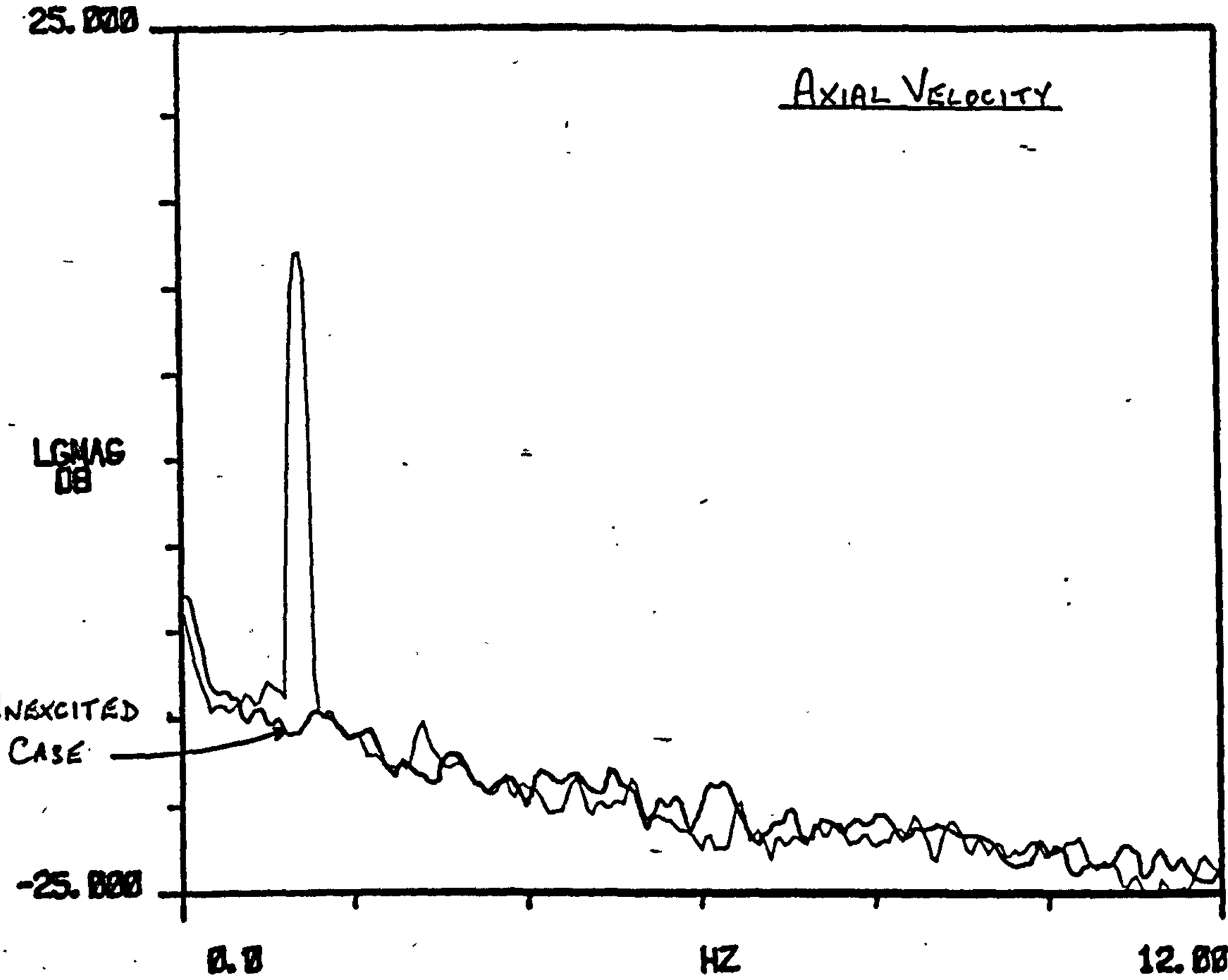

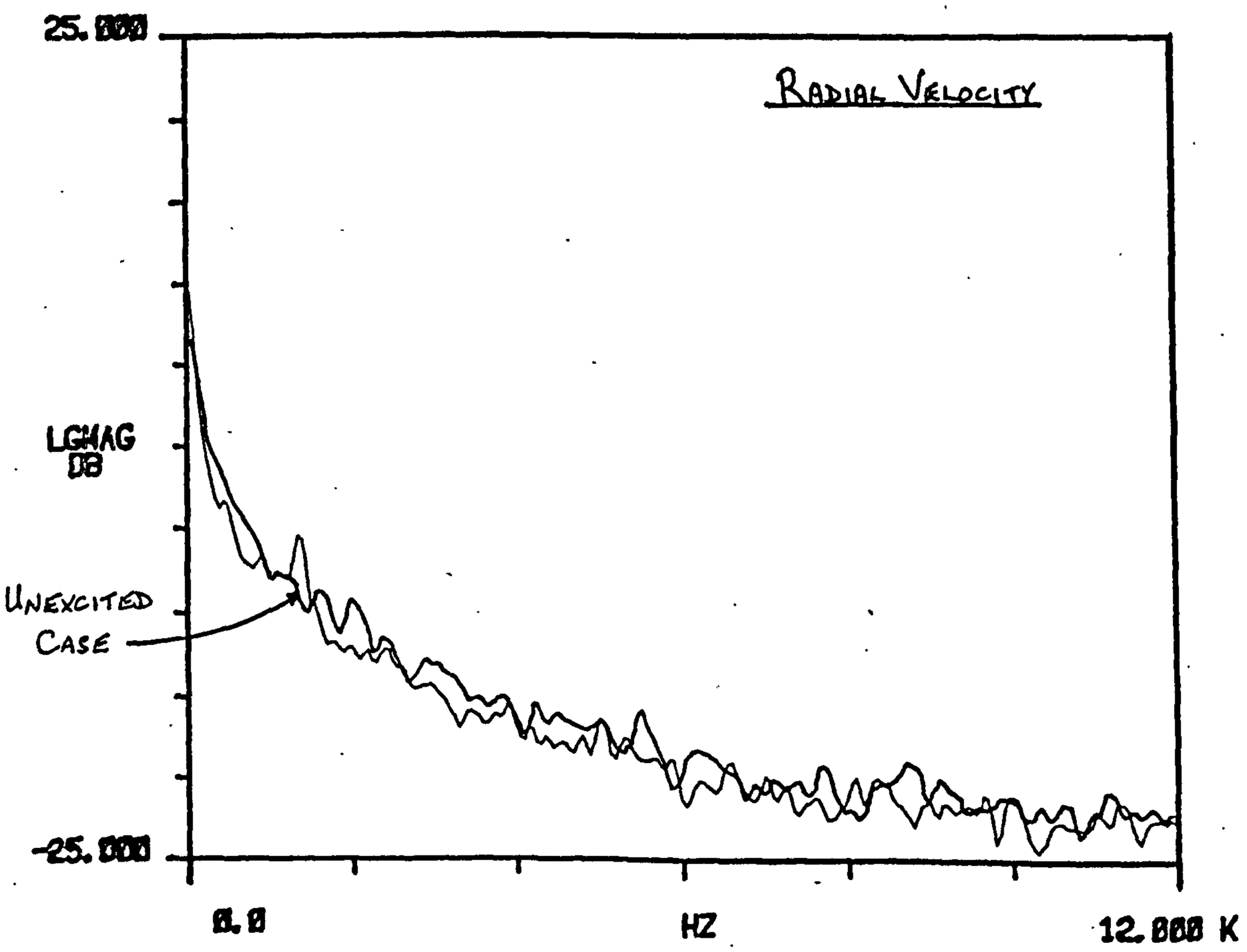

FIGURE 51 : FLUCTUATING VELOCITY SPECTRA AT X=1D, r=0.193D, M=0 MODE

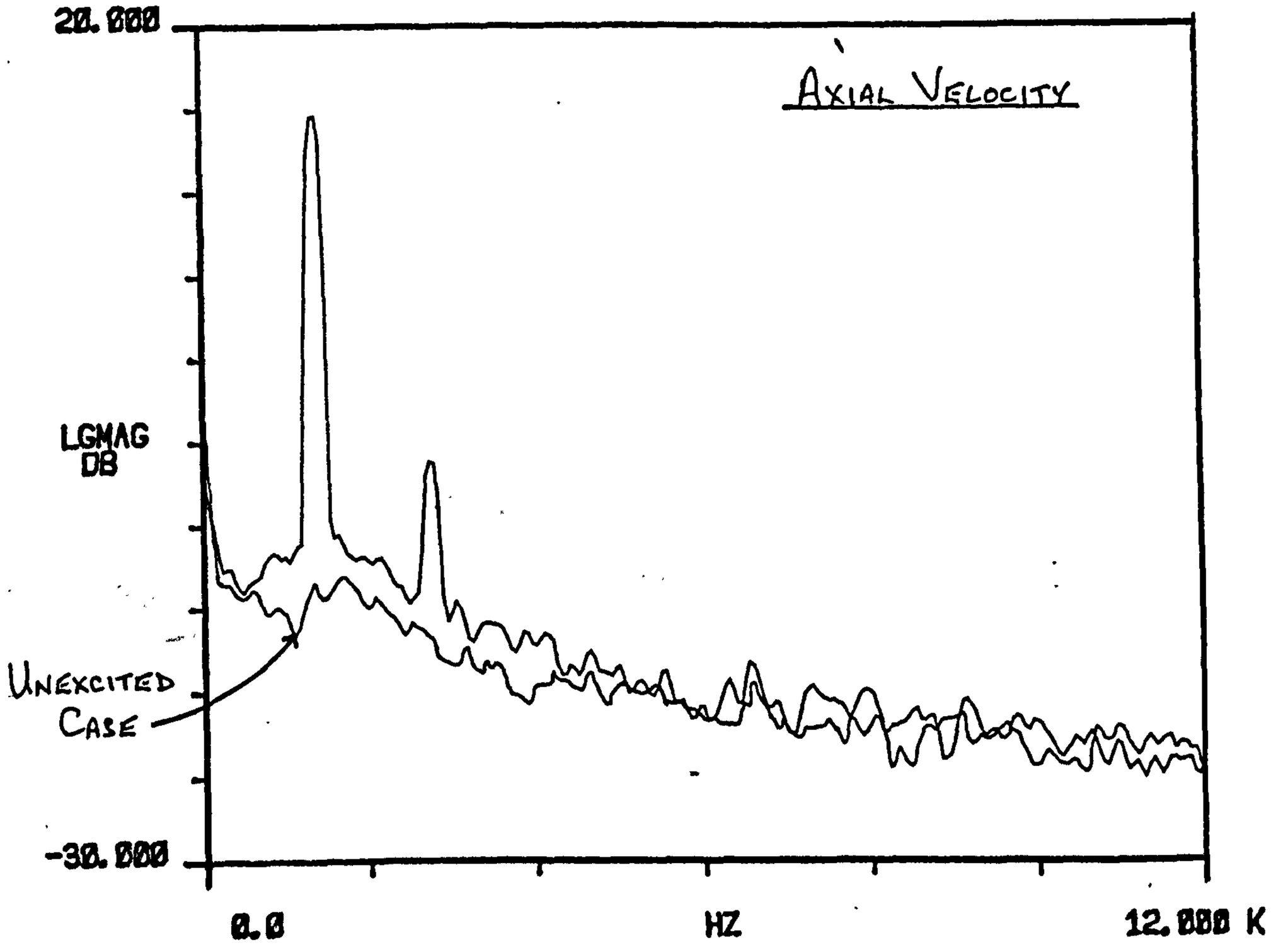

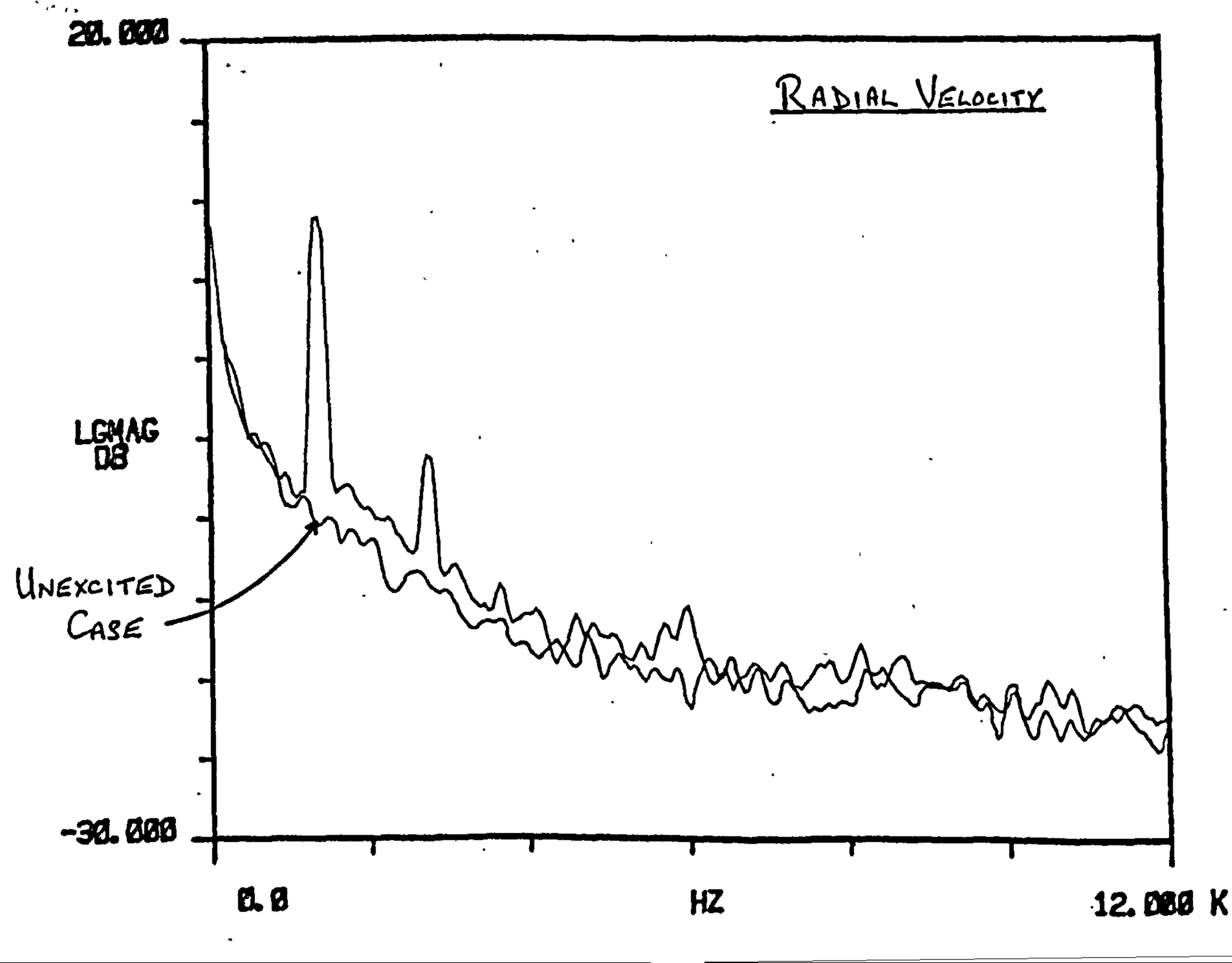

FIGURE 52 :- FLUCTUATING VELOCITY SPECTRA AT X=1D, r = 0·322D, M=0 MODE

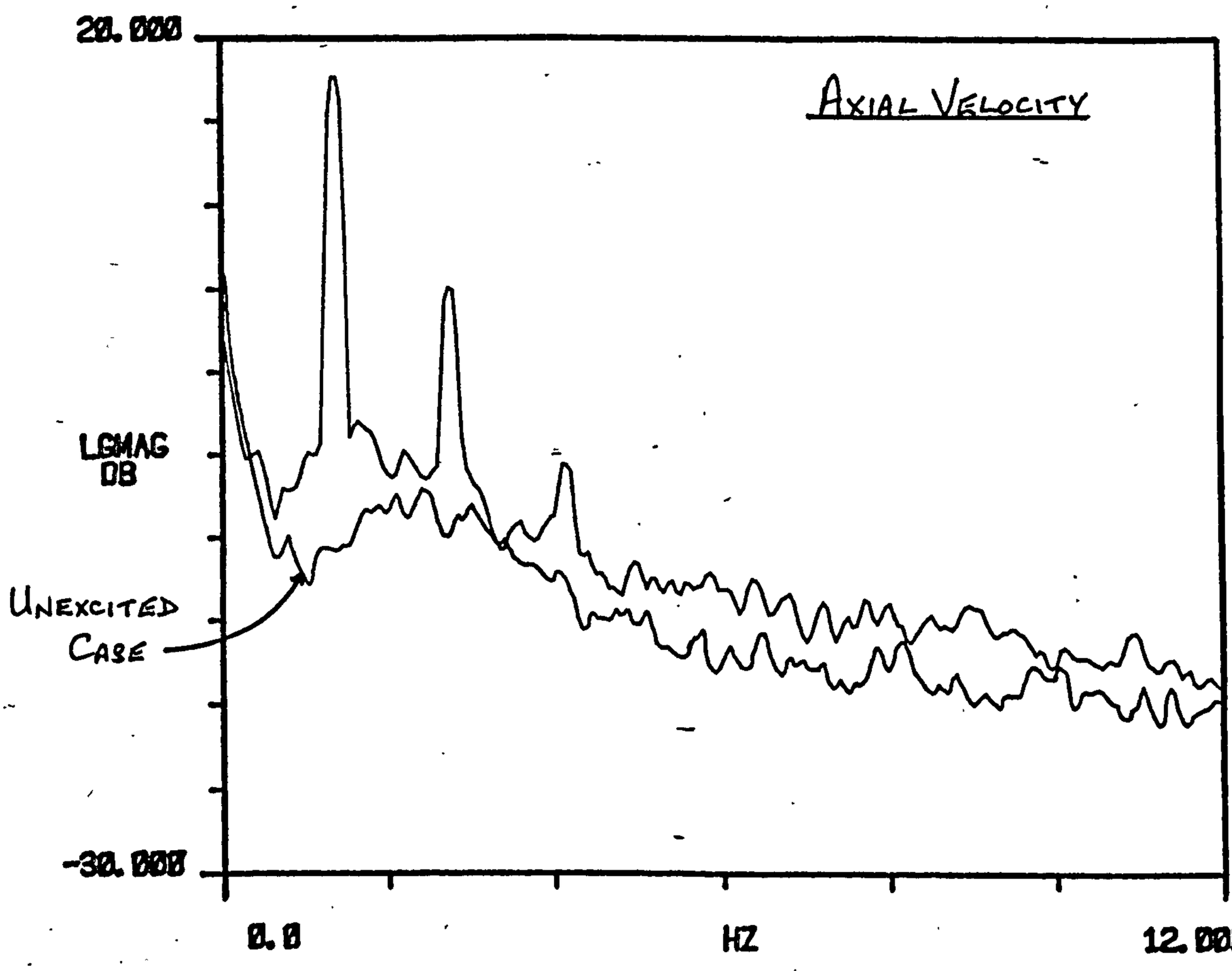

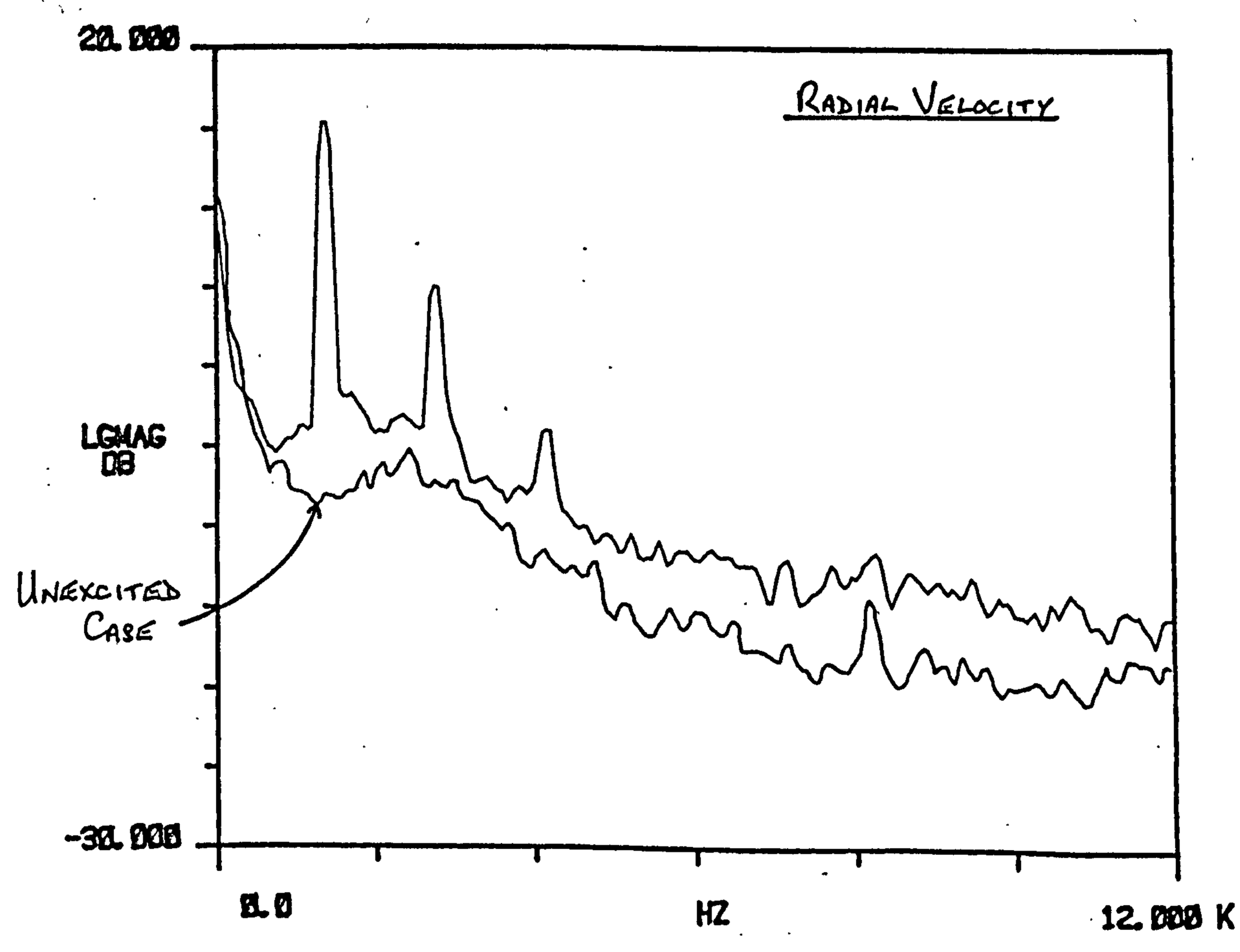

FIGURE 53 : FLUCTUATING VELOCITY SPECTRA AT X=1D, r=0·515D, M=0 MODE

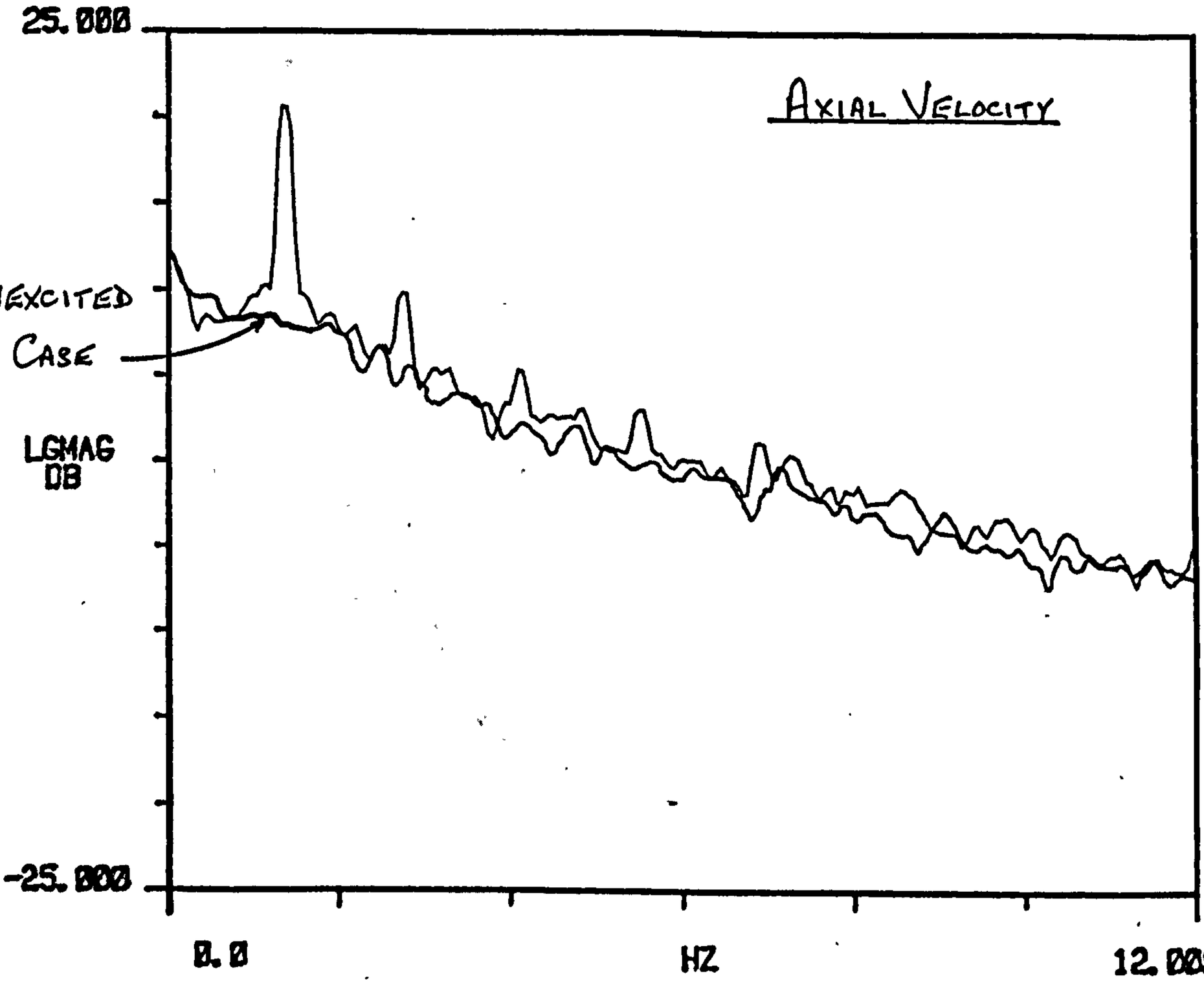

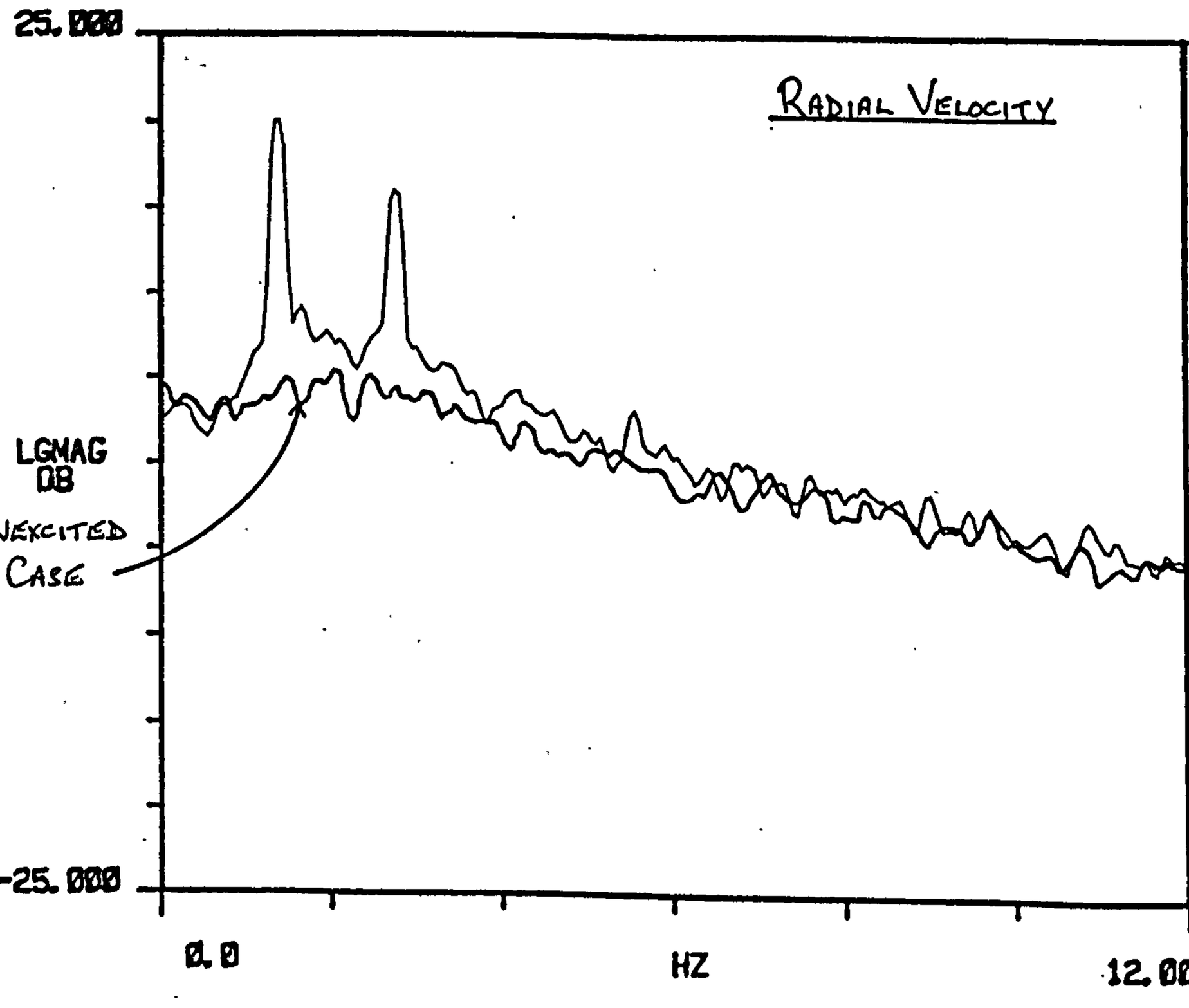

FIGURE 54 : FLUCTUATING VELOCITY SPECTRA AT X = 1D, r = 0.708D, m = 0 MODE

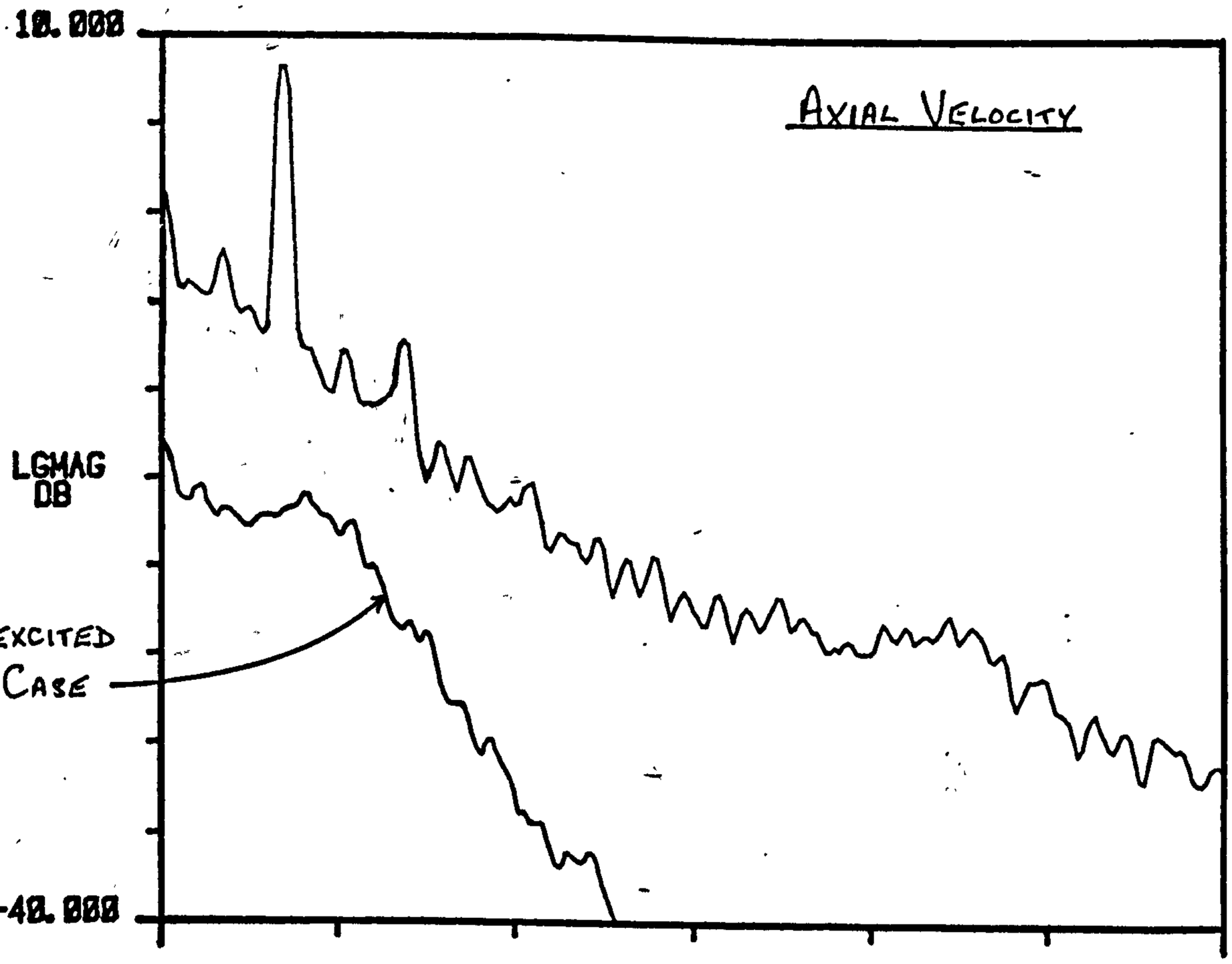

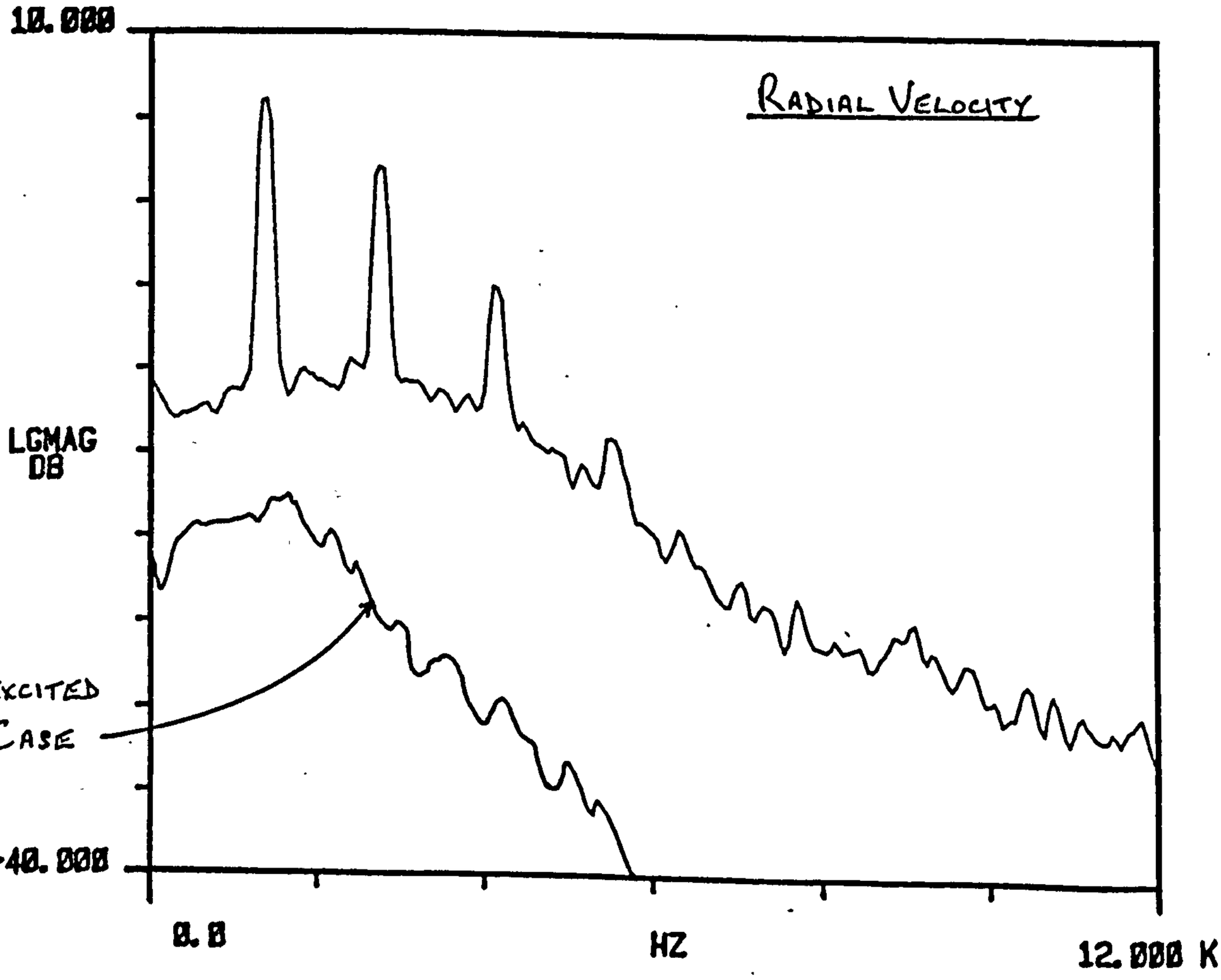

FIGURE 55 : FLUCTUATING VELOCITY SPECTRA AT X=1D,

r = 0·837D, m=0 MODE

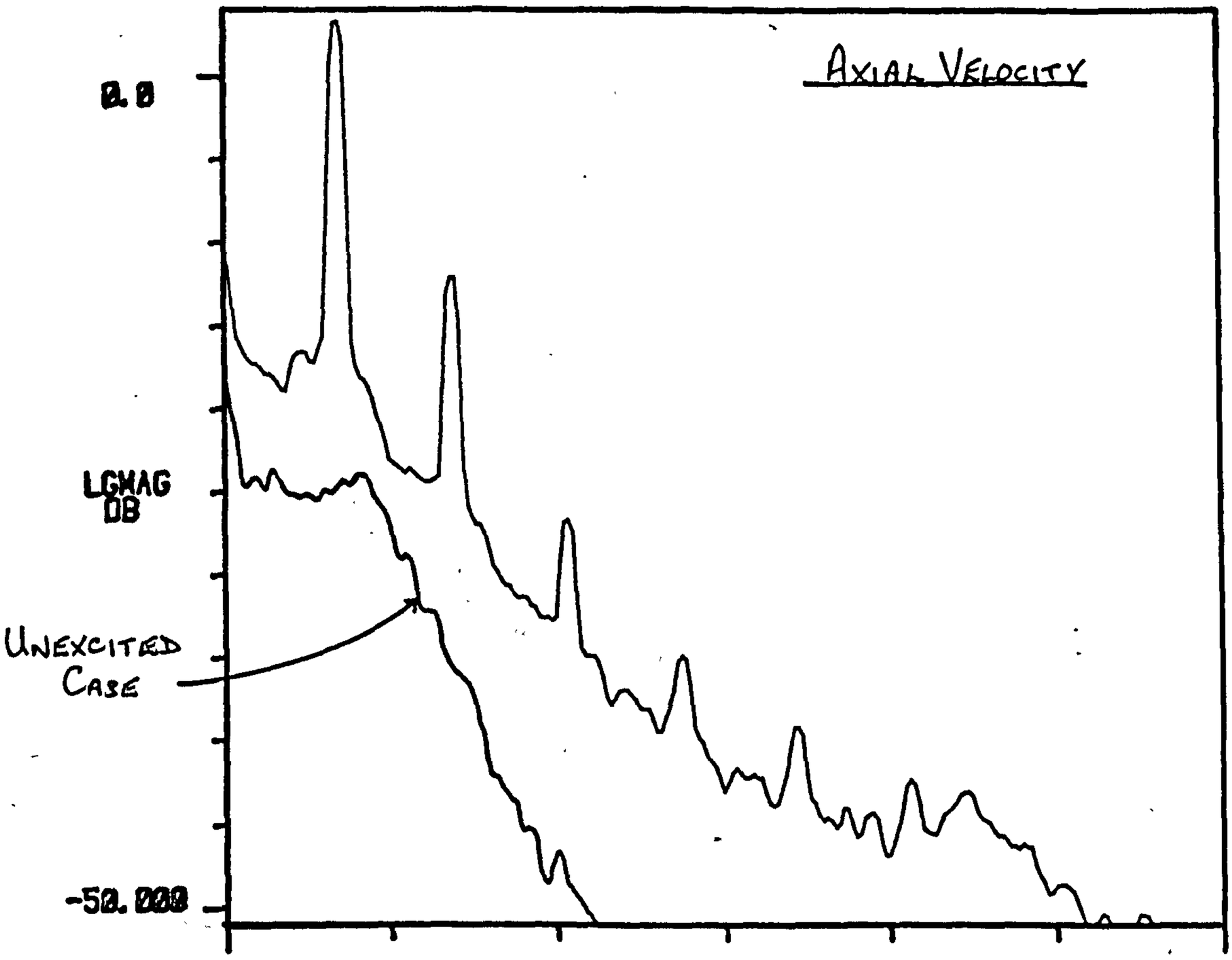

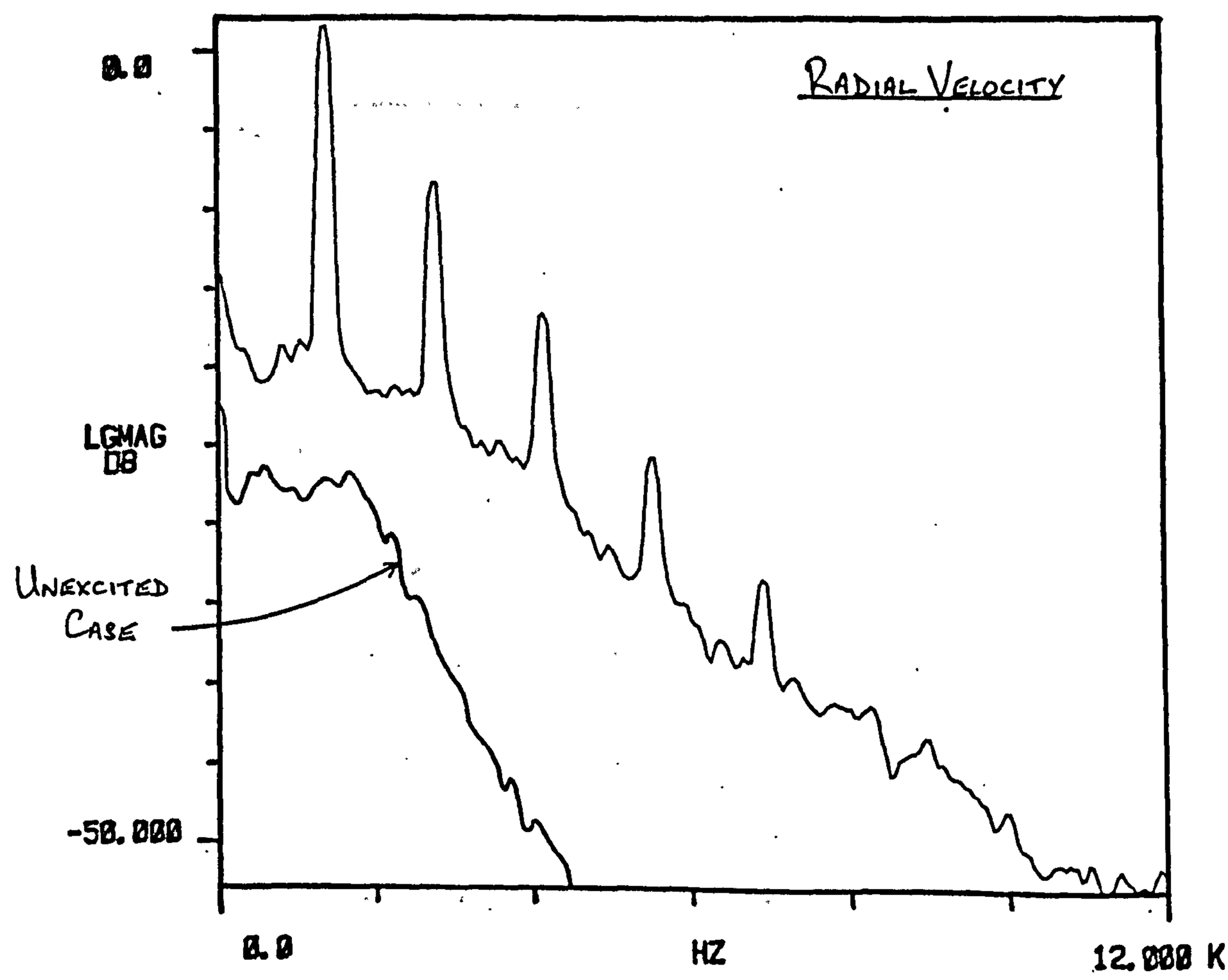

FIGURE 56:- FLUCTUATING VELOCITY SPECTRA AT X=1D, r=0·354D, M=±2 (MIN.)

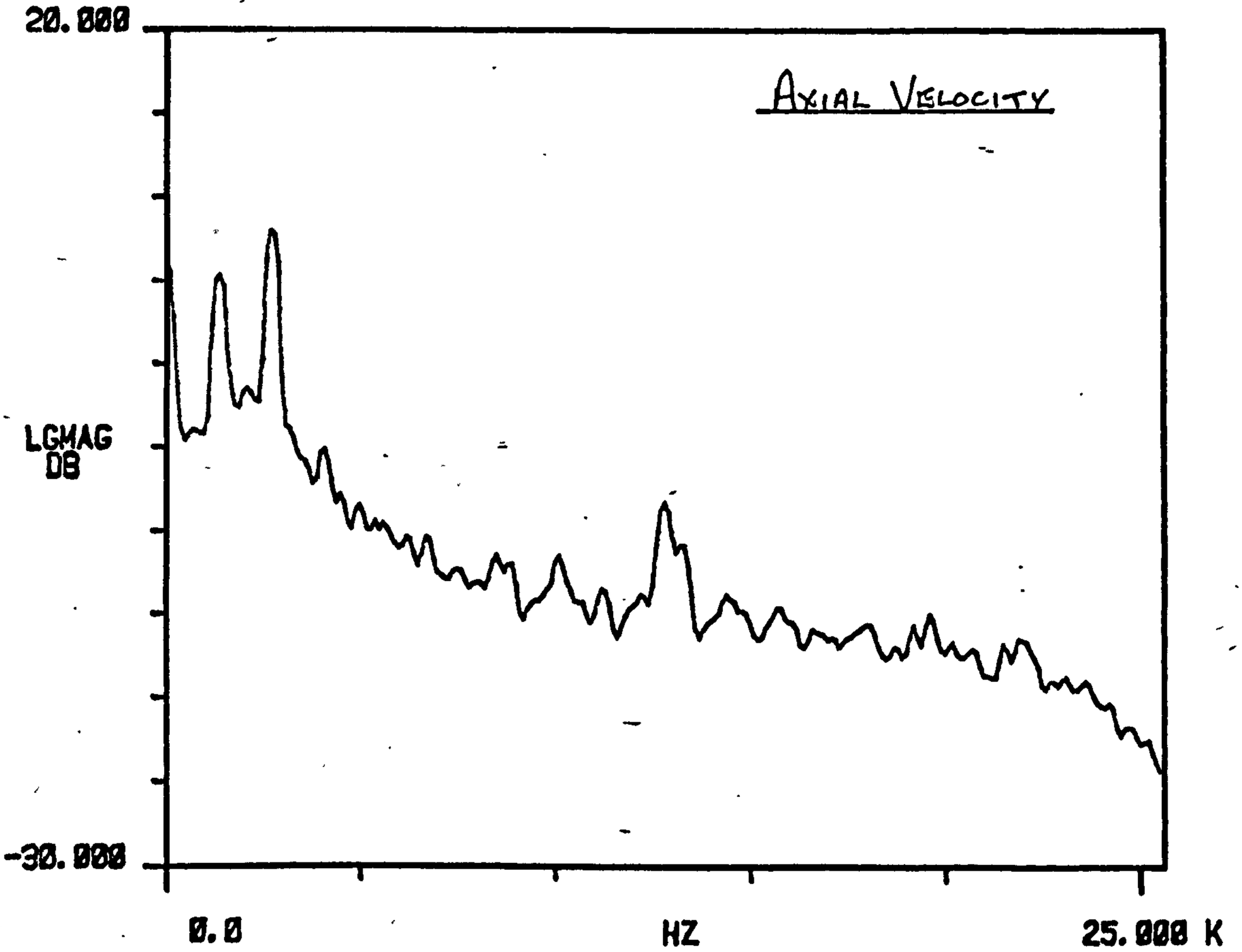

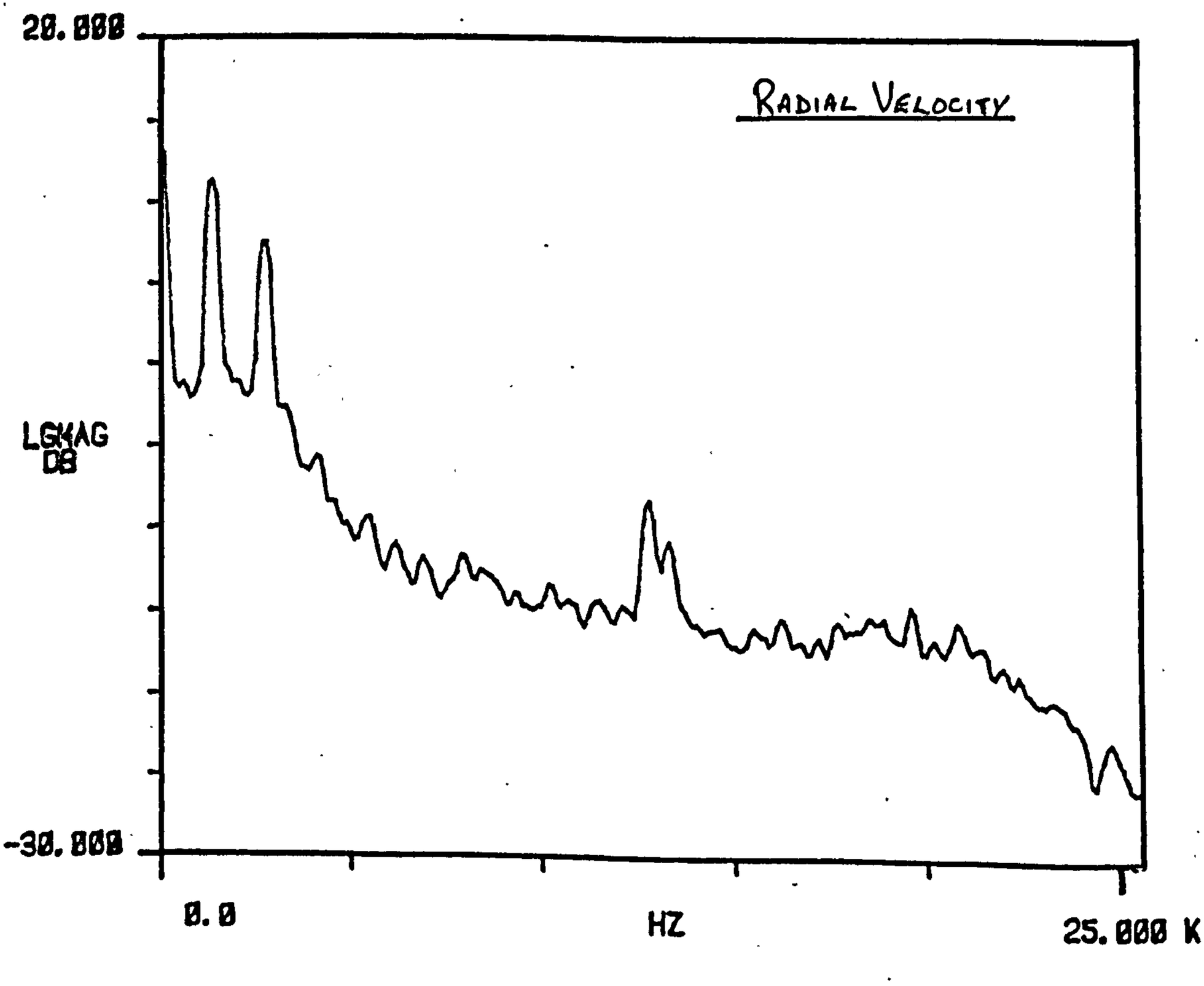

FIGURE 57 : FLUCTUATING VELOCITY SPECTRA AT X=1D, r=0.419D, M=±2 (MIN.)

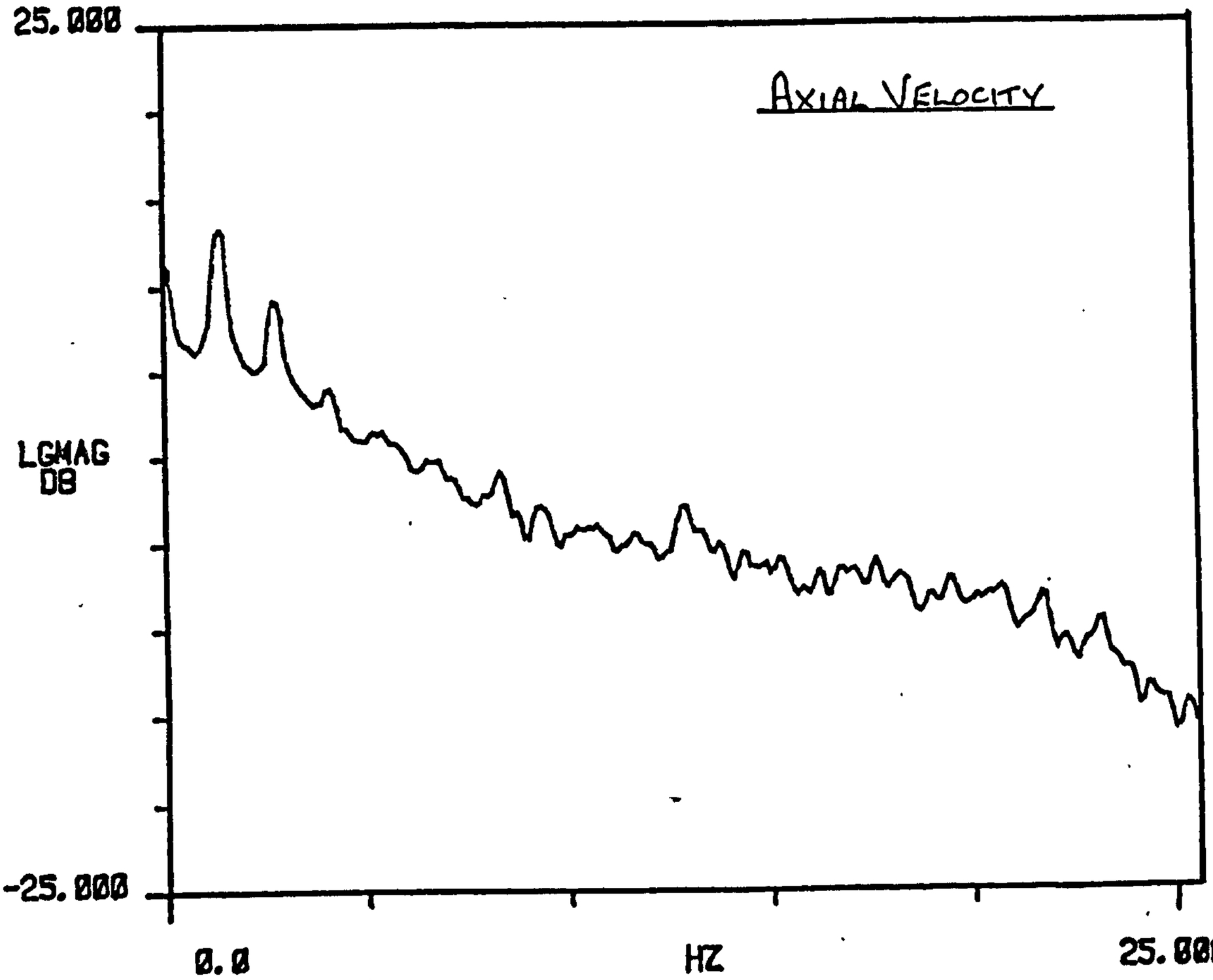

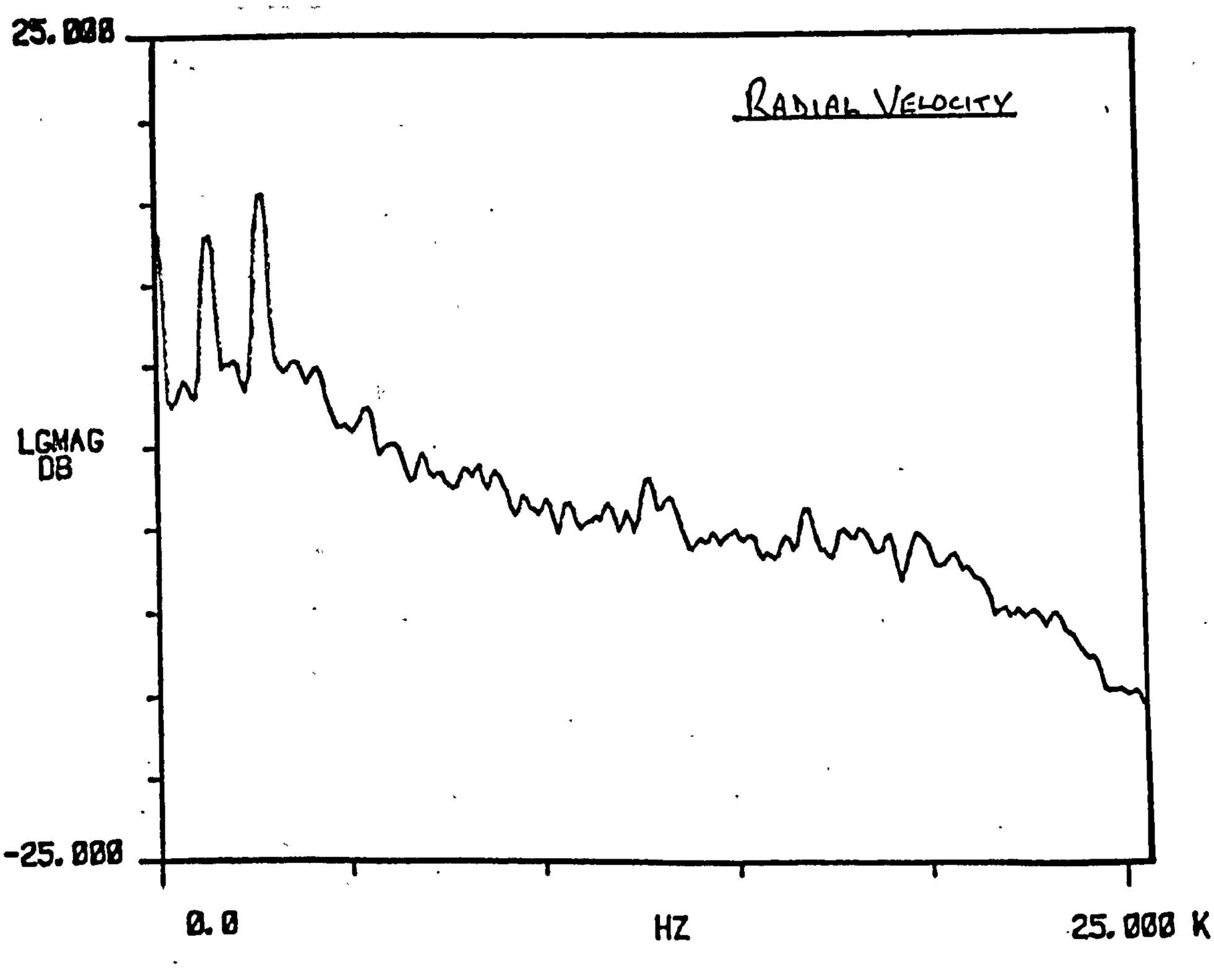

FIGURES 58 AND 59 : AXIAL VARIATION OF PRESSURE LEVEL AND PHASE ANGLE AT M = 0·5, WITH JET EXCITED AT 2250 Hz, DRIVE LEVEL 0 dB.

WITH FLOW :- $r = R/2$ ⊗ , $r = R$ ⊙ . WITHOUT FLOW :- $r = R/2$ ⊠ , $r = R$ ⊡

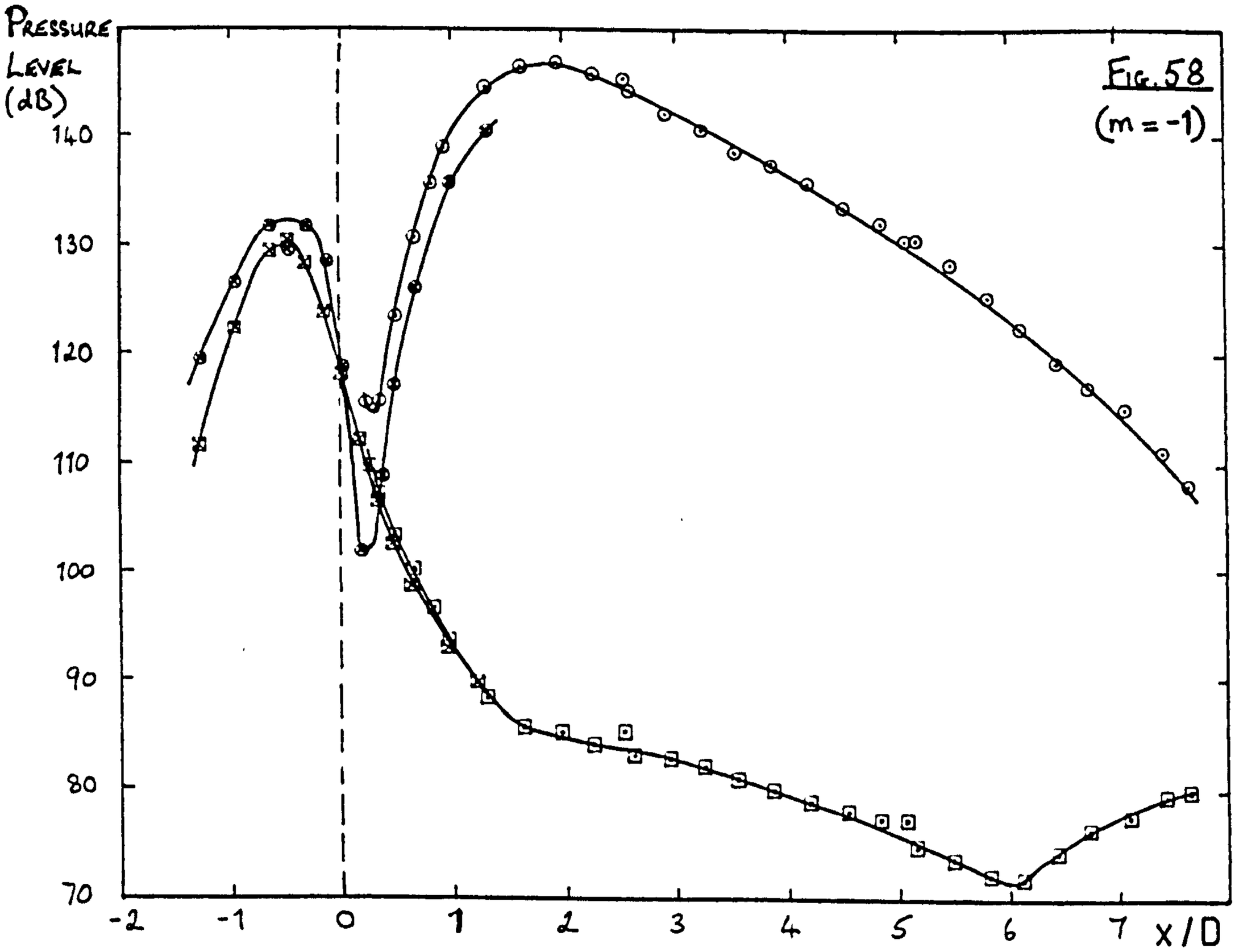

FIG. 58 (m = -1)

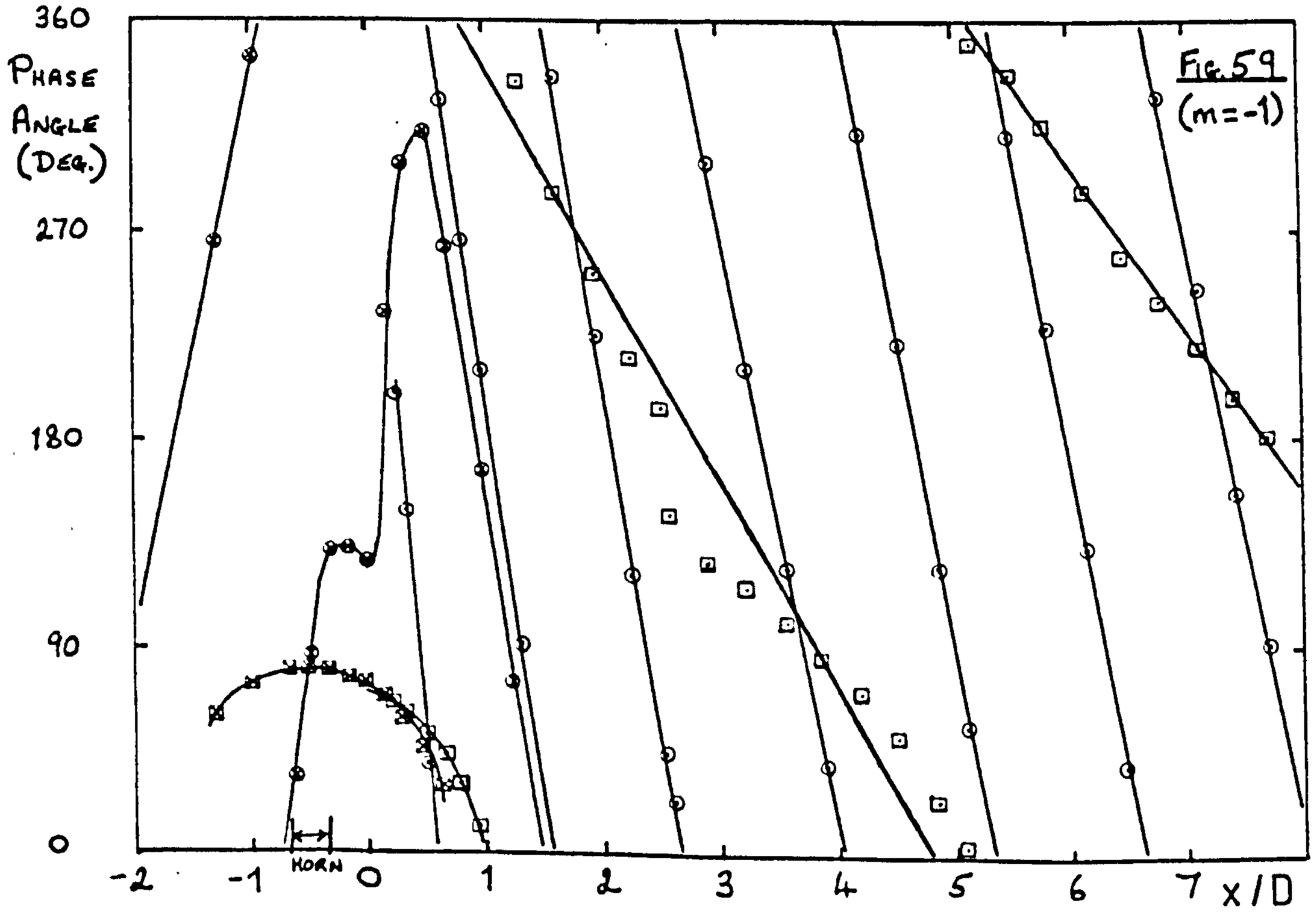

FIG. 59 (m = -1)

FIGURES 60 AND 61 : AXIAL VARIATION OF PRESSURE LEVEL AND PHASE ANGLE AT M=0.5, WITH JET EXCITED AT 2250 Hz, DRIVE LEVEL -20dB.

WITH FLOW :- r=R/2 ⊛, r=R ⊙ . WITHOUT FLOW :- r=R/2 ⊠, r=R ⊡

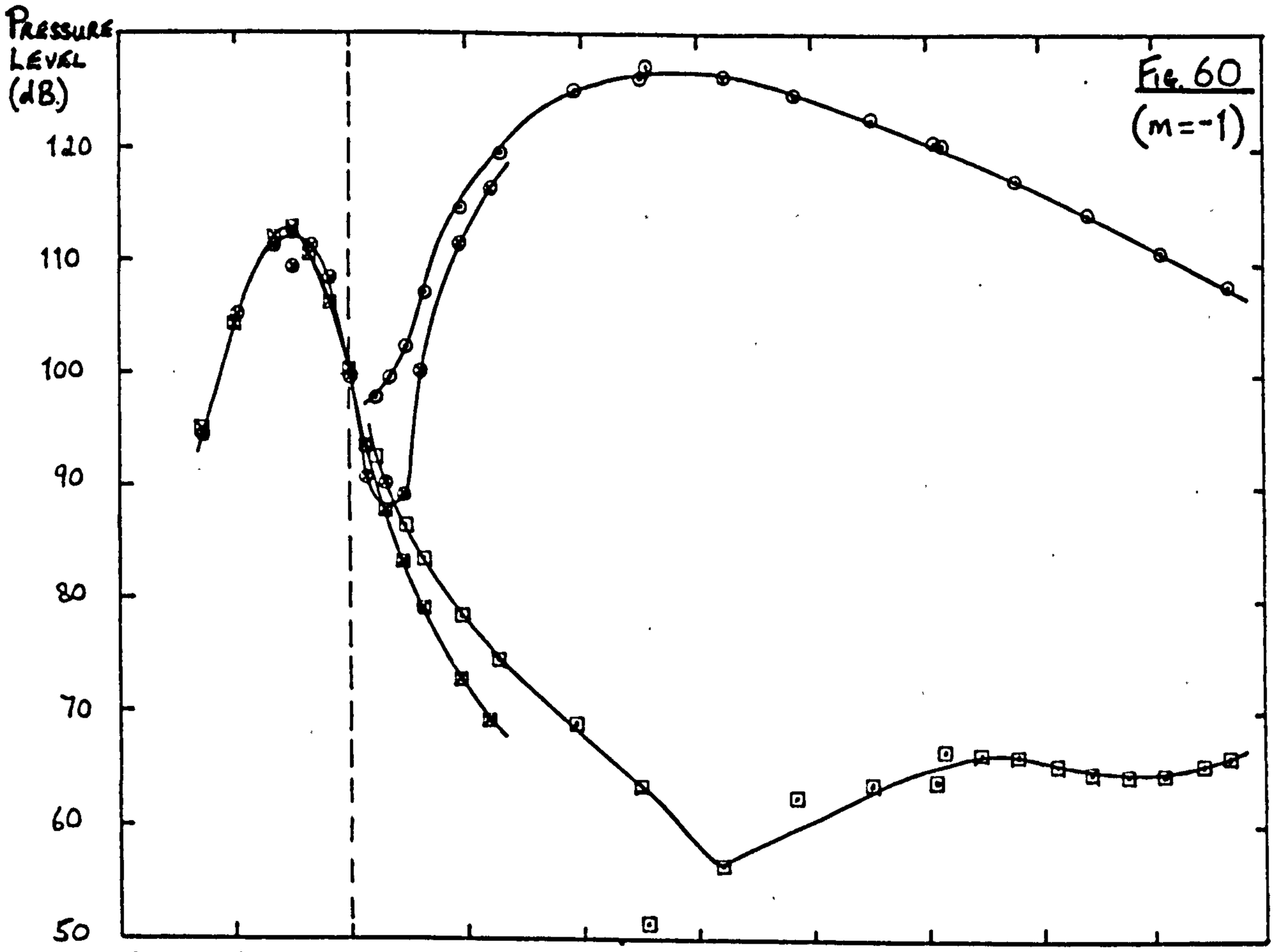

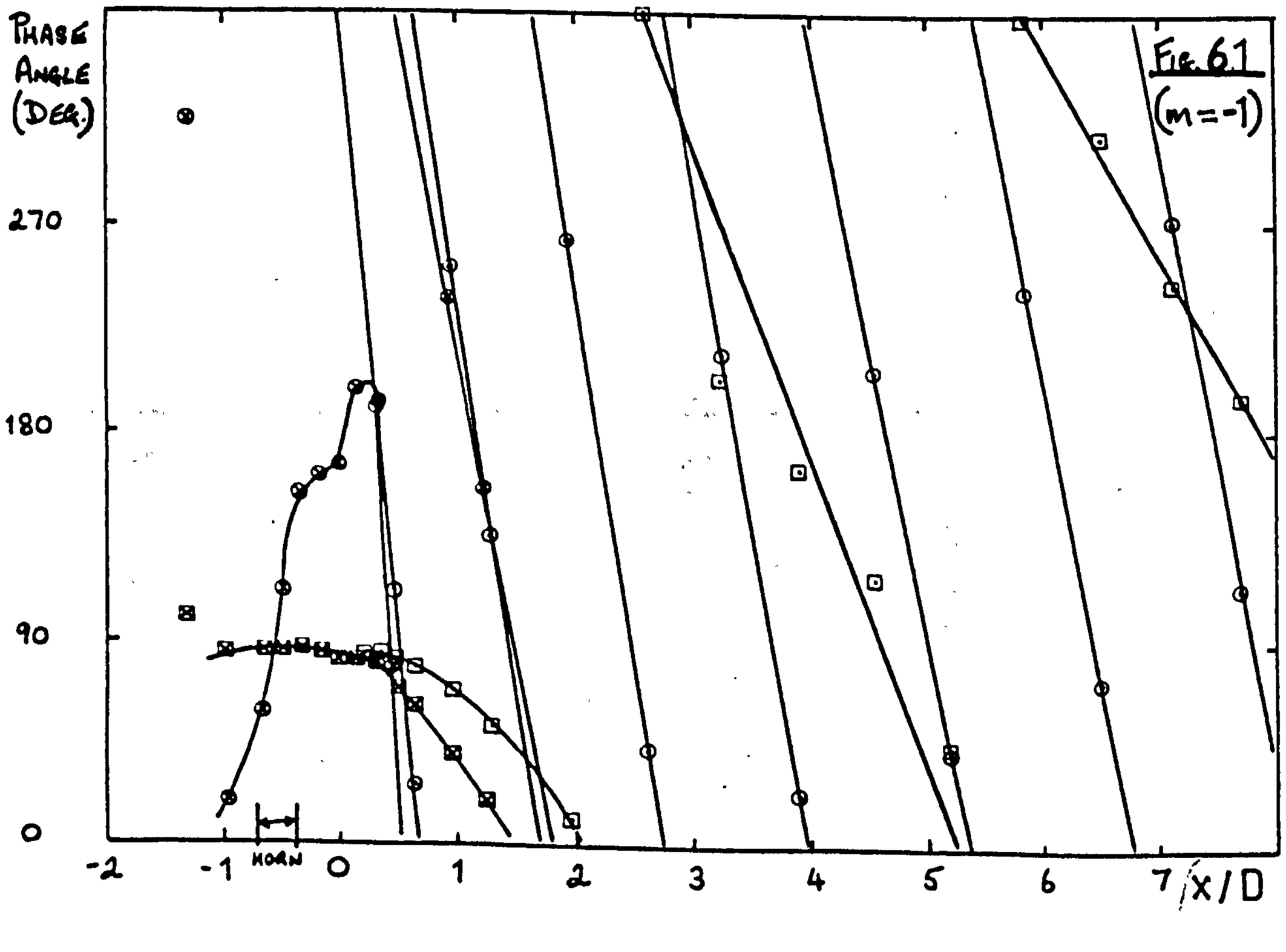

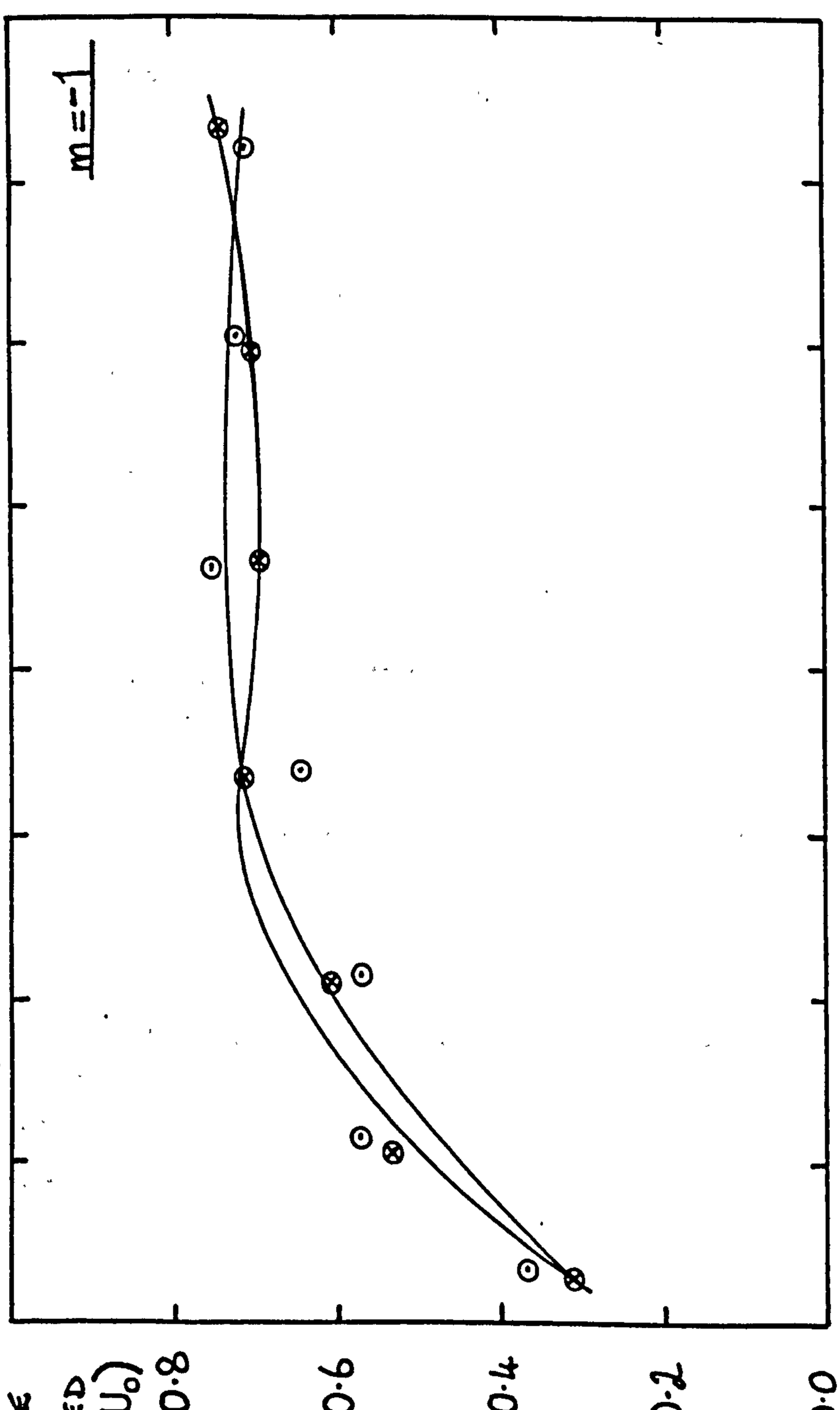

FIGURE 62: AXIAL VARIATION OF PHASE VELOCITY FROM PRESSURE MEASUREMENTS

FREQUENCY 2250Hz, MACH NUMBER 0·5. DRIVE LEVEL ONE ⊗ -20dB ⊙

FIGURES 63 AND 64 : RADIAL VARIATION OF PRESSURE LEVEL AND PHASE ANGLE AT M=0·5 WITH JET EXCITED AT 2250 Hz, DRIVE LEVEL 0dB, X=2D. WITH FLOW ⊙, WITHOUT FLOW ⊡. (m=-1)

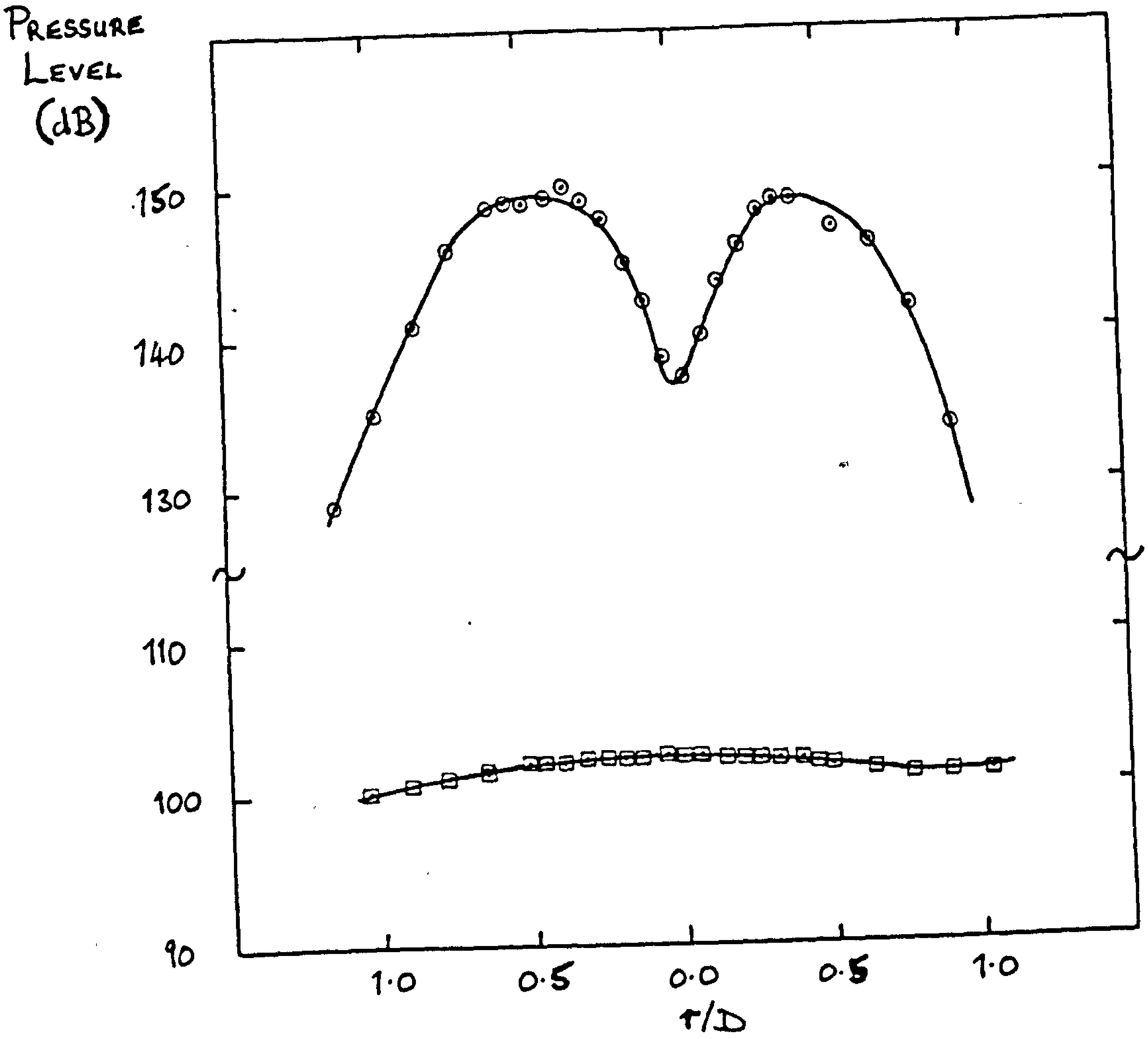

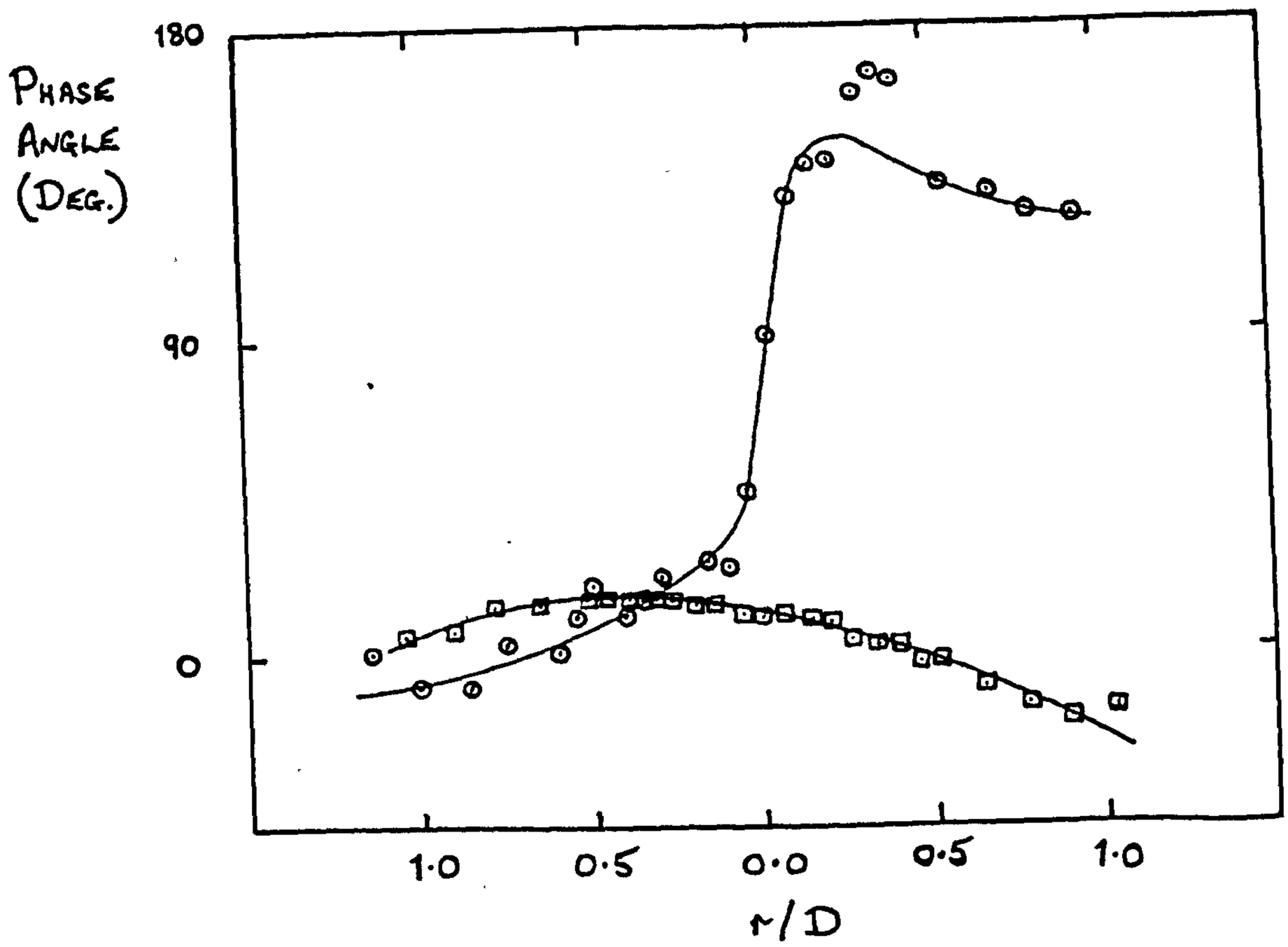

CHAPTER 3 A THEORETICAL STUDY OF SPINNING MODES ON A SLOWLY DIVERGING MEAN FLOW

3.1 Introduction

The organised behaviour of the large scale structures seen on a turbulent jet bears a close similarity to the high Reynolds number instability of the laminar jet, as first described by Reynolds [61]. It would therefore seem natural to construct a theoretical model for the observed coherent structures in terms of the instability modes of a hypothetical laminar flow, whose velocity profile is equivalent to the mean flow profile of the turbulent jet. However, a number of simplifying assumptions have first to be made. The linearisation of the Navier-Stokes equations to produce the governing equations for a small perturbation to a prescribed mean flow is not at all obvious when the mean flow is slowly diverging and, as such, does not itself satisfy the laminar flow equations of motion. The aim of this first section is to provide an explanation for this and to show that the assumptions are justified.

The basic concept, from which this justification will be realised, is that there is an asymptotic separation between both the length and time scales of the fine-grained turbulence and those of the large scale wave. In particular, if L is the shear layer thickness and D the jet diameter, this separation is characterised by the small parameter $\varepsilon = L/D \ll 1$. It is argued that the turbulence scales on L, U and the wave on D, U, where U is the mean velocity on the centre line at the nozzle exit.

The flow quantities are decomposed into an ensemble mean plus a random turbulent field (denoted by ′) plus a large scale field (denoted by ˜), so that the velocity is written as

$$\underline{u} = \underline{U}(\underline{x}/L) + \underline{u}'(\underline{x}/L,\ Ut/L) + \tilde{\underline{u}}(\underline{x}/D,\ Ut/D) \qquad (3.1.1a)$$

and the kinematic pressure as

$$p = P(\underline{x}/L) + p'(\underline{x}/L,\ Ut/L) + \tilde{p}(\underline{x}/D,\ Ut/D)\ . \qquad (3.1.1b)$$

The momentum equation is then

$$\left[\frac{U}{L}\,\underline{u}'_t + \frac{U}{D}\,\tilde{\underline{u}}_t\right] + (\underline{U} + \underline{u}' + \tilde{\underline{u}})\ .\ \left[\frac{1}{L}\ \nabla\underline{U} + \frac{1}{L}\,\nabla\underline{u}' + \frac{1}{D}\,\nabla\tilde{\underline{u}}\right]$$

$$= -\frac{1}{L}\,\nabla P - \frac{1}{L}\,\nabla p' - \frac{1}{D}\,\nabla\tilde{p} \qquad (3.1.2)$$

where we here use the suffix t and the ∇ operator to denote a differentiation with respect to the full time or space arguments expressed in (3.1.1), respectively.

When the terms in this equation are averaged over a long time T, such that $T \gg L/U,\ D/U$, (this average being denoted by $\langle\ \ \rangle$), the few surviving terms produce an equation relating the mean flow and the mean Reynolds stresses generated both by the fine-scale turbulence and by the large scale wave,

$$\frac{1}{L}\,\underline{U}.\nabla\underline{U} + \frac{1}{L}\,\langle\underline{u}'.\nabla\underline{u}'\rangle + \frac{1}{D}\,\langle\tilde{\underline{u}}.\nabla\tilde{\underline{u}}\rangle = -\frac{1}{L}\,\nabla P\ . \qquad (3.1.3)$$

Subtracting (3.1.3) from (3.1.2), we have

$$\left[\frac{U}{L}\underline{u}'_t + \frac{U}{D}\tilde{\underline{u}}_t\right] + \underline{U}\cdot\left[\frac{1}{L}\nabla\underline{u}' + \frac{1}{D}\nabla\tilde{\underline{u}}\right]$$

$$+ \frac{1}{L}\underline{u}'.\nabla\underline{u}' - \frac{1}{L}\langle\underline{u}'.\nabla\underline{u}'\rangle + (\underline{u}' + \tilde{\underline{u}})\cdot\left[\frac{1}{L}\nabla\underline{U} + \frac{1}{D}\nabla\tilde{\underline{u}}\right]$$

$$+ \frac{1}{L}\tilde{\underline{u}}.\nabla\underline{u}' = -\frac{1}{L}\nabla p' - \frac{1}{D}\nabla\tilde{p} \qquad (3.1.4)$$

where the term $\frac{1}{D}\langle\tilde{\underline{u}}.\nabla\tilde{\underline{u}}\rangle$ in (3.1.3) has been neglected since it is non-linear, of second order in the instability wave amplitude.

We proceed by taking a second time average, but this time such that $L/U \ll T \ll D/U$, (denoted by $\overline{(\quad)}$), and (3.1.4) gives

$$\frac{U}{D}\tilde{u}_t + \frac{1}{D}\underline{U}.\nabla\tilde{\underline{u}} + \frac{1}{L}\tilde{\underline{u}}.\nabla\underline{U} + \frac{1}{D}\tilde{\underline{u}}.\nabla\tilde{\underline{u}}$$

$$+ \frac{1}{L}\overline{\tilde{\underline{u}}.\nabla\underline{u}'} = -\frac{1}{D}\nabla\tilde{p} \quad . \qquad (3.1.5)$$

It can be seen that, neglecting the interaction between $\underline{u}'$ and $\tilde{\underline{u}}$ and the non-linear wave term $\frac{1}{D}\tilde{\underline{u}}.\nabla\tilde{\underline{u}}$, (3.1.5) is equivalent to the required equation for a small perturbation to a hypothetical mean flow,

$$\left(\frac{\partial}{\partial t} + \underline{U}.\nabla\right)\tilde{\underline{u}} + (\tilde{\underline{u}}.\nabla)\,\underline{U} = -\nabla\tilde{p} \quad . \qquad (3.1.6)$$

There is thus no requirement that the mean flow should be parallel, merely that it satisfies (3.1.3), and as a result, (3.1.6) and the continuity equation div $\tilde{\underline{u}} = 0$ will be taken as the governing

equations in the next section.

3.2 Analysis

The analysis which follows assumes an inviscid incompressible flow with no external forces. We adopt a cylindrical co-ordinate system and work from the appropriate form of the Euler equations; that is

$$\frac{\partial \underline{u}}{\partial t} + (\underline{u}.\nabla)\,\underline{u} = -\nabla p \qquad (3.2.1)$$

$$\text{div}\ \underline{u} = 0$$

where $\underline{u} = \underline{u}(x,r,\theta,t)$ is the total velocity and $p = p(x,r,\theta,t)$ is the kinematic pressure. The flow variables are normalised with respect to a typical length scale R, being the radius of the jet at $x = 0$, and a velocity U_o, the mean axial velocity on the centre line at $x = 0$ (the same normalisation is used in section 3.4).

We wish to examine the growth of small perturbations on an axisymmetric mean flow and thus consider the flow quantities to comprise a steady part and a time-dependent fluctuation

$$\underline{u}(x,r,\theta,t) = \underline{U}(x,r) + \tilde{\underline{u}}\,(x,r,\theta,t) \qquad (3.2.2)$$

and similarly $\qquad p = P + \tilde{p}$

where $\underline{u} = (u_x,u_r,u_\theta)$, $\tilde{\underline{u}} = (\tilde{u}_x,\tilde{u}_r,\tilde{u}_\theta)$ and the mean flow velocity

can be expressed in terms of a stream function Ψ, such that

$$\underline{U} = \left(\frac{1}{r}\frac{\partial \Psi}{\partial r}, -\frac{1}{r}\frac{\partial \Psi}{\partial x}, \ 0\right) .$$

The linearised equations of motion now correspond to those derived in section (3.1), namely

$$\frac{\partial \tilde{\underline{u}}}{\partial t} + (\underline{U}.\nabla)\ \tilde{\underline{u}} \ + (\tilde{\underline{u}}\ .\nabla)\ \underline{U} = -\nabla \tilde{p} \qquad (3.2.3)$$

and $$\text{div}\ \tilde{\underline{u}} = 0.$$

We further assume that the disturbances have a prescribed real frequency ω, that is they oscillate in time, but are allowed to grow in space.

Parallel Mean Flow

When we confine ourselves to a parallel mean flow, $\underline{U} = (U(r),0,0)$, and take, for example,

$$\tilde{u}_x(x,r,\theta,t) = \phi_x(r)\ \exp\left[i(\alpha x - \omega t + m\theta)\right] \qquad (3.2.4)$$

where $\phi_x(r)$ is the radial dependence of the axial eigenfunction $\tilde{u}_x$, α is the complex wavenumber in the axial direction and the prescribed azimuthal wavenumber m is an integer, then (3.2.3) becomes

$$\begin{pmatrix} U - \frac{\omega}{\alpha} & -\frac{i}{\alpha}\frac{dU}{dr} & 0 & 1 \\ 0 & U - \frac{\omega}{\alpha} & 0 & -\frac{i}{\alpha}\frac{d}{dr} \\ 0 & 0 & U - \frac{\omega}{\alpha} & \frac{m}{\alpha r} \\ 1 & -\frac{i}{\alpha}\left(\frac{d}{dr} + \frac{1}{r}\right) & \frac{m}{\alpha r} & 0 \end{pmatrix} \begin{pmatrix} \phi_x \\ \phi_r \\ \phi_\theta \\ \phi_p \end{pmatrix} = \begin{pmatrix} 0 \\ 0 \\ 0 \\ 0 \end{pmatrix}$$

or $\underline{L}(\alpha,\omega) \cdot \underline{\phi} = \underline{0}$. (3.2.5)

It is somewhat simpler to work in terms of a single variable, and (3.2.5) reduces to a second order differential equation for the pressure term

$$\frac{d^2\phi_p}{dr^2} + \left[\frac{1}{r} - \frac{2\frac{dU}{dr}}{(U - \frac{\omega}{\alpha})}\right]\frac{d\phi_p}{dr} - \left(\frac{m^2}{r^2} + \alpha^2\right)\phi_p = 0. \qquad (3.2.6)$$

Near $r = 0$, the mean velocity profile of Michalke [48], (3.3.1) becomes $U = 1 + O(e^{-1/r})$ and (3.2.6) is approximated by the modified Bessel equation in terms of the independent variable $z = \alpha r$,

$$\frac{d^2\phi_p}{dz^2} + \frac{1}{z}\frac{d\phi_p}{dz} - \left(1 + \frac{m^2}{z^2}\right)\phi_p = 0. \qquad (3.2.7)$$

Also, this form for the mean velocity decays rapidly as $r \to \infty$, and (3.2.7) is the appropriate equation to be satisfied for large r.

So the parallel flow solution is obtained by solving the eigenvalue problem defined by equation (3.2.6) and the boundary

conditions, with a suitable normalisation, say for definiteness, as one possibility

$$\phi_p \sim 1 \cdot I_m(\alpha r) \text{ as } r \to 0, \qquad \phi_p \sim BK_m(\alpha r) \text{ as } r \to \infty \tag{3.2.8}$$

which have been chosen so that the pressure fluctuation vanishes as $r \to \infty$ and takes a value derived from the physical conditions for the mth mode as $r \to 0$. The physical conditions at $r = 0$ are simply that the pressure fluctuation is finite for an $m = 0$ (plane wave) mode and zero for the higher order modes.

The eigenvalues to be found, for a fixed ω, are the complex wavenumber α and the complex constant B. There are thus four unknown quantities, for each real frequency ω, which are uniquely determined by solving the complex second order differential equation (3.2.6) with the given boundary conditions and a prescribed mean flow.

The parallel flow case has been presented at this stage in anticipation of the zeroth-order solution in the multiple scales expansion, which will satisfy a system of equations analogous to (3.2.5). It is also useful to note here that the adjoint eigenfunction for the pressure, which is required later in the derivation of the amplitude equation, is

$$\hat{\phi}_p = \frac{r\phi_p}{(U - \frac{\omega}{\alpha})^2} \tag{3.2.9}$$

from (3.2.6), by inspection.

Slowly Diverging Mean Flow

The mean flow is now assumed to be slowly varying in the axial

direction and we proceed, as in Crighton & Gaster [19], by introducing two new space variables. We define a slow space scale $X = \varepsilon x$, where ε is a small parameter which is a measure of the divergence of the jet, so that the mean velocity $\underline{U} \equiv \underline{U}(r,X)$ will now have a small component in the radial direction.

In addition, a strained fast variable $\eta = g(X)/\varepsilon$ is required to replace x in the exponential behaviour with axial distance. (This is analogous to the technique used in "Ray Theory" (Whitham [66]), whereby the solution of certain partial differential equations, in the context of a stable but slowly changing medium, is accomplished by expanding the dependent variable ϕ, say, in terms of a series of uniformly bounded amplitude functions $(A_o, A_1, \ldots)$. The exponential dependence is expressed in terms of a single strained fast variable Θ, such that

$$\phi(X,T) = e^{\frac{i}{\varepsilon}\Theta(X,T)} \left[A_o(X,T) + \varepsilon A_1(X,T) + \ldots\right] \quad ,$$

where we have considered a more general case having both slow space and time scales, X and T, respectively.) The only constraint on η is that $g(X) = O(X)$ as $X \to 0$, in order to recover the parallel flow results, and $g(X)$ is to be determined during the course of the analysis.

Expanding $\tilde{u}_x$, $\tilde{u}_r$, $\tilde{u}_\theta$ and $\tilde{p}$ in powers of ε, so that

$$\underline{\tilde{u}}(r,\theta,\eta,X,t) = e^{-i(\omega t - m\theta)} \left\{\underline{u}^o(r,\eta,X) + \varepsilon \underline{u}^1(r,\eta,X) + \ldots\right\}$$

$$\tilde{p}(r,\theta,\eta,X,t) = e^{-i(\omega t - m\theta)} \left\{p^o(r,\eta,X) + \varepsilon p^1(r,\eta,X) + \ldots\right\} \qquad (3.2.11)$$

and assuming further that

$$\begin{pmatrix} u_x^o \\ u_r^o \\ u_\theta^o \\ p^o \end{pmatrix} = e^{in} \begin{pmatrix} v_x^o \\ v_r^o \\ v_\theta^o \\ v_p^o \end{pmatrix} \quad (r,X) \quad ,$$

to the zeroth order, (3.2.3) becomes

$$\begin{pmatrix} U-\omega/g'(X) & 0 & 0 & 1 \\ 0 & U-\omega/g'(X) & 0 & -\frac{i}{g'(X)}\frac{\partial}{\partial r} \\ 0 & 0 & U-\omega/g'(X) & \frac{m}{rg'(X)} \\ 1 & \frac{-i}{g'(X)}\left(\frac{\partial}{\partial r}+\frac{1}{r}\right) & \frac{m}{rg'(X)} & 0 \end{pmatrix} \begin{vmatrix} v_x^o \\ v_r^o \\ v_\theta^o \\ v_p^o \end{vmatrix} = \begin{vmatrix} 0 \\ 0 \\ 0 \\ 0 \end{vmatrix} \qquad (3.2.12)$$

where U is the x-component of the mean velocity $\underline{U}$.

At a given axial position, (3.2.12) is simply the local parallel flow problem (3.2.5) relating to this station. The solution is thus

$$\underline{v}^o = A(X)\ \underline{\phi}(r,X) \text{ with } g(X) = \int_{X_o}^{X} \alpha(\xi)\ d\xi \qquad (3.2.13)$$

where $\alpha(X)$ and $\underline{\phi}(r,X)$ are the local wavenumber and eigenvector

satisfying

$$\underline{L}(\alpha(X),\omega) \cdot \underline{\phi}(r,X) = \underline{0} \qquad (3.2.14)$$

and $\underline{\phi}$ has been given a definite normalisation, that of (3.2.8), for example. Any convenient normalisation for $\underline{\phi}$ would be suitable, but it must be a smooth function of the slow axial co-ordinate. As will be seen later (3.2.20), the amplitude function A(X) at a given axial station involves a number of definite integrals containing $\underline{\phi}$ and its derivatives, and it is essential that there are no discontinuities arising from an arbitrary choice of normalisation at each axial position.

In terms of the pressure term v_p^o alone, (3.2.12) can be written as

$$\frac{\partial^2 v_p^o}{\partial r^2} + \left[\frac{1}{r} - \frac{2\,\frac{\partial U}{\partial r}}{(U - \omega/\alpha(X))}\right] \frac{\partial v_p^o}{\partial r} - \left(\frac{m^2}{r^2} + \alpha^2(X)\right) v_p^o = 0$$

$$\text{or } L\, v_p^o = 0. \qquad (3.2.15)$$

Amplitude Equation

We now derive an equation for the amplitude function A(X) by considering the $O(\varepsilon)$ terms in the expansion. At $O(\varepsilon)$, (3.2.3) gives

$$\begin{pmatrix} -i\omega + U\alpha\frac{\partial}{\partial\eta} & 0 & 0 & i\alpha \\ 0 & -i\omega + U\alpha\frac{\partial}{\partial\eta} & 0 & \frac{\partial}{\partial r} \\ 0 & 0 & -i\omega + U\alpha\frac{\partial}{\partial\eta} & \frac{im}{r} \\ i\alpha & \frac{\partial}{\partial r} + \frac{1}{r} & \frac{im}{r} & 0 \end{pmatrix} \begin{pmatrix} u_x^1 \\ u_r^1 \\ u_\theta^1 \\ p^1 \end{pmatrix}$$

$$= \exp(i\eta)\ \{\underline{F}\ .\ \underline{v}^o(r,X) - \underline{G}\ .\ \frac{\partial \underline{v}^o}{\partial X}(r,X)\}\ . \qquad (3.2.16)$$

Since the inhomogeneous terms in (3.2.16) involve the zeroth order solution $\underline{v}^o$, we would expect $\underline{u}^1$ to contain secular terms. We thus write

$$\underline{u}^1(r,\eta,X) = \gamma\ \eta\ \exp(i\eta)\ \underline{v}^o + \exp(i\eta)\ \underline{h}\quad ,$$

where $\underline{h} = \begin{pmatrix} h_x \\ h_r \\ h_\theta \\ h_p \end{pmatrix}$, and (3.2.16) becomes

$$i\alpha(X)\ \underline{L}(\alpha(X),\omega)\ \ \underline{h} = \underline{F}.\underline{v}^o - \underline{G}\ .\ (\frac{\partial \underline{v}^o}{\partial X} + \gamma\ \alpha\ \underline{v}^o)\ . \qquad (3.2.17)$$

When the velocity corrections h_x, h_r and h_θ are eliminated, the

single equation for the pressure term h_p is

$$L\, h_p = -i\alpha \left[\frac{\partial U}{\partial X} - \frac{1}{r}\frac{\partial \Psi}{\partial X}\frac{\partial}{\partial r}\right] v_x^o + \frac{im}{r}\left[\frac{1}{r}\frac{\partial \Psi}{\partial X}\frac{\partial}{\partial r} + \frac{1}{r^2}\frac{\partial \Psi}{\partial X}\right] v_\theta^o$$

$$+ \left[\frac{1}{r}\frac{\partial \Psi}{\partial X}\frac{\partial^2}{\partial r^2} + \left(2\frac{\partial U}{\partial X} - \omega\frac{1}{r^2}\frac{\partial \Psi}{\partial X}\right)\frac{\partial}{\partial r} + \frac{\partial^2 U}{\partial r \partial X} + \frac{1}{r^3}\frac{\partial \Psi}{\partial X}\right.$$

$$\left. + \frac{2\gamma\alpha\omega}{(U - \omega/\alpha)}\frac{\partial U}{\partial r}\left(\frac{1}{r^2}\frac{\partial \Psi}{\partial X} - \frac{\partial U}{\partial X}\right)\right] v_r^o$$

$$- i\omega\left(\frac{\partial v_x^o}{\partial X} + \gamma\alpha\, v_x^o\right) - \frac{imU}{r}\left(\frac{\partial v_\theta^o}{\partial X} + \gamma\alpha\, v_\theta^o\right) - i\alpha\left(\frac{\partial v_p^o}{\partial X} + \gamma\alpha\, v_p^o\right)$$

$$\left[\left(U + \frac{2}{r(U - \omega/\alpha)}\frac{\partial U}{\partial r}\frac{\partial \Psi}{\partial X}\right)\frac{\partial}{\partial r} + \left(1 - \frac{2U}{(U - \omega/\alpha)}\right)\frac{\partial U}{\partial r} + \frac{U}{r}\right]\left(\frac{\partial v_r^o}{\partial X} + \gamma\alpha\, v_r^o\right)$$

or
$$L\, h_p = \underline{r} \cdot \underline{v}^o + \underline{s} \cdot \left(\frac{\partial \underline{v}^o}{\partial X} + \gamma\alpha\, \underline{v}^o\right) \qquad (3.2.18)$$

We then apply an orthogonality condition to (3.2.18) to ensure that h_p is finite at $r = 0$ and vanishes as $r \to \infty$, and obtain

$$\int_o^\infty \hat{\phi}_p \left[\underline{r} \cdot \underline{v}^o + \underline{s} \cdot \left(\frac{\partial \underline{v}^o}{\partial X} + \gamma\alpha\, \underline{v}^o\right)\right] dr = 0 , \qquad (3.2.19)$$

where $\hat{\phi}_p$ is defined in (3.2.9). The first term in the expression for

† With reference to equation (3.2.21), this is not in the form of the parallel flow result plus an $O(\epsilon)$ correction for non-parallel effects — indeed the method of multiple scales never leads to results of that form because it is specifically designed to eliminate the non-uniformities at large x which would inevitably arise from such a form. For bounded ranges of x, however, (3.2.21) may readily be expanded in the form of the parallel flow result plus a correction, but this is useful only if the non-parallel effects are slow and small in total. In equation (3.2.21), on the other hand, the non-parallel effects must be slow and therefore locally small but over a sufficiently large downstream distance may lead to an $O(1)$ change from parallel flow theory. Similar remarks apply to the relation on p.136 between the local wavenumber α and the effective wavenumber $\bar{\alpha}$; $\bar{\alpha}-\alpha$ is small, $O(\epsilon)$, for $x = O(1)$, but $\bar{\alpha}-\alpha$ may well be $O(1)$ or larger if the downstream distance is sufficiently large.

p^1 above is $O(\varepsilon\eta)$ with respect to the zeroth order solution, but $\varepsilon\eta$ is $g(X)$, so the first order correction will be $O(1)$ when X is $O(1)$. In order for the expansion to be uniformly valid we must put $\gamma = 0$ and (3.2.19) then produces the required amplitude equation

$$m(X)\,\frac{dA(X)}{dX} + n(X)\,A(X) = 0\ , \qquad (3.2.20)$$

where $$m(X) = \int_o^\infty \hat{\phi}_p\,\underline{s}\cdot\underline{\phi}\,dr$$

and $$n(X) = \int_o^\infty \hat{\phi}_p\,(\underline{s}\cdot\frac{\partial\underline{\phi}}{\partial X} + \underline{r}\cdot\underline{\phi})\,dr\ .$$

So, to the zeroth order, the pressure can be written as

$$\tilde{p}(r,X,\theta,t) = A_o\,\phi_p(r,X)\,\exp\{i\int_{X_o}^{X}\frac{\alpha(\xi)}{\varepsilon}\,d\xi - \int_{X_o}^{X}\frac{n(\xi)}{m(\xi)}\,d\xi - i(\omega t - m\theta)\}, \qquad (3.2.21)$$

and similarly for each velocity component, e.g.,

$$\tilde{u}_x(r,X,\theta,t) = A_o\,\phi_x(r,X)\,\exp\{i\int_{X_o}^{X}\frac{\alpha(\xi)}{\varepsilon}d\xi - \int_{X_o}^{X}\frac{n(\xi)}{m(\xi)}\,d\xi - i(\omega t - m\theta)\},$$

since the problem is linear.†

It is evident at this stage that the slow space variable X has only served to distinguish the slow amplitude variation from the sinusoidal behaviour in the axial direction, and, since n/m is homogeneous in X, it can be replaced by x in (3.2.21). Thus, we can write

$$\tilde{p}(r,x,\theta,t) = A_o\ \phi_p(r,x)\ \exp\ \{i \int_{x_o}^{x} \alpha(x')\ dx'$$

$$- \int_{x_o}^{x} \frac{n(x')}{m(x')}\ dx' - i(\omega t - m\theta)\} \qquad (3.2.22).$$

For a given frequency and mode, there are three terms in this expression which contain both amplitude and phase information and this information is transferred between these three terms by choosing a different normalisation on ϕ_p. Furthermore, it is important to recognise that, unlike the parallel flow result, this expression can predict changes in growth rate (or phase) not only with axial position, but also with flow characteristic and radial position. Clearly, the wavenumber for the flow variable Q, defined by

$$\bar{\alpha}(x,\ r|Q) = -\ i\ \frac{\partial}{\partial x}\ \ln\ Q(r,x) \qquad (3.2.23)$$

has the same properties. For the pressure, say, this can be written as

$$\bar{\alpha}(x,\ r|\tilde{p}) = -\ i\ \frac{\partial}{\partial x}\ \ln\ \phi_p + \alpha(x) - \frac{n(x)}{m(x)}\ .$$

This demonstrates the meaninglessness of the comparison that has been made by a number of previous investigators (e.g., Mattingly & Chang [47]), between the axial variation of the quantity α, obtained from a quasi-parallel "slice" analysis, with that of the experimental wavenumber, since the former depends entirely on the normalisation used.

The expressions (3.2.22 - 23) have to be evaluated numerically

and this is described in section 3.4.

3.3 Mean Velocity Profile

Michalke [48], and later Mattingly & Chang [47], observed how crucially the stability problem depended on the details of the mean velocity profile. Michalke made a more realistic choice than had previously been made at the time, using (in dimensional form)

$$U(r) = \frac{U_o}{2} \{1 + \tanh [b (\frac{R}{r} - \frac{r}{R})]\} \qquad (3.3.1)$$

where $b = R/4\delta$, δ is a momentum thickness and R is the jet radius defined by $U(R) = U_o/2$. This, he found, gave reasonable agreement with the measured profile of Crow & Champagne [22] at the station $x = 2D$, provided $b = 25/16$.

This was generalised by Crighton & Gaster to give a slowly diverging profile over the first six diameters of the jet. They used

$$U(r,x) = \frac{U_o}{2} \{1 + \tanh [\frac{25R}{(3x + 4)} (\frac{R}{r} - \frac{r}{R})]\} \qquad (3.3.2)$$

which has a virtual origin at $x = \frac{2}{3} D$ and a divergence rate of 3/100.

This profile was calculated purely on the basis of the similarity rules which apply to the initial region of the jet ($x \lesssim 6D$), that the velocities are invariant with x and the turbulence length scales increase linearly with x, and it was chosen to agree with (3.3.1) at $x = 2D$.

There is close agreement between the above profile (3.3.2) and the experimental results of chapter 2 over the first four diameters of the jet, figure 65 : indeed, the agreement is much closer than Michalke had vis à vis Crow & Champagne's results. We have therefore chosen to use (3.3.2) as the mean velocity profile in the present calculations, not merely for its convenience, but more in the light of its experimental justification.

A detailed comparison of the theoretical and experimental flow results is presented in chapter 4, but in this chapter we confine ourselves to a more general discussion of the behaviour of the spinning modes on the same mean flow.

3.4 Numerical Procedure

The numerical formulation consisted of two main calculations, firstly the solution of the eigenvalue problem, (3.2.15) with the associated boundary conditions, and secondly, the evaluation of the integrals, m(x) and n(x), and subsequently the amplitude and the phase speed (or wavelength) of each flow variable. The input required was the mode number, the frequency, the mean velocity profile, the initial downstream station and a guess for the complex eigenvalue at that station.

The eigenvalue problem had to be solved at a set of axial stations and certain information needed to be retained in order to evaluate derivatives with respect to the downstream co-ordinate at each station. The downstream behaviour was sufficiently smooth to allow the distance between consecutive stations to be as large as

R/10, and the derivatives were expressed as central differences over this steplength.

At any given axial station, the eigenvalue problem in terms of the radial co-ordinate was solved using an iterative procedure which involved a finite difference method, to integrate numerically in the radial direction, and a standard routine (a combination of the Newton and steepest descent methods) to iterate from the initial guess.

The problem to be solved at each station x, consisted of the equation (3.2.15)

$$\frac{\partial^2 v_p^o}{\partial r^2} + \left[\frac{1}{r} - \frac{2\,\frac{\partial U}{\partial r}}{(U - \omega/\alpha)}\right] \frac{\partial v_p^o}{\partial r} - \left(\frac{m^2}{r^2} + \alpha^2\right) v_p^o = 0$$

and the boundary conditions

$$v_p^o \sim I_m(\alpha r) \text{ as } r \to 0$$

$$v_p^o \sim BK_m(\alpha r) \text{ as } r \to \infty, \qquad \text{where } \alpha = \alpha(x) \ .$$

The integration, using the finite different scheme, was started at both r = 0.0033 and at r = 5 ($r \to \infty$) with the boundary values

$$v_p^o = I_m(0.0033\alpha) \quad \text{and} \quad v_p^o = K_m(5\alpha) \ ,$$

respectively. The gradients of the pressures resulting from the forward and backward integrations were then matched at $r_m = 2.5$.

If at r_m

$$v_{p_f} = C\, v_{p_b}$$

where v_{p_f}, v_{p_b} are the pressures at r_m resulting from the forward and backward integrations, respectively, then the gradients, in the form of central differences,

$$\frac{\partial v_{p_f}}{\partial r}\Big|_{c.d.} \text{ and } \frac{\partial v_{p_b}}{\partial r}\Big|_{c.d.}, \text{ satisfy } \frac{\partial v_{p_f}}{\partial r}\Big|_{c.d.} = C\,\frac{\partial v_{p_b}}{\partial r}\Big|_{c.d.}, \text{ and}$$

$$\text{therefore } v_{p_f}\,\frac{\partial v_{p_b}}{\partial r}\Big|_{c.d.} - v_{p_b}\,\frac{\partial v_{p_f}}{\partial r}\Big|_{c.d.} = 0.$$

So the matching was achieved by minimising the expression

$$v_{p_f}\,\frac{\partial v_{p_b}}{\partial r}\Big|_{c.d.} - v_{p_b}\,\frac{\partial v_{p_f}}{\partial r}\Big|_{c.d.}$$

with respect to the complex wavenumber α, by iteration. This method, using a step length of 0.0033 (1500 points) in the radial direction, gave eigenvalues which differed by less than 10^{-4} from those obtained using a step length of 0.0025 (2000 points), and for which there was insufficient store to run the complete program.

The method is described in detail here, because prior to this, two more straightforward finite difference schemes had been tried : a single forward integration with matching at large r and a single backward integration with matching at small r; but within the confines of a respectable step length (i.e., storage space on the

computer), neither of these was found to be stable (not surprisingly in view of the fact that $I_m(\alpha r) \to \infty$ as $r \to \infty$ and $K_m(\alpha r) \to \infty$ as $r \to 0$). Plaschko (private communication) experienced similar difficulties and as such was not able to determine the radial distribution of the pressure eigenfunction for large r, a problem which is not encountered in the method used here.

After a number of eigenvalues had been found, extrapolation provided a fairly accurate estimate for the eigenvalue at the next axial station and only three or four iterations were then needed to obtain the required accuracy.

All the results presented in the next section correspond to axial integrations starting from $x_o = 2.0$, because for $\lesssim 1D$ it is quite unrealistic to model the jet as doubly infinite, especially at the Strouhal numbers of principal interest where the instability wavelengths are comparable to D. (Since the integrals m(x) and n(x) were obtained using a standard routine which required four points to evaluate a numerical integral, the first data point on each curve after x_o is at $1.15D$.)

Before any spinning mode calculations were attempted, a check was performed on the program by running it with m = 0, the plane wave mode. The results for the growth rates and phase speeds were in complete agreement with those of Crighton & Gaster.

3.5 Results and Discussion

We have discussed in the previous section why a slowly diverging mean flow calculation should produce a far more realistic picture of the flow field than is given by a parallel flow model. That the proposed multiple scales method is capable of predicting a variation of axial growth rate and phase speed with flow characteristic and radial position has already been demonstrated, by Crighton & Gaster, in the case of the plane wave mode. These features are also evident in the results presented here, but we shall concentrate on the variation with azimuthal wavenumber.

Results have been obtained for the first three modes, m = 0, 1 and 2, at three different Strouhal numbers, St = 0.3, 0.4 and 0.5 (with the exception of St = 0.3 in the m = 2 mode for which case the search for the initial eigenvalues was unsuccessful). For each flow characteristic, $\tilde{u}_x$, $\tilde{u}_r$, $\tilde{u}_\theta$ and $\tilde{p}$, we have considered the axial variation of the phase speed, the axial growth rate and the radial distribution. Furthermore, in relation to their axial development, we have made comparisons between quantities evaluated on the lip line (r = R), since in the case of the m = 1 and m = 2 modes the fluctuating pressure and axial velocity are zero on the centre line.

Figure 66 shows the gain in the pressure amplitude on the lip line (re x/D = 1) for m = 0, 1 and 2 at the three different Strouhal numbers. It can be seen that at the two higher Strouhal numbers, the m = 0 mode exhibits the largest initial growth rate, whereas at the lowest Strouhal number, it is the m = 1 mode. (This

result was also obtained by Plaschko [60].) The m = 2 mode shows the lowest gain at each Strouhal number at which it was considered.

The same qualitative behaviour is found in the radial velocity fluctuation on the lip line, as shown in figure 67. For the axial velocity fluctuation, though, both the initial amplification rate and the total gain increase with mode number, irrespective of Strouhal number (figure 68). However, the axial position at which the maximum gain is reached does not move towards the nozzle exit with increasing mode number.

We have also calculated the gain in the azimuthal velocity fluctuation (at r = R) in the first and second order modes and this is shown in figure 69. At St = 0.4 and 0.5 the two modes display the same initial growth rate. However, the peak amplitude is reached in a shorter axial distance for m = 2 and it is the m = 1 mode in which the higher total gain is achieved.

It will be observed that in a number of these figures, (66 - 69), the maximum gain condition is not obtained; in others, it cannot be reached for certain values of m; yet there are also those in which the calculation can be followed through until the disturbance has almost decayed to its original amplitude. In all of these cases the calculations are restricted to regions of x/D for which the local profile is unstable at the Strouhal number and mode number considered. So the "decay" is brought about entirely by the n(x)/m(x) term in the amplitude equation whose presence is excluded by the slice analyses. In the parallel flow situation it is necessary to bring in viscous forces or equivalently, in the high Reynolds number limit, to deform the integration path for the

inviscid equations above or below the complex critical point as described in Gotoh [32], for example. An alternative method of proceeding beyond the location of maximum gain appears to be provided by introducing non-parallel effects and in the present jet problem this approach may be more realistic.

The phase speeds for the four characteristics were calculated at the above conditions, too, using equation (3.2.23) and the definition $c_{ph} = \omega/\bar{\alpha}_r$, where $\bar{\alpha}_r$ denotes the real part of $\bar{\alpha}$. Figure 70 shows the axial variation of phase speed at a fixed Strouhal number, 0.4, for each mode. The results for the axial, radial and azimuthal velocity fluctuations and the pressure fluctuation are shown in (a), (b), (c) and (d), respectively. For each flow quantity an increase in mode number results in a decrease in phase speed and this is also true at St = 0.3 and 0.5.

For a given mode, an increase in Strouhal number produces a decrease in phase velocity at x = 1D. However, beyond a certain axial distance, which varies with both mode number and flow characteristic, this relationship is reversed and the largest phase speed corresponds to a Strouhal number of 0.5. Figure 71 shows this change in behaviour in the case of the m = 1 mode for (a) the axial velocity fluctuation and (b) the pressure fluctuation.

Finally, we would like to describe a number of interesting features which are present in the radial distributions of the pressure and velocity fluctuations. Figure 72 shows the radial velocity fluctuation in the m = 1 mode at two axial positions, x = 1D and x = 2D. The results corresponding to the three different Strouhal numbers are given at each axial station, and they have been

normalised such that $\tilde{u}_r = U_o$ on the centre line at x = 1D. With this particular normalisation, a Strouhal number of 0.5 produces the largest disturbance in the centre of the shear layer on this initial region of the jet. Also, the downstream amplification is much greater near the centre line than in the shear layer, at every Strouhal number. The twin peaks described in chapter 2 appear here, too, and the larger of the two moves towards the centre of the jet in agreement with figure 22. They are not so pronounced in the corresponding radial profiles for the m = 0 mode, figure 73, which are normalised in such a manner that $\tilde{p} = U_o^2$ on the centre line at x = 1D.

The radial profiles of the axial-velocity fluctuations in the m = 0 and m = 1 modes, under the same normalisations (in each mode), appear in figures 74 and 75 and the pressure fluctuation in the m = 1 mode is shown in figure 76. In contrast with the fluctuating velocity components, the pressure is always a slowly varying quantity. A smooth radial profile is also produced in the plane wave mode (not shown here). For completeness, figure 77 shows the azimuthal velocity fluctuation in the m = 1 mode.

The radial profiles of the flow characteristics in the m = 2 mode have not been included, since the results are very similar to those produced in the m = 1 mode.

FIGURE 65: MEAN VELOCITY PROFILES AT AXIAL DISTANCES OF (a) 1D, (b) 2D, (c) 4D AND (d) 6D. (○ EXPERIMENT, — ANALYTICAL FORM)

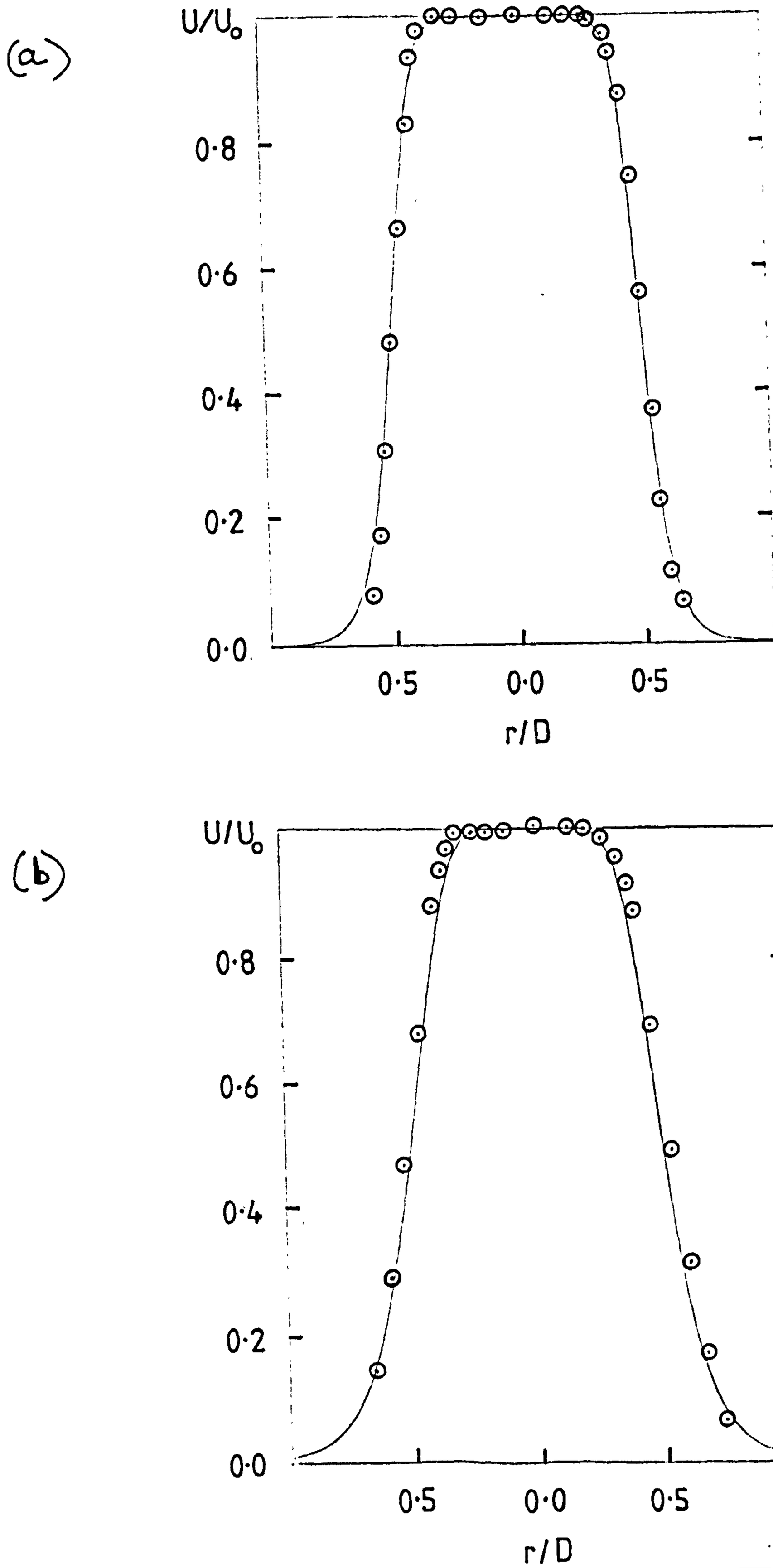

FIGURE 65 CNTD.

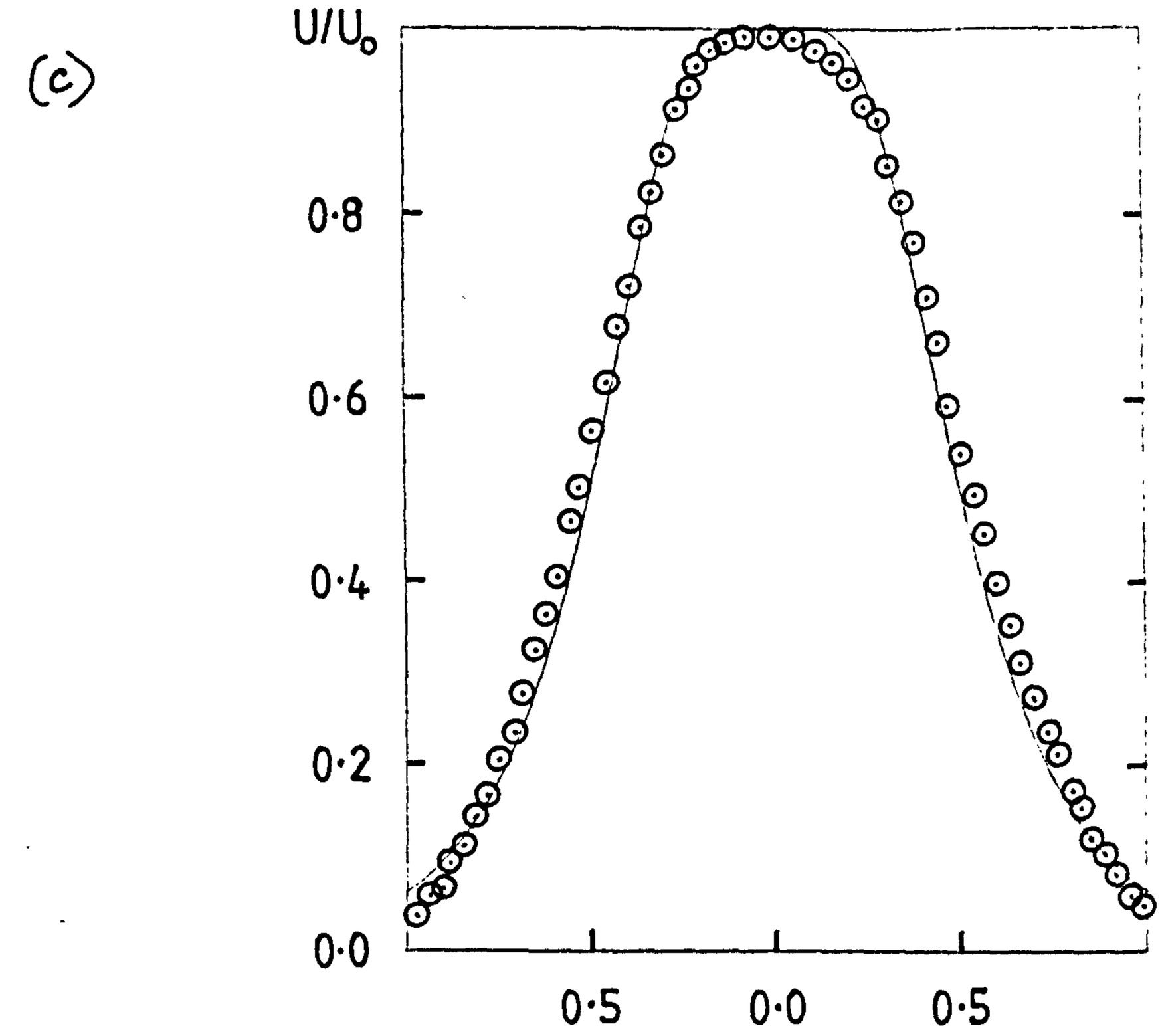

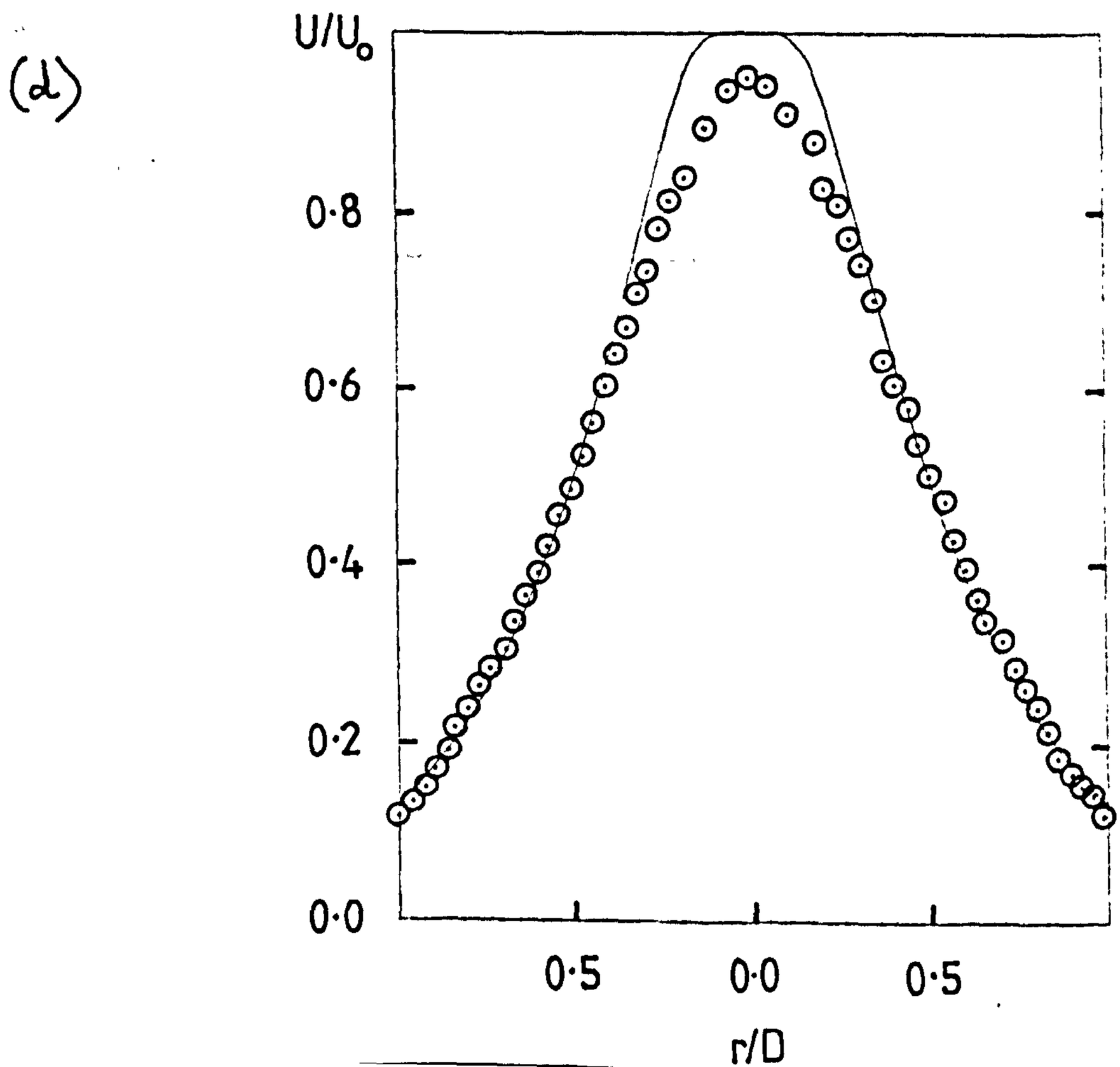

FIGURE 66 : GAIN IN SHEAR LAYER PRESSURE FLUCTUATION (r=R)

Re x/D=1

(a)

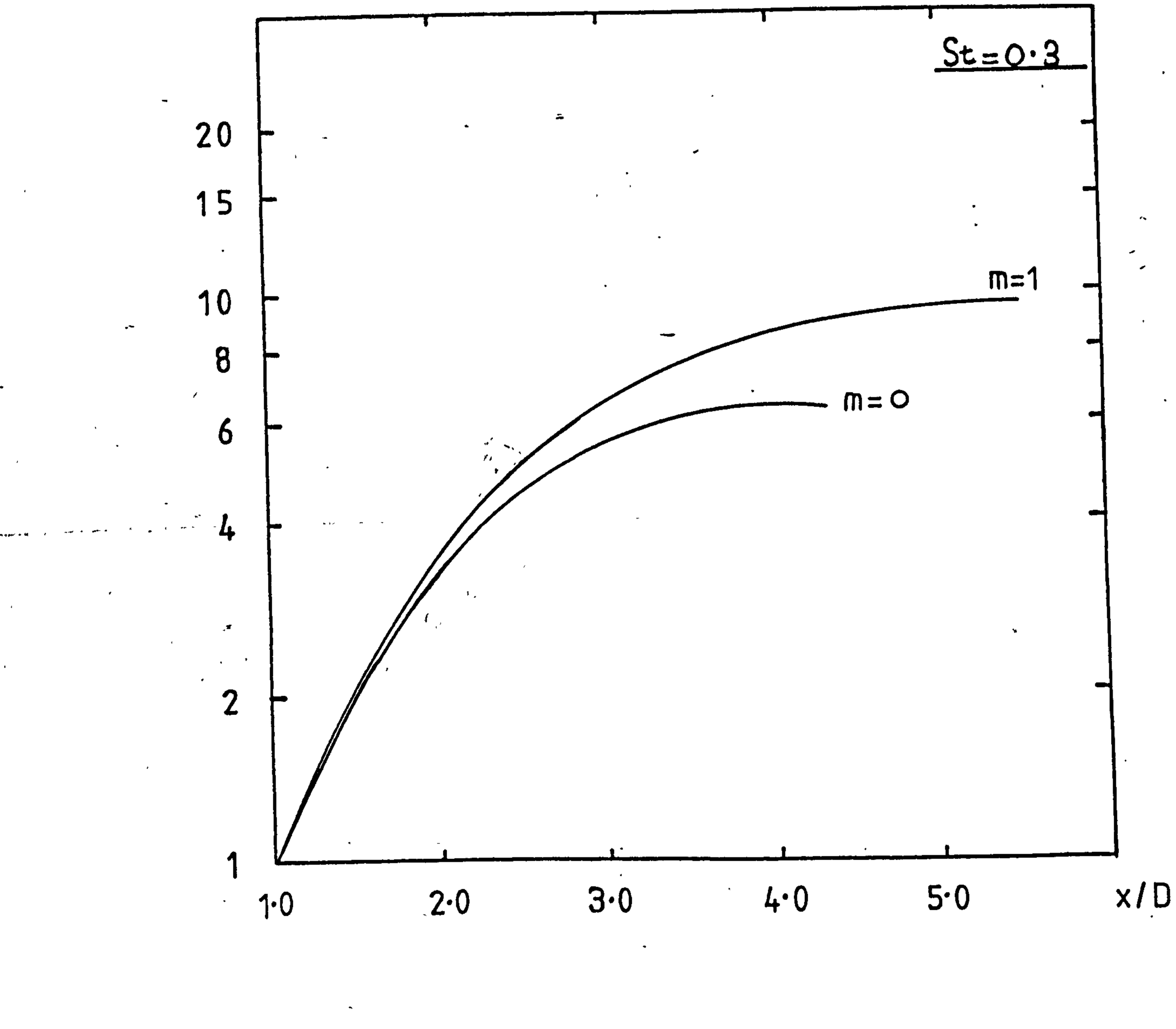

FIGURE 66 : GAIN IN SHEAR LAYER PRESSURE FLUCTUATION (r=R)

re x/D = 1

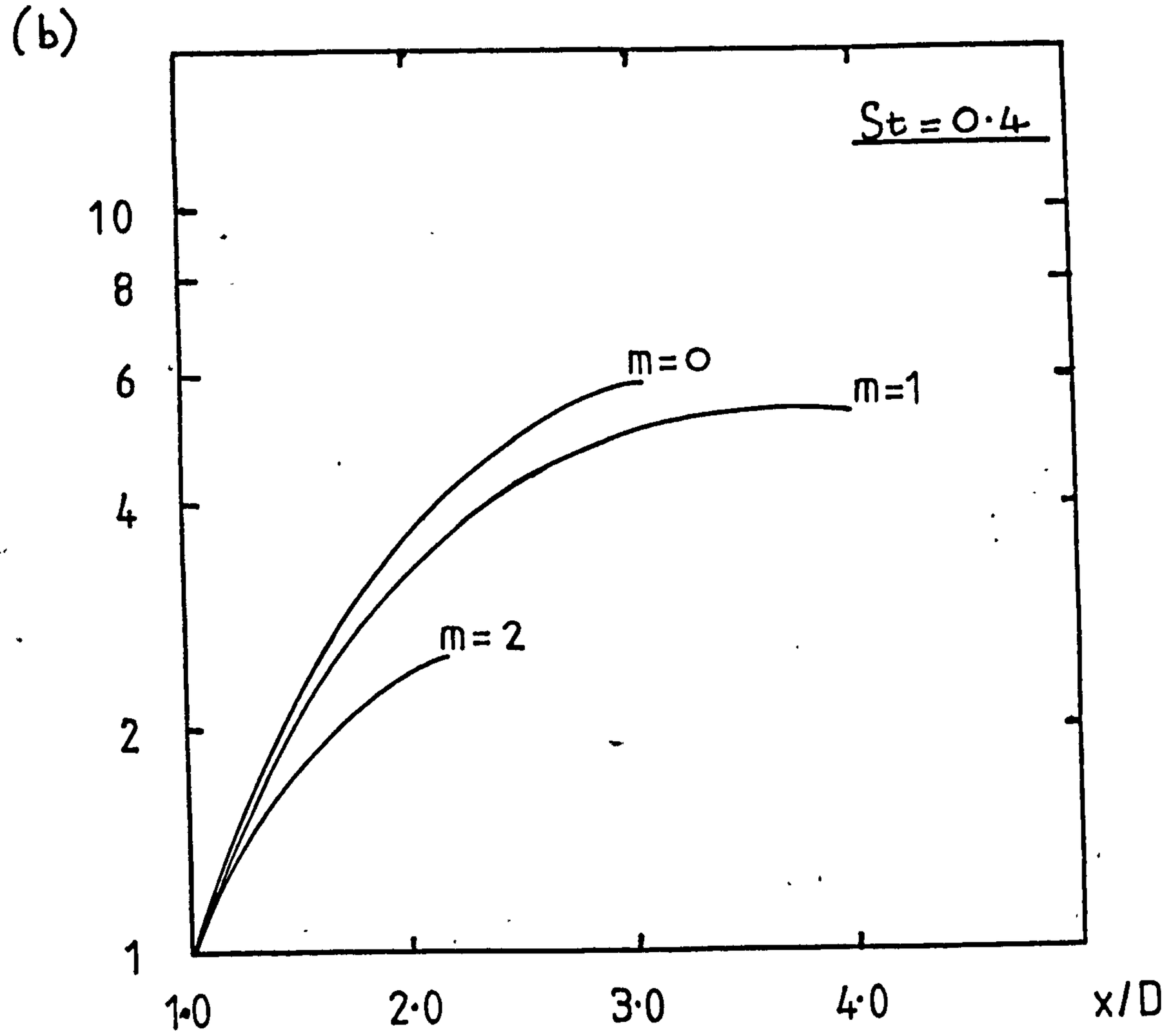

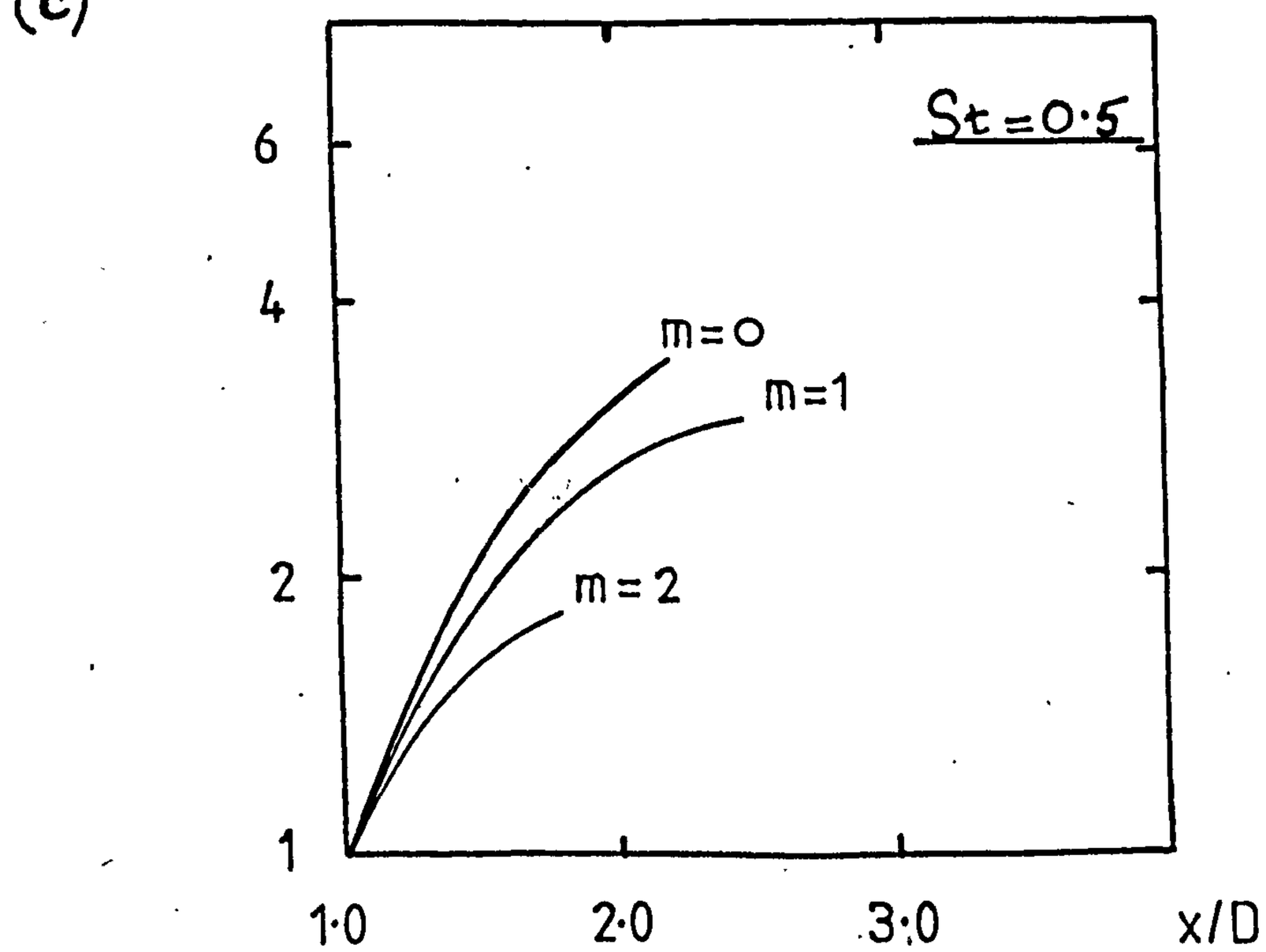

FIGURE 67 : GAIN IN SHEAR LAYER RADIAL VELOCITY FLUCTUATION (r=R)

re x/D = 1

(a)

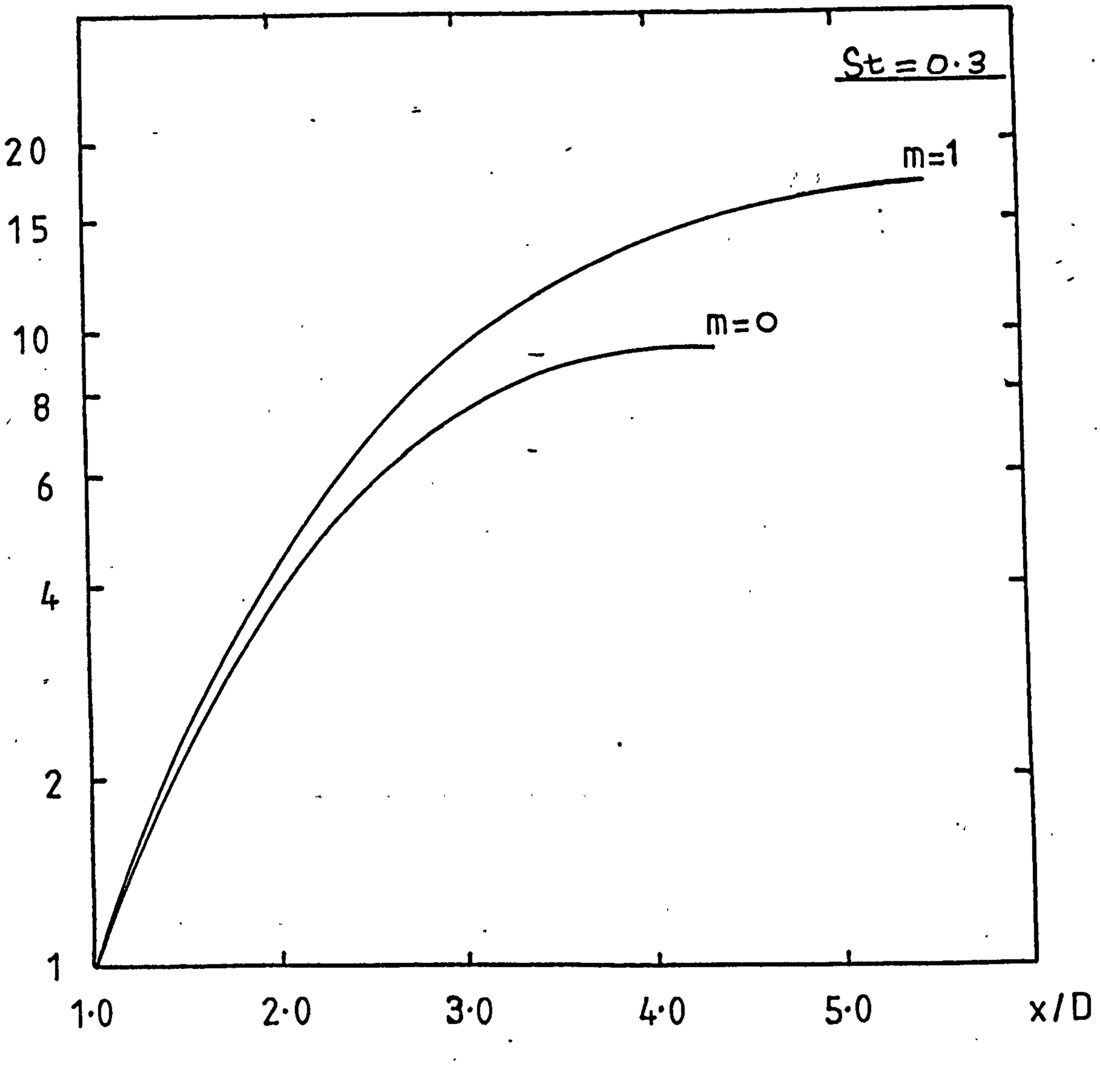

FIGURE 67 : GAIN IN SHEAR LAYER RADIAL VELOCITY FLUCTUATION ($r=R$)

re $x/D=1$

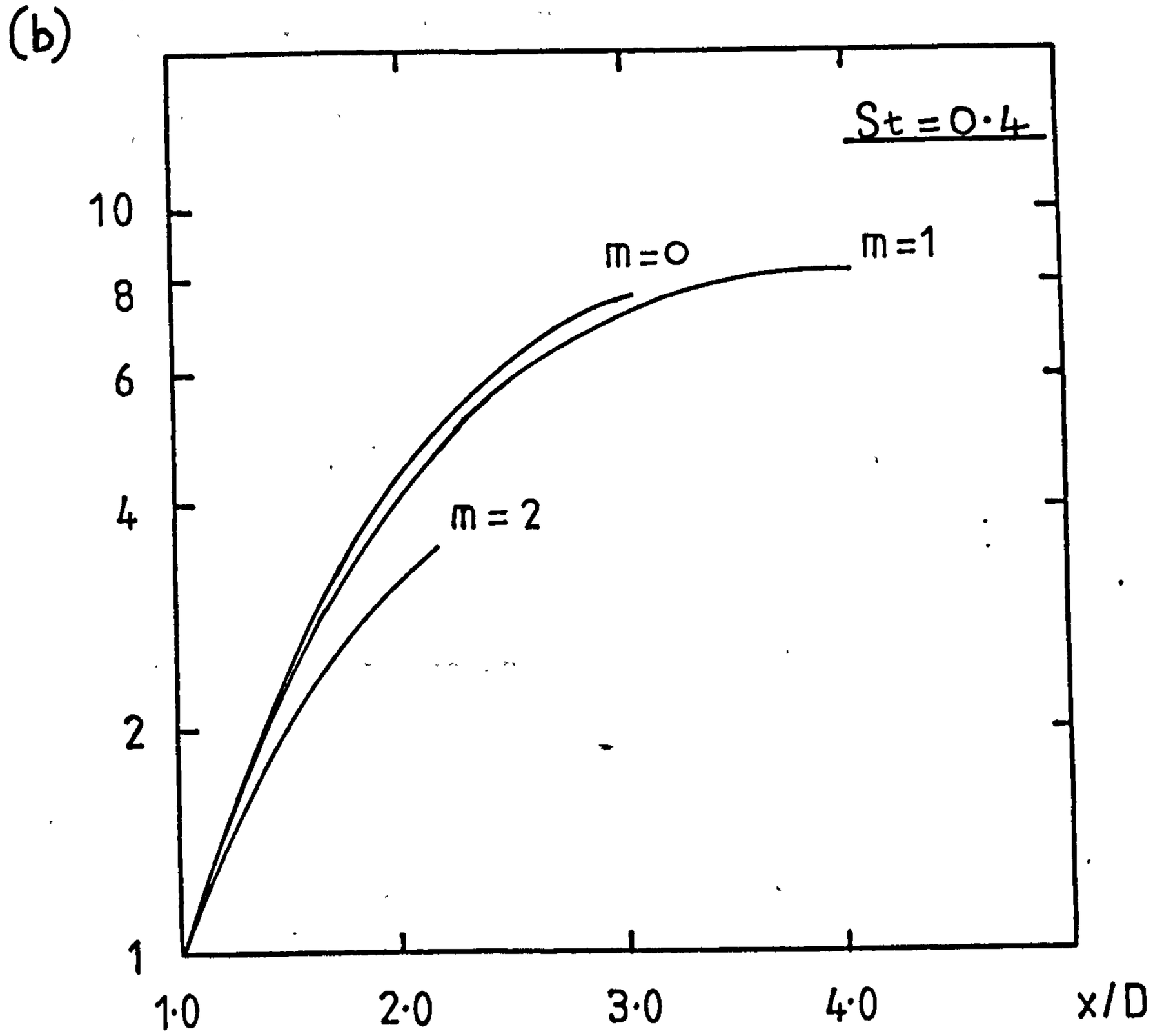

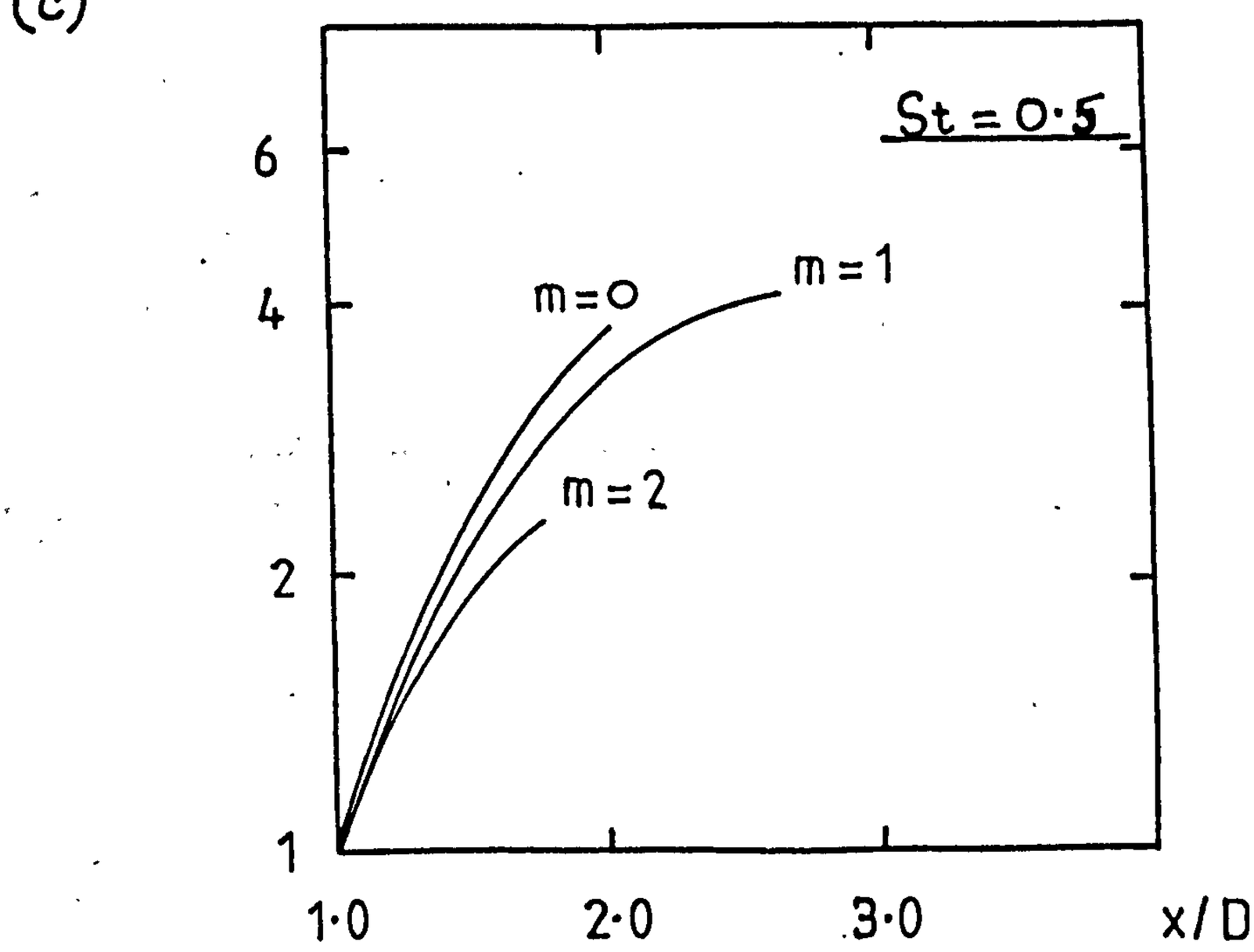

FIGURE 68: GAIN IN SHEAR LAYER AXIAL VELOCITY FLUCTUATION (r=R)

re x/D = 1

(a)

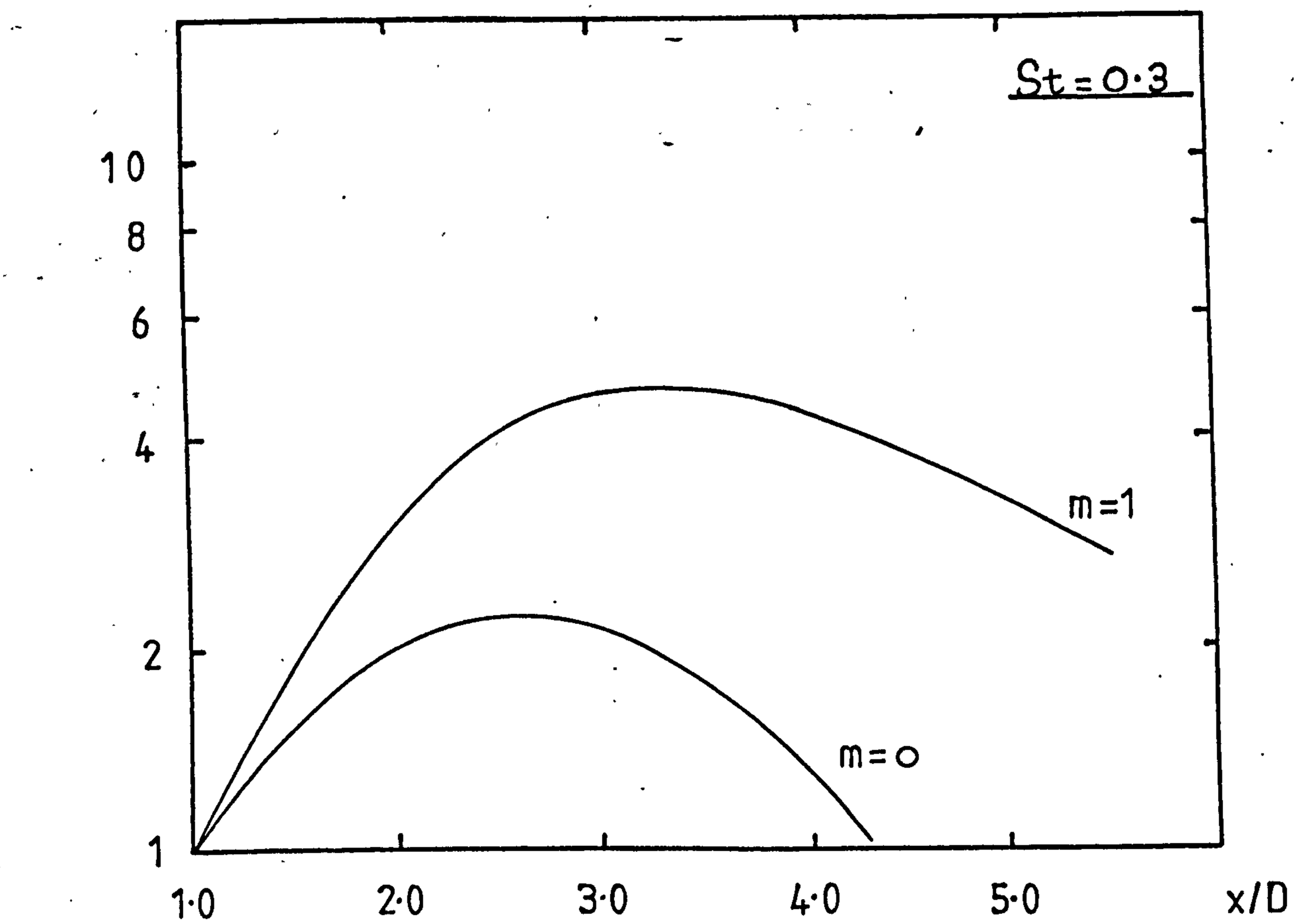

FIGURE 68 : GAIN IN SHEAR LAYER AXIAL VELOCITY FLUCTUATION ($r=R$)

re $x/D = 1$

(b)

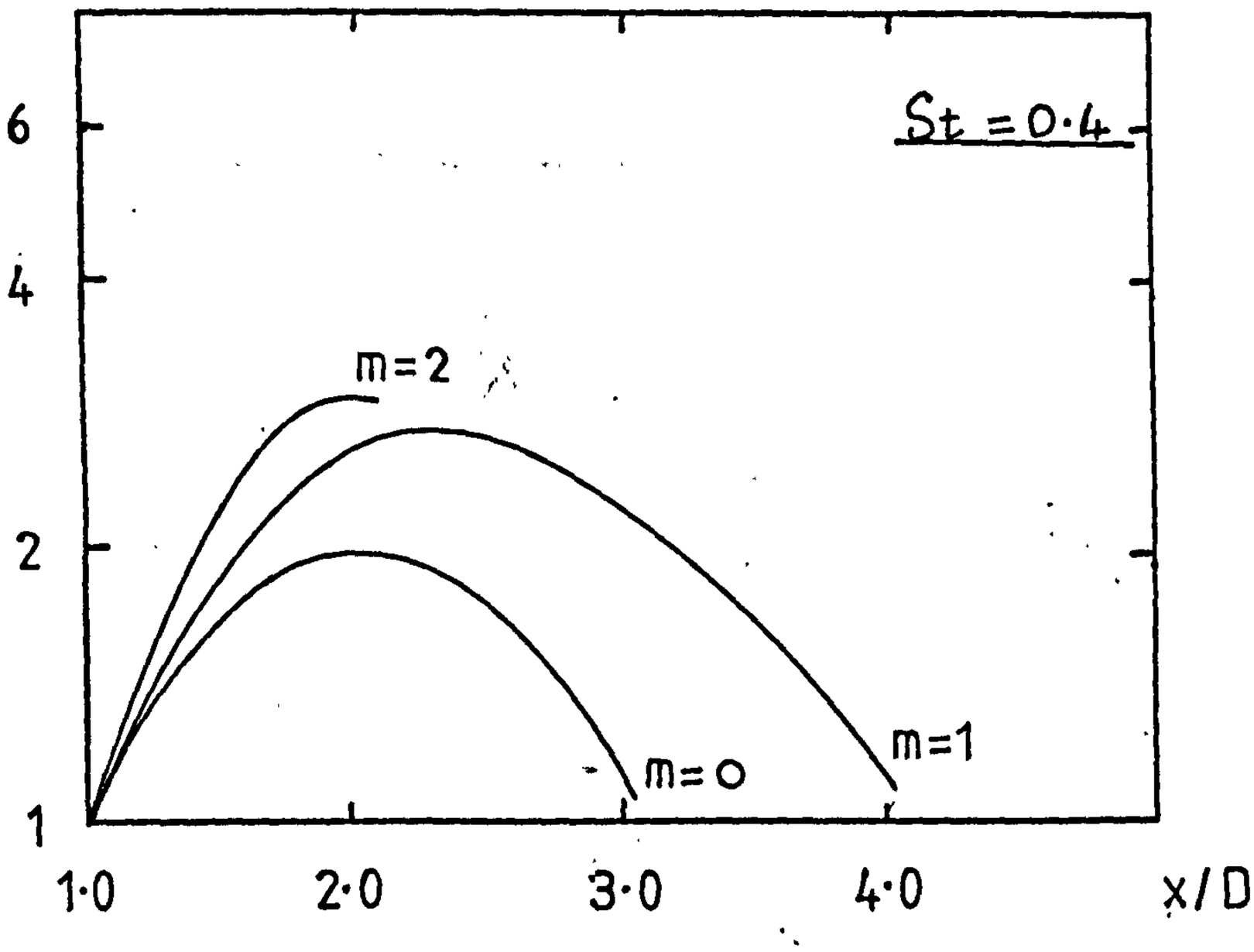

(c)

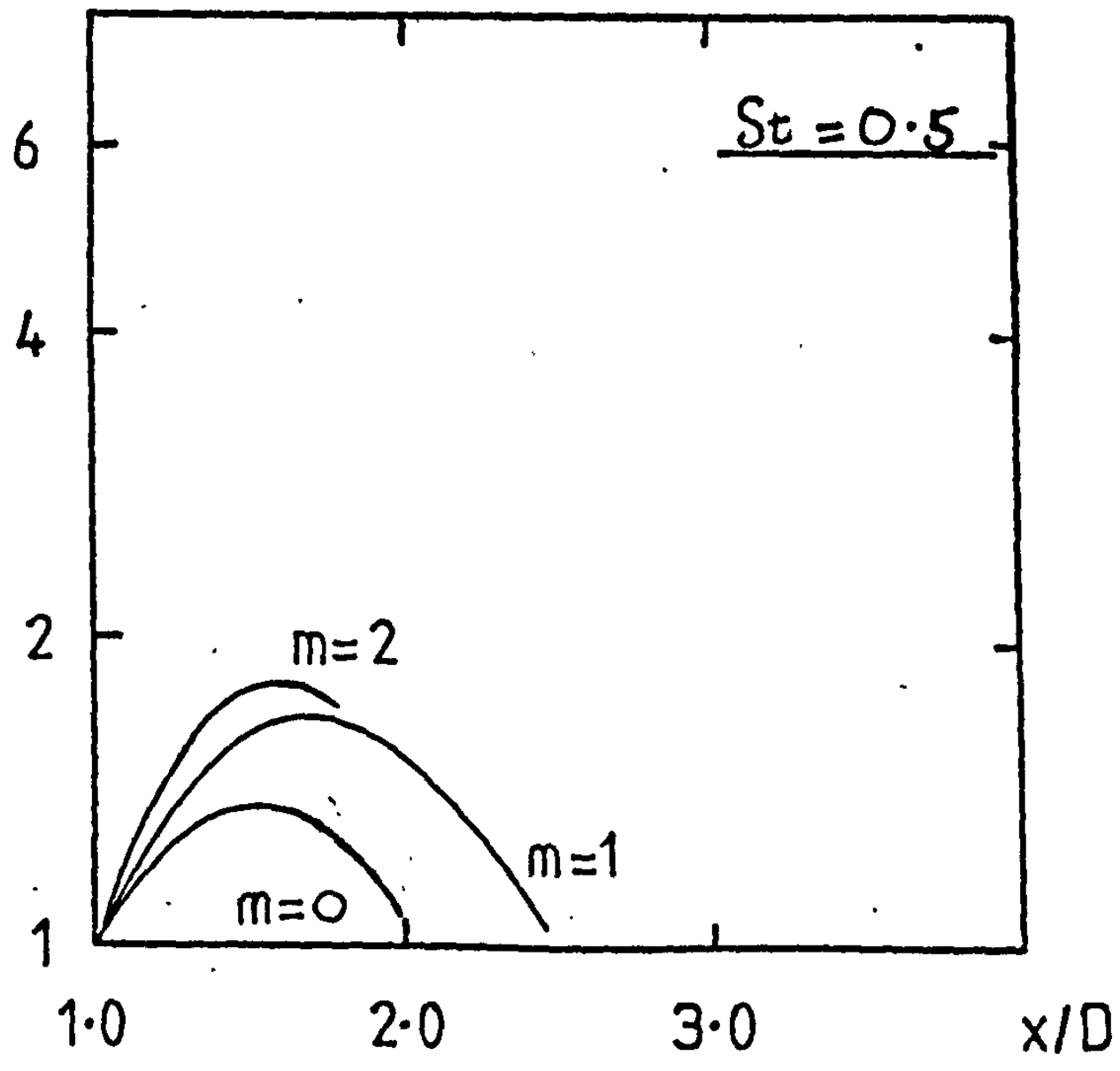

FIGURE 69 : GAIN IN SHEAR LAYER AZIMUTHAL VELOCITY FLUCTUATION (r=R) -

Re x/D = 1

(a)

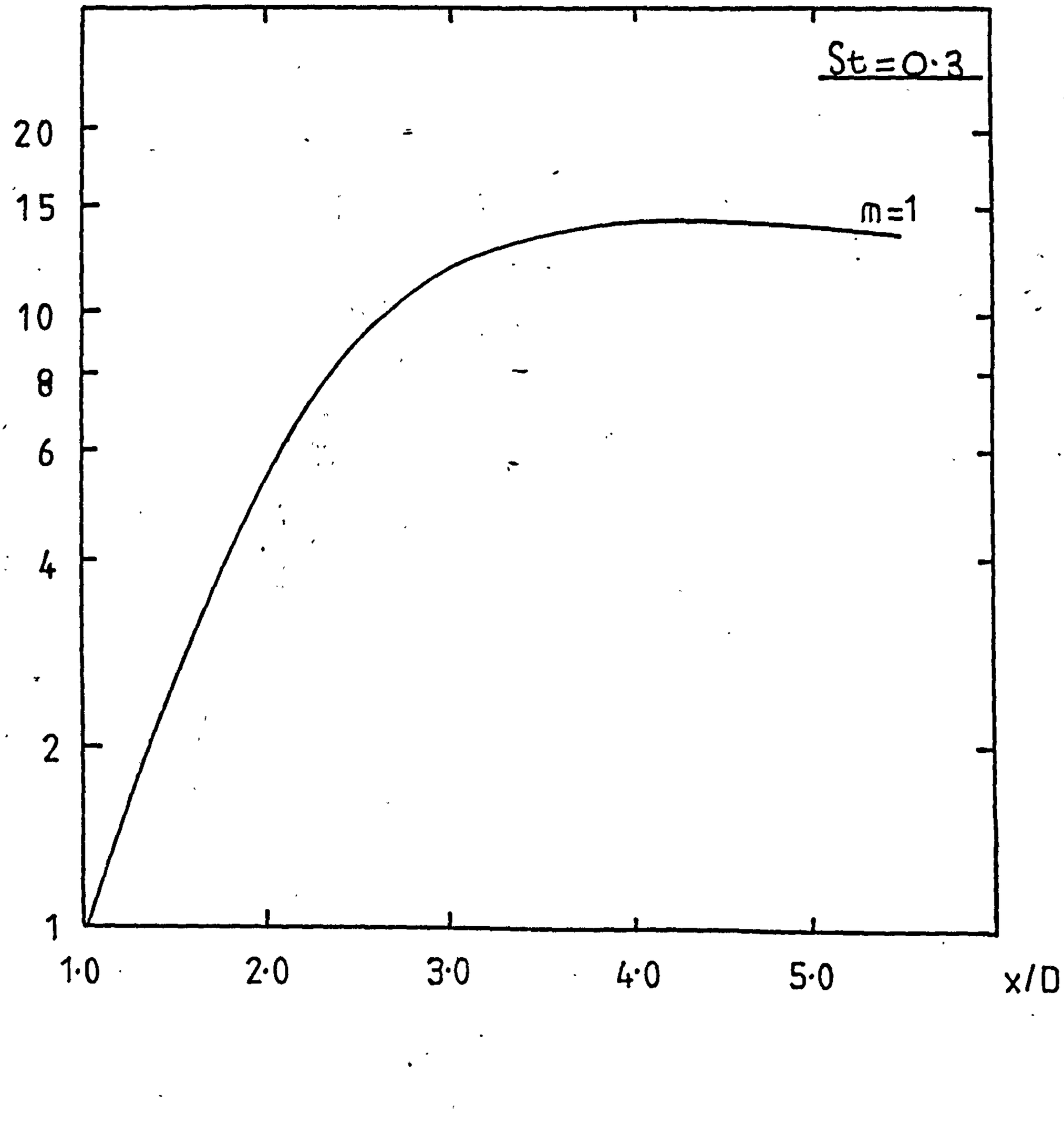

FIGURE 69 : GAIN IN SHEAR LAYER AZIMUTHAL VELOCITY FLUCTUATION ($r = R$)

$Re\ x/D = 1$

(b)

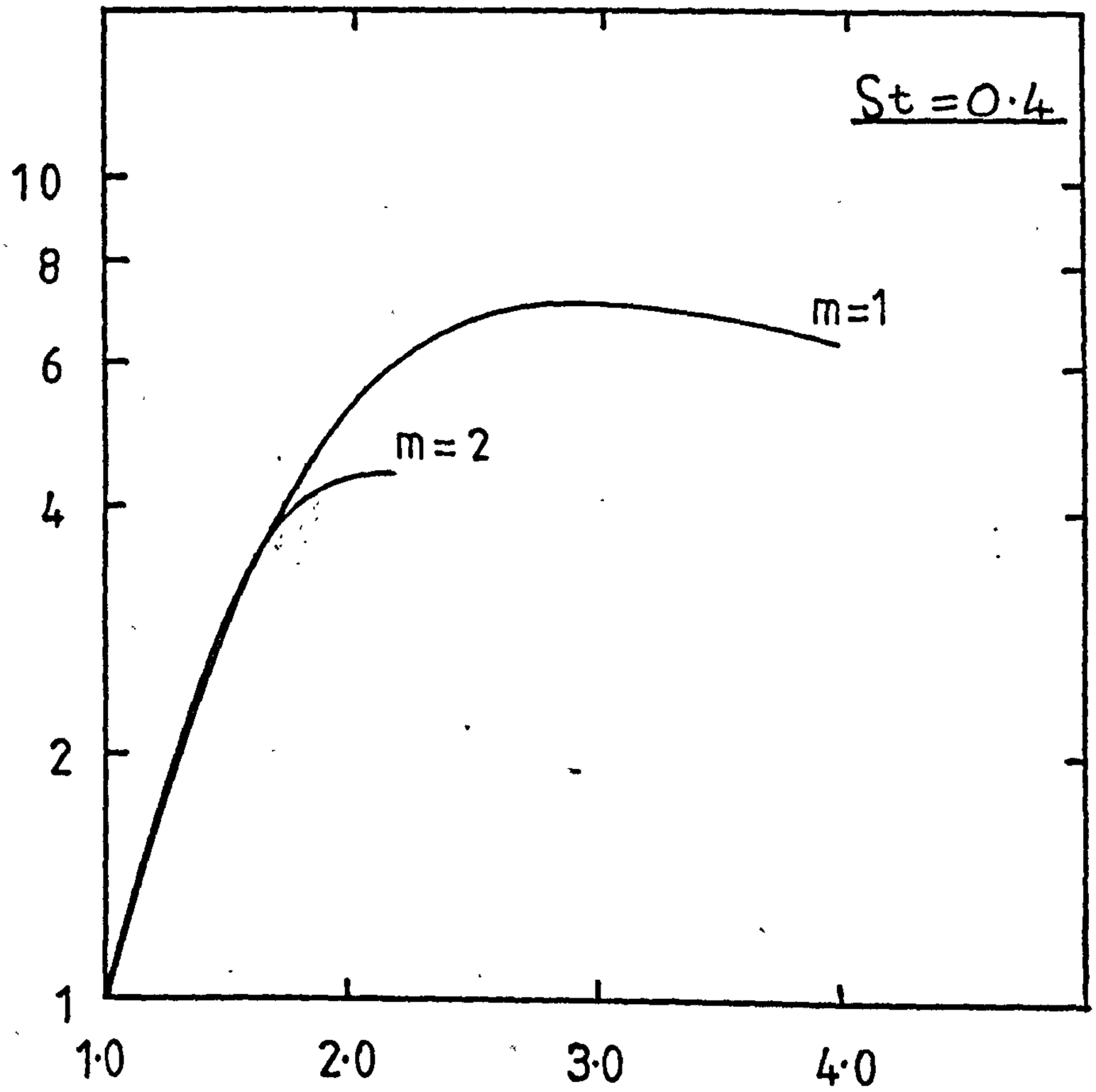

(c)

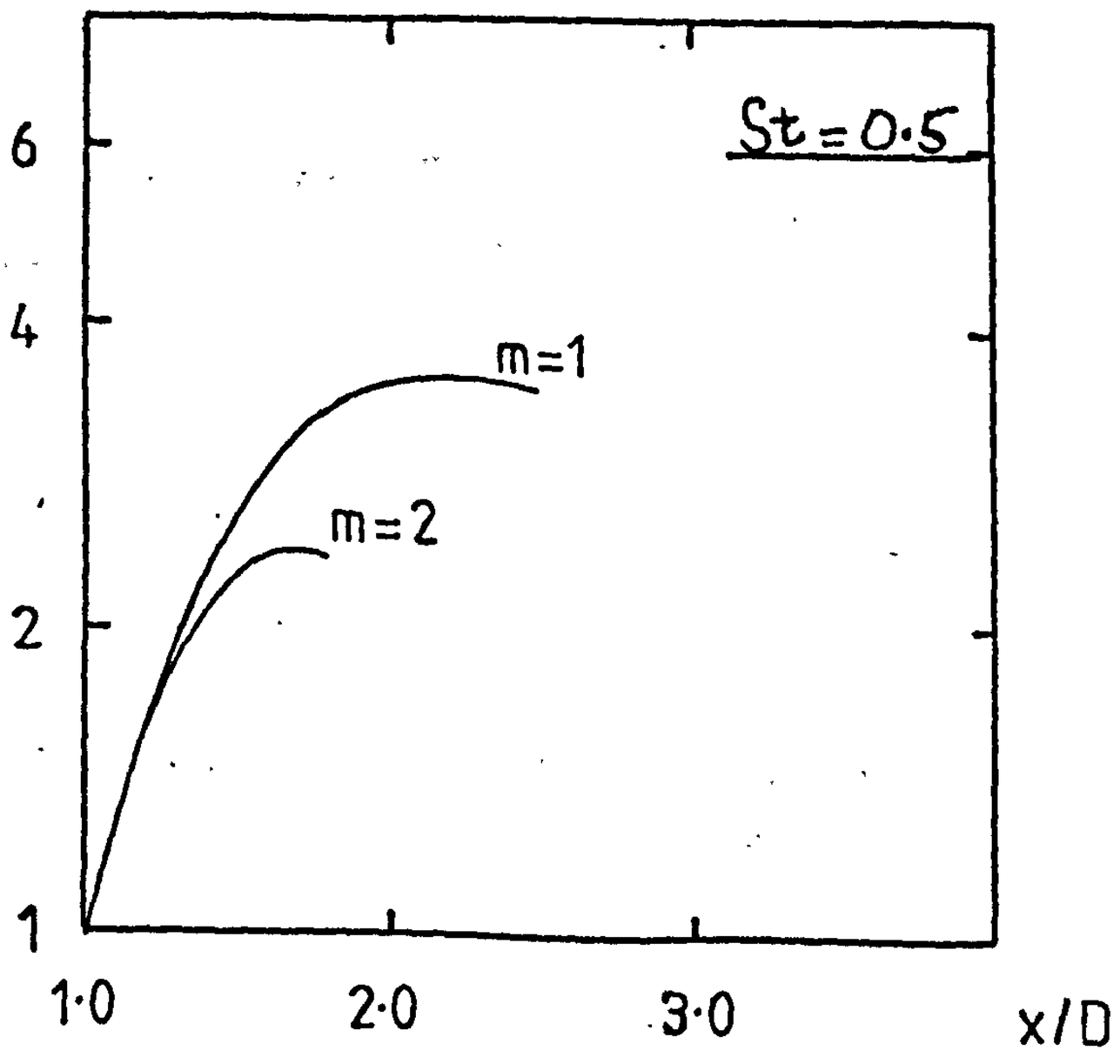

FIGURE 70 : AXIAL VARIATION IN PHASE SPEED AT $S_T = 0.4$

(a) AXIAL VELOCITY FLUCTUATION, $\tilde{u}_x$

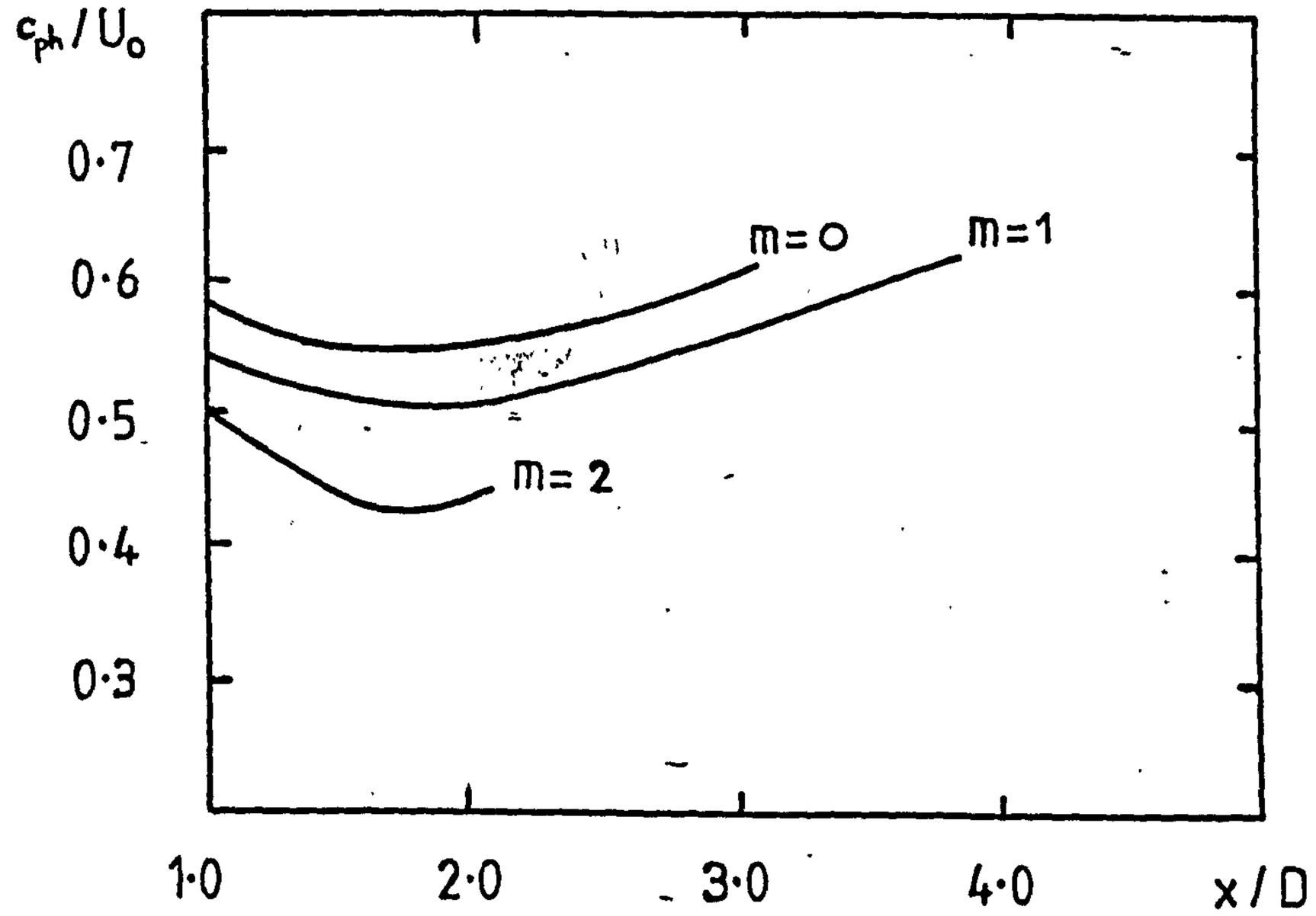

(b) RADIAL VELOCITY FLUCTUATION, $\tilde{u}_r$

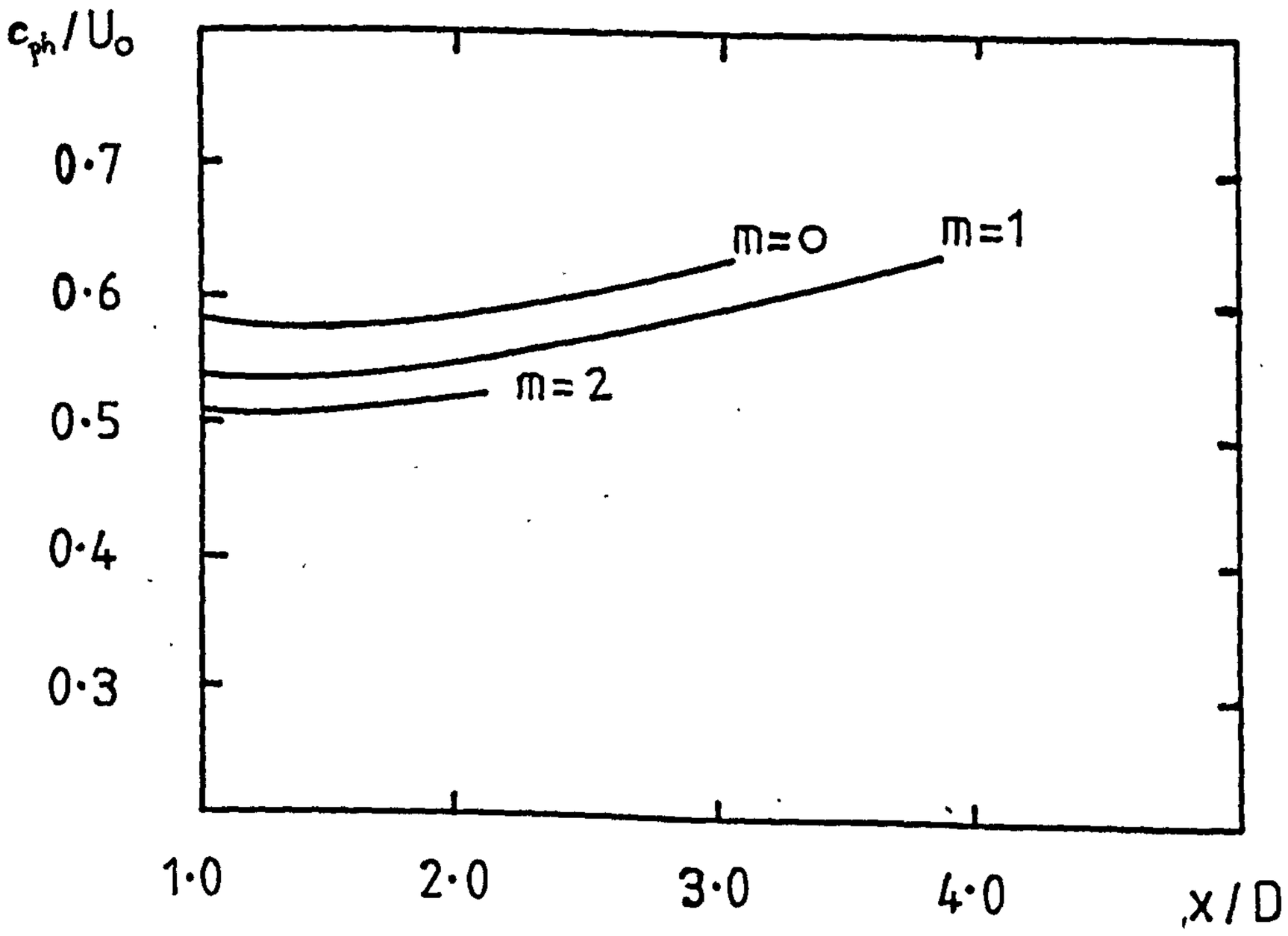

FIGURE 70 CNTD.

(c) AZIMUTHAL VELOCITY FLUCTUATION, $\tilde{u}_\theta$

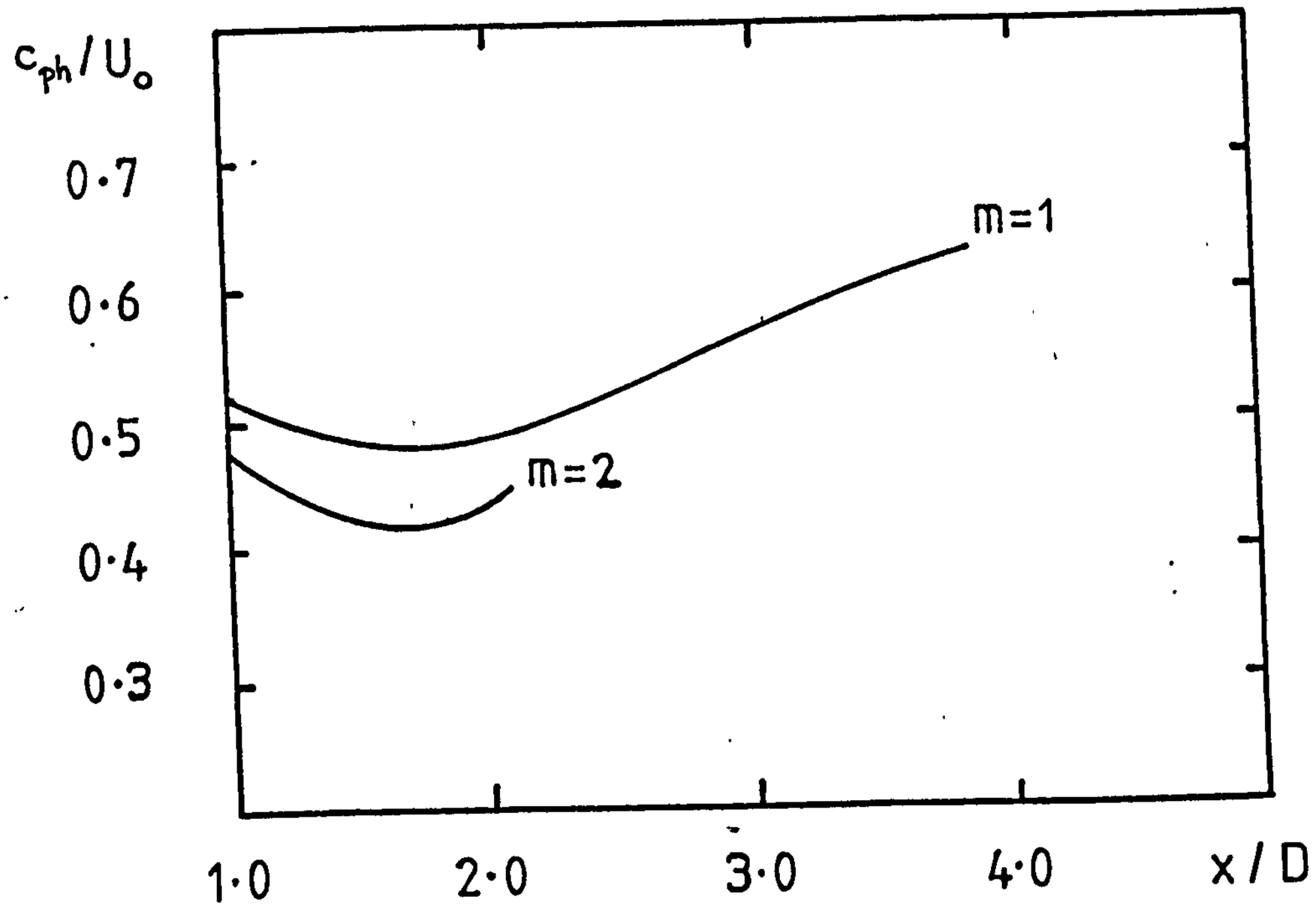

(d) PRESSURE FLUCTUATION, $\tilde{p}$

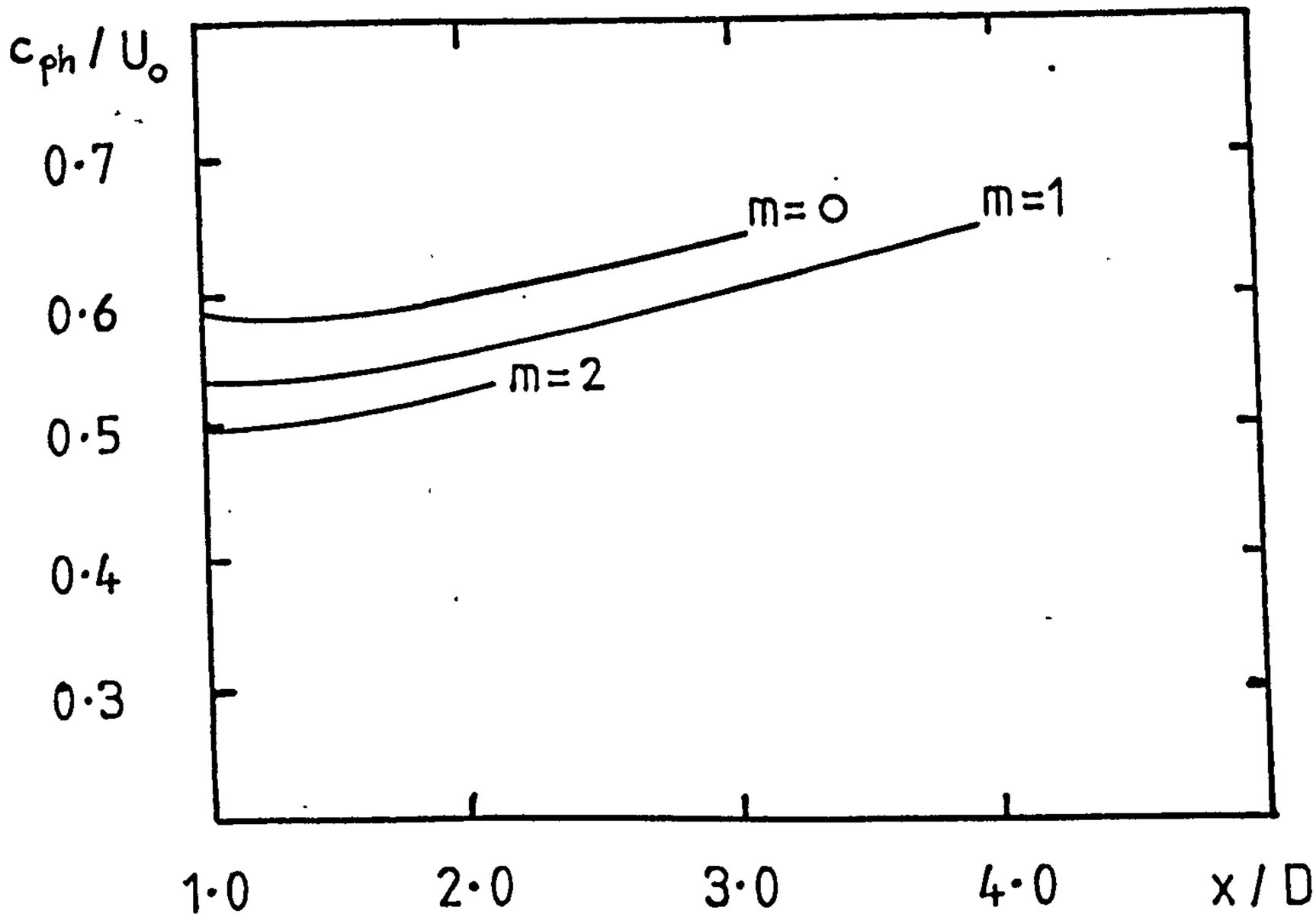

FIGURE 71 : AXIAL VARIATION IN PHASE SPEED : M=1 MODE

(a) AXIAL VELOCITY FLUCTUATION, $\tilde{u}_x$

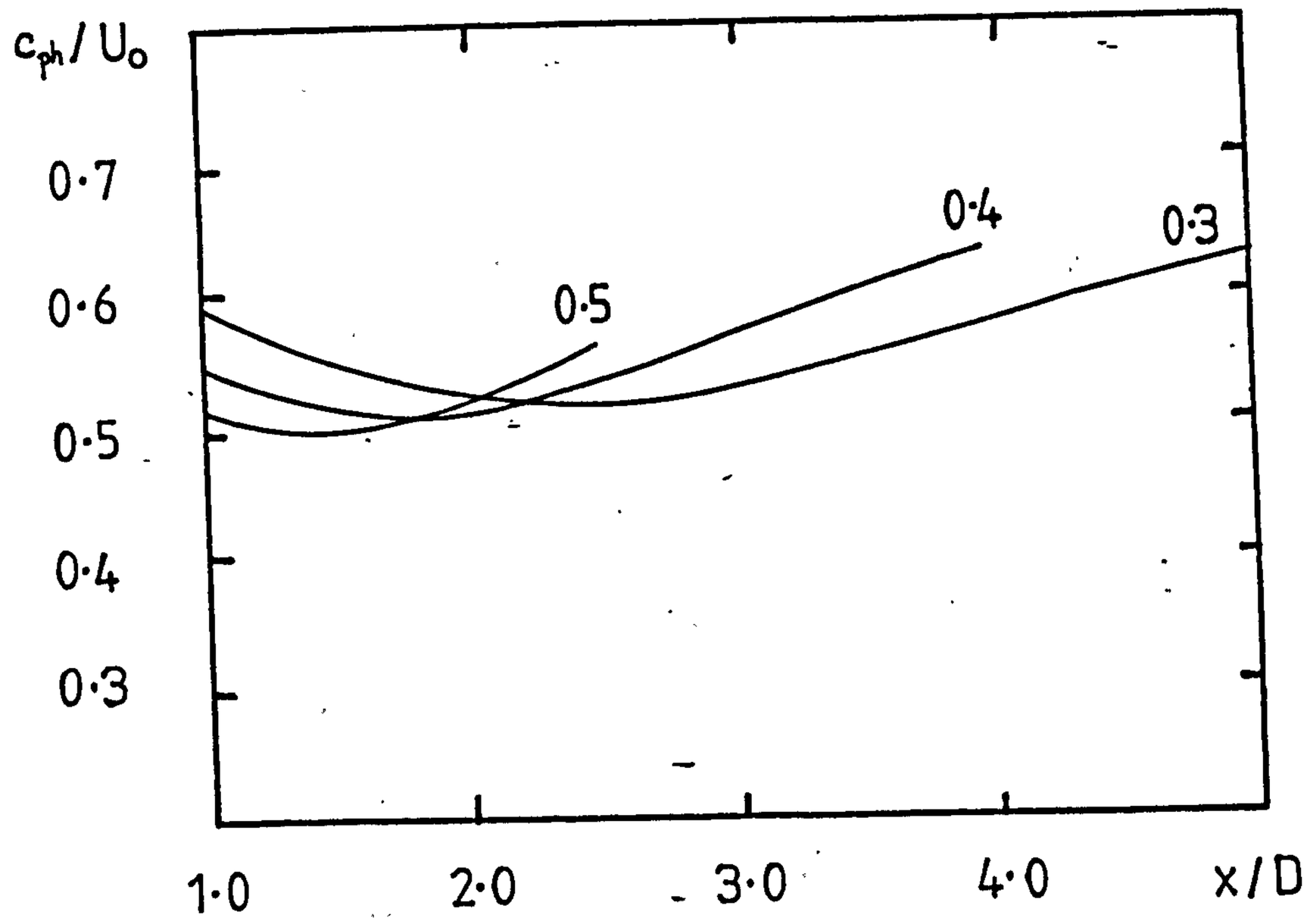

(b) PRESSURE FLUCTUATION, $\tilde{p}$

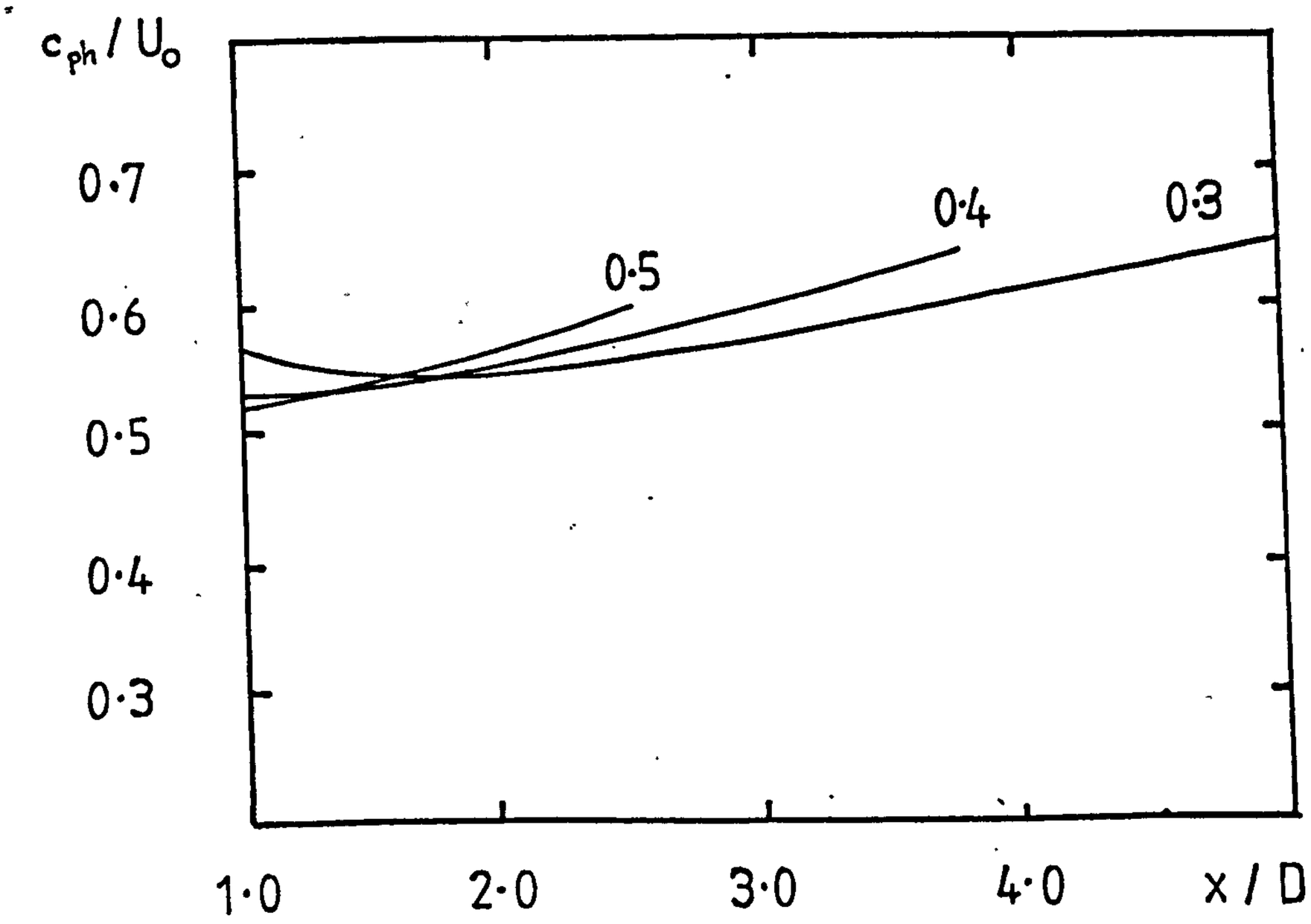

FIGURE 72 : RADIAL DISTRIBUTION OF RADIAL VELOCITY FLUCTUATION IN m=1 MODE AT (a) X=1D , (b) X=2D

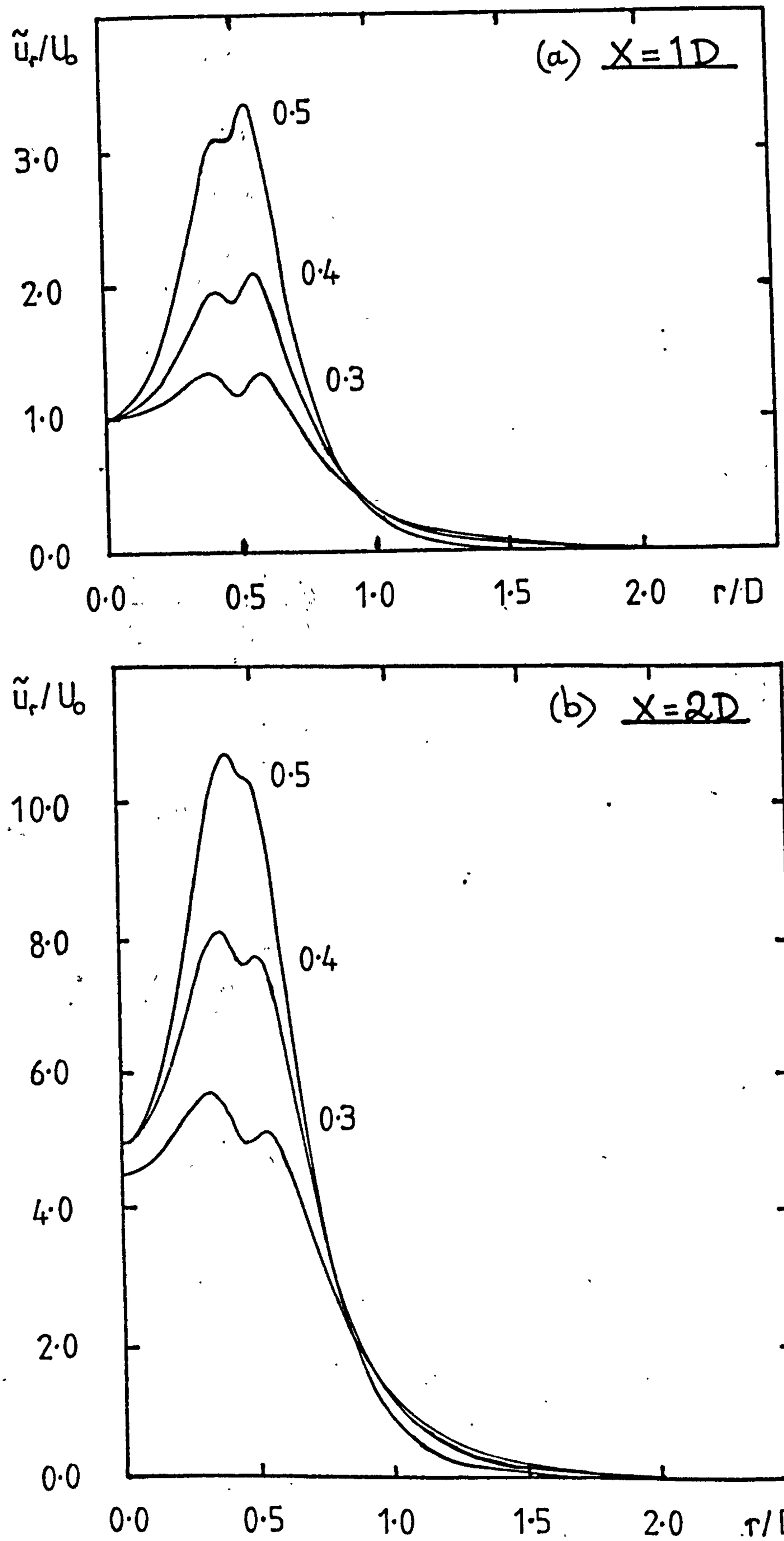

FIGURE 73 : RADIAL DISTRIBUTION OF RADIAL VELOCITY FLUCTUATION IN m=0 MODE AT (a) X=1D , (b) X=2D

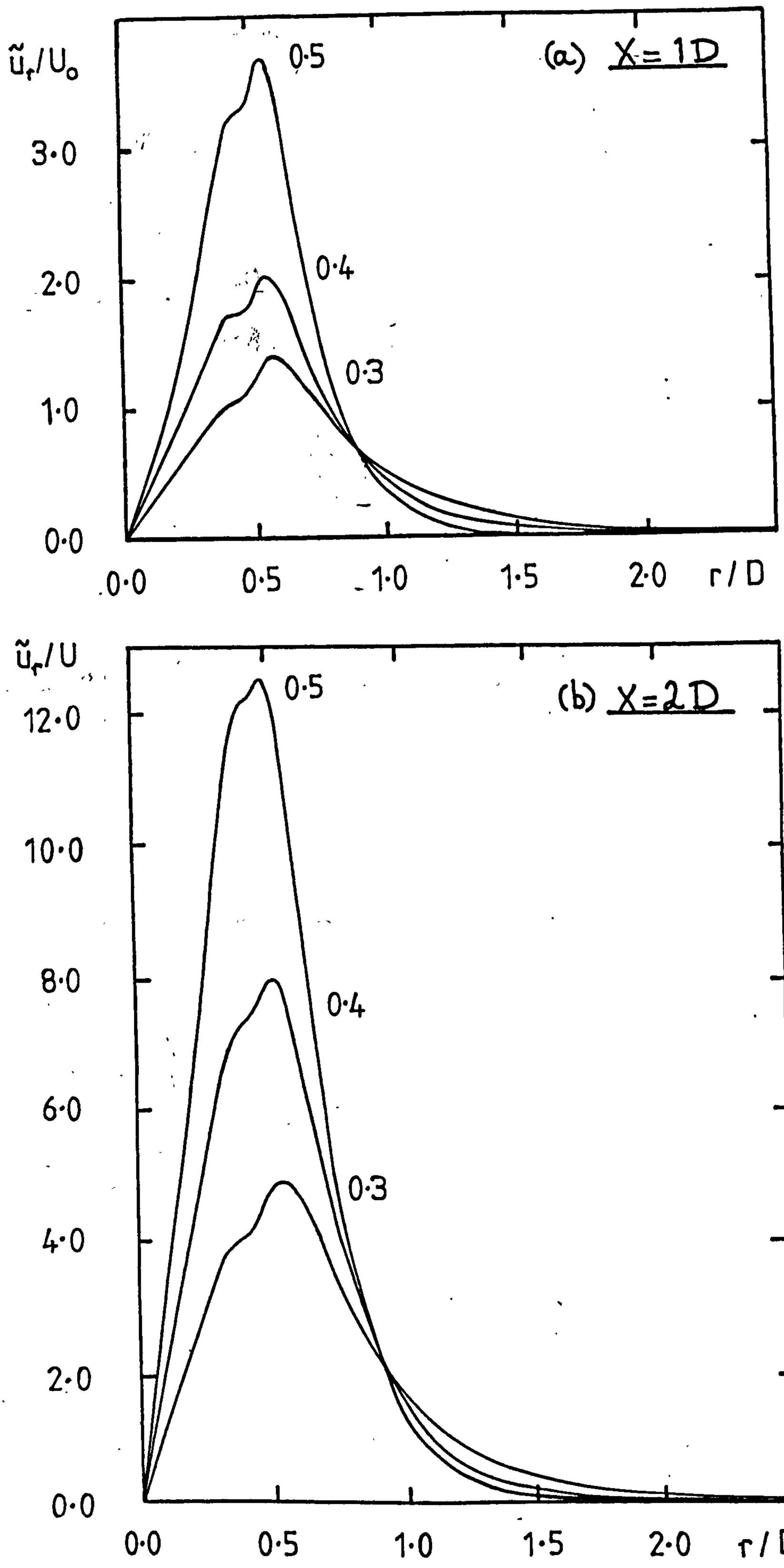

FIGURE 74 : RADIAL DISTRIBUTION OF AXIAL VELOCITY FLUCTUATION IN m=0 MODE AT (a) X=1D, (b) X=2D

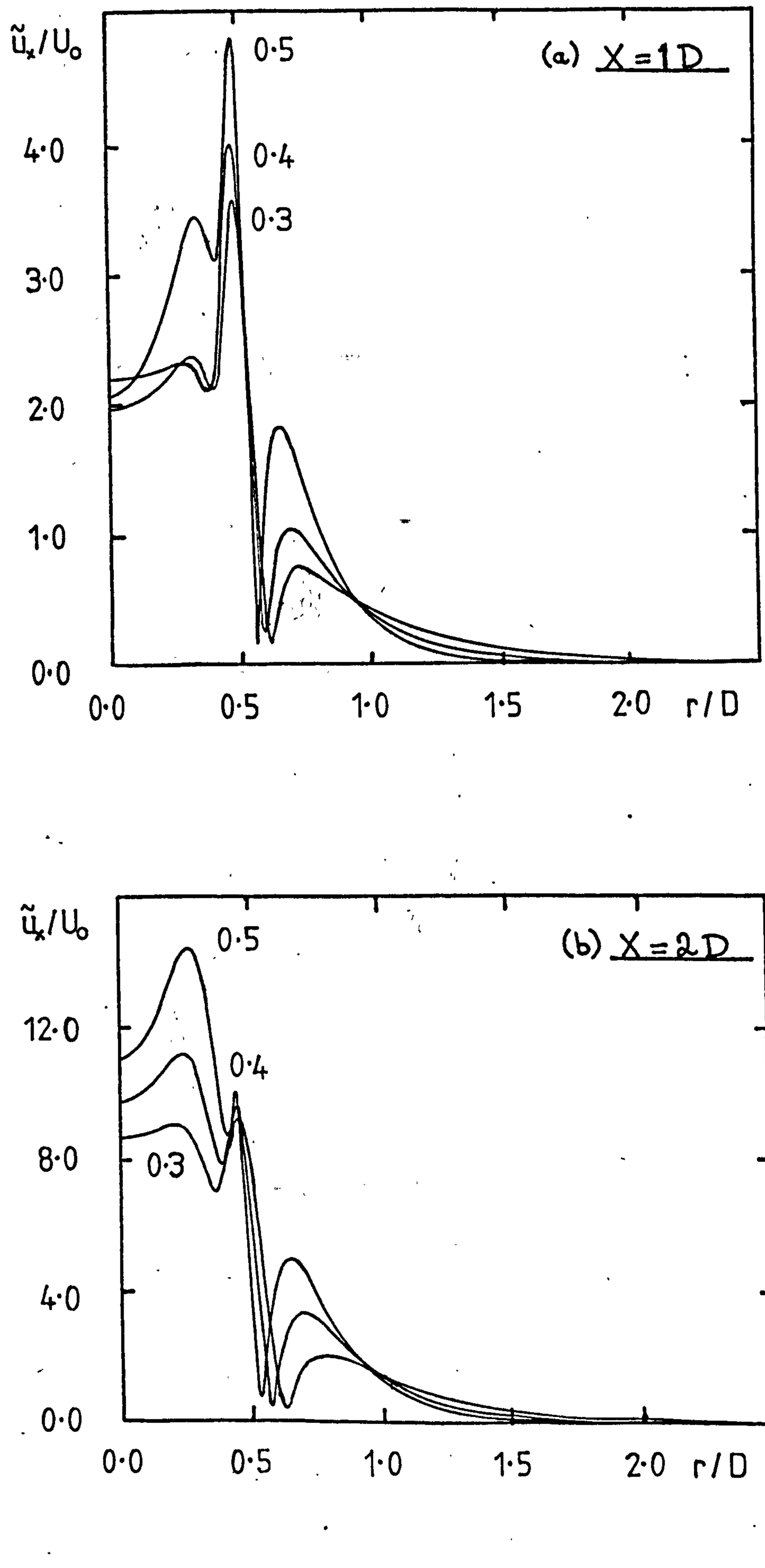

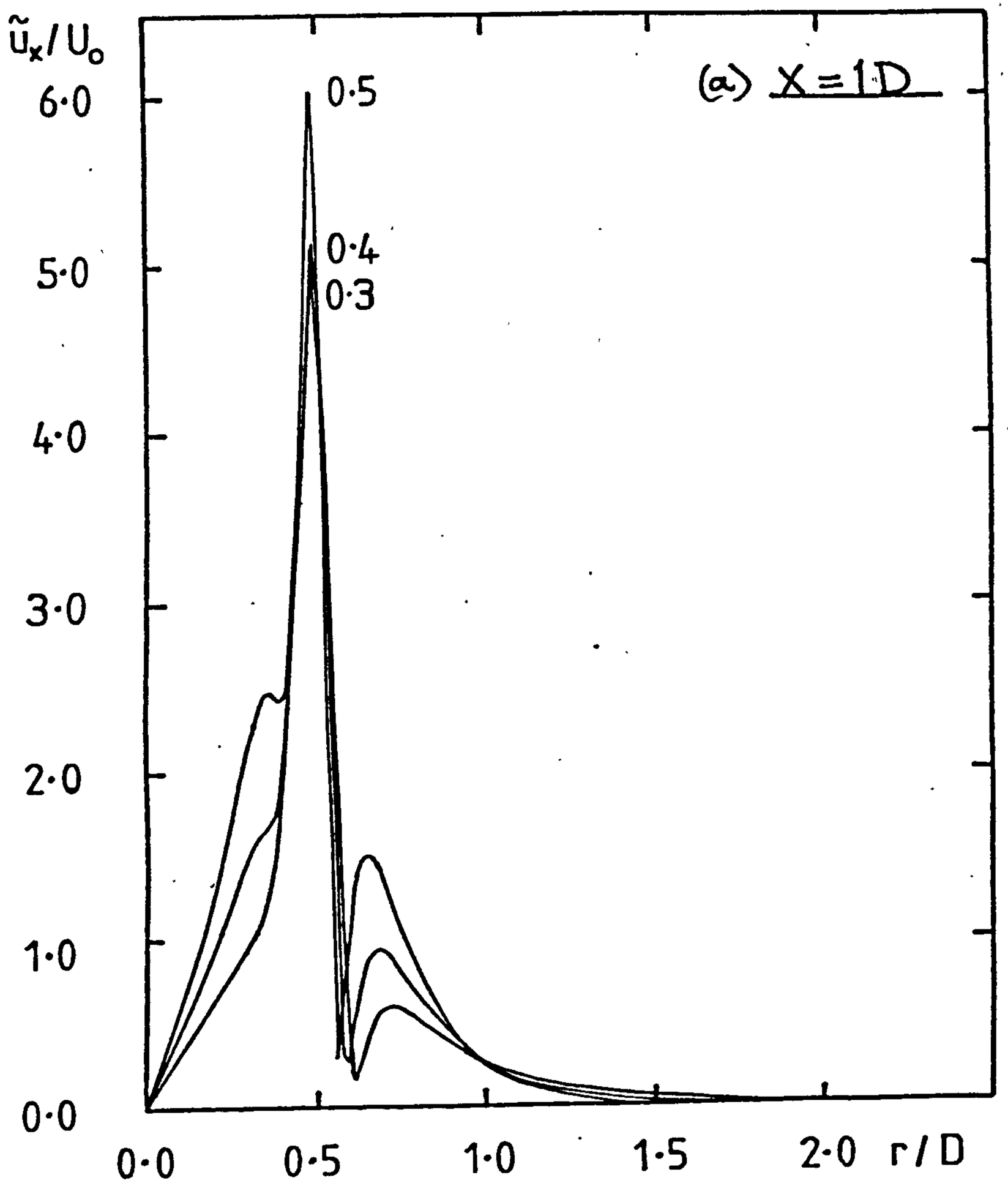

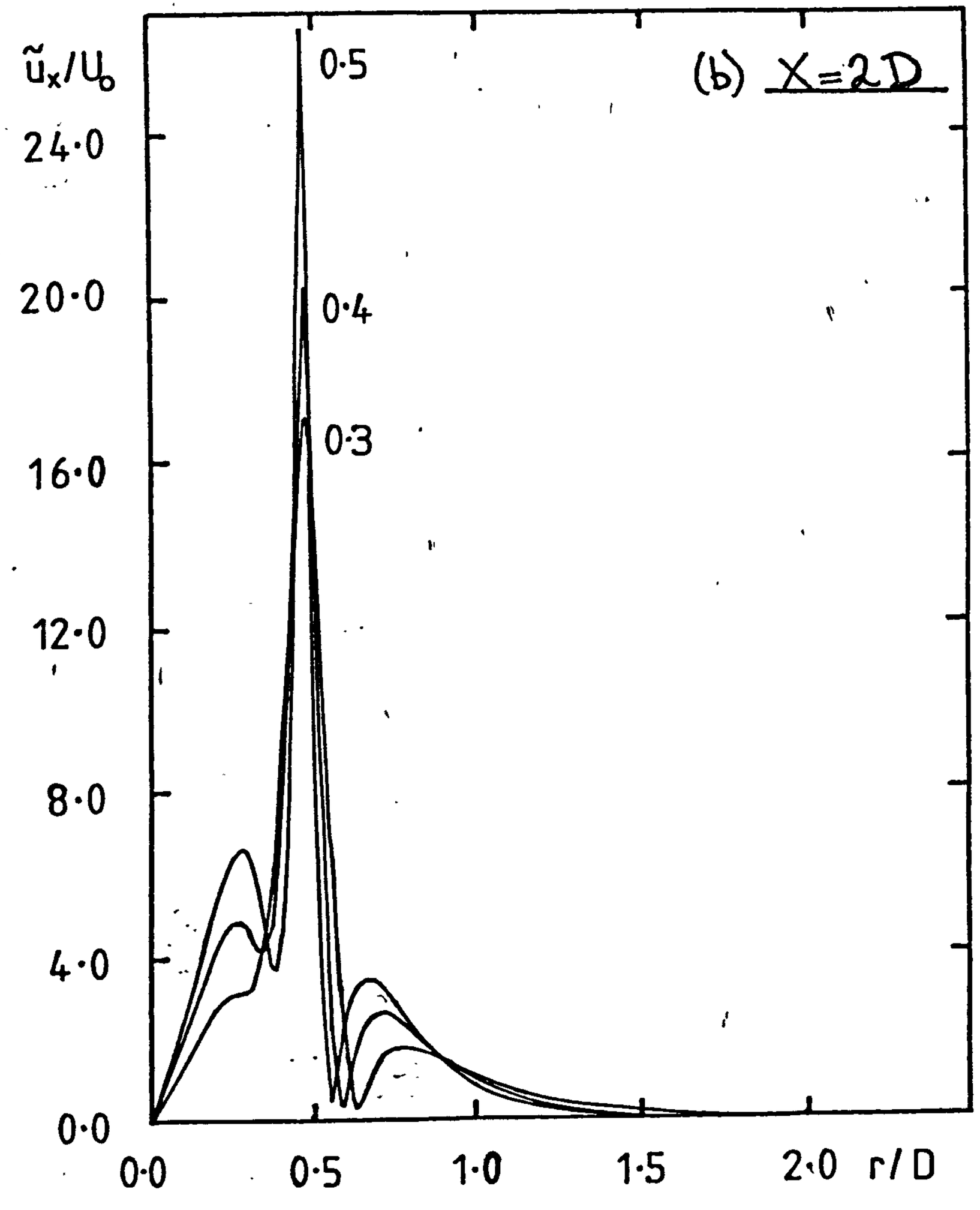

FIGURE 75 : RADIAL DISTRIBUTION OF AXIAL VELOCITY FLUCTUATION IN m=1 MODE AT (a) X=1D , (b) X=2D

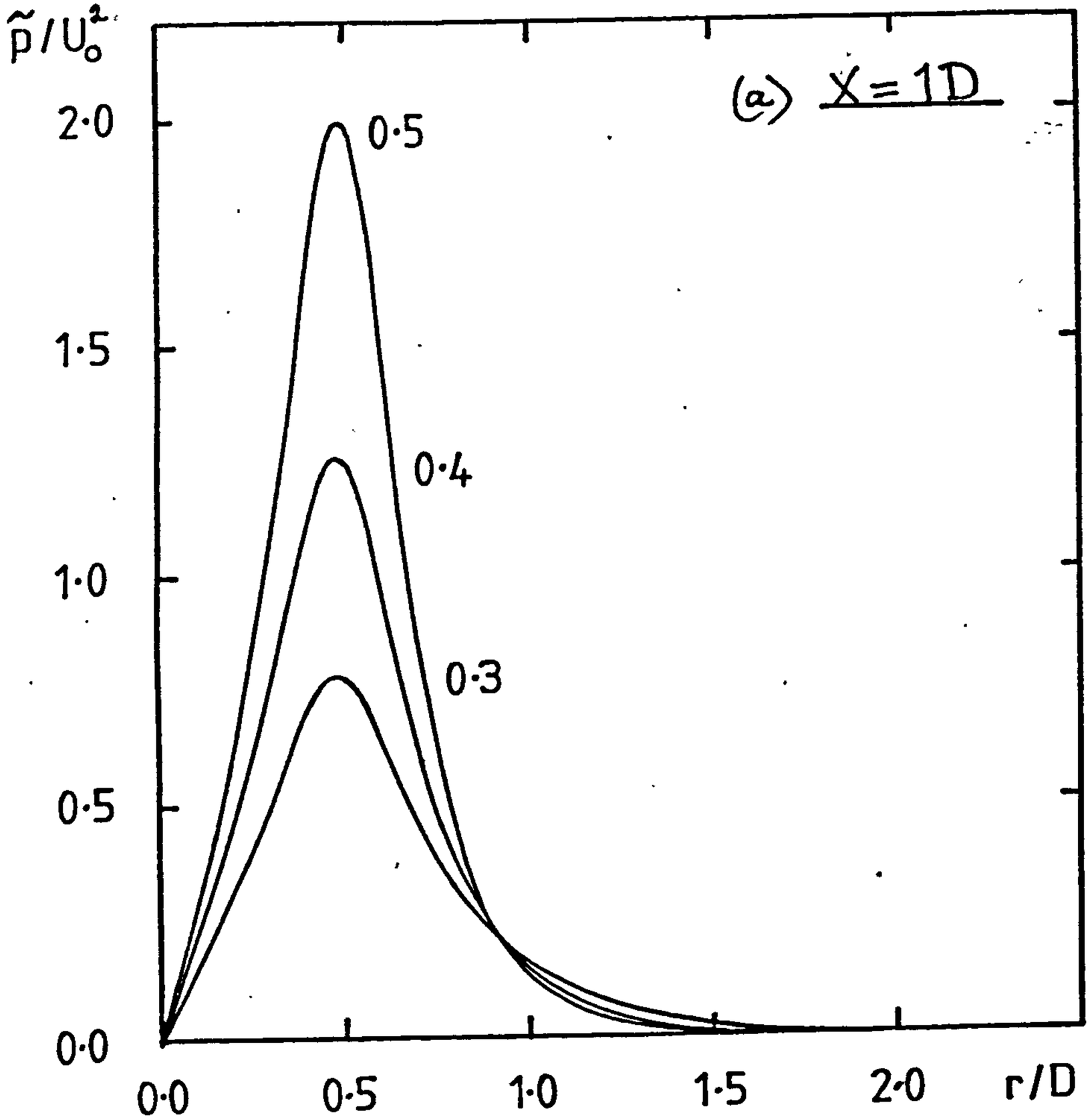

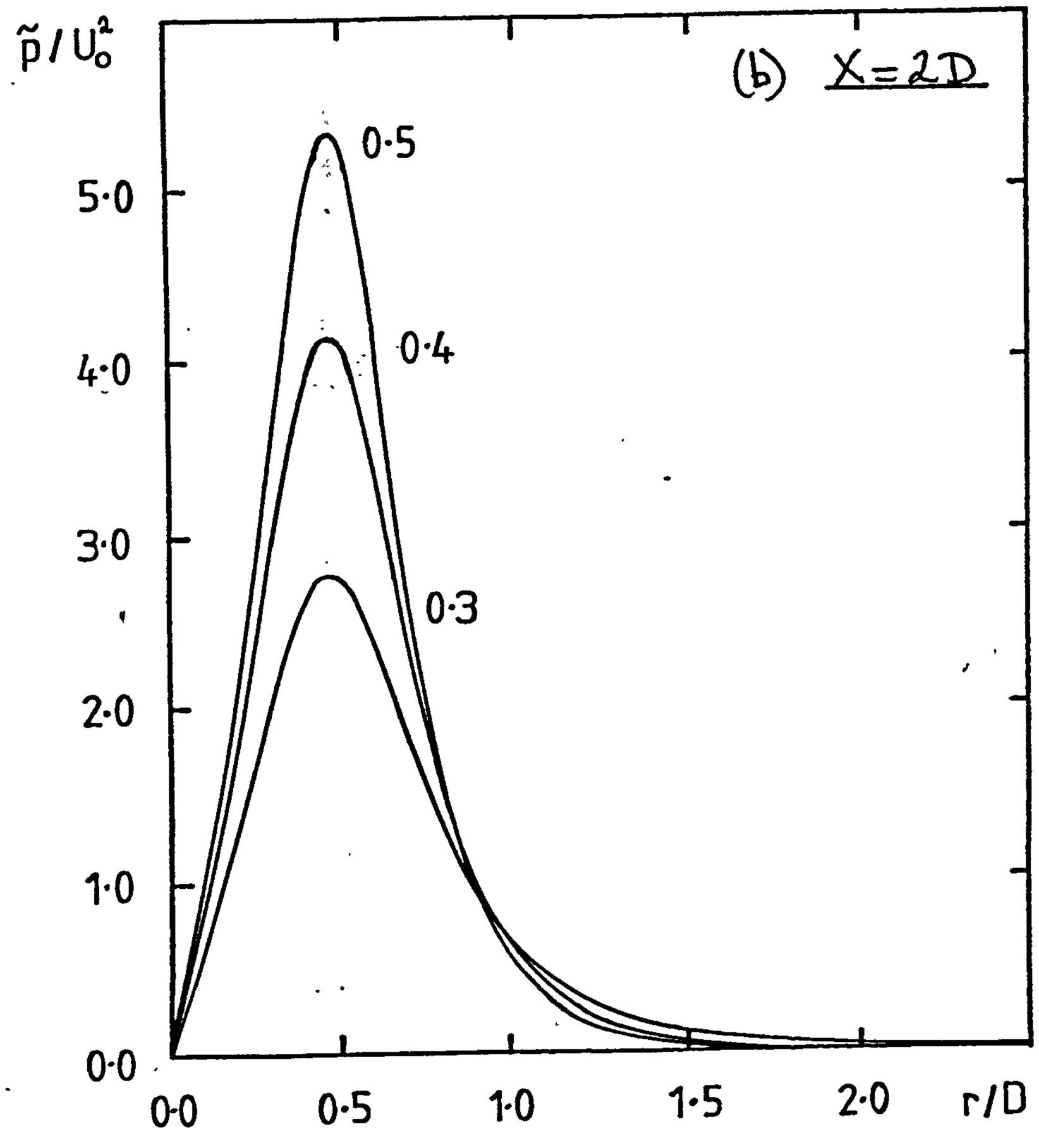

FIGURE 76 : RADIAL DISTRIBUTION OF PRESSURE FLUCTUATION IN m=1 MODE AT (a) X=1D , (b) X=2D

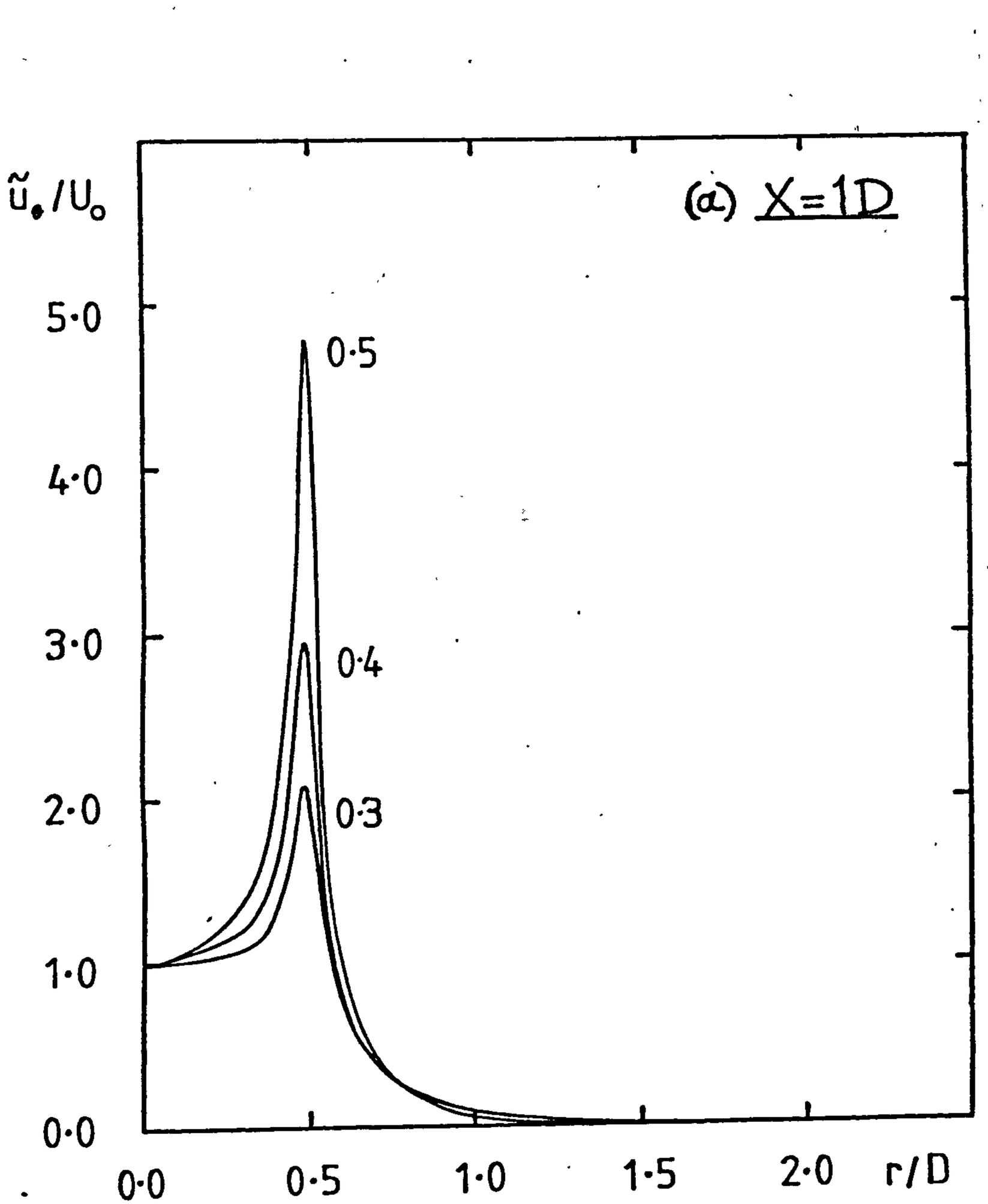

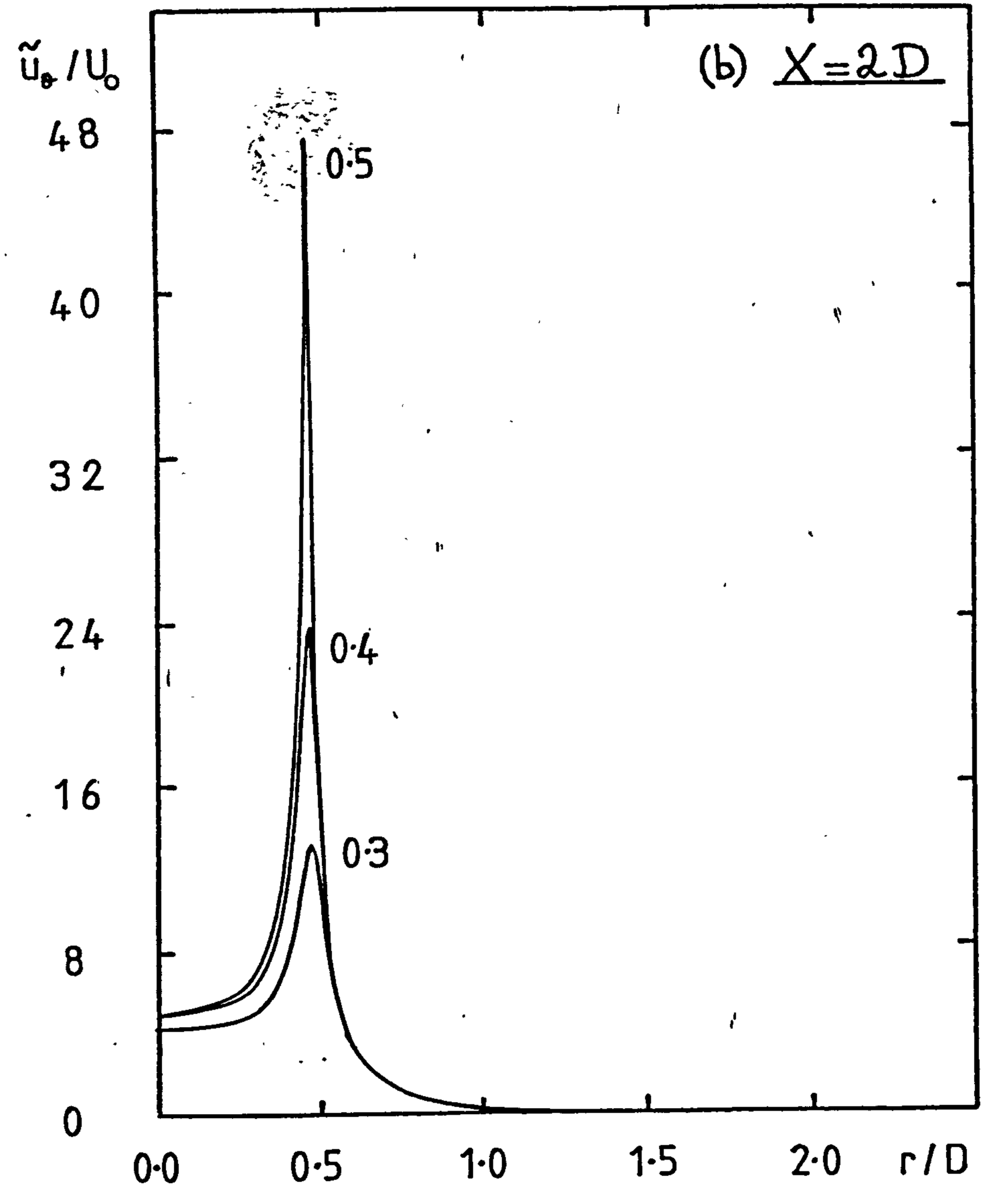

FIGURE 77 : RADIAL DISTRIBUTION OF AZIMUTHAL VELOCITY FLUCTUATION IN M=1 MODE AT (a) X=1D, (b) X=2D

CHAPTER 4 SPECIFIC COMPARISONS BETWEEN LINEAR STABILITY ANALYSIS AND EXPERIMENT

4.1 Introduction

In Chapter 3 we discussed the more general flow properties of a round turbulent jet when subjected to forcing in the form of helical disturbances, as predicted by a linear stability analysis of a slowly diverging laminar flow. We now describe, in greater detail, a number of specific comparisons of the present theory with the observations of recent workers. In particular, we shall first concern ourselves with the results presented in chapter 2 and later with the observations of Chan [17].

In [17], Chan describes an experiment involving a model jet, in which the development of a helical wave (m = 1, 2) was followed in terms of the filtered pressure fluctuation. Whilst comparisons have been made with these results, we do not consider them to constitute a very rigorous test of the theoretical model: such axial and radial pressure distributions are invariably slowly varying in nature. A far greater importance is attached to comparisons involving velocity fluctuations of which the present experimental work is the only known source at the time of writing. Furthermore, we feel that Chan's work is open to criticism on more than one count. The axial distributions of the pressure amplitude have been plotted against the normalised distance $(\frac{x}{D})$ St, which is a local Strouhal number, i.e., it is based on the local shear layer thickness. Such a normalisation is clearly invalid in the case of a circular jet for

which the instability wave scales on the nozzle diameter. Further, it has not been made clear at which axial positions the phase velocities have been measured.

A very high forcing level was used in Chan's experiments and therefore, as with some of the present results, the instability waves exhibit a highly non-linear behaviour. Indeed, at the Strouhal numbers of interest, the axial profiles show that the pressure waves begin to decay at about x = 1D. Since the present theory does not constitute a valid model upstream of this axial position and invariably predicts a region of growth downstream of it, we have had to restrict our comparison to the pressure distributions in the radial direction only.

4.2 Velocity Fluctuations

In this section we shall be concerned, primarily, with the radial distributions of the instability wave velocity components, for which the experimental results shown have been drawn exclusively from those presented earlier on in this work. It will have been observed that, away from the centre of the shear layer, the radial profiles determined experimentally show a satisfactory degree of symmetry about the axis of the jet, and consequently, only half diametral traverses have been plotted.

We have shown, in figure 78 (i), the fluctuating axial and radial velocity components in the m = 0 mode, at x = 1D. The predicted axial velocity fluctuation, shown in (a), has been normalised such that it matches the measured value on the centre line of the jet. The

predicted radial velocity fluctuation, shown in (b), has been obtained as a result of this normalisation on the axial component and has not itself been renormalised. By fixing the amplitude of one velocity component at a single radial position the radial distributions of both components are well predicted. The numerical agreement is particularly good for the axial component and, in general, the model accurately predicts the behaviour away from the centre of the shear layer.

Figure 78 (ii) shows comparisons of the same flow quantities in the m = 1 mode at x = 1D. The normalisation used here fixes the radial component on the centre line and, as in (i), it has been left unchanged for the other component. Again, with the exception of the peak values, the model provides an accurate representation of the physical situation.

As mentioned previously, the axial growth rates of the above quantities are overestimated since the theory is linear, whereas the experimental work involved a non-linear forcing of the jet. As an example, the discrepancies arising in the m = 1 mode, at x = 2D, are shown in figure 79 (a) and (b). A single normalisation (as described above) has been applied at x = 1D and the absolute levels are a consequence of the predicted growth rate. The theoretical prediction is in error by a factor of 2 over most of the profile for each velocity component. Despite this expected lack of agreement in quantities which are a result of cumulative effects in the axial direction, we proceed to show that the measured radial profiles of the eigenfunctions at a subsequent downstream station display, nevertheless, the same shapes as predicted by the linear theory.

When the normalisation applied at x = 1D is repeated at x = 2D, the results obtained are those shown in figure 80. The velocity components in the m = 0 and m = 1 modes appear in (i) and (ii), respectively. It must be realised that it is meaningless to compare the amplitudes shown here with those at x = 1D in figure 78 : the axial growth rate is not that predicted by the theory. We observe that, in the m = 0 mode, the position of the theoretical peak in the axial velocity is at variance with that obtained experimentally, but otherwise the measured and predicted shapes are very similar. There would also appear to be a lack of agreement regarding the peak axial velocity in the m = 1 mode, (although the peak is not very well defined from the experimental results), but again, the overall comparison is good.

We have observed that the Schlieren photographs in chapter 2 indicated that the non-linear behaviour is such that at this axial position (x = 2D), the instability wave has actually rolled up into a vortex on the shear layer and a little further downstream, vortex-pairing processes can be observed. It is therefore rather unexpected that the shapes of these radial profiles are relatively unaffected by the non-linearity. However, this result does provide a certain justification for the use of "shape functions" in non-linear stability analyses based on energy equations, of which the applications in this field by recent workers have been numerous (e.g., Mankbadi & Liu [46], Chan [16]).

4.3 Pressure Fluctuations

We find that the axial growth rate of the filtered pressure

fluctuation is not as grossly overestimated as that of the velocity fluctuations: the same observation was made by Crighton & Gaster in the case of the axisymmetric mode. Figure 81 shows the axial growth rate of the pressure fluctuation in the m = 1 mode along the lip line of the jet (St = 0.555). The two sets of measurements correspond to different forcing levels and it can be seen that it is the growth rate produced by the lower forcing level which is more closely approximated by the theory, as expected. (It will also be observed that a simple exponential behaviour, as given by parallel flow theory, would produce gains far in excess of those predicted by the slowly diverging analysis.) The experimental results were obtained at a Mach number of 0.5 for which the mean velocity profile will be somewhat different from that used in the model, which was shown to fit the measured profile at a Mach number of 0.3.†

The axial variation in the phase speed at these two forcing levels has also been drawn against the theoretical prediction in figure 82 and the agreement is good.

The measured radial pressure distribution in figure 83 has been taken from the present work and those in figures 84 to 86 have been reproduced from Chan [17]. Figure 83 shows the profile obtained at x = 2D in the m = -1 mode, the forcing level being 0 dB and the Strouhal number 0.555. Figures 84 to 86 show measured profiles in the m = 0, 1 and 2 modes at St = 0.513, 0.501 and 0.502, respectively. The axial positions are those at which the maximum amplitudes were reached at the given Strouhal numbers: x ≃ 1.8D (m = 0), x ≃ 1.7D (m = 1) and x ≃ 1.65D (m = 2).

Apart from the form of the mean velocity profile, the conditions

† Indeed, note also that the calculations were performed at zero Mach number throughout.

used in the theoretical prediction shown in figure 83 matched the experimental conditions. In figures 84 to 86, however, the theoretical curves shown were all determined at an axial distance of x = 2D, using a Strouhal number of 0.5 and since the experimental mean velocity profile is unknown, the profile given by (3.3.2) has been used.

In figure 83, the theoretical curve has been normalised such that the peak corresponds to an average of the levels at the two experimental points closest to the theoretical peak on both sides of the jet. The predicted profile is too narrow, but it is to be noted that the data has been plotted on a linear scale and the gradients in the "skirts" are similar to the measured ones. The situation is much the same in the comparisons with Chan's results. The theoretical curves shown here, though, have been normalised such that their gradients match the corresponding experimental pressure gradients in the near field of the jet (r ≃ 1D).

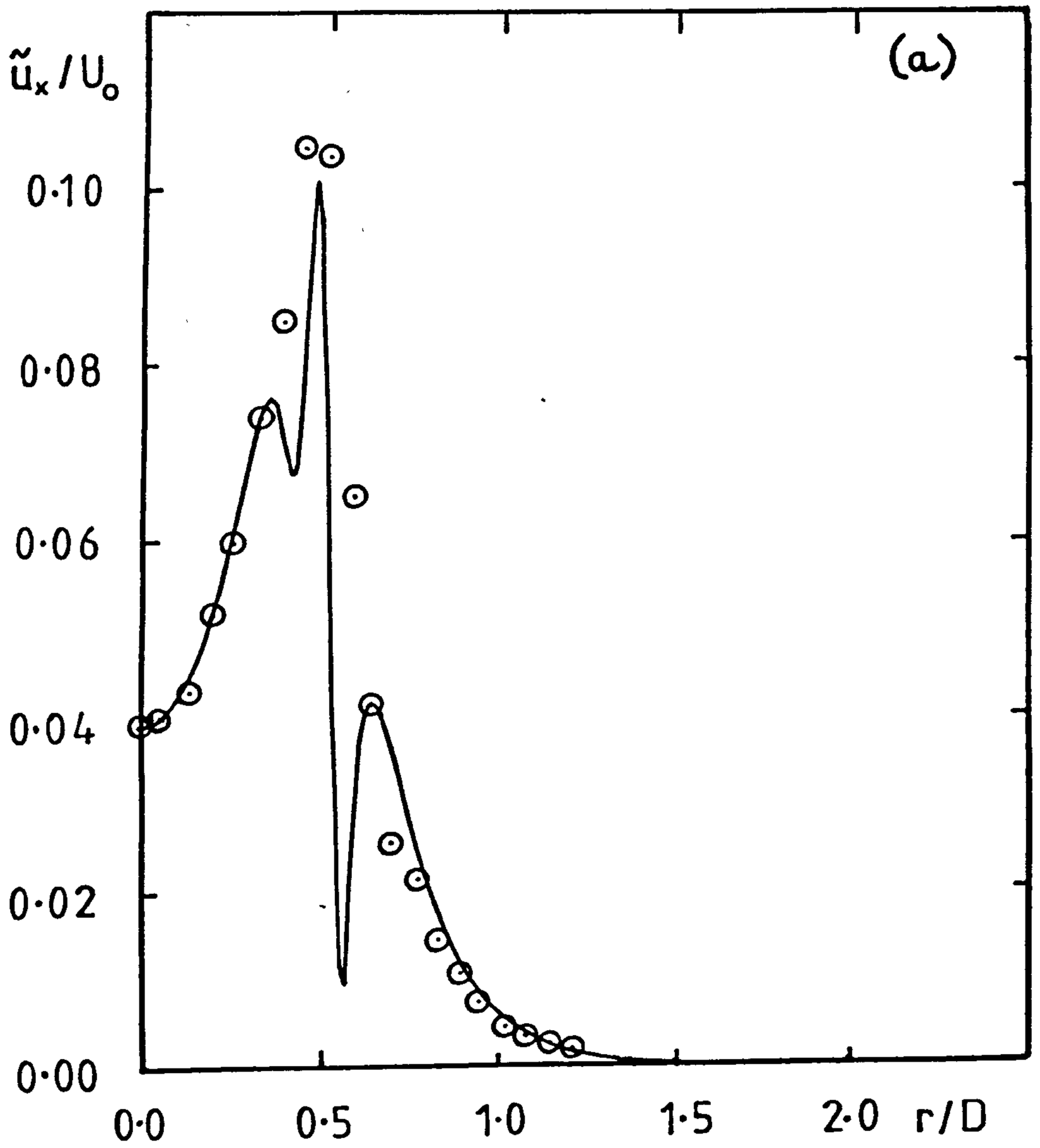

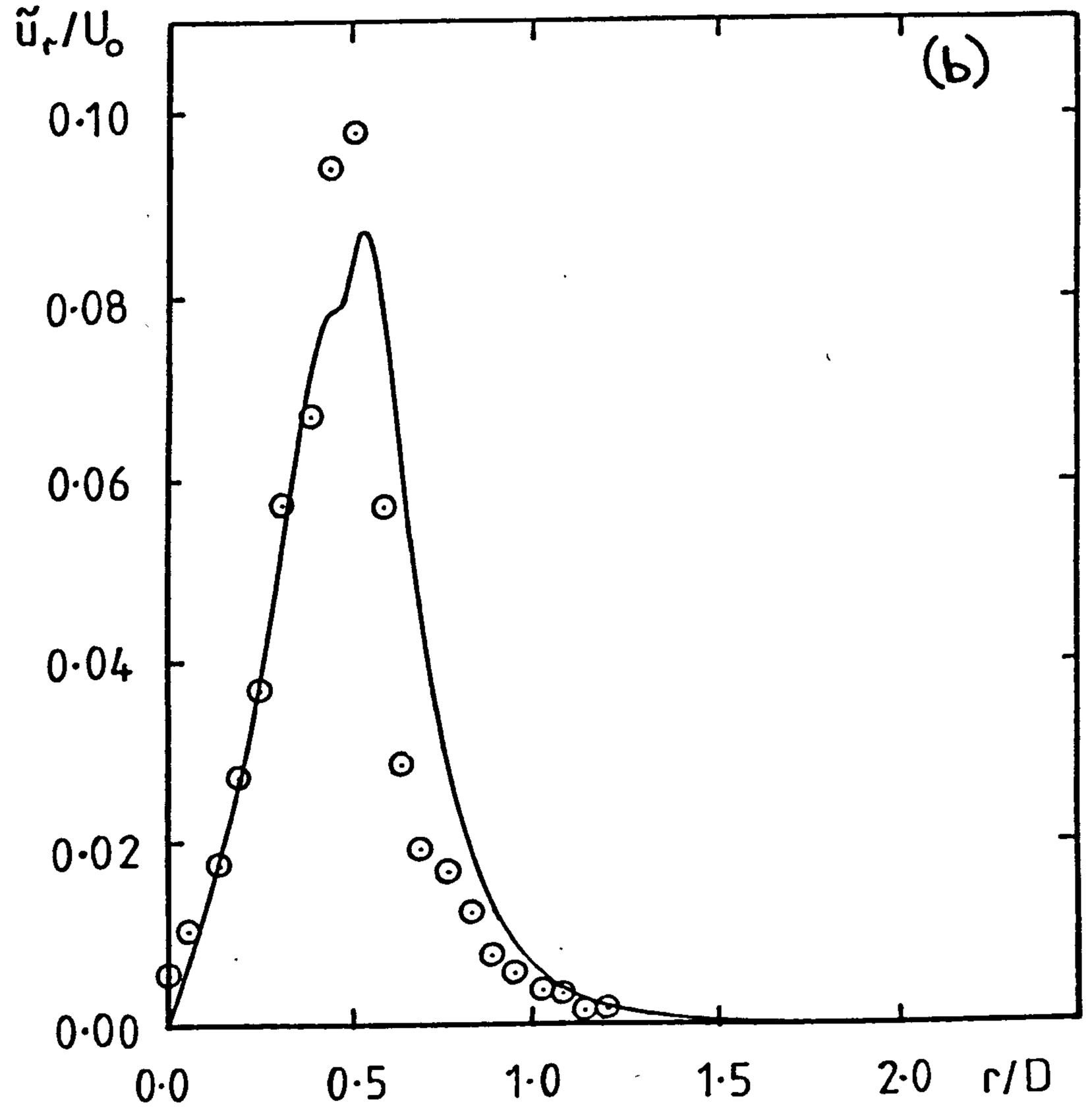

FIGURE 78 : RADIAL DISTRIBUTION OF FILTERED VELOCITY FLUCTUATIONS AT X=1D (i) m=0

(a) AXIAL COMPONENT, (b) RADIAL COMPONENT. (o EXPERIMENT, — PRESENT THEORY)

FIGURE 78 (ii) m=1

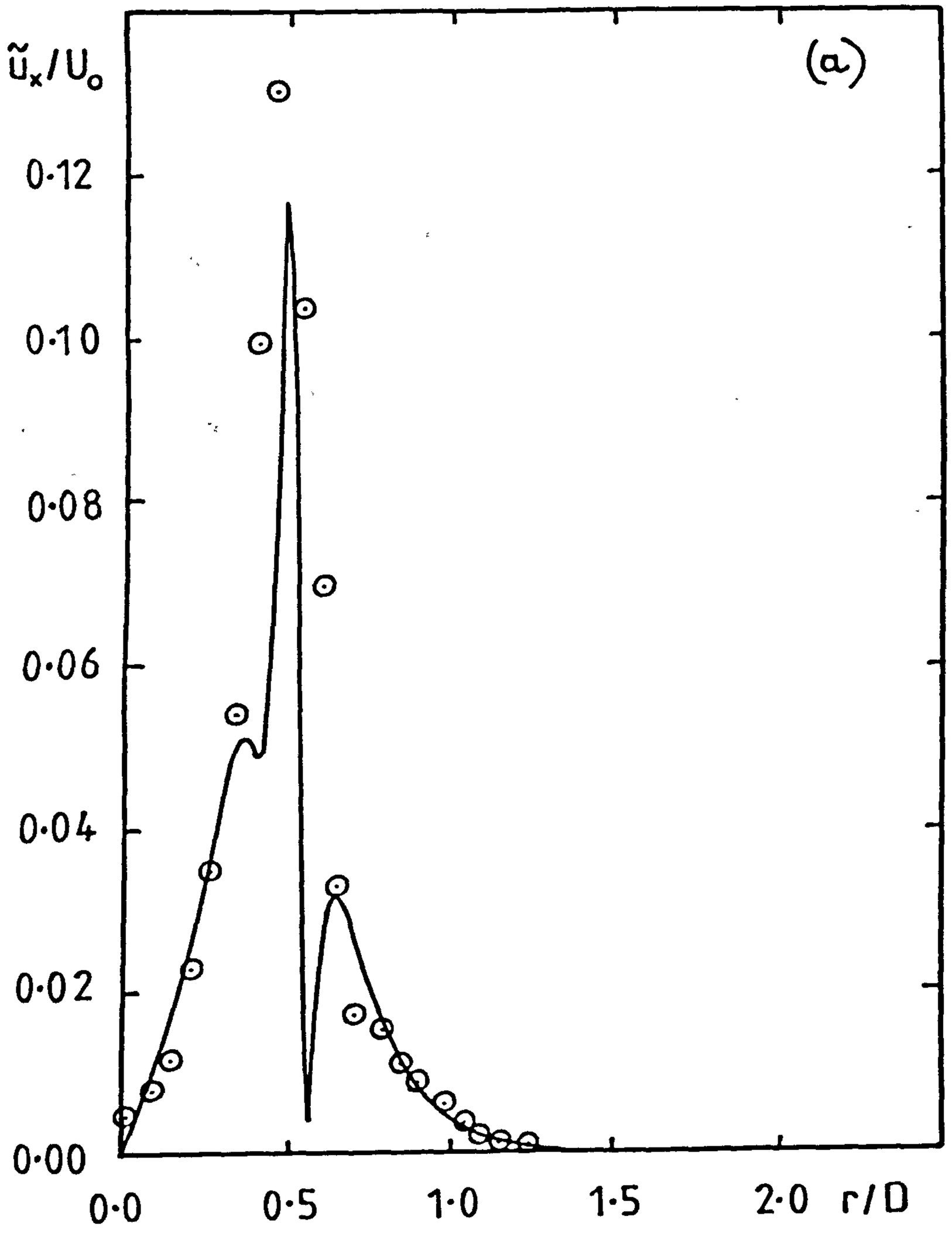

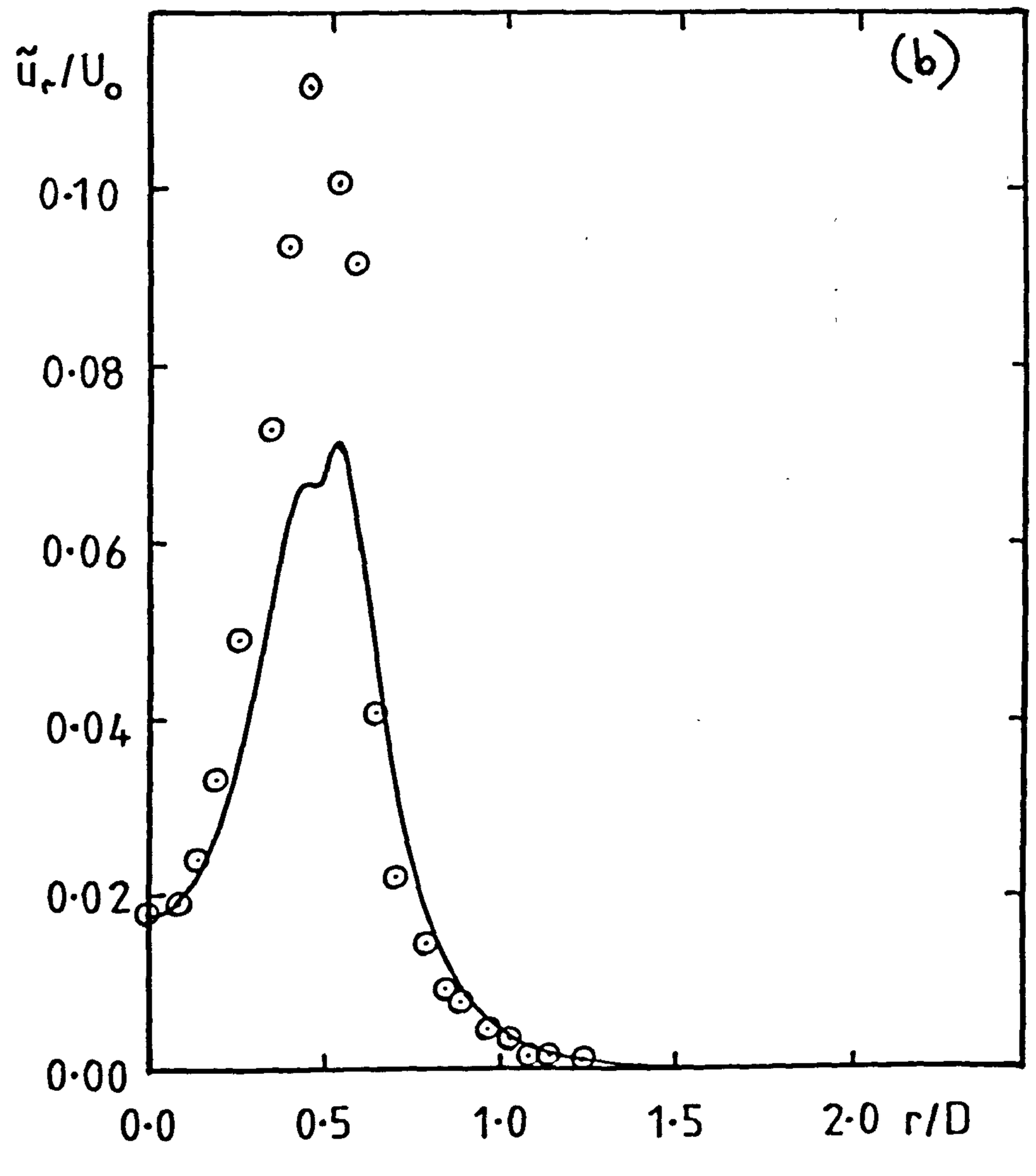

FIGURE 79 : RADIAL DISTRIBUTION OF FILTERED VELOCITY FLUCTUATIONS AT X=2D (GROWTH RATE AS PREDICTED BY THEORY)

m = 1

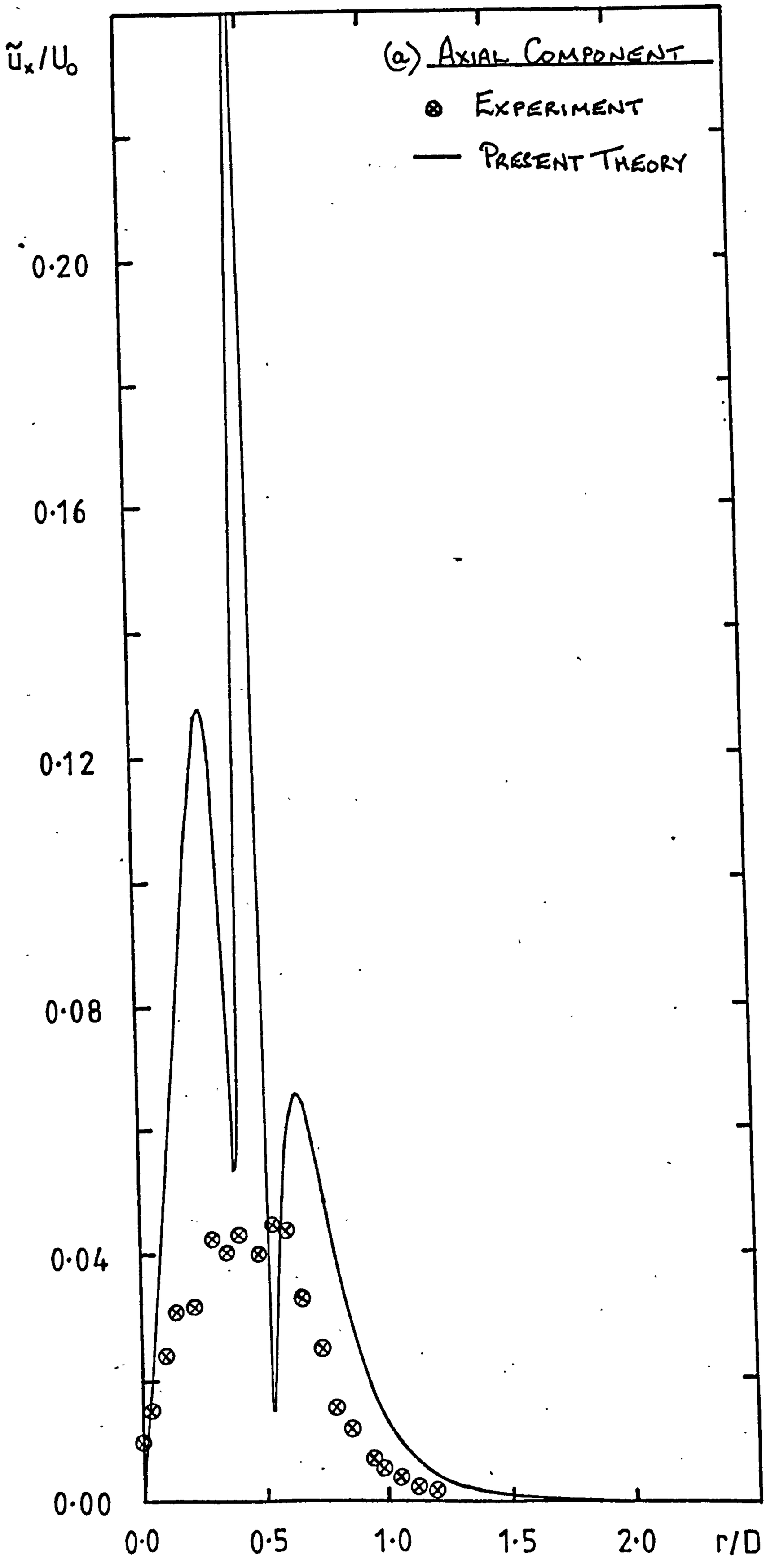

FIGURE 79 : CONTD.

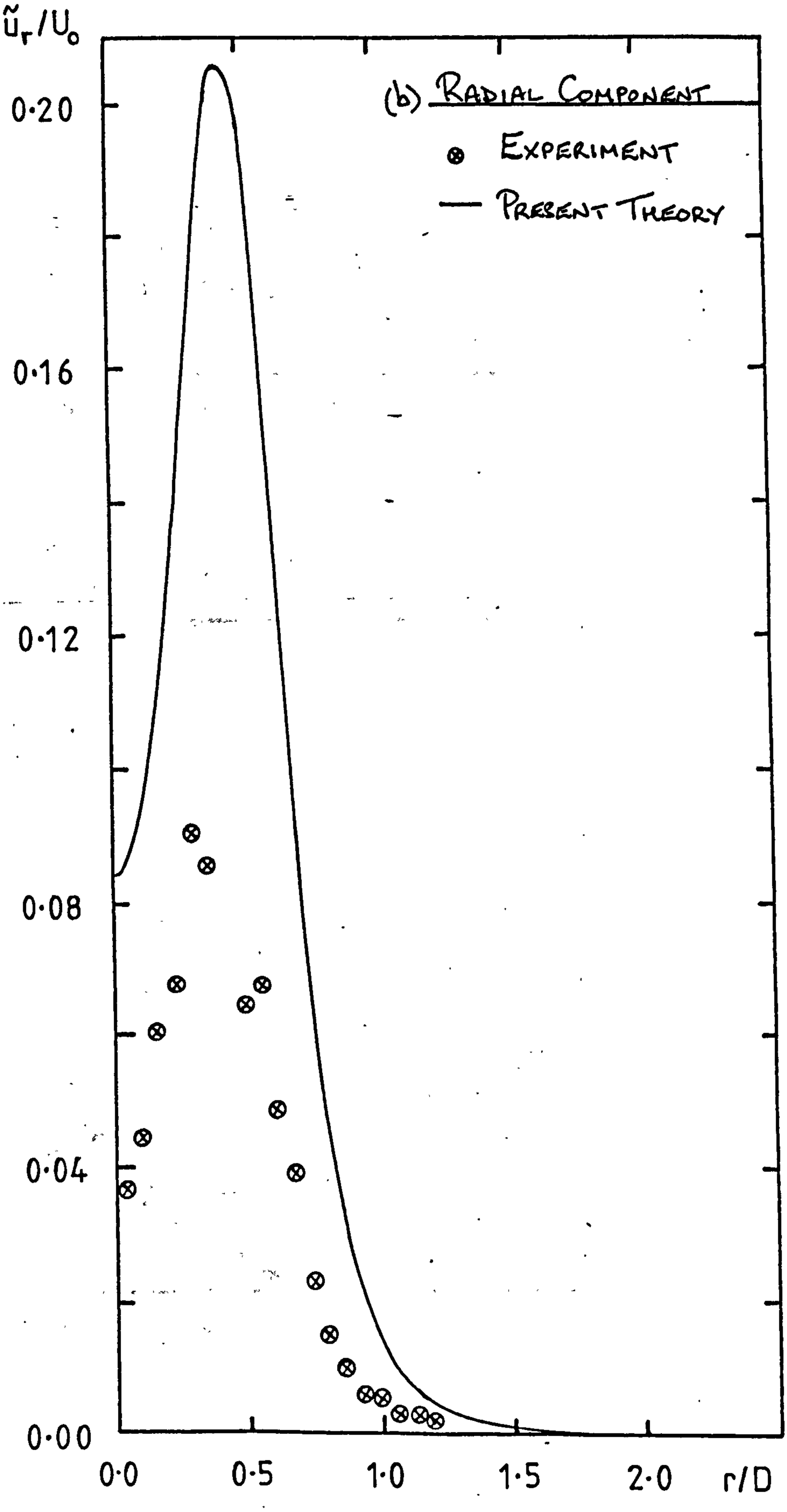

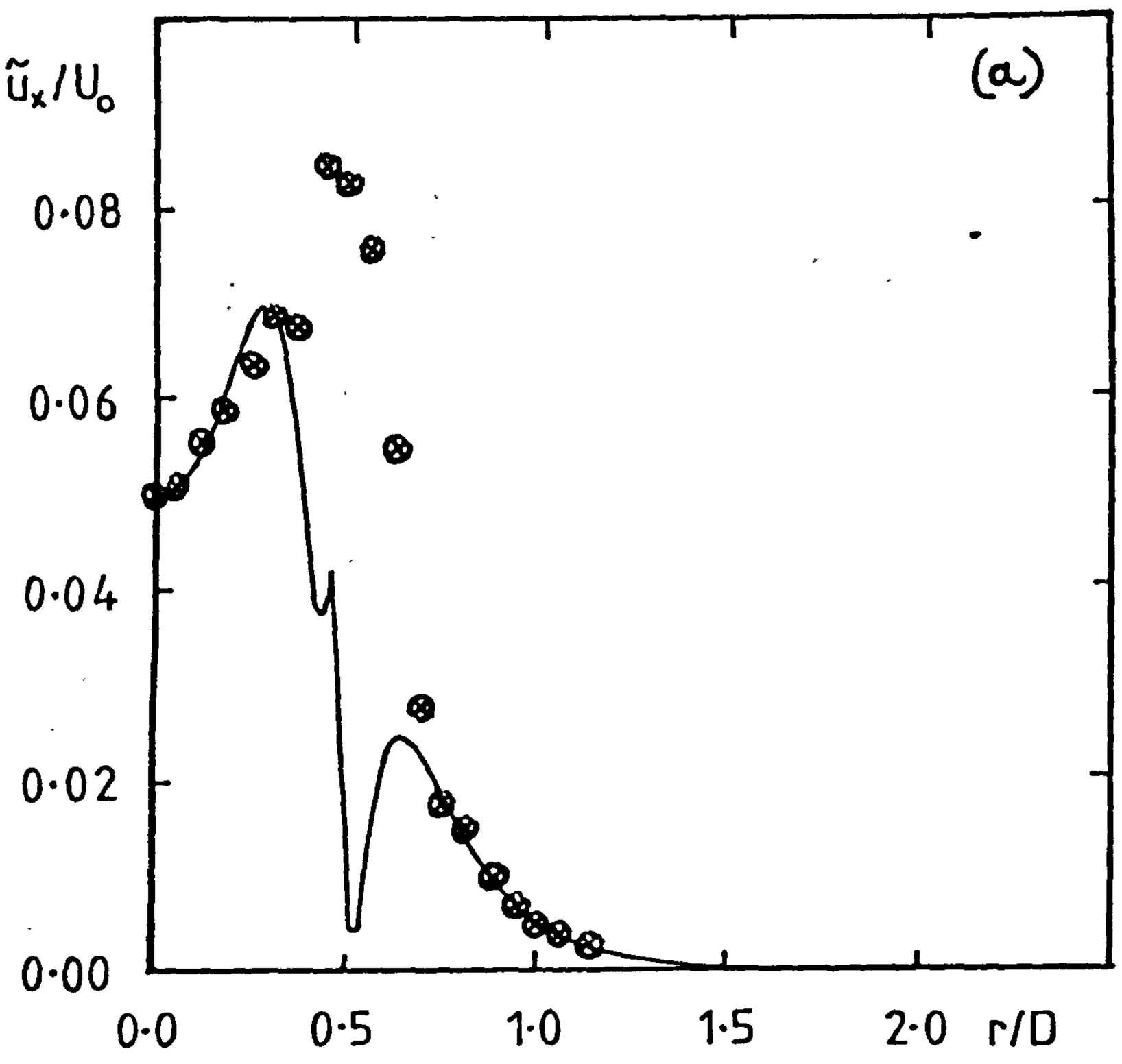

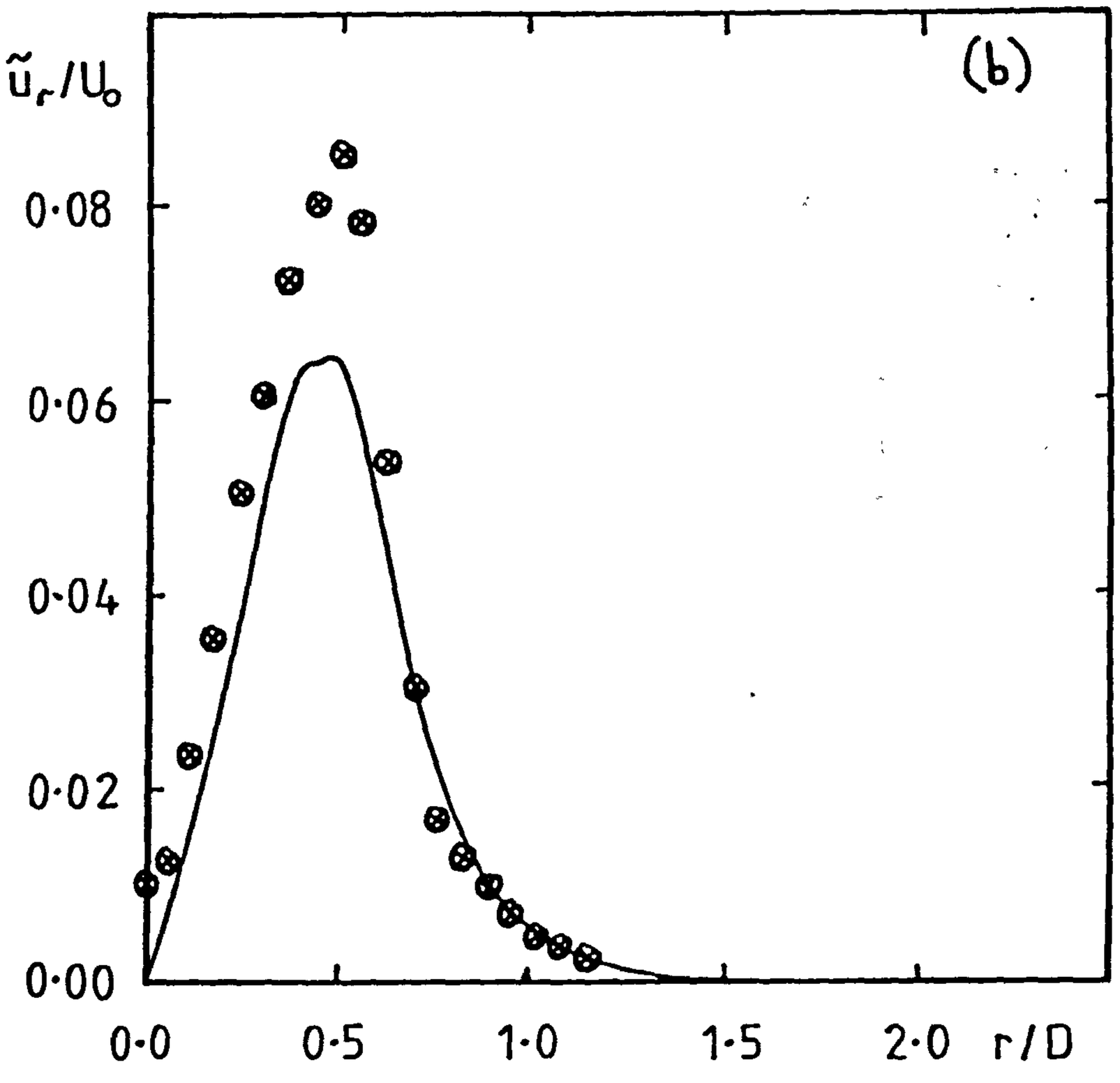

FIGURE 80 : RADIAL DISTRIBUTION OF FILTERED VELOCITY FLUCTUATIONS AT X=2D (i) m=0
(a) AXIAL COMPONENT, (b) RADIAL COMPONENT. (⊗ EXPERIMENT, —— PRESENT THEORY (RENORMALISED))

FIGURE 80 (ii) m=1

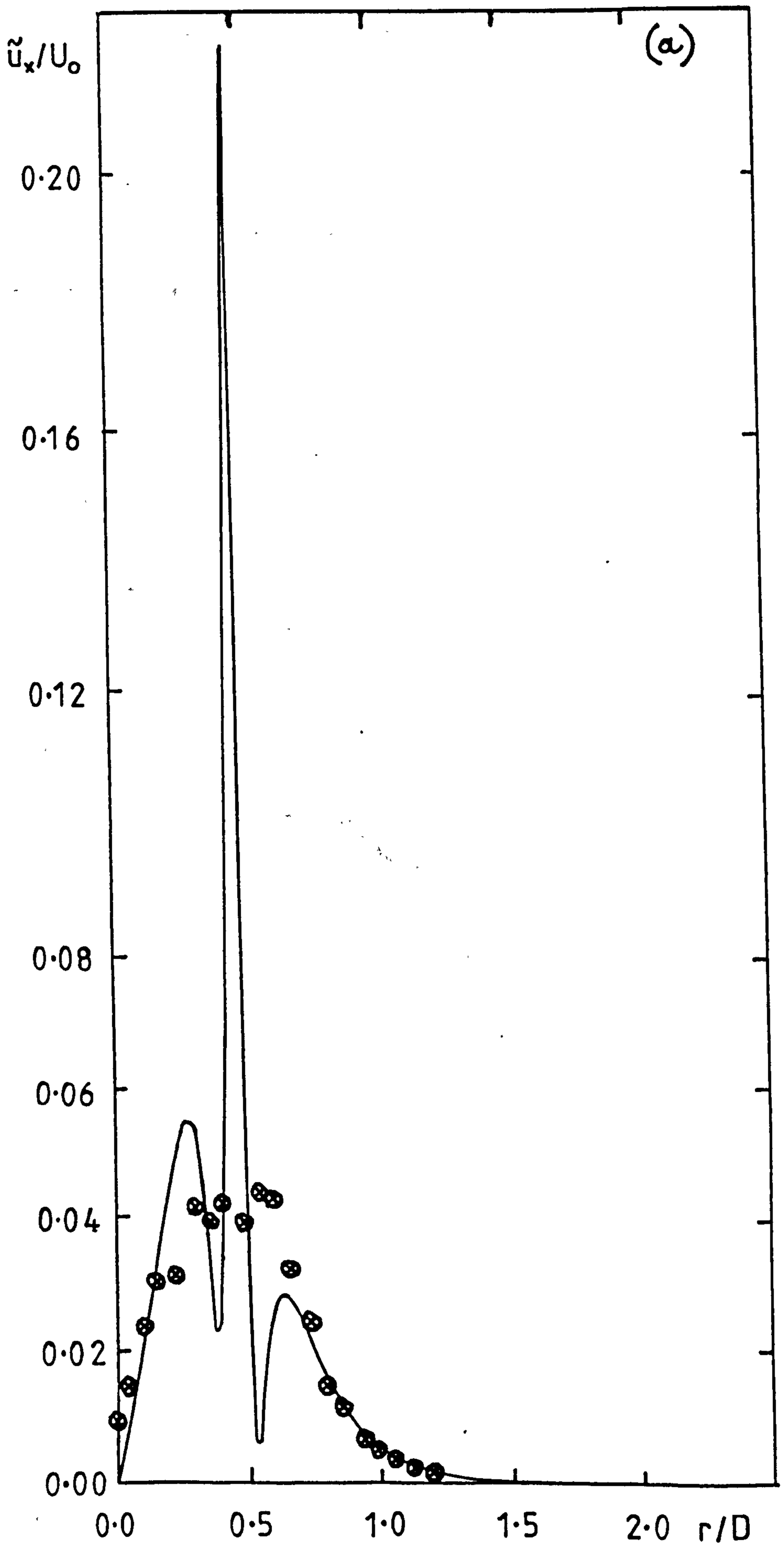

FIGURE 80 (ii) m=1

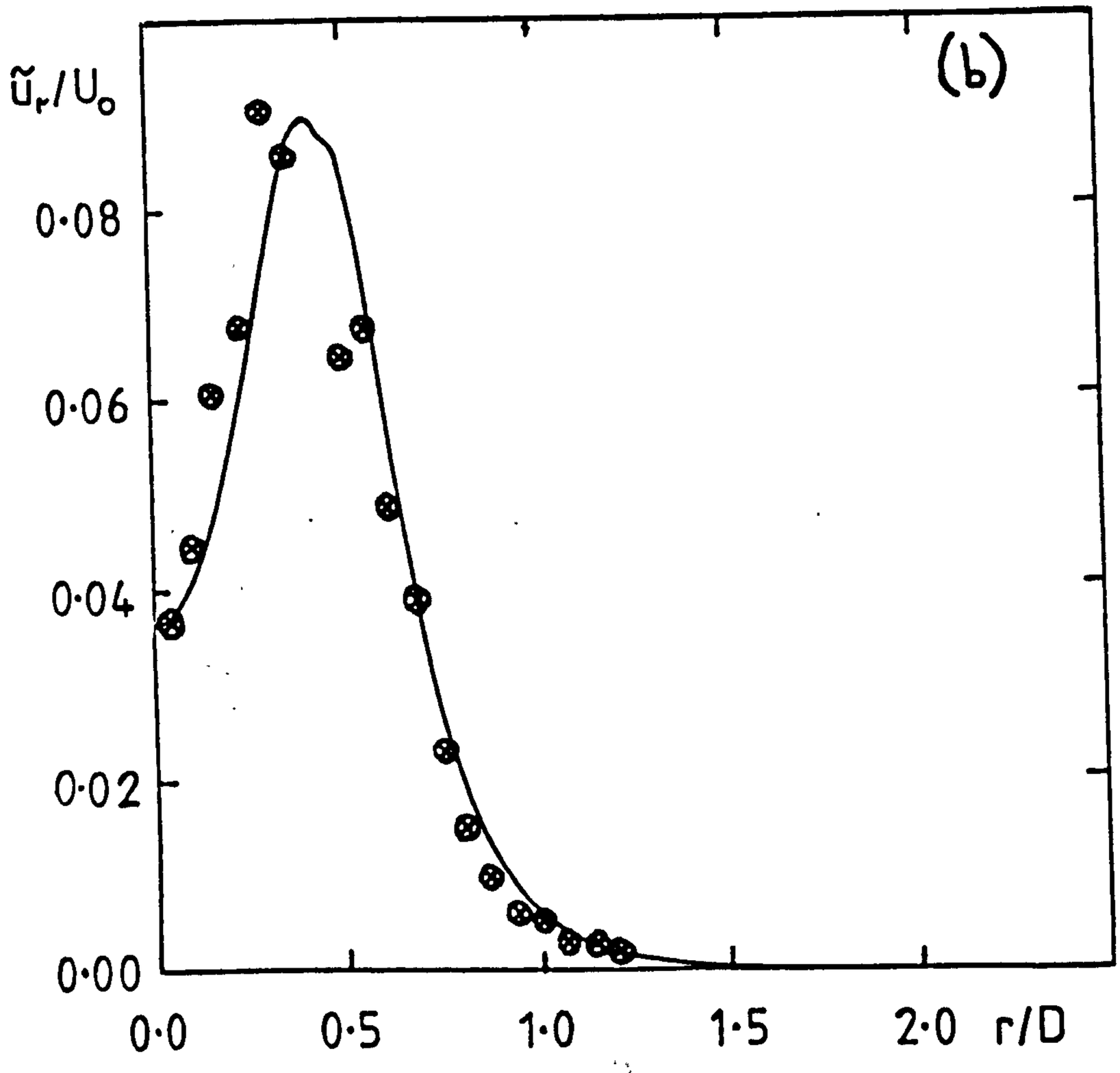

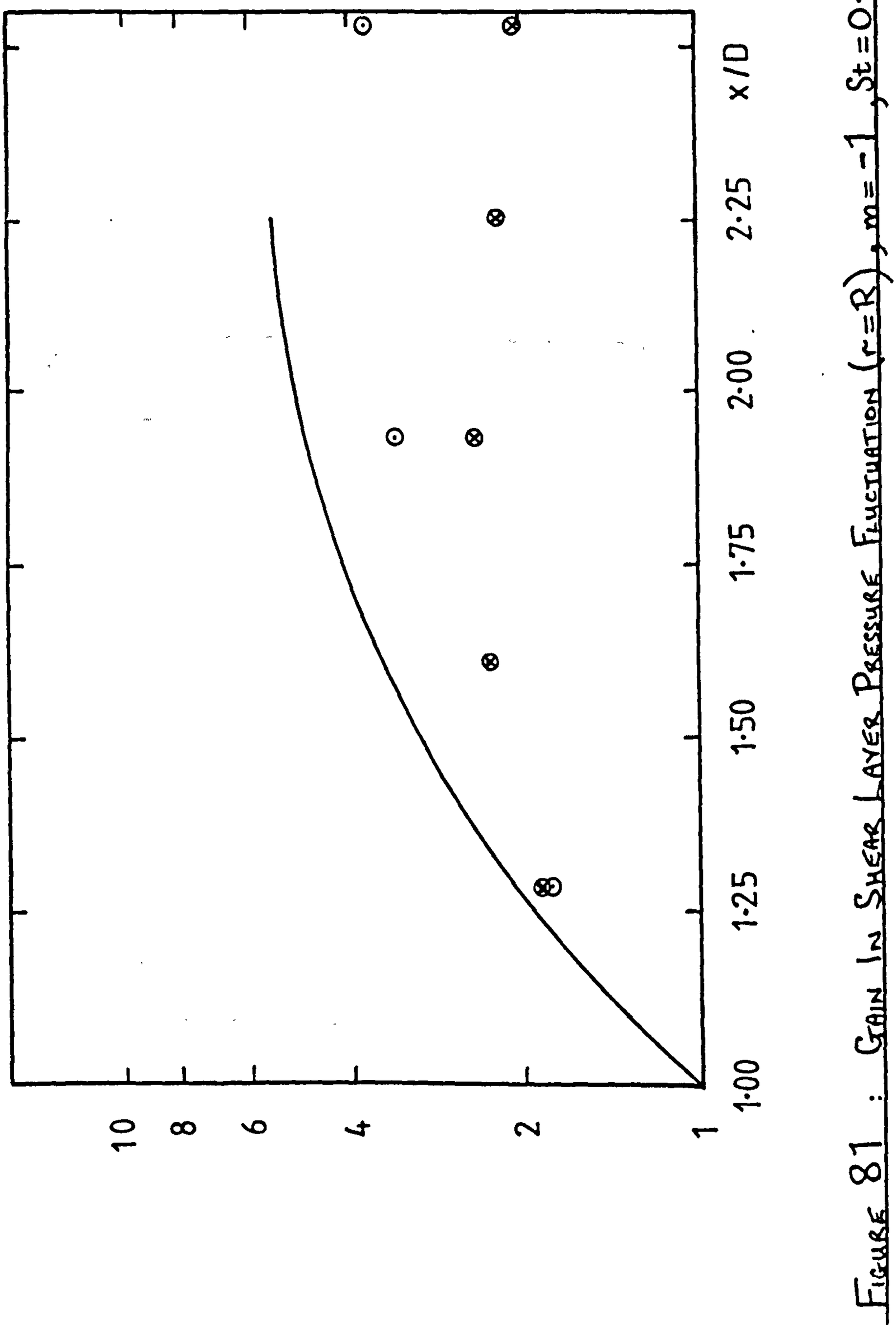

FIGURE 81 : GAIN IN SHEAR LAYER PRESSURE FLUCTUATION (r=R), m=-1, St=0.555

⊙ -20 dB ; ⊗ 0dB ; —— PRESENT THEORY

FIGURE 82 : PHASE SPEED OF SHEAR LAYER PRESSURE FLUCTUATION ($r=R$), $m=-1$, $St=0.555$

$\odot$ -20 dB, $\otimes$ 0 dB ; —⊡— PRESENT THEORY

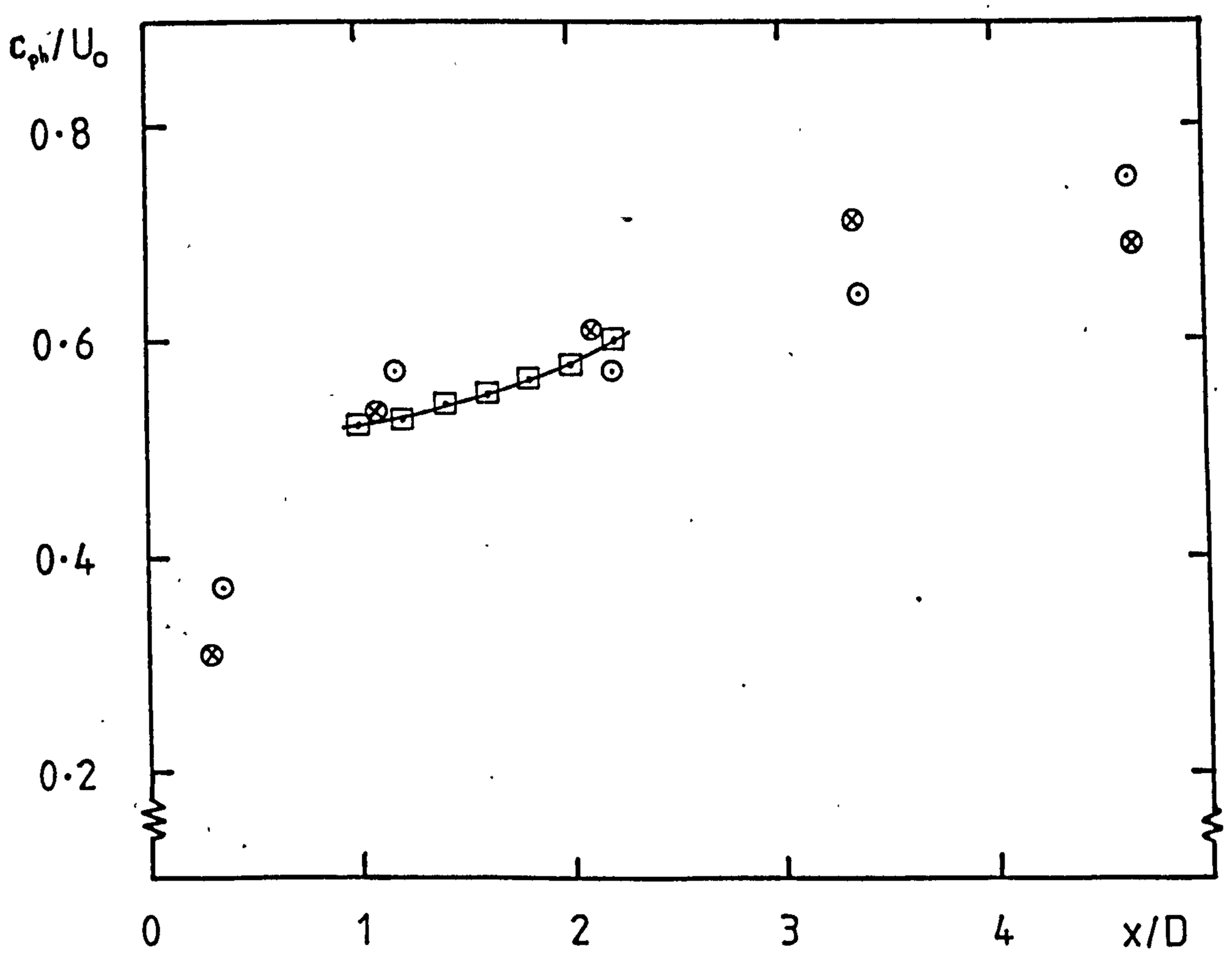

FIGURE 83 : RADIAL DISTRIBUTION OF PRESSURE FLUCTUATION IN m=-1 MODE AT X=2D, St=0·555, 0dB DRIVE LEVEL. ⊙ EXPERIMENT, ——— THEORY.

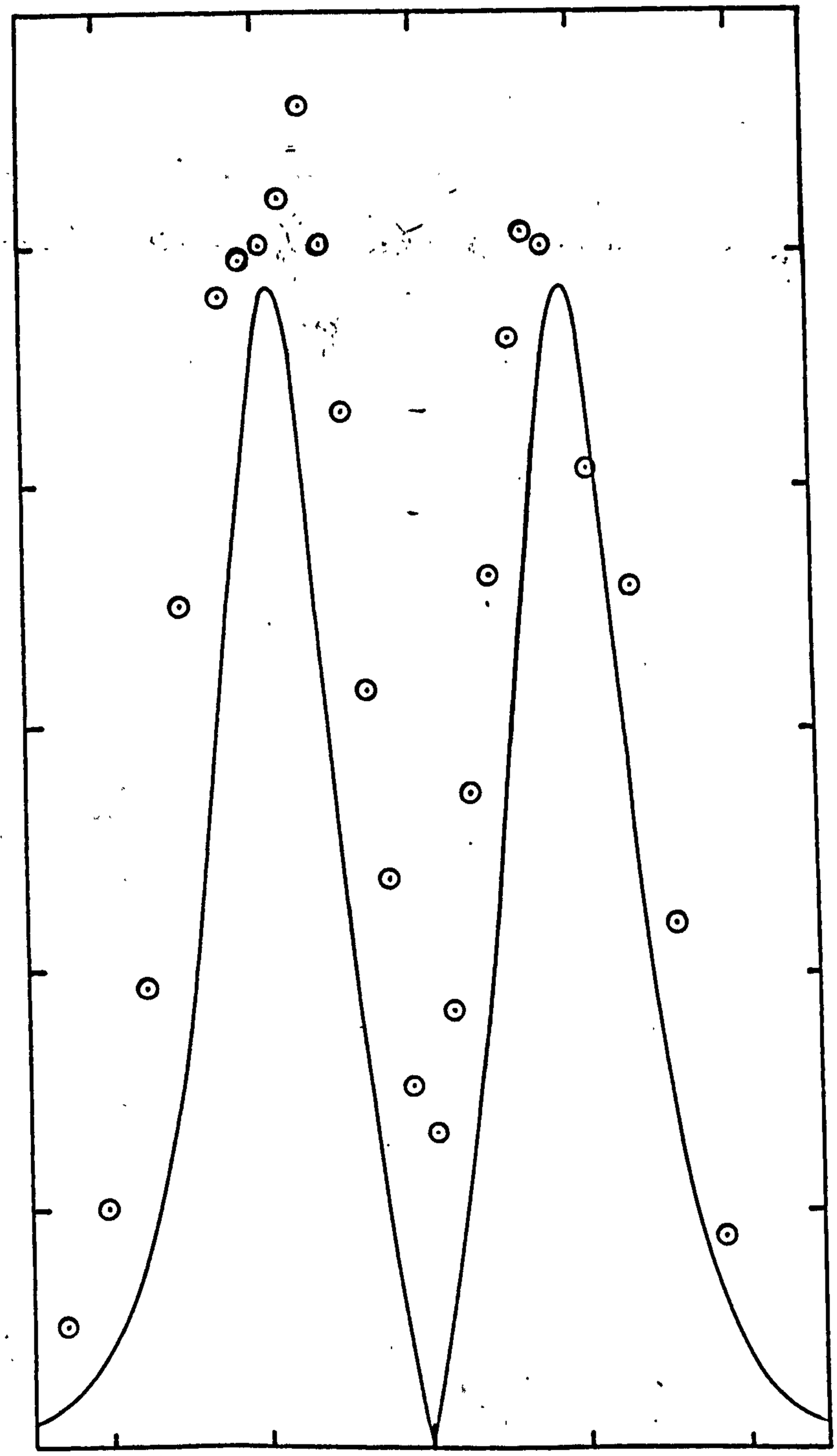

FIGURE 84 : RADIAL DISTRIBUTION OF PRESSURE FLUCTUATION

(o CHAN, St = 0·513, X = 1·8D ; — PRESENT THEORY, St = 0·5, X = 2D)

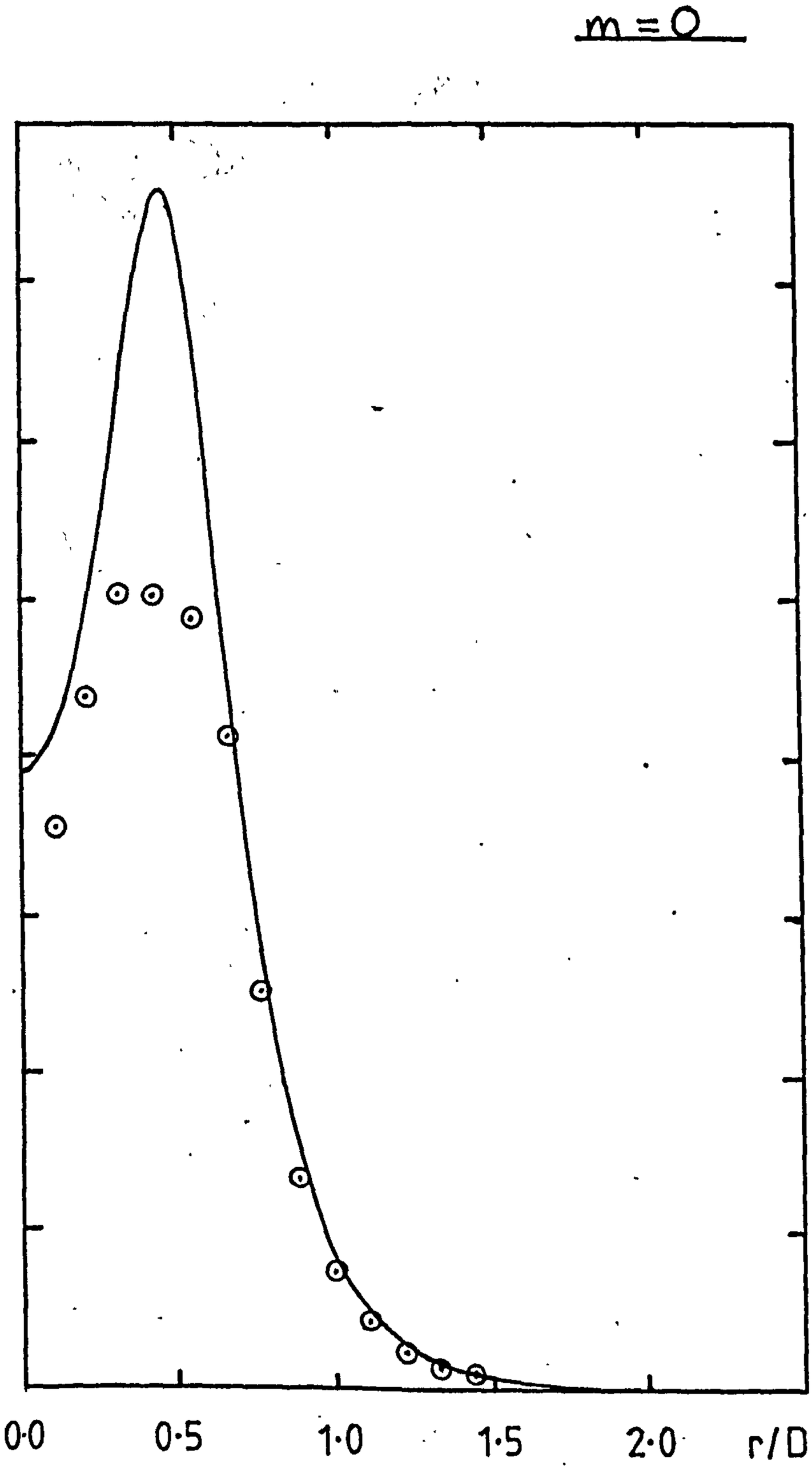

FIGURE 85 : RADIAL DISTRIBUTION OF PRESSURE FLUCTUATION

(⊙ CHAN, St = 0·501, X = 1·7D ; — PRESENT THEORY, St = 0·5, X = 2D)

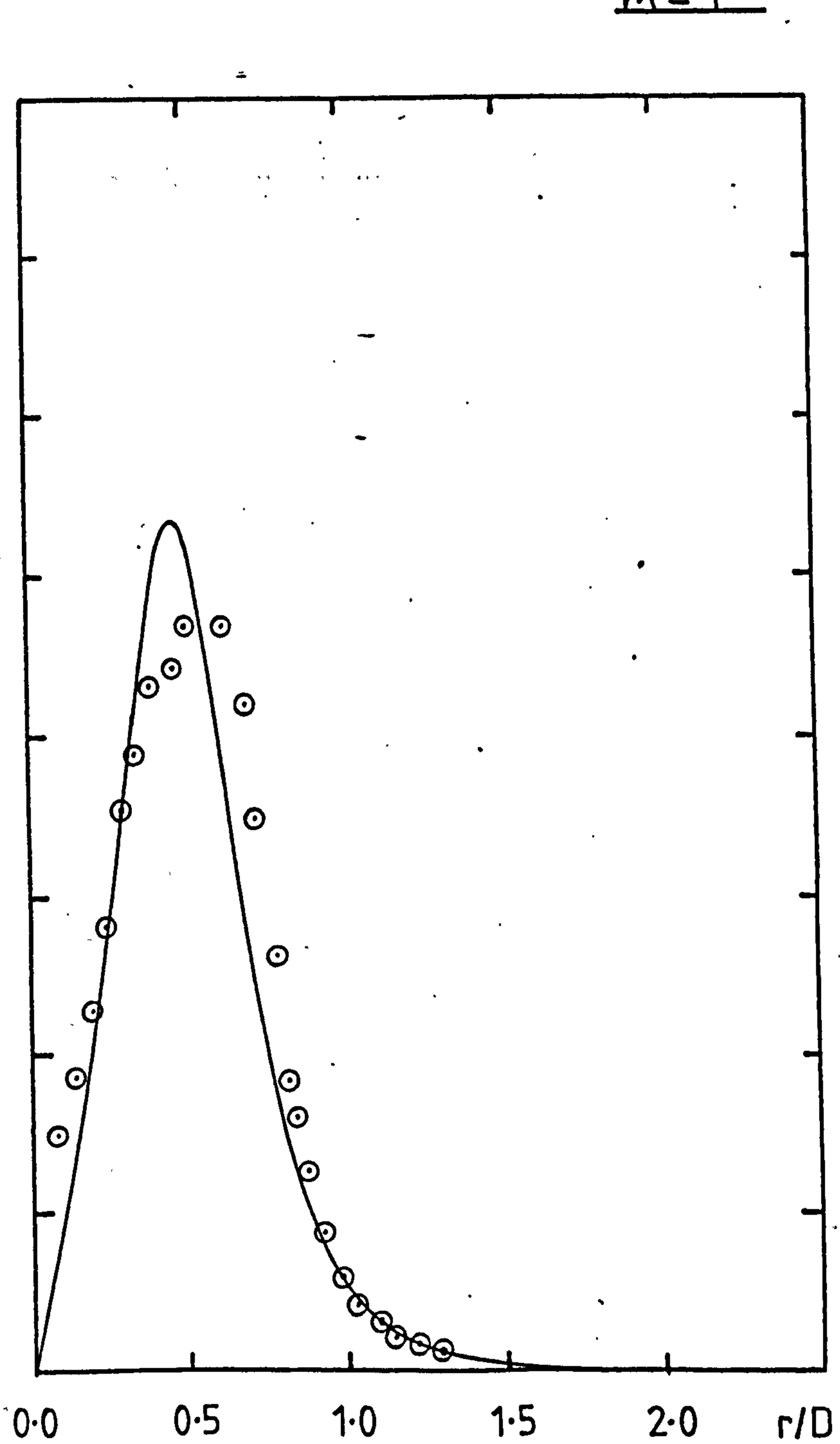

FIGURE 86 : RADIAL DISTRIBUTION OF PRESSURE FLUCTUATION

(⊙ CHAN, St = 0·502 , X = 1·65D ; — PRESENT THEORY, St = 0·5, X = 2D)

m = 2

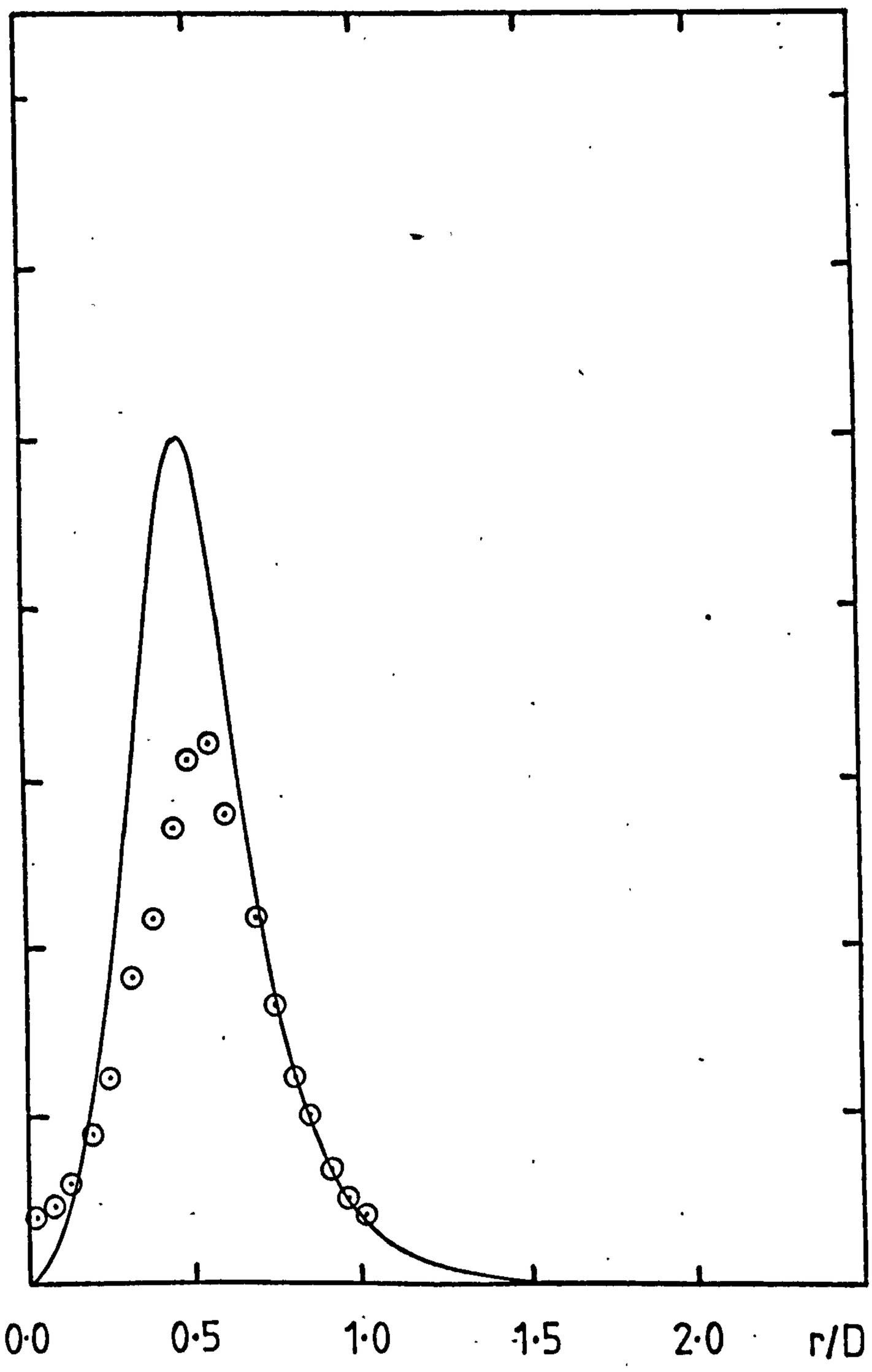

CHAPTER 5 STABILITY CHARACTERISTICS OF A SLOWLY DIVERGING CIRCULAR JET IN THE PRESENCE OF AN EXTERNAL FLOW

5.1 Introduction

In this chapter we are no longer concerned with the precise form taken by the excitation, but with the effect on an excited jet of yet a further deformation of the flow field: that produced by an external flow. Motivated by recent experimental work at the Advanced Research Laboratory, as reported in Moore & Brierley [54], which describes the effects of primary flow excitation on co-axial jets, we have adapted the program described in chapter 3 to take account of the presence of an external flow in a simple heuristic manner. There are no unsteady aerodynamic measurements shown in [54] and so no direct comparisons can be made (such comparisons would in any case have required the analytical form of the mean velocity profile to be rather more precise than the one to be used here). However, it is possible to draw a number of conclusions from the theoretical results presented (§5.3) in relation to the acoustic measurements and the flow visualisation results which appear in [54] and elsewhere (e.g., Sarohia & Massier [65]; Drevet, Duponchel & Jacques [26]; Bryce [12]).

In particular, the experimental work described in [54] details a number of noise measurements made on a clean co-axial model jet rig over a range of velocity ratios. Two different nozzle area ratios were used (0.9:1 and 6:1) and the primary jet excitation took place at a Strouhal number of 0.5. In the case of the 6:1 area ratio jet, which is more representative of a modern turbofan or a flight

situation, as the external flow velocity was increased from zero the noise level decreased over the whole acoustic field irrespective of whether the primary jet was excited or not. The levels reached a minimum at a velocity ratio of 0.5 in the excited case and 0.4 in the unexcited case, and then increased at higher velocity ratios in both cases. It was found that at all velocity ratios greater than 0.25 (approx.) the presence of an outer stream produced a larger decrease in the noise level when the primary jet was excited than when it was not excited. Since several different Strouhal numbers were subsequently used to the same effect, this seems to indicate that little or no broadband noise increase results from the excitation of a jet in the presence of a substantial ($V_a \gtrsim 0.25V_j$) external flow. This observation together with the evidence from the Schlieren films (described later) and the ensuing analysis all lend support to the theory that it is the vortex pairing process which is responsible for the broadband noise increase in an excited jet and that that pairing process cannot take place in the presence of a substantial external flow.

5.2 Mean Velocity Profile

The analysis used here is the same as that described in chapter 3. As will become clear, the boundary conditions determined there also remain unaltered in the external flow régime. The changes which had to be made to the program were therefore minimal and involved only the expressions for the mean velocity and its derivatives.

The profile given by (3.3.2) was modified such that as $r \to \infty$, the velocity decreases to a specified external flow velocity V_a, say.

It is then convenient to express the flow profile in terms of the external flow parameter

$$\Lambda \equiv \frac{V_j - V_a}{V_j}$$

where V_j is the centre line velocity of the jet. (We shall also have need to refer to the velocity ratio VR which is simply V_a/V_j.) The non-dimensionalised form of the mean velocity becomes

$$U(x,r) = 1 - \frac{\Lambda}{2} \{1 - \tanh \left[\frac{25}{(3x + 4)} (\frac{1}{r} - r)\right]\} \qquad (5.2.1)$$

The flow visualisation results presented in [54] and a number of previously unpublished mean velocity profiles obtained during that investigation (Moore, private communication) indicate that in the presence of a secondary flow, the potential core of the primary flow is lengthened since the mixing rate is reduced. Figure 87, showing the measured axial variation of the centre line mean velocity, with ($\Lambda = 0.5$) and without an external flow, is an illustration of this effect. Since we shall be considering only the first six diameters or so of the jet, the assumption of a constant centre line mean velocity would seem a valid one, at least for the case $\Lambda = 0.5$. The Schlieren films of the unexcited co-axial jet, shown in plate 9 (courtesy of Moore & Brierley [54]), confirm this behaviour for several other values of Λ. (It will be observed that when VR $\geq$ 1 ($\Lambda \leq 0$) the primary jet becomes entrained in the outer flow, but we shall restrict ourselves to the cases where $0 < \Lambda < 1$.)

It was felt that an additional effect which needed to be taken into account was that not only should the potential core of the primary jet be lengthened, but the shear layer ought to become narrower as the external flow velocity is increased. Furthermore, it did not seem unreasonable, in trying to model such an effect in as simple a manner as possible, to assume that the divergence rate of the primary flow varies linearly with Λ. Modifying the profile given by (5.2.1) accordingly gives

$$U(x,r) = 1 - \frac{\Lambda}{2}\left\{1 - \tanh\left[\frac{25}{\Lambda(3x + 4)}\left(\frac{1}{r} - r\right)\right]\right\}, \qquad (5.2.2)$$

where $0 < \Lambda < 1$. The profile given by (5.2.2), corresponding to $\Lambda = 0.7$, appears in figure 88, in a comparison with the profile used in the case of no external flow, at a number of axial positions. Clearly, this simple assumption of a linear variation of the divergence rate with Λ, when applied to (5.2.1), has only a secondary effect. The reason for this stems from the approximation used in the derivation of (5.2.1). In order to simulate an external flow, the condition $U = V_a$ should have been applied at least at a finite radius and preferably $O(R)$. However, in an attempt to keep the expression for the mean velocity as simple as possible, taking $U \to V_a$ as $r \to \infty$ has broadened the profile to such an extent as to make the adjustments made to the shear layer divergence ineffective.

Whilst the result of the change in the profile from (5.2.1) to (5.2.2) was not as first expected, we subsequently found that the previously unpublished mean flow measurements which correspond to a value of Λ in our range of interest show the same behaviour as the

co-axial profiles in figure 88. The experimental mean velocity profile of the primary jet in the presence of an external flow displays a broader potential core region than that measured for the primary jet alone, when the external flow is that produced by a secondary, annular jet (figure 89).

The mean velocity profile given by (5.2.2) was therefore the one used in the calculations and the results are presented in section 5.3. Comparisons with the measured profiles of the unexcited co-axial jet for $\Lambda = 0.5$, at axial positions of 1, 2 and 6 diameters, are shown in figure 90. A number of the details in the measured profiles are clearly not accounted for in the model. It was mentioned in [54] that the length to diameter ratio of the primary nozzle was quite large (approximately 20), which results in the flow in the primary nozzle being partially developed at the exit plane. We feel, however, that such a profile is unlikely to occur in the jet engine context and that the less stable profile given by (5.2.2) is more representative of the real situation. We are in any case considering only the more general, qualitative effects of an external flow field, for which purpose the details of the primary (jet) flow are of secondary importance. Furthermore, it must be emphasised that our intentions are no more definite than that : we have not attempted to describe the specific behaviour of either a coaxial jet or a jet in flight, but our investigations have been more speculative in nature, being concerned with the general effects of external flow on linear jet instabilities.

Finally, the measured profile displays a dip close to the nozzle exit plane, around $r = R$, because of the momentum deficit in

the boundary layer flows on the inner and outer walls of the primary nozzle. We have discussed the effects which this could have on the noise level in the forward arc in chapter 1, but this again is not a profile detail which has been included in (5.2.2).

Since the form of the mean velocity profile is such that its derivatives display the same asymptotic behaviour (as $r \to 0$ and as $r \to \infty$) as (3.3.2), the boundary conditions derived from (3.2.15) in chapter 3 remain unchanged and will not be restated.

5.3 Results

The results to be presented describe the variation with the external flow parameter Λ of the axial development of a plane wave mode on the mean velocity profile prescribed in the last section. We wished to examine the growth of a disturbance which was being forced by some perturbation created inside a jet engine. The disturbance would therefore be excited at a fixed frequency; the frequency associated with vortex shedding from nozzle guide vanes or flow interaction with fixed elements of the engine, for example. Since this frequency is the same for every value of Λ, the Strouhal numbers have been based on the centre line velocity V_j and not the velocity difference $(V_j - V_a)$. (It might be thought that the Strouhal number of the preferred mode would scale with the relative velocity, but we are unable to find evidence to support this. Indeed, the acoustic measurements of [54] could, indirectly, be taken to invalidate this claim. It was reported there that measurements were obtained with the excitation frequency corrected

for the relative velocity ($V_j - V_a$) and that the reduction in overall noise level with a secondary flow could not be said to have been caused only by the excitation being at the wrong diameter-based Strouhal number for the primary jet.)

The graphs in figures 91 and 92 show the axial growth of the fluctuations in the pressure, axial velocity and radial velocity on the lip line at two Strouhal numbers, 0.3 and 0.5. At St = 0.3, results are presented for Λ = 0.5, 0.7, 0.8 and 0.9. However, at the higher Strouhal number it was not possible to determine the eigenvalues for the inviscid calculation at the lowest of these values for Λ, because the wave was too close to the neutral condition. The plotted gains have been normalised with respect to the wave amplitude at x = 1D.

For each flow quantity an increase in the external flow velocity results in a downstream displacement of the axial position of maximum gain. At the higher Strouhal number, the maximum amplitude itself also increases with the external velocity. This increase is observed to a lesser extent in the pressure and radial velocity fluctuations at the lower Strouhal number, but the maximum amplitude of the axial velocity fluctuation actually decreases with increasing external flow velocity. It is also of interest to note that at St = 0.5, the initial growth rate is larger for Λ = 0.9 than for Λ = 1 for every flow quantity. For Λ < 0.9, however, the initial growth rate decreases with Λ, as is the case for each flow quantity at St = 0.3. No phase speed results are shown here, but at each Strouhal number an increase in the external flow velocity produced a decrease in the phase speed of each flow variable along r = R.

5.4 Discussion

It would appear that in the present model the variations in the axial growth rates with external flow fall into two categories. The mean velocity profile near to the nozzle exit more closely approaches the unstable top hat profile in the presence of a small external flow velocity than in its absence. At the higher Strouhal number, which is close to that which produces the largest initial amplification on the core profile ($\Lambda = 1.0$), a small external flow velocity ($\Lambda \gtrsim 0.8$) therefore results in an <u>increase</u> in the growth rate. As the external flow velocity is increased, the initial growth rate decreases, but the total amplification becomes greater than that for $\Lambda = 1.0$ at some distance further downstream, presumably because the potential core is longer. When the external flow velocity is as large as 0.5 V_j, the disturbance at St = 0.5 grows at a much slower rate than for $\Lambda = 1.0$ and too slowly to be followed using the present analysis. At St = 0.3, the initial growth rate decreases with increasing external flow velocity from $\Lambda = 1.0$ because this Strouhal number is not close to the maximally amplified one and the disturbance is therefore not as sensitive to the thinning of the shear layer.

It can thus be said that when the external flow velocity is sufficiently large, $\Lambda \approx 0.5$, the disturbances grow more slowly and reach a lower maximum amplitude than in the absence of an external flow. This is in agreement with the flow visualisation results in plate 9 where, at $\Lambda = 0.5$ (VR = 0.5), for example, the vortices on the primary jet which are first seen around x = 3D maintain their coherent structure until at least x = 10D. If the vortex pairing

process is assumed to be the main noise generation mechanism, as claimed by Laufer et al [39] and Ffowcs Williams & Kempton [29], this structural analysis provides a possible explanation for the observed reduction in overall noise level in the presence of an external flow as reported by Moore & Brierley [54]. Moreover, their paper also indicates that the extra noise produced by the excitation of a co-axial jet decreases to a minimum as the secondary flow velocity is increased to 0.5 V_j.

Figure 87 : Variation Of Centre Line Mean Velocity With Axial Position From Brierley [9]

PLATE 9

EXCITED

UNEXCITED

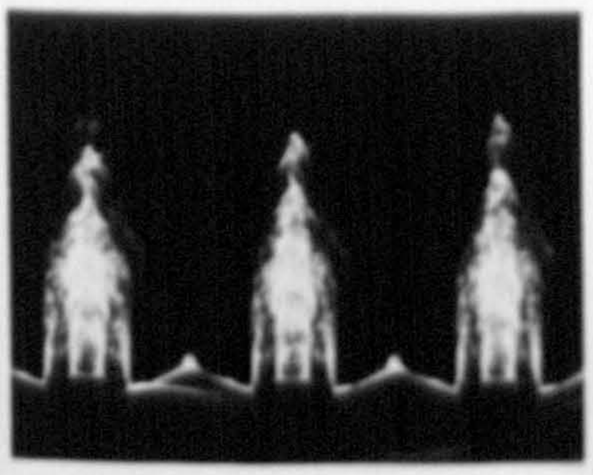

VR = 0.125

Mpri = 0.7

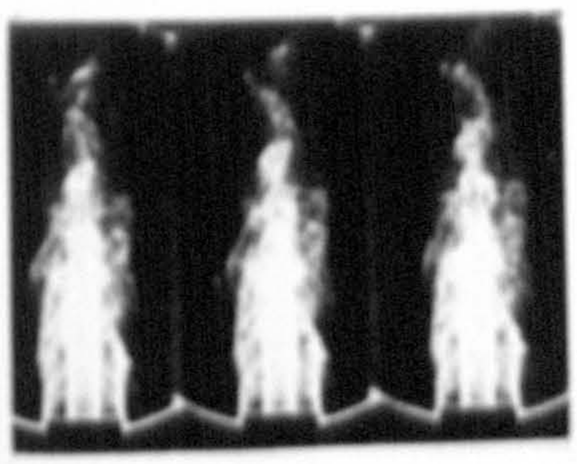

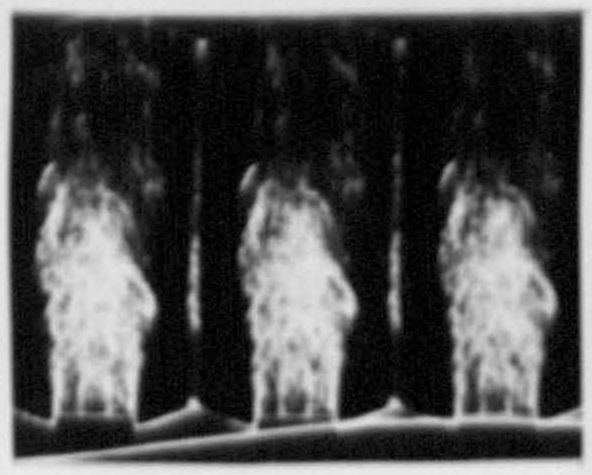

VR = 0.25

Mpri = 0.3

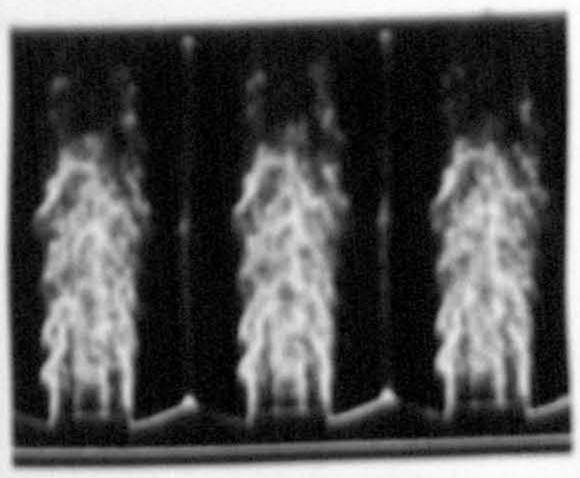

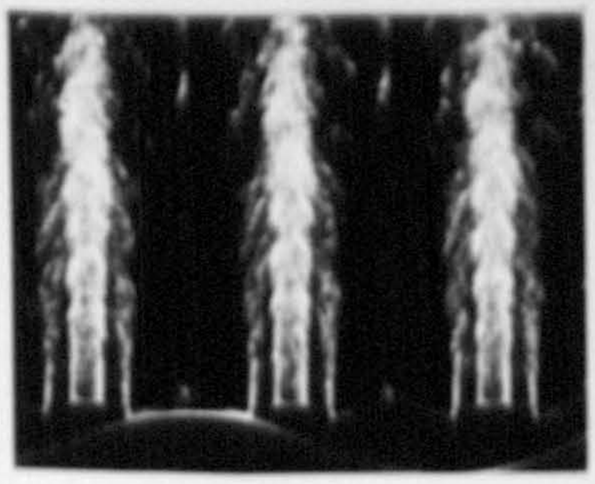

VR = 0.5

Mpri = 0.7

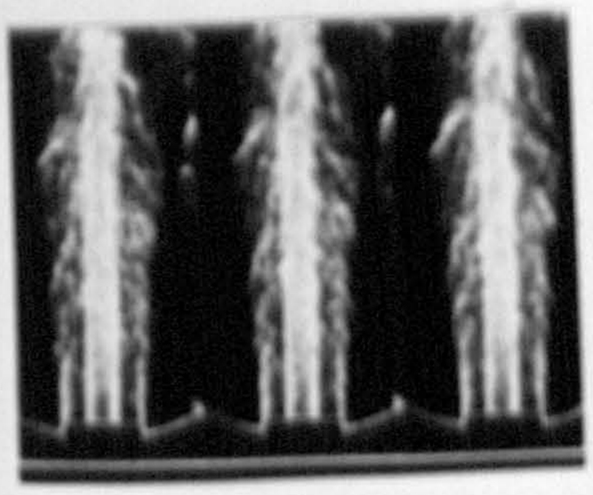

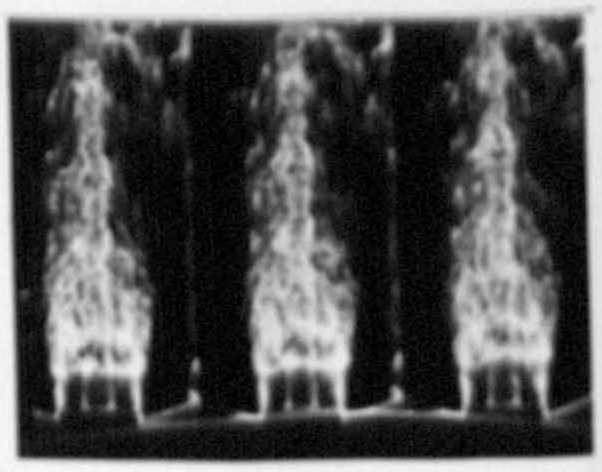

VR = 1.0

Mpri = 0.3

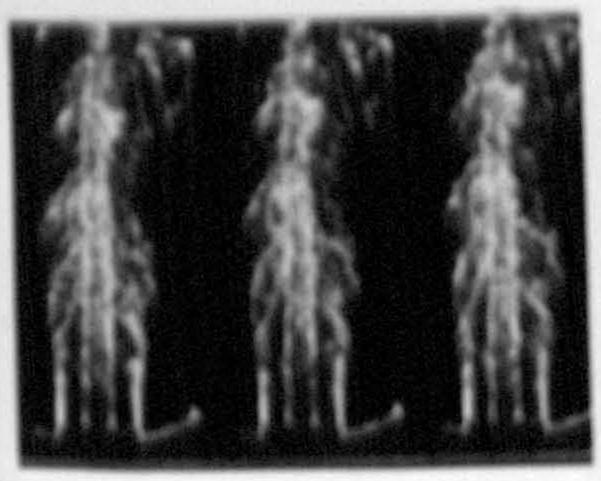

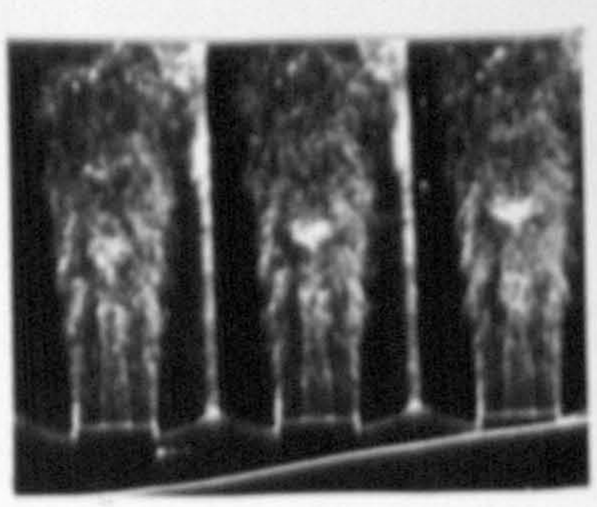

VR = 2.0

Mpri = 0.3

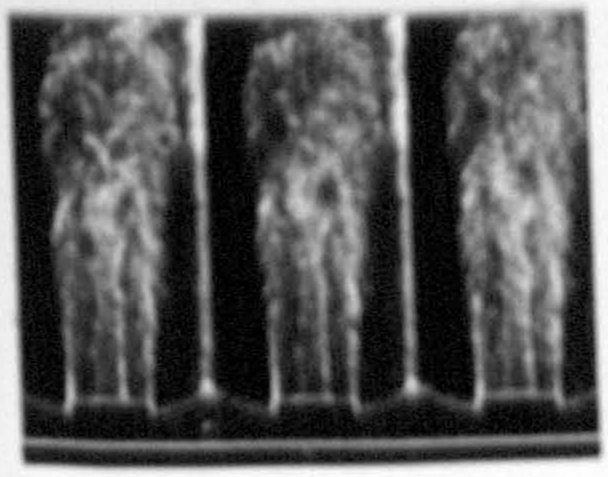

Summary of effect of primary flow excitation
on 6-1 AR coaxial jet system

FIGURE 88 : COMPARISON OF MEAN VELOCITY PROFILES WITH (i) EXTERNAL FLOW PARAMETER $\Lambda = 0.7$ AND (ii) NO EXTERNAL FLOW. AXIAL DISTANCES : (a) X=1D , (b) X=2D , (c) X=4D , (d) X=6D.

(a)

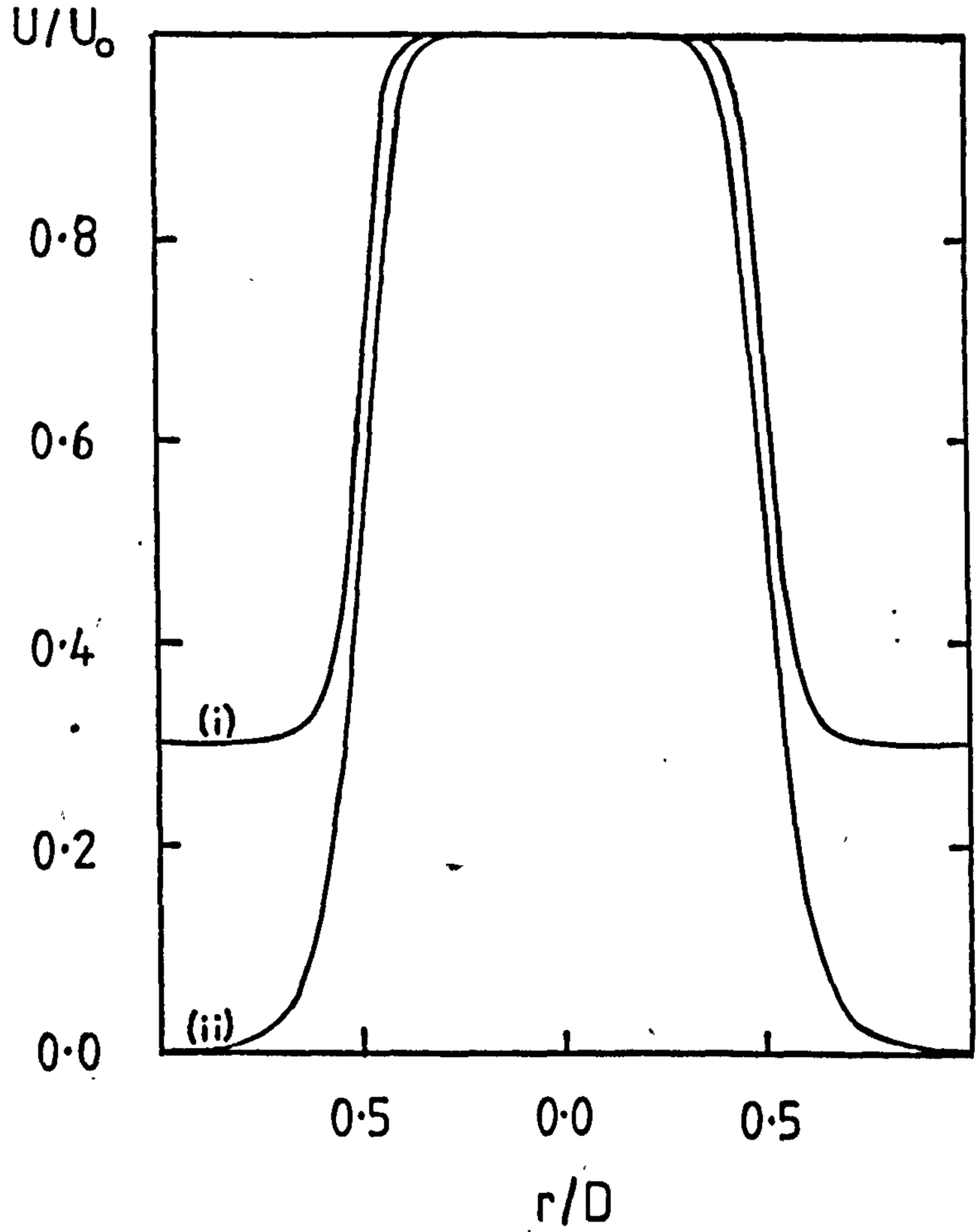

(b)

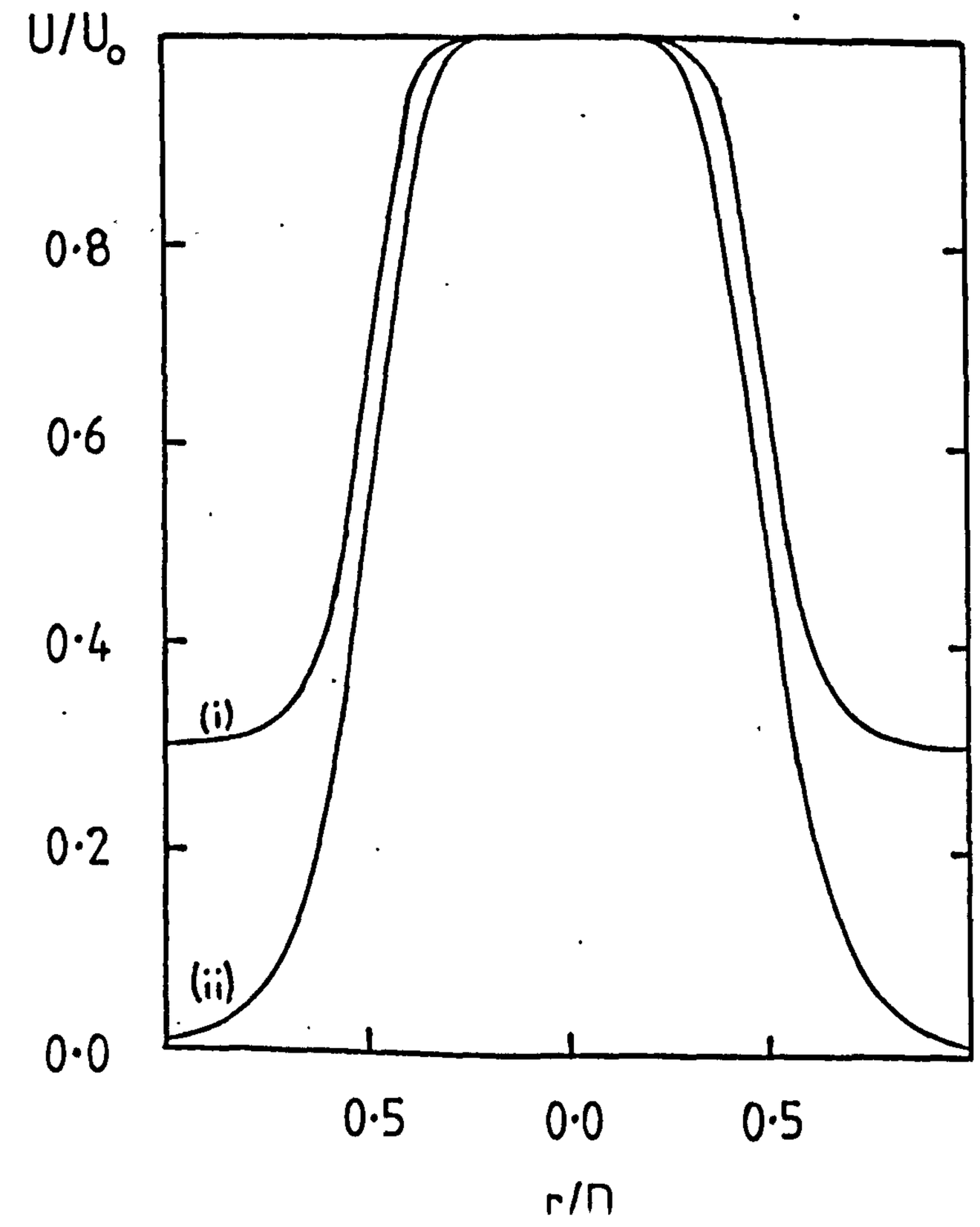

FIGURE 88- CNTD.

(c)

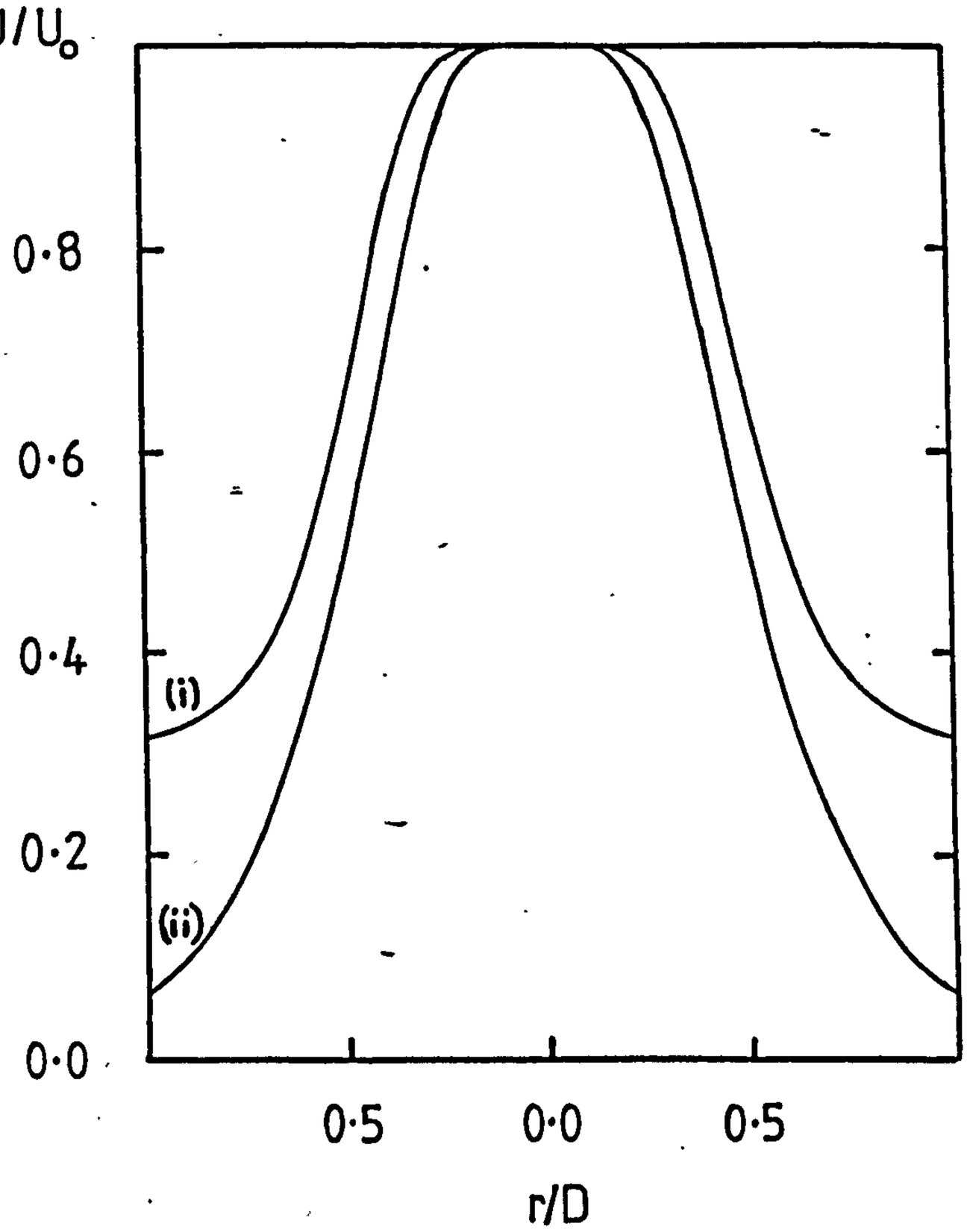

(d)

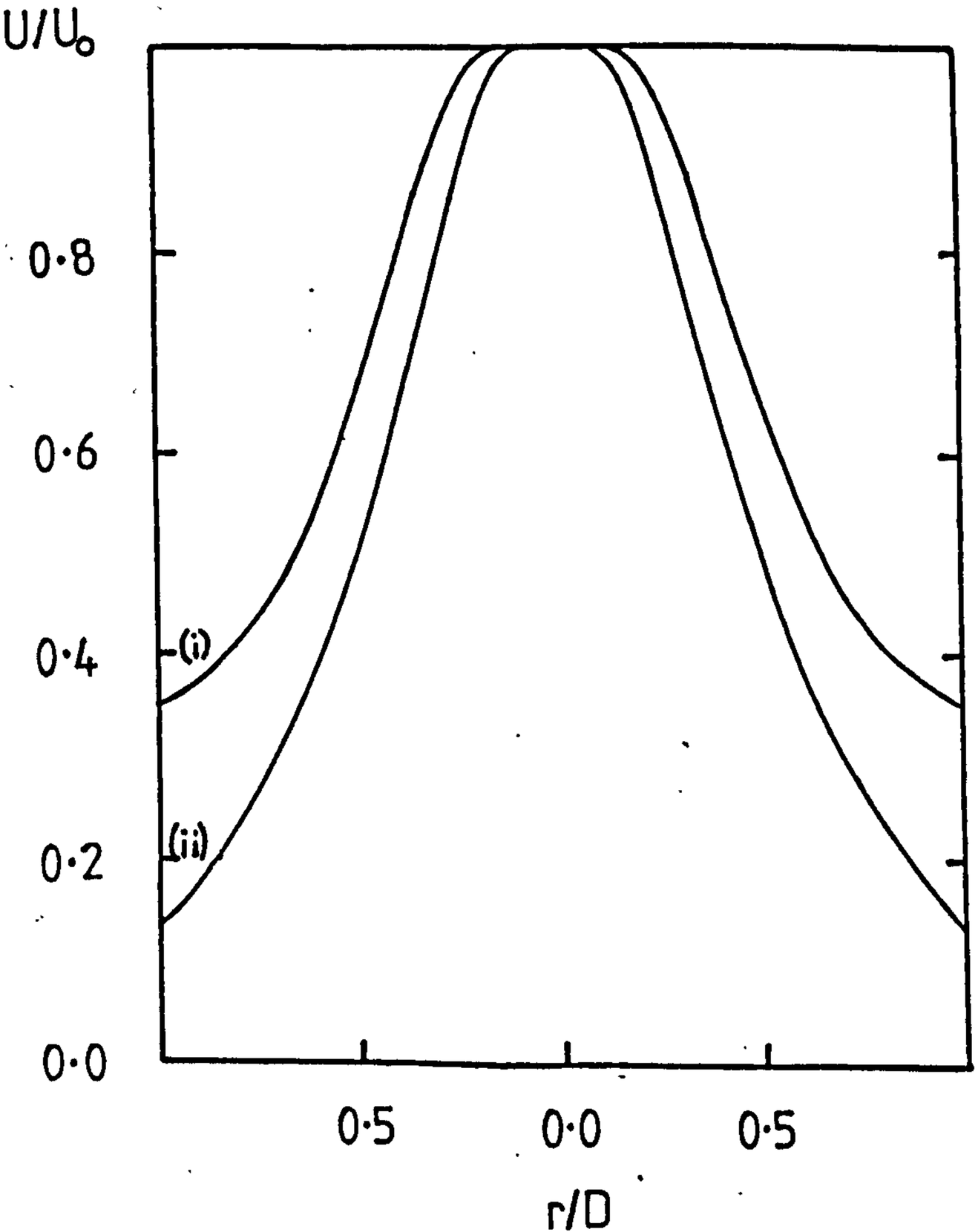

FIGURE 89 : COMPARISON OF MEASURED MEAN VELOCITY PROFILES FOR CO-AXIAL FLOW ($\Lambda = 0.5$) AND PRIMARY FLOW ALONE.

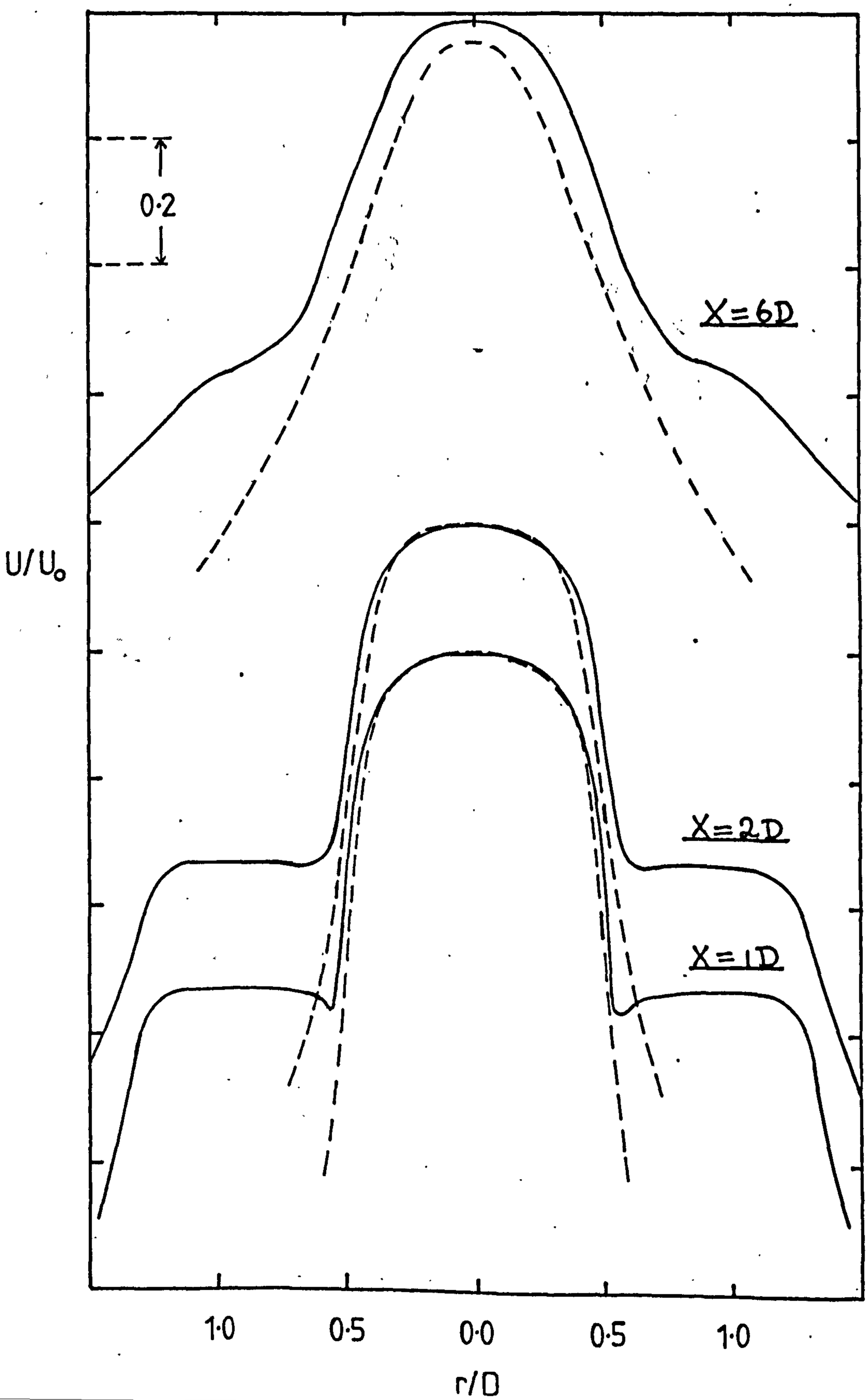

FIGURE 90 : COMPARISON OF ANALYTICAL FORM OF MEAN VELOCITY PROFILE (——) WITH MEASURED MEAN VELOCITY PROFILE OF BRIERLEY (⊙), $\Lambda = 0.5$. AXIAL DISTANCES : (a) X = 1D, (b) X = 2D, (c) X = 6D.

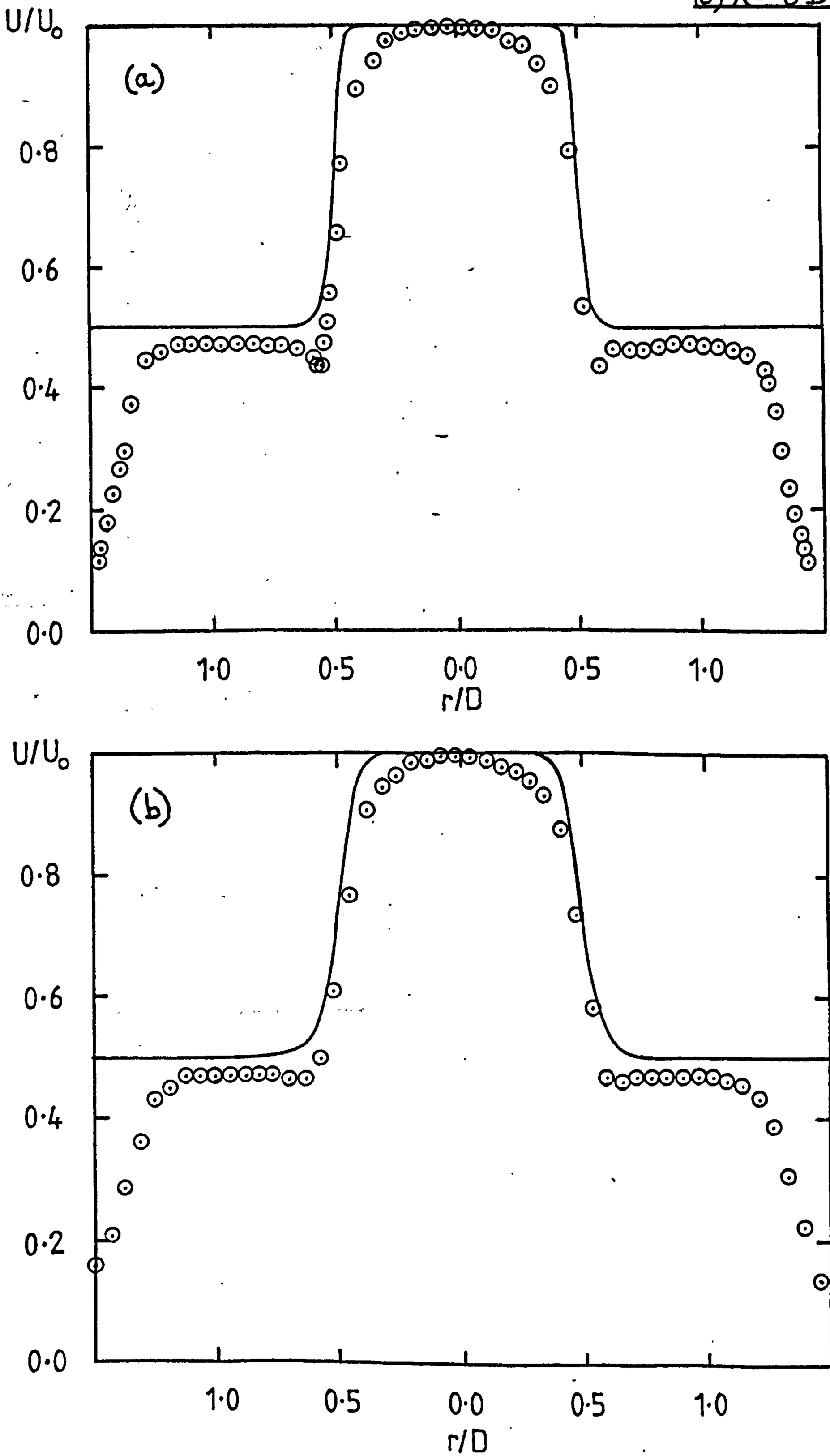

FIGURE 90 CNTD.

(c)

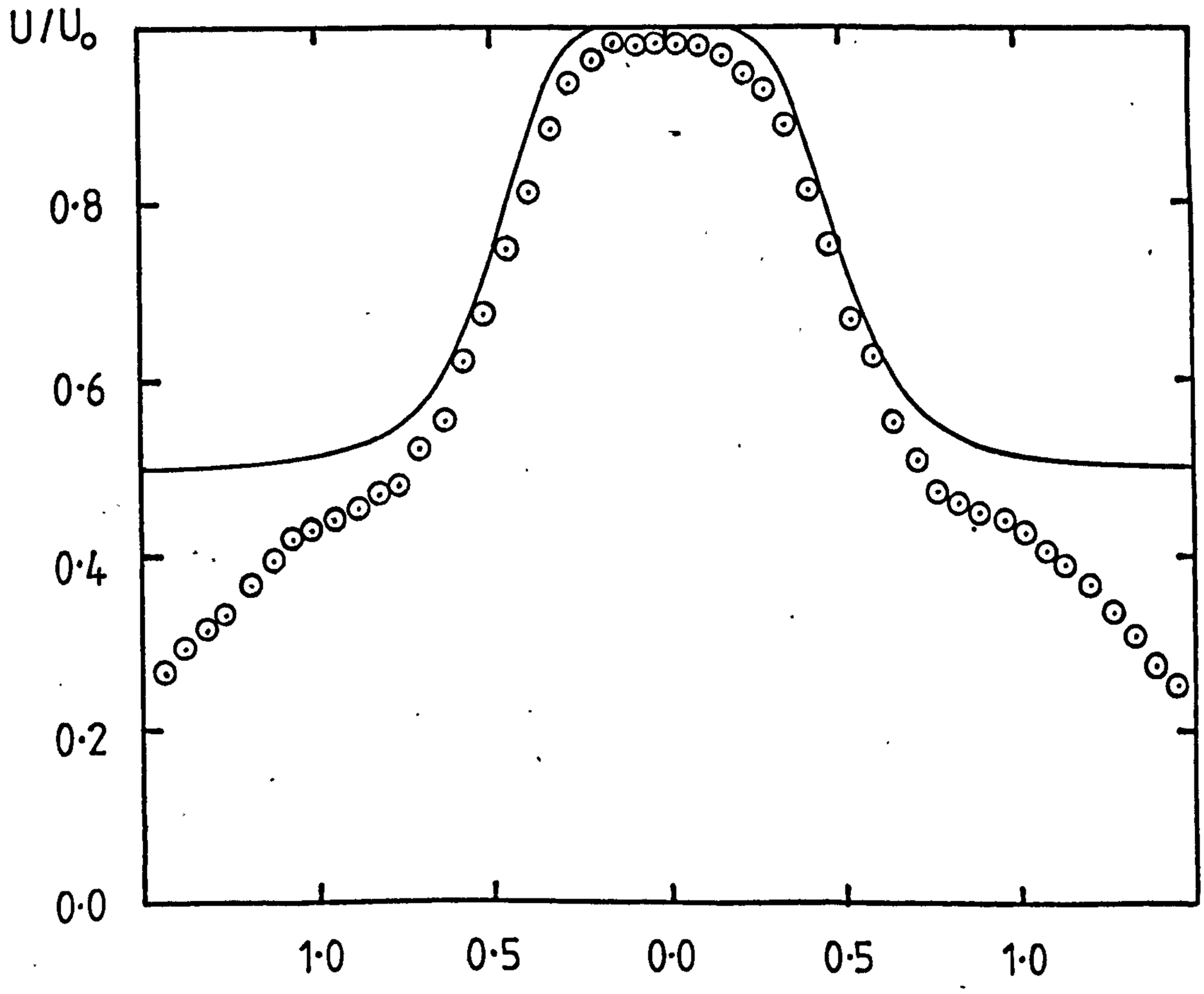

FIGURE 91 : EFFECT OF EXTERNAL FLOW ON AXIAL VARIATION OF (a) FLUCTUATING PRESSURE, (b) FLUCTUATING AXIAL VELOCITY AND (c) FLUCTUATING RADIAL VELOCITY IN m=0 MODE AT St = 0·3 . ---, Λ = 1·0 ; ——, (i) Λ = 0·9, (ii) Λ = 0·8, (iii) Λ = 0·7 AND (iv) Λ = 0·5.

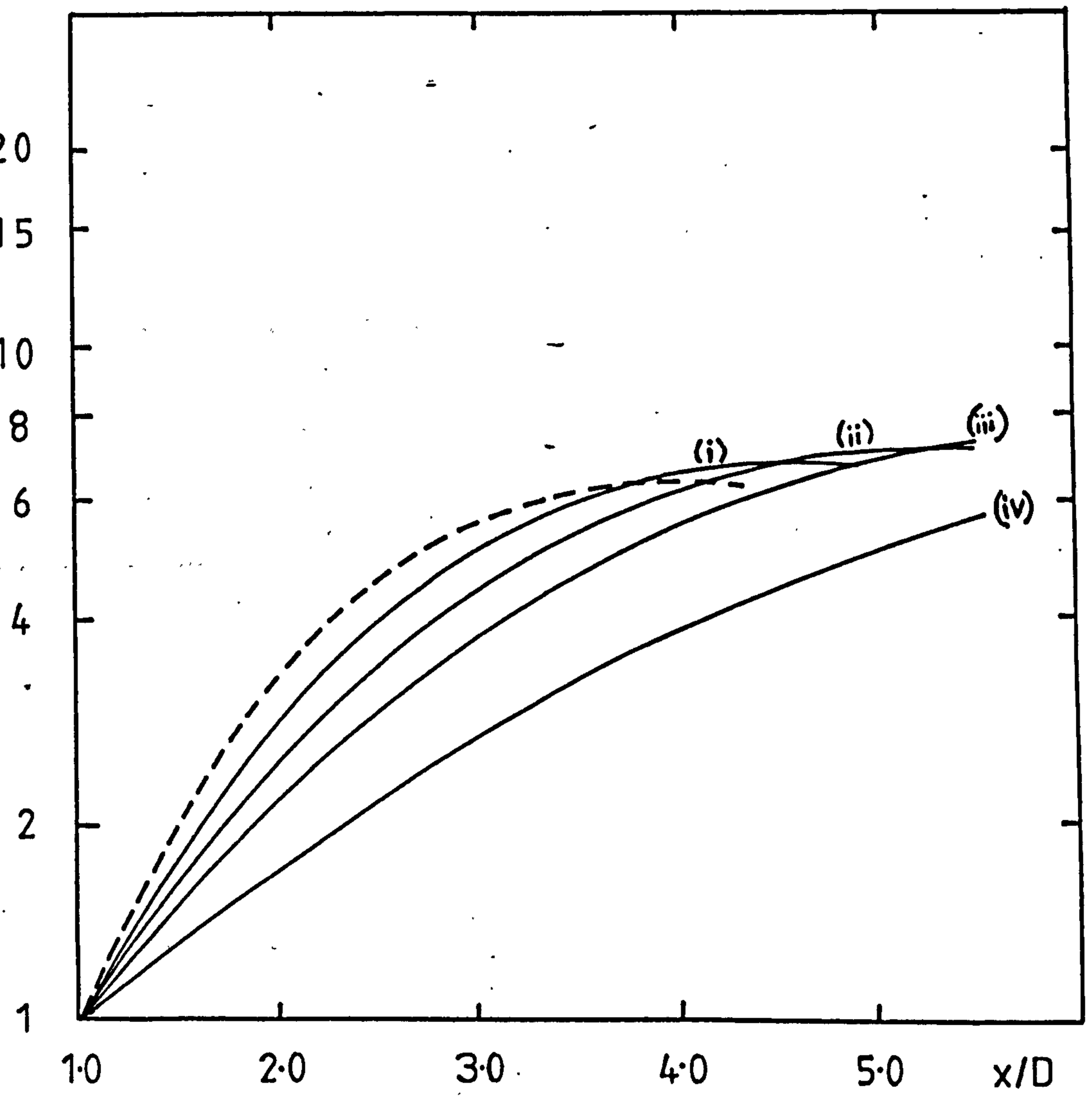

(a) FLUCTUATING PRESSURE

FIGURE 91 CNTD.

(b) FLUCTUATING AXIAL VELOCITY

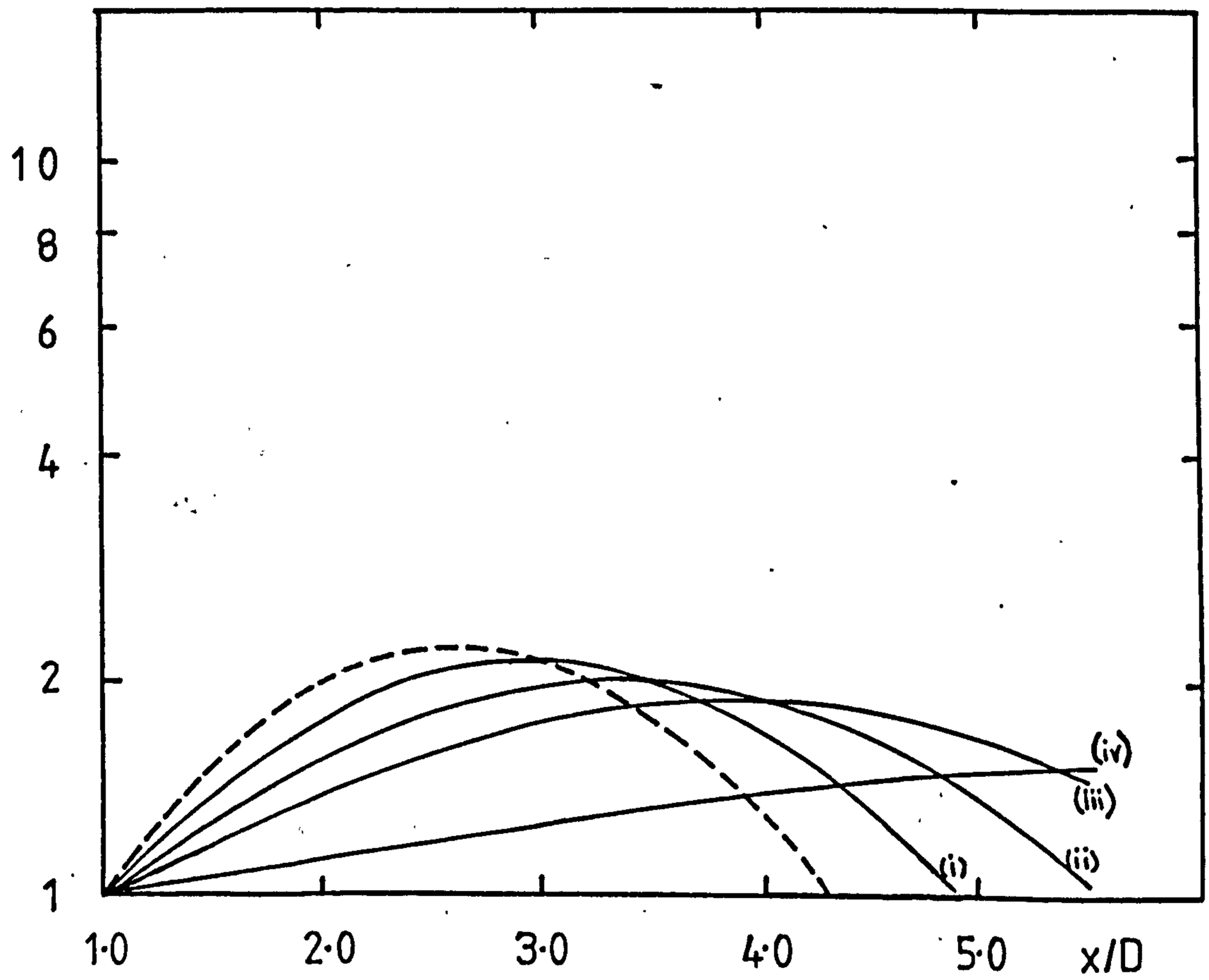

FIGURE 9-1 CNTD.

(c) FLUCTUATING RADIAL VELOCITY

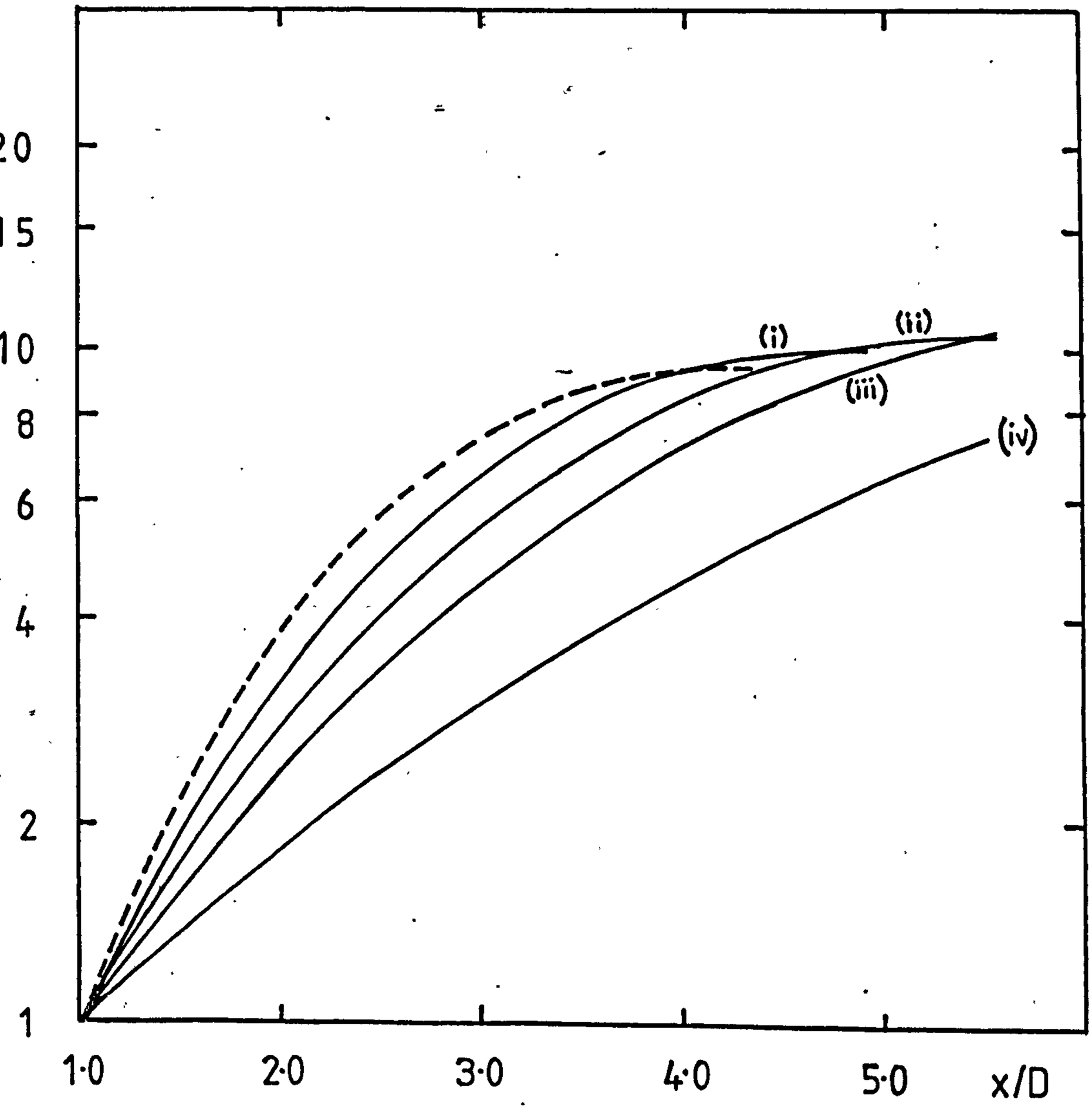

FIGURE 92 : FOR CAPTION SEE NEXT PAGE

(a) FLUCTUATING PRESSURE

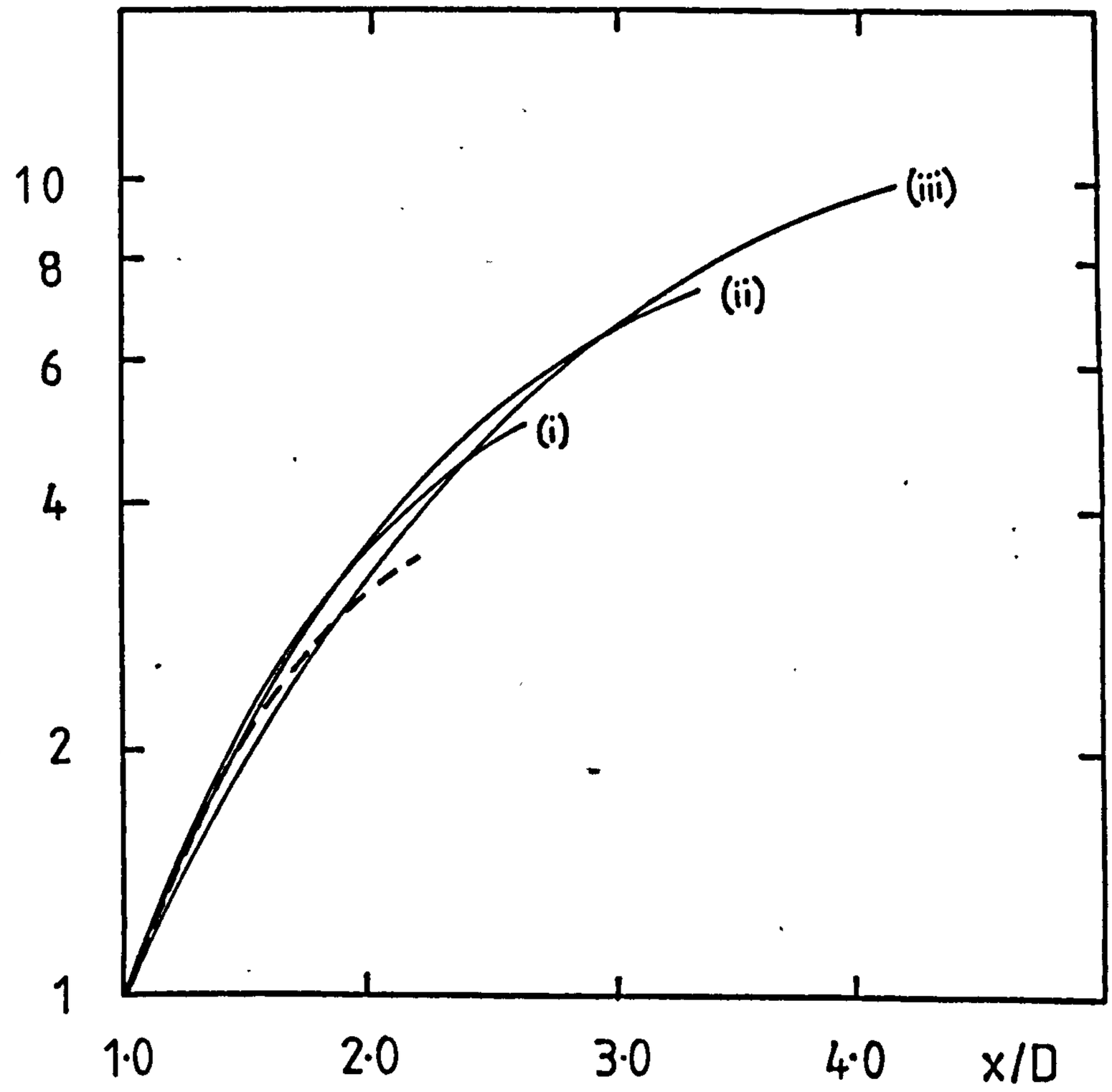

(b) FLUCTUATING AXIAL VELOCITY

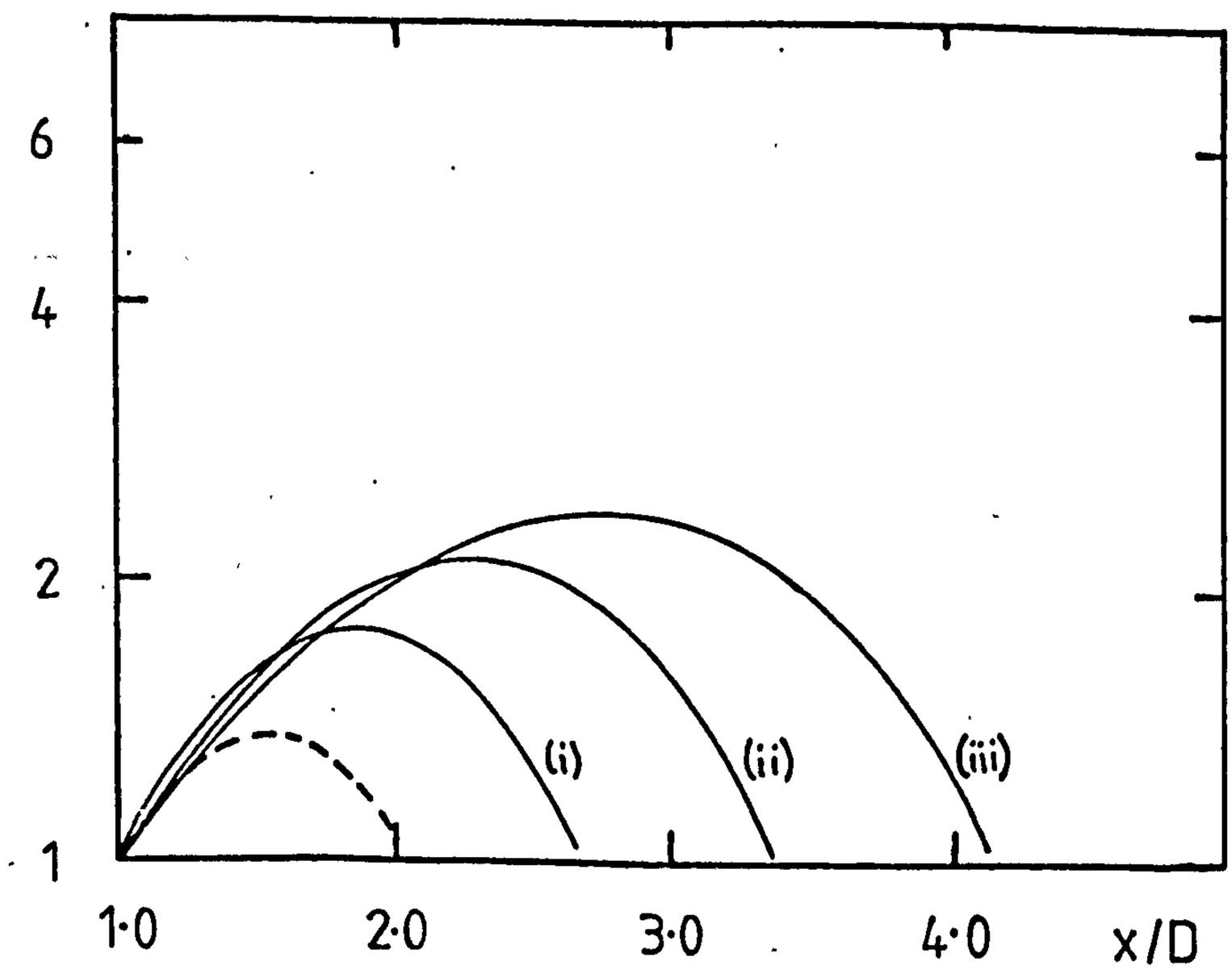

FIGURE 92 : EFFECT OF EXTERNAL FLOW ON AXIAL VARIATION OF (a) FLUCTUATING PRESSURE, (b) FLUCTUATING AXIAL VELOCITY AND (c) FLUCTUATING RADIAL VELOCITY IN m=0 MODE AT St = 0·5. ---, $\Lambda = 1.0$; ——, (i) $\Lambda = 0.9$, (ii) $\Lambda = 0.8$ AND (iii) $\Lambda = 0.7$.

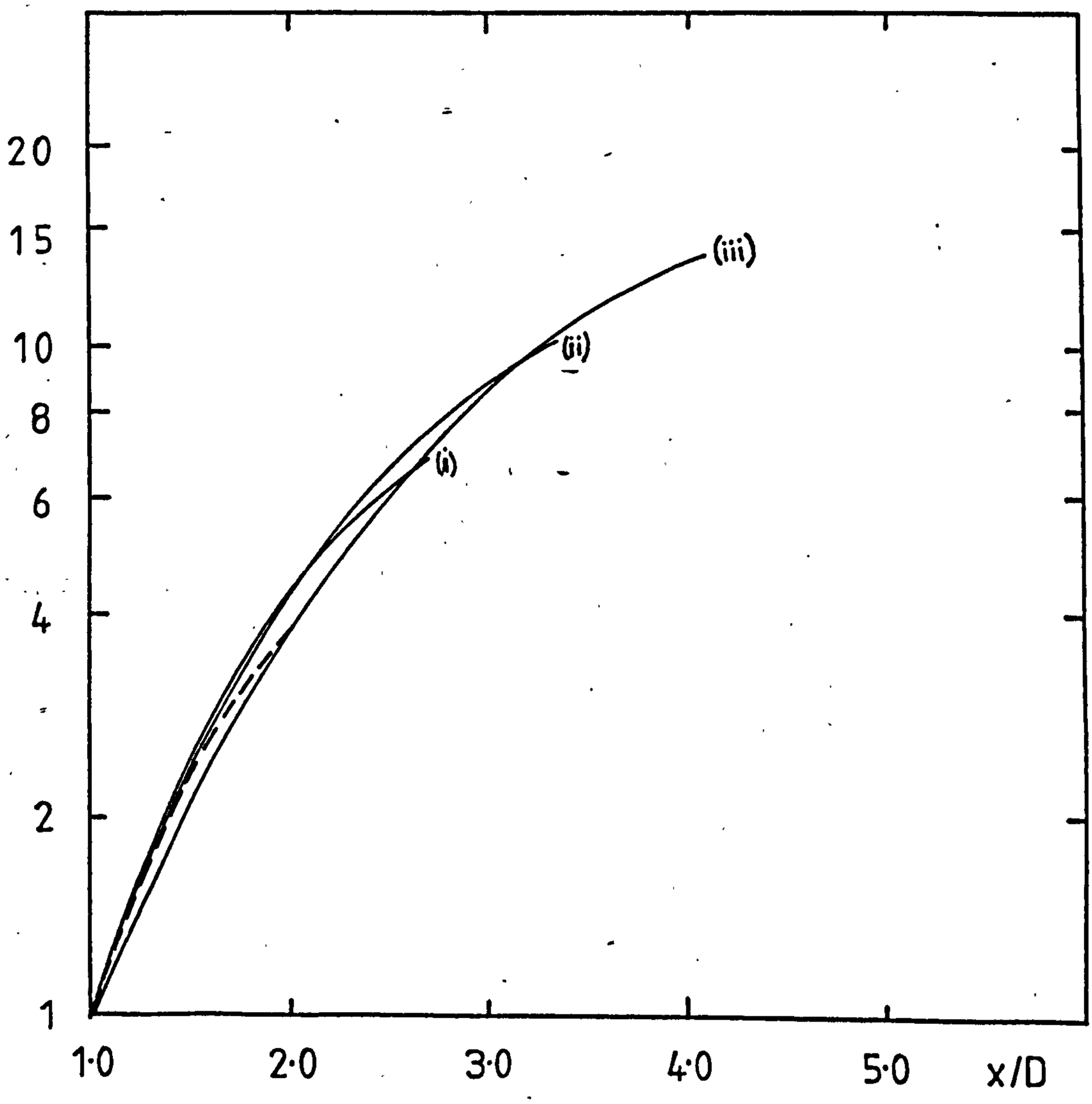

(c) FLUCTUATING RADIAL VELOCITY

CHAPTER 6 SUMMARY AND CONCLUSIONS

A detailed investigation has been undertaken of the aerodynamic response of a high Reynolds number jet to controlled excitation. Acoustic forcing has been applied just upstream of the nozzle exit plane both in the form of a single circumferential mode, which here included the plane wave and first order (spinning) modes, and in a combination of either two counter-rotating first order modes ($m = \pm 1$) producing a "flapping" mode, or two such second order modes ($m = \pm 2$). A Strouhal number close to that of the "preferred" mode and, for the most part, a high forcing level which resulted in a non-linear instability wave response, produced a large broadband far-field noise increase ($\sim$ 6 dB) over the level of the unexcited jet.

Extensive aerodynamic measurements have been made on the initial mixing region of the jet. Hot wire anemometry was used to obtain radial profiles of the mean, turbulent and instability wave components of the axial and radial velocities. In addition, a large number of pitot tube readings has been taken from which a more comprehensive set of mean velocity profiles was obtained covering the first twelve diameters of the jet. In the first order mode, axial and radial profiles of both the amplitude and phase of the instability wave pressure have also been determined including results which correspond to an additional, much lower, forcing level at which the jet response would be expected to be almost linear. Finally, ciné Schlieren films of the excited jet have been taken to provide a visual aid in assessing the structural deformations brought about by the different forcing patterns.

The instability wave measurements have shown that on the initial region of the jet both the spinning and the flapping first order modes were amplified at a rate comparable with that of the axisymmetric mode. This was also true of the particular second order mode configuration used here, but a modal analysis revealed that a substantial amount of the plane wave mode was present in the forcing field and so this result is not representative of the true growth rate of a 'pure' second order mode.

However, changes in growth rates have been observed with radial position. In general, the peak in the shear layer velocity fluctuations was found to occur between one and two diameters downstream of the nozzle exit whereas the peak in the centre line fluctuations was reached further downstream, between two and four diameters. The flapping mode produced the largest gain in the velocity fluctuations at x = 2D (with respect to x = 1D) and indeed this was the only mode in which an axial growth was achieved across the whole jet at this position.

At axial distances greater than two diameters, the mean velocity profile of the unexcited jet suffered appreciable distortion when the jet was excited, which was characterised by a shortening of the potential core and a broadening of the shear layer. A particularly sizeable deformation was evident across the widest profiles of the asymmetric m = ±1 and m = ±2 modes between x = 4D and x = 8D. In the case of the flapping mode the profile was still strongly asymmetric at x = 12D.

The turbulence profiles, too, showed that the growth of the mixing region was more rapid in the excited jet than the unexcited

jet. On the whole, the measured turbulence levels were comparable under all the forms of excitation. An exceptionally high axial velocity component was noted in the m = ±2 mode across the narrowest profile at x = 4D,though, which coincided with a low instability wave amplitude and a large deformation in the mean velocity profile. The instability wave in this mode thus appeared to be the most rapidly decaying one at this station.

The flow visualisation results have emphasised the rapid growth of all the modes considered. The now familiar vortex pairing process in the case of the plane wave mode has again been observed here and the sinuous nature of the first order modes is clearly shown.

The primary objective of this study was to establish the relative importance of the non-axisymmetric modes on a turbulent jet. Conclusive evidence has been shown to demonstrate that both the spinning and the flapping first order modes are as significant as the axisymmetric mode in their effect on the jet structure; yet for the first order modes no phenomenon corresponding to the pairing of axisymmetric vortex rings has been observed.

The experimental results have been compared with the results of a linear stability analysis of higher order modes growing on a circular jet with a slowly diverging mean flow. The predicted axial growth rates of the velocity perturbations were inevitably too large, the discrepancy being attributable to the fact that the theory is linear whereas the measured growth rates were the result of a highly non-linear forcing. At the lower forcing level, however, at which pressure measurements were made in the first order spinning mode, the theoretical results were much more consistent with the observed

growth rates. No mean velocity measurements were taken at this flow condition, the experiment being conducted at a higher Mach number (M = 0.5) than for the velocity measurements (M = 0.3), but the improvement is nonetheless encouraging.

The computed transverse structures of the velocity components compare very favourably with the profiles measured in the non-linear régime. In a given mode, by simply matching the amplitude of a single component at one radial position to the corresponding experimental value, the profiles of both the axial and radial velocity components were determined to a good approximation. This was shown at x = 1D and x = 2D separately, but the choice of a single normalisation at x = 1D could not be used to determine the amplitudes at both axial stations because of the disagreement in the axial growth rates between theory and experiment. Nevertheless, this is still an important result which lends support to the hitherto unjustified use of shape functions in integral methods for predicting the axial development of other than very low level perturbations.

The forcing level does not appear to affect the measured phase speeds of the pressure fluctuations either, and these too have been well predicted by the analysis. The shapes of the experimental radial pressure distributions of the present work and those of Chan [17] have been less well predicted. This can almost certainly be ascribed to the use of the incorrect mean velocity profile in the computations, which was unknown in these cases.

The theory has been limited to axial distances upstream of the axial position at which the local parallel flow sustains a neutral

wave and this has been particularly restrictive for disturbances at high Strouhal numbers. Further, the limits of its applicability have been stretched in the comparison with the non-linear instability wave response of the experimental work, but with a good measure of success. There is still a need for further work on the decay process which has not been considered here. The possible amplification of spinning modes on the fully developed jet would appear less significant. It seems improbable that an azimuthally coherent structure could survive the turbulent mixing process, which encompasses the whole jet at the end of the potential core, and such a structure is unlikely to exist on the far downstream profile in order to be able to grow. Non-linear effects, however, are considered to be essential in modelling the growth of disturbances in the real jet engine context, particularly if the present emphasis on the vortex pairing process as a major noise generation mechanism is vindicated. That emphasis may, however, be shown by the present work to be misplaced; we have found that first order modes produce large mean flow distortions and large broadband acoustic gains, but there is no trace of any process akin to vortex pairing.

Finally, in chapter 5, the effect of an external flow on the growth of an axisymmetric disturbance has been studied. Linear stability theory was applied to a plane wave mode growing on a slowly diverging circular jet immersed in an infinite co-flowing external stream. A number of different velocity ratios and two Strouhal numbers were considered, and the mean velocity profiles used were given a certain amount of justification by the experimental work of Moore & Brierley [54].

The results indicated that the external flow inhibits the growth of disturbances on the primary jet. At a Strouhal number of 0.5 and a velocity ratio of 0.5 the theory indicated that a disturbance would not grow on the corresponding mean velocity profile. Moore & Brierley found that it was under just these conditions that the overall noise reduction of their model co-axial jet, with respect to the noise level of the primary jet alone, reached its maximum value. This result also supports the view that the vortex pairing process is a major noise generation mechanism when it can occur, the external flow reducing growth rates and thereby inhibiting such a process. However, the fact that a jet in an external flow cannot be appreciably excited does not offer any explanation of the observed static to flight differences in noise level (see, for example, Bryce [12]). Indeed, the situation is made worse because for the excited jet the difference in the rear arc is greater.

Overall, it is felt that these studies have shown that linear spatial instability theory for the mean velocity profile is able to indicate significant aspects of the development of large scale structures on high Reynolds number turbulent jets and, in particular, that they have shown important aspects of the behaviour of non-axisymmetric modes and of the influence of external flow on jet response.

List of References

1. Acton, E.
The modelling of large eddies in a two-dimensional shear layer. J. Fluid Mech. (1976) Vol. 76, part 3, pp. 561-592.

2. Acton, E.
A modelling of large eddies in an axisymmetric jet. J. Fluid Mech. (1980) Vol. 98, part 1, pp. 1-32.

3. Ahuja, K.K.
An experimental study of subsonic jet noise with particular reference to the effects of upstream disturbance. M. Phil. thesis (1972), Queen Mary College, London University.

4. Alper, A. and Liu, J.T.C.
On the interactions between large-scale structure and fine-grained turbulence in a free shear flow II The development of spatial interactions in the mean. Proc. R. Soc. London A (1978) 359, pp. 497-523.

5. Bechert, D.W. and Pfizenmaier, E.
On the amplification of broadband jet noise by a pure tone excitation. J. Sound and Vib. (1975) Vol. 43, pp. 581-587.

6. Bechert, D.W. and Pfizenmaier, E.
Amplification of jet noise by a higher-mode acoustical excitation.AIAA Journal (1977), Vol. 15, No.9, pp. 1268-1271.

7. Bendat, J.S. and Piersol, A.G.
Measurement and analysis of random data. Wiley, 1958.

8. Bradshaw, P.
An introduction to turbulence and its measurement. Pergamon Press, 1971.

9. Bradshaw, P., Ferriss, D.H. and Johnson, R.F.
Turbulence in the noise producing region of a circular jet. J. Fluid Mech. (1964) Vol. 19, pp. 591-621.

10. Brooks, J.R. and Woodrow, R.J.
The effects of forward speed on a number of turbojet exhaust silencers. AIAA paper no. 75-056.

11. Brown, G.L. and Roshko, A.
On density effects and large-scale structures in turbulent mixing layers. J. Fluid Mech. (1974) Vol. 64, pp. 775-816.

12. Bryce, W.D.
A review of the research at NGTE concerning the effects of flight on engine exhaust noise. NGTE report no. 78007 (1978).

13. Bushell, K.W.
A survey of low velocity and co-axial jet noise with application to prediction. J. Sound and Vib. (1971) pp. 271-282.

14. Bushell, K.W.
Measurement and prediction of jet noise in flight. AIAA paper no. 75-461.

15. Chan, Y.Y.
Spatial waves in turbulent jets. Part I. Phys. Fluids Vol. 17 pp. 46-53.

16. Chan, Y.Y.
Spatial waves in turbulent jets. Part II. Phys. Fluids Vol. 17 pp. 1667-1670.

17. Chan, Y.Y.
Noise generated wavelike eddies in a turbulent jet. I.C.A.S. conference (1976) paper no. 76-42.

18. Crighton, D.G.
Jet noise and the effects of jet forcing. To appear in 'Proceedings of the International Conference on Turbulent Flows' Madrid 25-27th June 1980. Ed. J. Jimenez, Springer Lecture Notes in Physics.

19. Crighton, D.G. and Gaster, M.
Stability of slowly diverging jet flow. J. Fluid Mech. (1976), Vol. 77, part 2, pp. 397-413.

20. Crow, S.C.
Viscoelastic properties of fine-grained incompressible turbulence. J. Fluid Mech. (1968) Vol. 33, pp. 1-20.

21. Crow, S.C.
Acoustic gain of a turbulent jet. Paper IE.6 Am. Phys. Soc. Fluid Dynamics Meeting, Boulder, Colorado, Nov. 1972.

22. Crow, S.C. and Champagne, F.H.
Orderly structure in jet turbulence. J. Fluid Mech. (1971) Vol. 48, part 3, pp. 547-591.

23. Davies, P.O.A.L., Fisher, M.J. and Barratt, M.J.
The characteristics of the turbulence in the mixing region of a round jet. J. Fluid Mech. (1963) Vol. 15, pp. 337-367.

24. Damms, S.M. and Küchemann, D.
On a vortex sheet model for mixing between two parallel streams 1. Description of the model and the experimental evidence. Proc. R. Soc. London A 339, p. 451 (1974).

25. Deneuville, P.M. and Jacques, J.R.
Jet noise amplification - a practically important problem. AIAA paper no. 77-1368.

26. Drevet, P., Duponchel, J.P. and Jacques, J.R.
Effect of flight on the noise from a convergent nozzle as observed on the Bertin Aerotrain. AIAA paper no. 76-557.

27. Ffowcs Williams, J.E.
The noise from turbulence convected at high speed. Phil. Trans. Roy. Soc. London (1963) 255, pp. 469-503.

28. Ffowcs Williams, J.E. and Hawkings, D.L.
Sound generation by turbulence and surfaces in arbitrary motion. Phil. Trans. Roy. Soc. A 264, pp. 321-342 (1969).

29. Ffowcs Williams, J.E. and Kempton, A.J.
The noise from the large scale structure of a jet. J. Fluid Mech. (1978). Vol. 84, pp. 673-694.

30. Fuchs, H.V.
Space correlations of the fluctuating pressure in subsonic turbulent jets. J. Sound and Vib. (1972) Vol. 23 pp. 77-99.

31. Fuchs, H.V.
Resolution of turbulent jet pressure into azimuthal components. AGARD-CP-131 (1974), paper no. 27.

32. Gotoh, K.
The equilibrium-state of the finite disturbance in free flows. Journal of the Physical Society of Japan (1968), Vol. 24 No. 5, pp. 1137-1146.

33. Grant, A.J.
A numerical modelling of instability in axisymmetric jets. J. Fluid Mech. (1974) Vol. 66, pp. 707-724.

34. Huerre, P.
The nonlinear stability of a free shear layer in the viscous critical layer regime. Phil. Trans. Roy. Soc. London A 293, pp. 643-675 (1980).

35. Huerre, P. and Scott, J.F.
Effects of critical layer structure on the nonlinear evolution of waves in free shear layers. Proc. Roy. Soc. London A 371, pp. 509-524 (1980).

36. Jubelin, B.
New experimental studies on jet noise amplification. AIAA paper no. 80-0961.

37. Kibens, V.
Discrete noise spectrum generated by an acoustically excited jet. AIAA paper no. 79-0592.

38. Lau, J.C., Fisher, M.J. and Fuchs, H.V.
The intrinsic structure of turbulent jets. J. Sound and Vib. (1972) Vol. 22, pp. 379-406.

39. Laufer, J., Kaplan, R.E. and Cu, W.T.
On the generation of jet noise. AGARD-CP-131 (1974), paper no. 21.

40. Lee, B.H.K.
Some measurements of spatial instability waves in a round jet. AIAA Journal (1976) Vol. 14, pp. 348-351.

41. Lighthill, M.J.
On sound generated aerodynamically I General theory. Proc. R. Soc. London A (1952) 211, pp. 564-587.

42. Lighthill, M.J.
On sound generated aerodynamically II Turbulence as a source of sound. Proc. R. Soc. London A (1954), 222, pp. 1-32.

43. Liu, J.T.C. and Merkine, L.
On the interactions between large scale structure and fine-grained turbulence in a free shear flow. I. The development of temporal interactions in the mean. Proc. R. Soc. London A (1976) 352, p.213.

44. Lush, P.A.
Measurements of subsonic jet noise and comparison with theory. J. Fluid Mech. (1971) Vol. 46, pp. 477-500.

45. Mani, R.
The issue of convective amplification in jet noise. AGARD-CP-131 (1974), paper no. 10.

46. Mankbadi, R. and Liu, J.T.C.
A study of the interactions between large scale coherent structures and fine-grained turbulence in a round jet. Phil. Trans. R. Soc. (in press).

47. Mattingly, G.E. and Chang, C.C.
Unstable waves on an axisymmetric jet column. J. Fluid Mech. (1974) Vol. 65, part 3, pp. 541-560.

48. Michalke, A.
Instabilität eines kompressiblen runden Freistrahls unter Berücksichtigung des Einflusses der Strahlgrenzschichtdicke. Z. Flugwiss. (1971) Vol. 19, pp. 319-328.

49. Michalke, A. and Fuchs, H.V.
On turbulence and noise of an axisymmetric shear flow. J. Fluid Mech. (1975) Vol. 70, part 1, pp. 179-205.

50. Mollo-Christensen, E.
Jet noise and shear flow instability seen from an experimenter's viewpoint. J. Appl. Mech. Vol. 34, pp. 1-7.

51. Moore, C.J.
Aerodynamic data and flow visualisation techniques for the ARL jet noise rig. Internal report RR(OH) 585, Rolls Royce Ltd.(1974).

52. Moore, C.J.
The role of shear-layer instability waves in jet exhaust noise. J. Fluid Mech. (1977) Vol. 80, part 2, pp. 321-367.

53. Moore, C.J.
The effect of shear layer instability on jet exhaust noise. Structure and Mechanisms of Turbulence Vol. II pp. 254-264, Springer Lecture Notes in Physics, 76, Ed. H. Fiedler.

54. Moore, C.J. and Brierley, D.H.
Shear layer instability noise produced by various jet nozzle configurations. Mechanics of Sound Generation in Flows, pp. 48-54, Ed. E.-A. Müller, Springer, Berlin (1979).

55. Morfey, C.L.
Sound radiation from a simulated jet flow. Mechanics of Sound Generation in Flows, pp. 12-18, Ed. E.-A. Müller, Springer, Berlin (1979).

56. Morris, P.J.
The spatial viscous instability of axisymmetric jets. J. Fluid Mech. (1976). Vol. 77, part 3, pp. 511-529.

57. Morris, P.J.
A model for broadband jet noise amplification. AIAA paper no. 80-1004.

58. Morris, P.J. and Tam, C.K.W.
On the radiation of sound by the instability waves of a compressible axisymmetric jet. Mechanics of Sound Generation in Flows, pp. 55-61, Ed. E.-A. Müller, Springer, Berlin (1979).

59. Morrison, G.L. and McLaughlin, D.K.
Noise generation by instabilities in low Reynolds number supersonic jets. J. Sound and Vib. (1979). Vol. 65, part 2, pp. 177-191.

60. Plaschko, P.
Helical instabilities of slowly divergent jets. J. Fluid Mech. (1979) Vol. 92, pp. 209-216.

61. Reynolds, A.J.
Observations of a liquid-into-liquid jet. J. Fluid Mech. Vol. 14, p. 552.

62. Ribner, H.S.
The generation of sound by turbulent jets.
Advances in Applied Mechanics. Vol. 8, pp. 103-182, Academic Press (1964).

63. Ronneberger, D.
Experimentelle Untersuchungen zum akustichen Reflexionsfactor von unstetigen Querschnittsänderungen in einem luftdurchströmten Rohr. Acustica (1967) Vol. 19, part 4, pp. 222-235.

64. Roshko, A.
Structure of turbulent shear flows : a new look.
AIAA Journal (1976) Vol.14, No.10, pp.1349-1357.

65. Sarohia, V. and Massier, P.F.
Effects of external boundary layer flow on jet noise in flight. AIAA paper no. 76-558.

66. Whitham, G.B.
Linear and Non-linear waves. Wiley, New York (1974), p. 397.

67. Winant, C.D. and Browand, F.K.
Vortex pairing : the mechanism of turbulent mixing layer growth at moderate Reynolds numbers. J. Fluid Mech. (1974) Vol. 63, pp. 237-255.